

UC Berkeley

UC Berkeley Electronic Theses and Dissertations

Title

Computational Methods for the Design and Operations of Electric Power Systems: Towards Resiliency and Security

Permalink

<https://escholarship.org/uc/item/1m109050>

Author

Park, SangWoo

Publication Date

2022

Peer reviewed|Thesis/dissertation

Computational Methods for the Design and Operations of Electric Power Systems:
Towards Resiliency and Security

By

SangWoo Park

A dissertation submitted in partial satisfaction of the
requirements for the degree of
Doctor of Philosophy
in
Engineering - Industrial Engineering and Operations Research
in the
Graduate Division
of the
University of California, Berkeley

Committee in charge:

Associate Professor Javad Lavaei, Chair
Professor Shmuel Oren
Associate Professor Duncan Callaway

Summer 2022

©August, 2022
SangWoo Park
All rights reserved

Abstract

State estimation is an important tool for continuously monitoring the power system and aims to recover the underlying system voltage phasors, given supervisory control and data acquisition (SCADA) measurements and a model that encompasses the system topology and specifications. To ensure an accurate state estimation, it is essential to have the capability of detecting bad data. Assuming that the network parameters are known and the measurement devices are correctly calibrated, the main source of bad data is topological errors in the model. In this dissertation, we propose a methodology for robust power system state estimation (PSSE) modeled by AC power flow equations when there exists a small number of topological errors. The developed technique utilizes the availability of a large number of SCADA measurements and minimizes the ℓ_1 norm of nonconvex residuals augmented by a nonlinear, but convex, regularizer. Representing the power network by a graph, we first study the properties of the solution obtained from the proposed NLAV estimator and demonstrate that, under mild conditions, this solution identifies a small subgraph of the network that contains the topological errors in the model used for the state estimation problem. Then, we introduce a method that can efficiently detect the topological errors by searching over the identified subgraph. In addition, we develop a theoretical upper bound on the state estimation error to guarantee the accuracy of the proposed state estimation technique.

The power flow equations are nonlinear, and may admit multiple solutions. In the past, the conventional wisdom was to assume that the solution becomes unique by restricting it to “realistic” or “physically realizable” values. However, various examples in the literature show that multiple solutions may persist even after restricting either voltage magnitudes or phase angle differences to “physically realizable” values. This dissertation establishes sufficient conditions for the uniqueness of AC power flow solutions via the monotonic relationship between real power flow and the phase angle difference. More specifically, we prove that the $P - \Theta$ power flow problem has at most one solution for any acyclic or *GSP* graph. In addition, for arbitrary cyclic power networks, we show that multiple distinct solutions cannot exist under the assumption that angle differences across the lines are bounded by some limit related to the maximal girth of the network. We also introduce a series-parallel operator and show that this operator obtains a reduced and easier-to-analyze model for the power system without changing the uniqueness of power flow solutions.

In the next part of this dissertation, the above work is extended and we establish general necessary and sufficient conditions for the uniqueness of $P - \Theta$ power flow solutions in an AC power system using properties of the monotone regime and the power network topology. We show that the necessary and sufficient conditions can lead to tighter sufficient conditions for the uniqueness in several special cases. Our results are based on the previously introduced notion of maximal girth and a new notion of maximal eye. Moreover, we develop a series-parallel reduction method and search-based algorithms for computing the maximal eye and maximal girth, which are necessary for the uniqueness

analysis. Reduction to a single line using the proposed reduction method is guaranteed for 2-vertex-connected Series-Parallel graphs.

In the final part of this dissertation, we present a methodology based on homotopy to find the globally optimal solutions of nonconvex optimization problems. Optimal power flow (OPF) is a fundamental problem in power systems analysis for determining the steady-state operating point of a power network that minimizes the generation cost. In anticipation of component failures, such as transmission line or generator outages, it is also important to find optimal corrective actions for the power flow distribution over the network. The problem of finding these post-contingency solutions to the OPF problem is challenging due to the nonconvexity of the power flow equations and the large number of contingency cases in practice. In this paper, we introduce a homotopy method to solve for the post-contingency actions, which involves a series of intermediate optimization problems that gradually transform the original OPF problem into each contingency-OPF problem. We show that given a global solution to the original OPF problem, a global solution to the contingency problem can be obtained using this homotopy method, under some conditions. With simulations on Polish and other European networks, we demonstrate that the effectiveness of the proposed homotopy method is dependent on the choice of the homotopy path and that homotopy yields an improved solution in many cases.

Acknowledgement

The time that I spent in Berkeley for my doctoral degree have been blessed with so many brilliant people and wonderful memories. First and foremost, I would like to thank my advisor, Prof. Javad Lavaei, for providing me with the opportunity to work with him. Throughout my time at Berkeley, Prof. Javad Lavaei has constantly supported me and guided me towards becoming a good researcher. During the toughest times of my studies, his encouragement is what got me to persevere and constantly believe in myself. His unceasing passion for research and intellectual excellence will continue to motivate me even after graduation.

My sincere respect and gratitude go to Prof. Benjamin Hobbs, Prof. Ross Baldick and Prof. Somayeh Sojoudi for mentoring me and providing valuable insight during our collaborative research projects. My interactions with them helped me gain better understanding of power systems and important technical matters. I would also like to thank Prof. Shmuel Oren and Prof. Duncan Callaway for serving on my committee and providing valuable feedbacks and comments on my research and dissertation.

The materials of this dissertation benefited from the collaborations and discussions with current and former members of our research group: Richard Y. Zhang, Reza Mohammadi-Ghazi, Ming Jin, Elizabeth Glista, Julie Mulvaney-Kemp and Haixiang Zhang. I would like to thank them for their great efforts and contributions, and for being wonderful friends and work-partners. Special thanks to my dearest friend, Han Feng, for supporting me and spending time with me ever since we joined the program together. You are the best friend that I can ever have. My deepest gratitude and appreciation go to all my IEOR friends. Thank you Salar Fattahi, Igor Molybog, Richard Y. Zhang, Cedric Jozs, Yuhao Ding, Matt Olfat, George Patsakis and Pedro Hespanhol for the wonderful trips and memories that we enjoyed together. Thank you Jiung Lee for deeply caring about me and reaching out to help me all the time.

Outside of work, my biggest hobby/second-profession has been soccer. To all my Galacticos brothers, thank you for your love and support on and off the field. I will treasure the moments that I shared with you forever. As I have said before, teams come and go, but Galacticos will always be there, b-b-bro!

I thank my parents for their unwavering love and support. Without them, I would not have been able to stand strong and become the person who I am right now. They have been my inspiration, motivation, hope and shelter. Mom and dad, dad and mom, I love you very much. Finally, my deepest affection and appreciation for the love of my life, Saebom Lee, for her unconditional love and support for me. Thank you for sharing the journey of life with me.

SangWoo Park
May 18, 2022

Dedicated to

My mother Yoon-Mi Hwang, my father Yong-Bum Park and my sister Jung-Woo Park

Contents

Abstract	1
Acknowledgement	i
Dedication	ii
List of Figures	viii
List of Tables	ix
I Background and Motivation	1
II Nonlinear LAV Estimator for Topology Error Detection and Robust State Estimation	6
1 Introduction	6
1.1 Previous studies on topological error detection	6
1.2 Contributions	7
1.3 Notations	8
2 Preliminaries	8
3 Main Results	10
3.1 Nonlinear least-squares state estimation	10
3.2 Proposed NLAV formulation	11
3.3 Estimation error	12
3.4 Sparse suspect-subgraph	14
3.5 Algorithm	15
3.6 Unpenalized NLAV estimator and unique solution	16
4 Simulation Results	18
4.1 Simulation setup	18
4.2 Example: Sparse residuals for NLAV	19
4.3 57-bus system	20

5	Conclusion	20
6	Appendix	21
6.1	Proof of Theorem 1	21
6.2	Proof of Theorem 2	24
6.3	Proof of Theorem 3	25
6.4	Theorem 4 and its proof	25
 III Uniqueness of Power Flow Solutions Using Monotonicity and Network Topology		30
1	Introduction	30
1.1	Monotonicity between phase angles and power flow	30
1.2	Main results	31
1.3	Related work	32
2	Notations	34
3	P-Theta problem formulation	34
4	Acyclic Networks	35
4.1	Single line properties	35
4.2	Tree networks	37
5	Cyclic Networks	38
6	Series-Parallel Reduction	41
7	Algorithm	44
7.1	Linear-time algorithm	44
7.2	Graphs that do not satisfy the assumption in Theorem 7.1	47
8	Numerical and simulation results	48
8.1	Series-parallel reduction of IEEE test cases	49
8.2	Calculation of $\kappa(\mathbb{G})$	49
8.3	Performance of linear-time algorithm	49
9	Conclusion	52
10	Appendix	53
10.1	Proof of Lemma 4.1	53
10.2	Proof of Theorem 4.2	54
10.3	Lemma 10.1 and its proof	55

10.4 Proof of Lemma 5.1	56
10.5 Proof of Theorem 5.2	57
10.6 Proof of Theorem 5.3	58
10.7 Lemma 10.2 and its proof	59
10.8 Proof of Theorem 6.1	59
10.9 Proof of Theorem 7.1	60
10.10 Additional Figures	61

IV Uniqueness of Power Flow Solutions Using Graph-theoretic Notions 66

1 Introduction 66	
1.1 Main results	67
1.2 Related work	68
1.3 Notations	69
1.4 Paper organization	69
2 Preliminaries 70	
2.1 P - Θ problem formulation	70
2.2 Monotone regime and allowable sets	70
2.3 Notions of weak and strong uniqueness	72
3 Uniqueness Theory for General Graphs 73	
4 Uniqueness Theory for Three Special Cases 77	
4.1 Single cycles	77
4.2 Series-Parallel graphs	78
4.3 Lossless networks	79
5 Algorithms and Numerical Results 80	
5.1 Successive Series-Parallel Reduction method	80
5.2 Numerical results	85
6 Conclusion 86	
7 Appendix 87	
7.1 Algorithms for computing maximal eye and maximal girth	87
7.2 Proof of Lemma 3.1	90
7.3 Proof of Lemma 3.2	93
7.4 Proof of Corollary 3.4	94
7.5 Proof of Theorem 3.6	95
7.6 Proof of Lemma 4.1	96
7.7 Proof of Theorem 4.2	97

7.8	Proof of Lemma 4.4	98
7.9	Proof of Theorem 4.6	103
7.10	Proof for Successive Series-Parallel Reduction Method	105
7.11	Proof of Lemma 5.1	105
7.12	Proof of Lemma 5.3	107
7.13	Proof of Theorem 5.5	109
7.14	Numerical results of SSPR method for computing the maximal girth . . .	109
7.15	Algorithm for Computing The Maximal Girth	111
7.16	More details and results of numerical experiments	112

V An Efficient Homotopy Method for Solving the Post-contingency Optimal Power Flow to Global Optimality 117

1	Introduction	117
1.1	Notations	119
2	Homotopy for Optimization	120
3	Formulation of Two-stage Security-constrained Optimal Power Flow	122
3.1	Base-case Optimal Power Flow	122
3.2	Post-contingency Optimal Power Flow	123
4	Methods	125
4.1	Homotopy Method for a Line Outage	125
4.2	Homotopy Method for a Generator Outage	125
4.3	Implementation of Homotopy-OPF	126
5	Analysis of Homotopy Paths	129
5.1	Convergence and Complexity of Homotopy-OPF	129
5.2	Genericity of Unique Global Minimizer with SSOC	131
5.3	Geometry of the homotopy path: Two-bus example	133
6	Simulations	134
7	Conclusions	139
8	Appendix	142
8.1	Proof of Theorem 5.1	142
8.2	Proof of Theorem 5.2	142
8.3	Proof of Lemma 5.3	144
8.4	Proof of Lemma 5.4	144
8.5	Proof of Lemma 5.5	145
8.6	Proof of Corollary 5.6	146

8.7 Proof of Lemma 5.7 146
8.8 Computation of Participation Factors for Generator Outage 149

List of Figures

1	(a) A power network, (b) the state estimation error graph \mathcal{S} , (c) the extended state estimation error graph $\tilde{\mathcal{S}}$, and (d) the line residual graph \mathcal{R}^L .	13
2	A diagram showing the relationship between different subgraphs.	14
3	Noiseless state estimation error for (a) NLS, (b) NLAV; and residuals for (c) NLS, (d) NLAV.	17
4	Simulation results on the IEEE 57-bus system.	19
5	Cycle example showing multiple solutions.	39
6	A simple diagram illustrating a sequence of series-parallel reductions for the IEEE 14-bus system.	42
7	A two-cycle network sharing an edge.	46
8	A simple diagram of the IEEE 14-bus system.	47
9	(a) IEEE 30-bus system before reduction, (b) IEEE 30-bus system after reduction, (c) IEEE 39-bus system before reduction, and (d) IEEE 39-bus system after reduction.	50
10	Further decomposition of a directed chordless cycle.	51
11	Comparison of average errors and solving times for Algorithm1 and matpower-NR.	52
12	Errors for the 36 (out of 400) simulations when matpower-NR converged successfully for $\mu = 10$.	53
13	A test network consisting of triangles.	61
14	A simple graph with dangling vertex.	61
15	A simple graph with multiple edges in series.	61
16	Evaluating the performance of homotopy on one-dimensional unconstrained minimization problems.	121
17	An example of the set \mathbb{U}' (blue) and an effective homotopy path (red) that can reach the origin without passing through a point in \mathbb{U}' .	133
18	Performance of proposed homotopy method on the 3375-bus Polish network (case3375wp with real and reactive power demand scaled up by 10%) with single line outages.	136
19	Performance of proposed homotopy method on the 3120-bus Polish network (case3120sp with real and reactive power demand scaled up by 10%) with a multiple line outages.	137
20	Performance of proposed homotopy scheme 1 tested with a varying number of iterations.	138
21	Performance of proposed homotopy method for generator outages.	139
22	Performance of proposed homotopy method on the 3375-bus Polish network (case3375wp with real and reactive power demand scaled up by 10%) with a single generator outage.	139

23	Comparison of solution for homotopy and one-shot methods for the 3375-bus Polish network (case3375wp with real and reactive power demand scaled up by 10%) with a single generator outage (generator out ID: 100).	140
24	Comparison of solution for homotopy and one-shot methods for the 3375-bus Polish network (case3375wp with real and reactive power demand scaled up by 10%) with a single generator outage (generator out ID: 100).	141
25	An example of two-bus network for which there are two global solutions to an instance of the homotopy-OPF.	148

List of Tables

1	Upper-bounds on maximal girth for IEEE test cases.	49
2	Number of vertices and edges before and after the SSPR method for maximal eye along with values computed during the reduction process. . . .	86
3	Number of vertices and edges before and after the SSPR method for maximal girth along with values computed during the reduction process. . . .	110
4	Distance measure for different test cases.	113
5	Percent of simulations where 5-iteration homotopy scheme outperformed one-shot method for 1354-bus PEGASE network.	140

Chapter I

Background and Motivation

"The electric utility industry is probably the largest and most complex industry in the world. The electrical engineer who works in that industry will encounter challenging problems in designing future power systems to deliver increasing amounts of electrical energy in a safe, clean, and economical manner [1]."

A power system is a large scale network deployed to supply, transfer, and use electric power. Power systems around the globe are currently undergoing a major paradigm-shift following the need for more resilient and secure systems, and our society's commitment towards a carbon-free and sustainable future. This transformation of the power grid is met with many challenges. The already large-scale network is growing even bigger and more fine-grained as new components and participants are added to the grid. Higher penetration of renewable energy sources promotes sustainability, but it also brings more uncertainty and instability to the grid. Increasing volumes of data are produced through sensors, communication networks and human activities, which can bring great value in operating the system but also contains the risk of derailing the system if noise, gross errors, and malicious attacks are not dealt with properly. On top of all these issues, the innate nature of AC power poses serious difficulties in various computational methods. As a result, the design and operation of these systems needs major innovations in computational techniques.

We take electricity for granted, but behind the scenes there are actually multiple entities such as the independent system operators (ISOs), that solve various large-scale and NP-hard optimization problems in order to make the power system functional. To give you a few examples, an optimal power flow (OPF) problem aims to optimize generation levels and power flow across the network in order to meet system demand in an economical way. The state estimation problem aims to estimate complex valued voltages (in other words the state of the power system) given noisy and tainted measurement values coming from sensors. Also, there is the fundamental problem of solving power flow equations, which involves solving a system of highly nonlinear equations to find steady-state voltages given a power system set-point. Finally, there are also design and planning problems, where the goal is to make decisions on long-term investments (such as transmission lines).

Many of these problems are solved on a large-scale system with up to millions of variables and constraints and often with a tight time restriction. Therefore, the ability of

computational methods that can efficiently come up with high-quality solutions is essential in the safe, reliable and economic operations of the power grid. There are many factors that make computational methods difficult for power systems. One of the most important factor that is common to many problems stems from the nonlinear physics of power. For optimization problems, the nonlinear laws of physics often results in nonconvex problems, which has two types of solutions. A local solution is locally the best solution and is relatively easy to find with modern optimization techniques but has a suboptimal cost. A global solution has the smallest possible objective value but is difficult to find. Finding the global solution is important because implementing a local solution can mean inefficient use of resources and money, and can also mean large violations in the system constraints that lead to insecure operations. For finding the root of a system of equations, nonlinearity leads to multiple solutions, that can potentially grow exponentially with the size of the network. This can lead to solutions that are isolated and far away from each other, causing ambiguity in monitoring and controlling the system.

1 Nonlinear LAV Estimator for Topology Error Detection and Robust State Estimation

Topology error, a modeling misrepresentation of the power system network configuration, can impair the quality of state estimation. The current industry practice for state estimation uses the most recent topology of the power system, previously determined by the system operator. In a longer time frame, topology errors can be fixed by restoring communication and observability on the system. However, state estimation is solved on the time-frame of several minutes, and until the system operator obtains full recovery, the state estimation tool itself could be the only resource available to detect and fix those topology errors. Misrepresenting the system topology typically creates gross errors, which can lead to significant state estimation errors across the entire network. Since the output of state estimation is utilized for many other important applications such as real-time nodal market and voltage stability analysis, the ability of state estimators to detect and correct topology errors in real-time holds considerable value. In this paper, we propose a new technique for robust state estimation in the presence of a small number of topological errors for power systems modeled by AC power flow equations. The developed method leverages the availability of a large volume of SCADA measurements and minimizes the ℓ_1 norm of nonconvex residuals augmented by a nonlinear, but convex, regularizer. Noting that a power network can be represented by a graph, we first study the properties of the solution obtained by the proposed estimator and argue that, under mild conditions, this solution identifies a small subgraph of the network that contains the topological errors in the model used for the state estimation problem. Then, we propose a method that can efficiently detect the topological errors by searching over the identified subgraph. Furthermore, we develop a theoretical upper bound on the state estimation error to guarantee the accuracy of the proposed state estimation technique. The efficacy of the developed

framework is demonstrated through numerical simulations on IEEE benchmark systems.

2 Uniqueness of Power Flow Solutions Using Monotonicity and Network Topology

The AC power flow equations are nonlinear, and may admit multiple solutions. In the past, the conventional wisdom was to assume that the solution becomes unique by restricting it to “realistic” or “physically realizable” values. However, various examples in the literature/industry show that multiple solutions may persist even after restricting either voltage magnitudes or phase angle differences to “physically realizable” values. Therefore, in principle, system operators may encounter operating points that are very different from what they had expected. In order to avoid these situations, it is important to understand whether or not there is a unique “physically realizable” power flow solution for real-world power systems. This paper establishes sufficient conditions for the uniqueness of AC power flow solutions via the monotonic relationship between real power flow and the phase angle difference. More specifically, we prove that the $P - \Theta$ power flow problem has at most one solution for any acyclic or *GSP* graph. In addition, for arbitrary cyclic power networks, we show that multiple distinct solutions cannot exist under the assumption that angle differences across the lines are bounded by some limit related to the maximal girth of the network. In these cases, a vector of voltage phase angles can be uniquely determined (up to an absolute phase shift) given a vector of real power injections within the realizable range. The implication of this result for classical power flow analysis is that, under the conditions specified above, the problem has a unique physically realizable solution if the phasor voltage magnitudes are fixed. We also introduce a series-parallel operator and show that this operator obtains a reduced and easier-to-analyze model for the power system without changing the uniqueness of power flow solutions.

3 Uniqueness of Power Flow Solutions Using Graph-theoretic Notions

This paper extends the uniqueness theory in the previous paper (Project 2) and establishes general necessary and sufficient conditions for the uniqueness of $P - \Theta$ power flow solutions in an AC power system using some properties of the monotone regime and the power network topology. We show that the necessary and sufficient conditions can lead to tighter sufficient conditions for the uniqueness in several special cases. Our results are based on the existing notion of maximal girth and our new notion of maximal eye. Moreover, we develop a series-parallel reduction method and search-based algorithms for computing the maximal eye and maximal girth, which are necessary for the uniqueness analysis. Reduction to a single line using the proposed reduction method is guaranteed for 2-vertex-connected Series-Parallel graphs. The relations between the parameters of the network before and

after reduction are obtained. It is verified on real-world networks that the computation of the maximal eye can be reduced to the analysis of a much smaller power network, while the maximal girth is computed during the reduction process.

4 An Efficient Homotopy Method for Solving the Post-contingency Optimal Power Flow to Global Optimality

Optimal power flow (OPF) is a fundamental problem in power systems analysis for determining the steady-state operating point of a power network that minimizes the generation cost. In anticipation of component failures, such as transmission line or generator outages, it is also important to find optimal corrective actions for the power flow distribution over the network. The problem of finding these post-contingency solutions to the OPF problem is challenging due to the nonconvexity of the power flow equations and the large number of contingency cases in practice. A major drawback of current industry practice is that the post-contingency variables are not optimized with respect to each corresponding contingency configuration to minimize the violation of the constraints in case there is no feasible operating point. It is important to find at least a locally optimal solution, if not a globally optimal solution, because approximate solutions can be much more costly (higher constraint violations) and can threaten the security of the power system. In this paper, we introduce a homotopy method to solve for the post-contingency actions, which involves a series of intermediate optimization problems that gradually transform the original OPF problem into each contingency-OPF problem. We show that given a global solution to the original OPF problem, a global solution to the contingency problem can be obtained using this homotopy method, under some conditions. With simulations on Polish and other European networks, we demonstrate that the effectiveness of the proposed homotopy method is dependent on the choice of the homotopy path and that homotopy yields an improved solution in many cases.

The remainder of this dissertation is organized as follows. In the following Parts II–V, we provide a detailed write-up explaining the methods and results of each corresponding research project. Part VI provides further directions and research problems ¹.

Bibliography

- [1] J. D. Glover, M. S. Sarma, and T. Overbye, *Power System Analysis and Design*, 5th ed. Cengage Learning, 2012.

¹This dissertation includes materials from [2], [3], [4] and [5] that are previously published.

- [2] S. Park, R. Mohammadi-Ghazi, and J. Lavaei, "Nonlinear least absolute value estimator for topology error detection and robust state estimation," *IEEE Access*, vol. 9, pp. 137 198–137 210, 2021.
- [3] S. Park, R. Zhang, J. Lavaei, and R. Baldick, "Uniqueness of power flow solutions using monotonicity and network topology," *IEEE Transactions on Control of Network Systems*, vol. 8, no. 1, pp. 310–330, 2020.
- [4] H. Zhang, S. Park, J. Lavaei, and R. Baldick, "Uniqueness of power flow solutions using graph-theoretic notions," *IEEE Transactions on Control of Network Systems*, vol. 9, no. 1, pp. 100–112, 2022.
- [5] S. Park, E. Glista, J. Lavaei, and S. Sojoudi, "Homotopy method for finding the global solution of post-contingency optimal power flow," *American Controls Conference (ACC)*, 2020.

Chapter II

Nonlinear LAV Estimator for Topology Error Detection and Robust State Estimation

1 Introduction

Safeguarding energy infrastructures against progressive failures of stressed components is an important challenge in operating these systems and preventing blackouts [3, 2]. In doing so, the power system condition should be continuously monitored so that, if needed, required actions can be taken. This condition monitoring is performed through real-time state estimation that aims to recover the underlying system voltage phasors, given supervisory control and data acquisition (SCADA) measurements and a model that encompasses the system topology and specifications [10, 14]. In fact, state estimation not only helps prevent failures in the power network, but it also underpins every aspect of real-time power system operation and control. To ensure an accurate state estimation, it is essential to have the capability of detecting bad data. Assuming that the network parameters are known and the measurement devices are correctly calibrated, the main source of bad data is topological errors in the model. Topological errors refer to the inaccurate modeling of the current network configuration and are often initiated by the misconception of the system operator about the on/off switching status of a few lines in the network due to faults or unreported network reconfigurations. Due to their significant impact on the accuracy of state estimation, dealing with bad data and identifying topological errors have received considerable attention in the past few years.

1.1 Previous studies on topological error detection

The existing topological error detection methods take either a statistical or a geometric approach. Bayesian hypothesis testing [26], collinearity tests [25], and fuzzy pattern machine [27] are examples of statistical approaches for topology error detection. These methods usually need prior information about states and/or a decently-sized dataset from previous measurements.

The geometric approaches, on the other hand, aim to design state estimation techniques that are robust against topological errors and measurement noise. Using normalized Lagrange multipliers of the least-squares state estimation problem is one such technique

that has been shown to be effective in some cases [21], although it is a heuristic method. Recent studies, such as the one proposed in [22], improve this technique; however, they may fail to detect certain scenarios called ‘critical parameter and measurement pairs’. Another important approach in this category is the least absolute value (LAV) estimator introduced in [30] for power systems. By minimizing the ℓ_1 norm of the linearized measurement residual vector, the LAV is capable of finding a minimum set of measurements free of large errors, thus rejecting bad data and yielding a robust estimate. Despite its robustness, the LAV is vulnerable to leverage points as explained in [32, 33]. Further investigation and suggestion of different methods to mitigate this issue have been presented in [34, 35]. In [31], the authors have shown that the effect of leverage points can be eliminated if measurements consist only of phasor measurement units (PMUs). The caveat of these methods is their reliance on a linearized DC model. Only few studies have addressed the fully nonlinear, non-convex problem with power measurements, e.g., [23] where a semidefinite programming (SDP) relaxation is proposed to convexify the nonlinear LAV state estimator; however, no theoretical guarantees have been developed to ensure the recovery of a high-quality solution. Moreover, the computational demand of solving the surrogate SDP problem may restrict the application of this method to small-sized problems in practice. These issues motivate further research on developing robust state estimation techniques with the capability of handling nonconvexities associated with various types of measurements.

1.2 Contributions

In light of the recently developed theoretical guarantees for the ℓ_2 -norm to avoid spurious local solutions in nonconvex optimization [15] and arising promises for the ℓ_1 -norm [17], this study proposes a local search algorithm to find the global solution of the nonlinear LAV (NLAV) state estimator. The proposed method provides a robust approach for estimating the system’s states in presence of a modest number of topological errors as well as detecting such errors. In doing so, the main contributions of this work can be summarized as: (1) proposing an algorithm for detecting modest topological errors and finding the state of the power system using an NLAV state estimator with local search algorithms, (2) formulating a regularized NLAV state estimator to handle severe nonconvexities, (3) finding error bounds and necessary properties for the regularization parameters. As explained later in this paper, local search algorithms would efficiently find global solutions of the underlying NLAV estimators given a sufficient number of noiseless measurements and a proper initialization of the algorithm. Also, many of the implications provided in this paper are all valid even if one uses an SDP relaxation of the proposed nonconvex estimators. The remainder of this paper is organized as follows. Preliminary materials are presented in Section 2, followed by formulation of the algorithm in Section 3. A comprehensive set of numerical simulations on the IEEE 57-bus system is presented in Section 4. Concluding remarks are drawn in Section 9. The proofs are provided in the Appendix.

1.3 Notations

Throughout this paper, lower (resp. upper) case letters represent column vectors (resp. matrices) and calligraphic letters stand for sets and graphs. The symbols \mathbb{R} and \mathbb{C} denote the sets of real and complex numbers, respectively. \mathbb{R}^N and \mathbb{C}^N denote the spaces of N -dimensional real and complex vectors, respectively; \mathbb{S}^N and \mathbb{H}^N stand for the sets of $N \times N$ complex symmetric matrices and Hermitian matrices, respectively. The symbols $(\cdot)^T$ and $(\cdot)^*$ denote the transpose and conjugate transpose of a vector or matrix. $\text{Re}(\cdot)$, $\text{Im}(\cdot)$, $\text{rank}(\cdot)$ and $\text{Tr}(\cdot)$ denote the real part, imaginary part, rank and trace of a given scalar or matrix. The notations $\|x\|_1$, $\|x\|_2$ and $\|X\|_F$ denote the ℓ_1 -norm and ℓ_2 -norm of vector x respectively, and the Frobenius norm of matrix X . The symbol $\langle X, Y \rangle$ denotes the Frobenius inner product of the matrices X and Y . The symbol $|\cdot|$ is the absolute value operator if the argument is a scalar, vector, or matrix; otherwise, it is the cardinality of a measurable set. The relation $X \succeq 0$ means that the matrix X is Hermitian positive semidefinite. The (i, j) entry of X is denoted by $X_{i,j}$. The notation $X[\mathcal{S}_1, \mathcal{S}_2]$ denotes the submatrix of X whose rows and columns are chosen from the index sets \mathcal{S}_1 and \mathcal{S}_2 , respectively. I_N shows the $N \times N$ identity matrix. The symbol $\text{diag}(x)$ denotes a diagonal matrix whose diagonal entries are given by the vector x , whereas $\text{diag}(X)$ forms a column vector by extracting the diagonal entries of the matrix X . The imaginary unit is denoted by $\mathbf{j} = \sqrt{-1}$. The symbol $\mathbf{1}$ denotes a vector of all ones with appropriate dimension. $\lambda_i(X)$ denotes the i -th smallest eigenvalue of the matrix X . Given a graph \mathcal{G} , the notation $\mathcal{G}(\mathcal{V}, \mathcal{E})$ implies that \mathcal{V} and \mathcal{E} are the vertex set and the edge set of this graph, respectively.

2 Preliminaries

Consider an electric power network represented by a graph $\mathcal{G}(\mathcal{V}, \mathcal{E})$, where $\mathcal{V} := \{1, \dots, n\}$ and $\mathcal{E} := \{1, \dots, r\}$ denote the sets of buses and branches, respectively. Also, suppose that the slack bus is also the reference bus. Let $v_k \in \mathbb{C}$ denote the nodal complex voltage at bus $k \in \mathcal{V}$, whose magnitude and phase are given as $|v_k|$ and $\angle v_k$. The net injected complex power at bus k is denoted as $s_k = p_k + q_k \mathbf{j}$. Define $s_{l,f} = p_{l,f} + q_{l,f} \mathbf{j}$ (resp. $i_{l,f}$) and $s_{l,t} = p_{l,t} + q_{l,t} \mathbf{j}$ (resp. $i_{l,t}$) as the complex power flows (resp. currents) entering the line $l \in \mathcal{E}$ through the ‘from’ and ‘to’ end of the branch. Note that the currents $i_{l,f}$ and $i_{l,t}$ may not add up to zero due to the existence of transformers and shunt capacitors. Let v and i be the vectors of nodal complex voltages and net current injections, respectively. The Ohm’s law dictates that

$$i = Yv, \quad i_f = Y_f v, \quad \text{and} \quad i_t = Y_t v, \quad (1)$$

where $Y = G + B\mathbf{j} \in \mathbb{C}^{n \times n}$ is the admittance matrix of the power network, whose real and imaginary parts are the conductance matrix G and susceptance matrix B , respectively. Furthermore, $Y_f \in \mathbb{C}^{r \times n}$ and $Y_t \in \mathbb{C}^{r \times n}$ represent the ‘from’ and ‘to’ branch admittance

matrices. The injected complex power can thus be expressed as $p + q\mathbf{j} = \text{diag}(vv^*Y^*)$. Let $\{e_1, \dots, e_n\}$ denote the canonical vectors in \mathbb{R}^n . Define

$$\begin{aligned} E_k &:= e_k e_k^T, & Y_{k,p} &:= \frac{1}{2}(Y^* E_k + E_k Y), \\ Y_{k,q} &:= \frac{\mathbf{j}}{2}(E_k Y - Y^* E_k). \end{aligned} \quad (2)$$

Moreover, let $\{d_1, \dots, d_r\}$ be the canonical vectors in \mathbb{R}^r . Define $Y_{l,p_f}, Y_{l,p_t}, Y_{l,q_f}$ and Y_{l,q_t} associated with the l -th branch from node i to node j as

$$\begin{aligned} Y_{l,p_f} &:= \frac{1}{2}(Y_f^* d_l e_i^T + e_i d_l^T Y_f), & Y_{l,p_t} &:= \frac{1}{2}(Y_t^* d_l e_j^T + e_j d_l^T Y_t) \\ Y_{l,q_f} &:= \frac{\mathbf{j}}{2}(e_j d_l^T Y_f - Y_f^* d_l e_i^T), & Y_{l,q_t} &:= \frac{\mathbf{j}}{2}(e_j d_l^T Y_t - Y_t^* d_l e_i^T) \end{aligned} \quad (3)$$

The traditional measurable quantities can be expressed as

$$|v_k|^2 = \text{Tr}(E_k v v^*) \quad (4a)$$

$$p_k = \text{Tr}(Y_{k,p} v v^*), \quad q_k = \text{Tr}(Y_{k,q} v v^*) \quad (4b)$$

$$p_{l,f} = \text{Tr}(Y_{l,p_f} v v^*), \quad p_{l,t} = \text{Tr}(Y_{l,p_t} v v^*) \quad (4c)$$

$$q_{l,f} = \text{Tr}(Y_{l,q_f} v v^*), \quad q_{l,t} = \text{Tr}(Y_{l,q_t} v v^*) \quad (4d)$$

These equations show that the nodal and line measurements can be expressed as simple quadratic functions of the complex voltage vector v . In this paper, we only focus on traditional voltage and power measurements. However, if we have linear PMU measurements (e.g., certain entries of v and i), they can be regarded as quadratic equations with a zero quadratic term and the results of this paper are all valid in this scenario as well. To proceed with the paper, we lay out several definitions. First, we define the *set of measurement matrices* based on (2)–(4):

Definition 2.1. *Given a power system model Ω characterized by the tuple (Y, Y_f, Y_t) and an index set of measurements $\mathcal{M} = \{1, \dots, m\}$ specifying m measurements of the form (4), the mapping from the measurement index set to the set of measurement matrices is defined as*

$$C^\Omega(\mathcal{M}) \triangleq \{M_j(\Omega)\}_{j \in \mathcal{M}} \quad (5)$$

where each $M_j(\Omega)$ corresponds to one of the matrices $E_k, Y_{k,p}, Y_{k,q}, Y_{l,p_f}, Y_{l,p_t}, Y_{l,q_f}, Y_{l,q_t}$ defined in (2) and (3), depending on the type of measurement j .

Second, we define the real-valued state vector and the corresponding real-valued matrices. This enables us to solve optimization problems involving complex voltages in the real-domain. The dimension of the real-valued state vector is $2n - 1$ because the voltage angle at the slack/reference bus is fixed to be zero. Accordingly, the matrices also have $2n - 1$ rows and columns.

Definition 2.2. Given a complex-valued state vector $v \in \mathbb{C}^n$, define $\bar{v} \triangleq [\text{Re}\{v[\mathcal{Q}]^T\} \text{Im}\{v[\mathcal{O}]^T\}]^T \in \mathbb{R}^{2n-1}$ as the real-valued state vector of the power system's operating point with \mathcal{Q} denoting the set of all buses and \mathcal{O} indicating the set of all buses except for the slack bus. Furthermore, define $\bar{X} \in \mathbb{S}^{2n-1}$ as the real-valued symmetrization of $X \in \mathbb{H}^n$. To further clarify this notation, note that a general $n \times n$ Hermitian matrix can be mapped into a $(2n-1) \times (2n-1)$ real-valued symmetric matrix as follows:

$$\bar{X} = \begin{bmatrix} \text{Re}\{X[\mathcal{Q}, \mathcal{Q}]\} & -\text{Im}\{X[\mathcal{Q}, \mathcal{O}]\} \\ \text{Im}\{X[\mathcal{O}, \mathcal{Q}]\} & \text{Re}\{X[\mathcal{O}, \mathcal{O}]\} \end{bmatrix} \quad (6)$$

Finally, we define an operator that maps the state vector to the vector of measurement values, and also its Jacobian:

Definition 2.3. Given a system model Ω and a set of measurements \mathcal{M} , define the function $h^\Omega(\bar{v}) : \mathbb{R}^{2n-1} \rightarrow \mathbb{R}^m$ as the mapping from the real-valued state of the power system to the vector of noiseless measurement values:

$$h^\Omega(\bar{v}) \triangleq [v^T M_1(\Omega)v \ \cdots \ v^T M_m(\Omega)v]^T \quad (7)$$

$$= [\bar{v}^T \bar{M}_1(\Omega)\bar{v} \ \cdots \ \bar{v}^T \bar{M}_m(\Omega)\bar{v}]^T \quad (8)$$

Furthermore, define $J^\Omega(\bar{v}) \in \mathbb{R}^{(2n-1) \times m}$ to be the Jacobian of $h^\Omega(\bar{v})$. In other words,

$$J^\Omega(\bar{v}) = 2[\bar{M}_1(\Omega)\bar{v} \ \bar{M}_2(\Omega)\bar{v} \ \cdots \ \bar{M}_m(\Omega)\bar{v}] \quad (9)$$

3 Main Results

In this section, we first briefly discuss the most widely used nonlinear least-squares (NLS) state estimation formulation and its limitations. Then, we present the *NLAV* formulation and provide a theoretical upper bound on the state estimation error obtained by the NLAV problem. Finally, we uncover certain properties of the vector of residual errors and develop a novel algorithm that jointly performs state estimation and topology error detection.

3.1 Nonlinear least-squares state estimation

NLS is the most common state estimation technique, which was first proposed by Schweppe [8, 9]. Recent studies have shown that local search algorithms, such as Gauss-Newton, are able to find a global solution of this nonconvex problem in the case where the number of measurements is relatively higher than the degree of the freedom of the system and the measurements are noiseless [14, 15]. Similar to other estimators, this method requires that the system's measurement matrices (see Definition 2.1) be known. However, the model that power system operators use may be different from the true system due to the presence of topological errors arising from faults or recent changes in the switching status

of some lines. The measurements at the vicinity of the incorrectly modeled lines are potentially the outliers, which can impact the solution of the state estimation problem over a large portion of the network. This is due to the incapability of the ℓ_2 -norm in dealing with outliers and simulation results supporting this fact are shown in Figure 3 followed by further discussions in Section 4.2. Despite the drawbacks of *NLS*, the work [26] develops an effective tool for topology error detection using Bayesian-based hypothesis testing and the covariance matrix of the states. The method that we propose in this paper does not require the covariance information but takes advantage of the favorable aspects of ℓ_1 -norm minimization.

3.2 Proposed NLAV formulation

A line whose presence in the system is misrepresented by the system operator is called *erroneous* in the remainder of this paper, and the set of all *erroneous* lines is denoted by Ξ . Let $C^{\tilde{\Omega}}(\mathcal{M})$ be the set of measurement matrices corresponding to the model $\tilde{\Omega}$ that the power system operator has access to, and $C^{\Omega}(\mathcal{M})$ be the set of measurement matrices corresponding to the true system Ω . Assume that Ω and $\tilde{\Omega}$ are sparsely different in the sense that there is a small subset of lines in the system for which the operator misunderstands their on/off statuses. In this work, we only focus on sparse errors for two reasons. If Ω and $\tilde{\Omega}$ are relatively different, then the state is not observable from a static set of measurements and dynamic time-stamped data is required. Second, topological errors often occur due to low probability events and it is unlikely that the operator's model be significantly different from the true model. To design an algorithm that jointly performs state estimation and sparse topological error detection, we propose the following optimization problem:

$$\min_{\bar{v} \in \mathbb{R}^{2n-1}} f(\bar{v}) \quad (10)$$

where

$$f(\bar{v}) = \bar{v}^T \bar{M}_0 \bar{v} + \rho \sum_{j=1}^m |\bar{v}^T \bar{M}_j(\tilde{\Omega}) \bar{v} - b_j| \quad (11)$$

and b_j is the j^{th} element of the measurement vector $b \in \mathbb{R}^m$ that is

$$b = h^{\Omega}(\bar{z}) + \eta. \quad (12)$$

Here, $\bar{z} \in \mathbb{R}^{2n-1}$ denotes the true underlying state of the system and η is the noise vector. Notice that the measurement values b are based on the true system Ω and the true system state \bar{z} . Also, $M_0 \in \mathbb{S}^n$ is a regularization matrix and ρ is a regularization coefficient. As will be discussed later, these two parameters assist with the convexification of the problem for finding a robust solution using local search algorithms. From here on, we assume that the measurement set \mathcal{M} is observable. A necessary condition for observability is that the Jacobian of the measurement equations (i.e. $J^{\Omega}(\bar{z})$) be full row rank [40]. Let \bar{v}_* denote

a globally optimal solution of (10), as in

$$\bar{v}_* = \operatorname{argmin}_{\bar{v} \in \mathbb{R}^{2n-1}} f(\bar{v}) \quad (13)$$

Then, let $\epsilon \in \mathbb{R}^{2n-1}$ be the state estimation error vector and $r \in \mathbb{R}^m$ be the residual error vector, defined as

$$\epsilon = \bar{v}_* - \bar{z} \quad (14a)$$

$$r_j = |\bar{v}_*^T \bar{M}_j(\tilde{\Omega}) \bar{v}_* - b_j|, \quad \forall j \in \mathcal{M} \quad (14b)$$

The problem (10) aims to push the insignificant residual errors to hard zeros, while some of the r_j 's associated with the outlier measurements are expected to remain nonzero. This phenomenon is supported empirically via an example in Figure 3(d). The performance of this estimator has a striking contrast with that of the ℓ_2 minimization (Figure 3(c)) where the residuals are spread out throughout all the measurements. In the remainder of this article, we use this intuition to design an efficient topological error detection algorithm. Note that, similar to the NLS state estimation, the objective function of (10) is nonlinear and nonconvex, which makes local search algorithms prone to falling into spurious local solutions. However, recent studies have shown that increasing the number of redundant measurements helps with reducing the non-convexity of NLS problems and hence, improves the likelihood of finding their global solutions using local search algorithms [15, 14]. Therefore, having access to many measurements is the key for real-world state estimation problems. This property is expected to hold for the NLAV estimator too, as partially proven in [17]. The risk of becoming stuck at a local optimum is further avoided by starting the algorithm close to the unknown state. This is possible because in power systems, voltage magnitudes are kept close to 1 and voltage angles are maintained to be small. Therefore, choosing the initial point to be the nominal point $\mathbf{1}$ would likely ensure that it is relatively close to the true state.

3.3 Estimation error

Given a design matrix M_0 , we intend to prove a theoretical upper bound on the state estimation error obtained by the NLAV problem (10). To this end, it is useful to introduce the concept of dual certificate:

Definition 3.1. *Given a positive-semidefinite regularization matrix $M_0 \in \mathbb{S}^n$, a system model Ω , and a set of measurement matrices $C_\Omega(\mathcal{M})$, define $H_\mu^\Omega \triangleq M_0 + \sum_{j=1}^m \mu_j M_j(\Omega)$. A vector $\mu \in \mathbb{R}^m$ is called a dual certificate for the voltage vector $v \in \mathbb{C}^n$ of the system model Ω if it satisfies the following three conditions:*

$$H_\mu^\Omega \succeq 0, \quad H_\mu^\Omega v = 0, \quad \operatorname{rank}\{H_\mu^\Omega\} = n - 1 \quad (15)$$

In essence, the existence of a dual certificate ensures that the second-smallest eigenvalue of H_μ^Ω is strictly positive, which enables us to derive an upper-bound of the form presented in the following theorem.

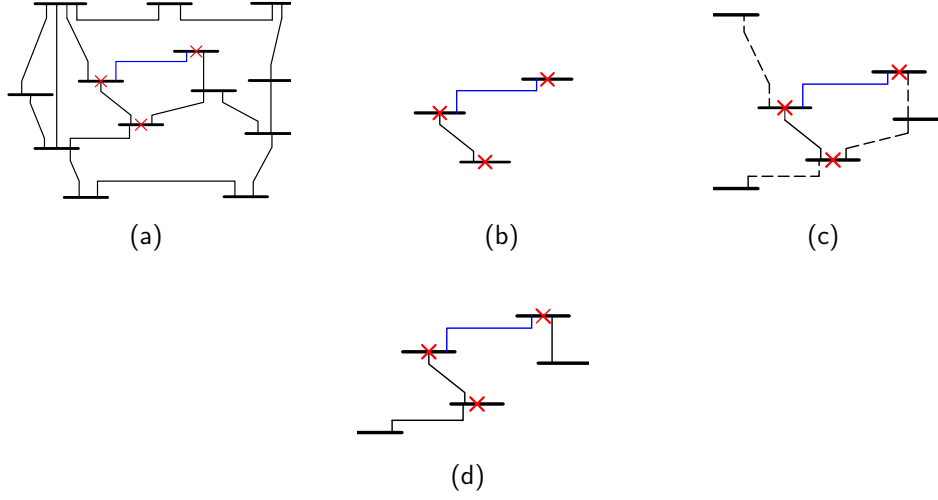


Figure 1: (a) A power network, (b) the state estimation error graph \mathcal{S} , (c) the extended state estimation error graph $\tilde{\mathcal{S}}$, and (d) the line residual graph \mathcal{R}^L . Unsolvable nodes are marked with red crosses, the blue line is the only erroneous line, and the dotted lines correspond to the edges added to \mathcal{S} to obtain $\tilde{\mathcal{S}}$. The graphic of the node residual graph \mathcal{R}^N is omitted.

Theorem 3.1. *Suppose that the power system operator has a network model $\tilde{\Omega}$ and a set \mathcal{M} of measurement indices. For this model, assume that there exists a dual certificate μ for the true state vector z . Also, consider a parameter ρ satisfying the inequality $\rho \geq \max_{j \in \mathcal{M}} |\mu_j|$. Then, there exists a real-valued scalar β such that*

$$\frac{\|\bar{v}_* - \beta \cdot \bar{z}\|_2^2}{\|\bar{v}_*\|_2} \leq \sqrt{\frac{4n \cdot g(\bar{z}, \eta, \rho)}{\lambda_2(H_\mu^{\tilde{\Omega}})}} \quad (16)$$

where $g(\bar{z}, \eta, \rho)$ is equal to

$$\rho \left[\sum_{j \in \mathcal{N}} |\bar{z}^T (\bar{M}_j(\Omega) - \bar{M}_j(\tilde{\Omega})) \bar{z}| + \sum_{j=1}^m |\eta_j| \right] \quad (17)$$

By recalling that \bar{z} and \bar{v}_* are, respectively, the true and recovered states of the system, the above inequality quantitatively bounds the error of the state estimation. There are several important characteristics of this bound.

First, if there is no topology error and the measurements are noiseless, NLAV recovers a high-quality solution if not the actual state. On the other hand, if there are topology error and measurement noise, the upper bound for the state estimation error increases proportionally to the number of topology errors and the magnitude of noise. Furthermore, the upper-bound is a decreasing function of the second smallest eigenvalue of the matrix

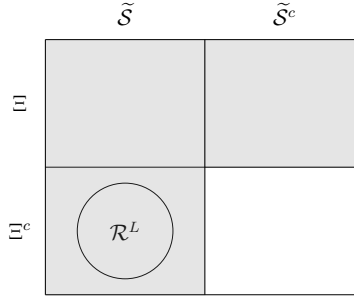


Figure 2: A diagram showing the relationship between different subgraphs. Each rectangle represents the intersection between two different sets. For example, the upper-left rectangle represents $\Xi \cap \tilde{\mathcal{S}}$. \mathcal{R}^L is equivalent to the gray-colored area.

$H_\mu^{\tilde{\Omega}}$, which acts as the Laplacian of a weighted graph obtained from the power network. The second smallest eigenvalue of this matrix, also called the algebraic connectivity [36], is a parameter that measures how well connected a weighted graph is. For example, a complete graph has the algebraic connectivity of n while this value is equal to 2 for a star graph and $2(1 - \cos\frac{\pi}{n})$ for a path graph (where n denotes the number of nodes in the graph). In the special case when M_0 reflects the connectivity of the original network \mathcal{G} (i.e., $i \neq j$ and $(i, j) \notin \mathcal{E} \implies M_0(i, j) = 0$), the second smallest eigenvalue of $H_\mu^{\tilde{\Omega}}$ represents the algebraic connectivity of the original network with different weights assigned to different edges. Finally, note that the bound in equation (16) does not guarantee a unique solution of the NLAV. For conditions that guarantee the uniqueness of solution, the reader is referred to Theorem 3.3.

3.4 Sparse suspect-subgraph

As shown above, the quality of the state estimation deteriorates under the presence of topological errors. Our approach for detecting and correcting these topological errors can be summarized as follows. First, we solve (10) and use the pattern of the nonzero residuals errors to find a (small) subset of lines that are potentially *erroneous* in the model. We call this subset the *suspect-subgraph*, which we then efficiently search through to identify the topological errors. This is followed by a correction of the model and a re-estimation of the system states. To formalize this approach, we first introduce some relevant subgraphs.

Definition 3.2. A node $i \in \mathcal{V}$ is called *unsolvable* if ϵ_i is nonzero. On the other hand, if ϵ_i is zero, node i is called *solvable*. Define the following four induced subgraphs² of \mathcal{G} :

- 1) The state estimation error graph $\mathcal{S}(\mathcal{V}_S, \mathcal{E}_S)$ is such that \mathcal{V}_S is the set of unsolvable nodes.

²Note that, by definition, the edge set of an induced subgraph of $\mathcal{G} = (\mathcal{V}, \mathcal{E})$ consists of all edges in \mathcal{E} that have both endpoints in the node set of the induced graph [37].

- 2) The extended state estimation error graph $\tilde{\mathcal{S}}(\mathcal{V}_{\tilde{\mathcal{S}}}, \mathcal{E}_{\tilde{\mathcal{S}}})$ is such that $\mathcal{V}_{\tilde{\mathcal{S}}}$ includes all nodes in $\mathcal{V}_{\mathcal{S}}$ and also those nodes that are adjacent to any node in $\mathcal{V}_{\mathcal{S}}$.
- 3) The node residual graph $\mathcal{R}^N(\mathcal{V}_N, \mathcal{E}_N)$ is such that \mathcal{V}_N is the set of nodes whose associated entries in r are nonzero.
- 4) The line residual graph $\mathcal{R}^L(\mathcal{V}_L, \mathcal{E}_L)$ is such that \mathcal{V}_L is the set of nodes that are either at the 'from' or 'to' end of a line whose associated entry in r is nonzero.

In order to help the reader visualize the different subgraphs, we illustrate Definition 3.2 for a small system in Figure 9. In Theorem 3.2, we reveal how the set of erroneous lines, namely Ξ , relates to these subgraphs.

Theorem 3.2. *Suppose that the noise vector η is zero. In addition, assume that there do not exist any two distinct vectors of voltages resulting in the same measurement values, i.e.,*

$$\bar{x} \neq \bar{y} \implies \|h^\Omega(\bar{x}) - h^\Omega(\bar{y})\|_1 \neq 0 \quad (18)$$

Then,

$$\mathcal{R}^L \subseteq (\Xi^c \cap \tilde{\mathcal{S}}) \quad (19)$$

Moreover, if no two erroneous lines share the same node, the following statements hold:

$$\mathcal{R}^N = \tilde{\mathcal{S}} \cup \Xi \quad (20)$$

The relationships between different subgraphs are illustrated in Figure 2. It is important to note that due to the sparsity of the state estimation error (as shown in Figure 3(b)) and the sparsity assumption on Ξ , most lines belong to the set $\tilde{\mathcal{S}}^c \cap \Xi^c$. From the diagram, we can also easily infer that $\Xi \subseteq (\mathcal{R}^N \setminus \mathcal{R}^L) \subseteq (\tilde{\mathcal{S}}^c \cap \Xi^c)^c$. Therefore, the practical benefit of Theorem 3.2 is that it enables us to develop a technique for efficiently detecting topological errors by searching over a small subgraph of the original power network. We call this small subgraph, namely $(\mathcal{R}^N \setminus \mathcal{R}^L)$, the *suspect-subgraph*.

3.5 Algorithm

Based on the above results, we propose Algorithm 1 for topological error detection. This algorithm initializes the set of detected erroneous lines, denoted by \mathcal{D}_L , with the empty set. Then, the algorithm searches over all branches in the *suspect-subgraph* $(\mathcal{R}^N \setminus \mathcal{R}^L)$, and evaluates the effect of the presence of each line on the accuracy of the solution. In doing so, the proposed method switches the line off if it is on in the model and vice versa, updates the model based on this change, and re-solves the NLAV problem with the updated model. If the norm of residual errors is decreased, the line is added to \mathcal{D}_L ; otherwise, the change of line status is rejected and the algorithm proceeds to check the next line or terminates if all lines of $(\mathcal{R}^N \setminus \mathcal{R}^L)$ have already been evaluated. Justification for using such an algorithm is provided in the Appendix section 6.4. Algorithm 1 summarizes the proposed topological error detection method.

Algorithm 1 Subgraph search algorithm

Given: Hypothetical model $\tilde{\Omega}$ and measurement vector b

Initialize: Set $\mathcal{D}_L = \emptyset$, $\epsilon > 0$, $\delta > 0$, $\mu > 0$

and calculate $\mathcal{C}_{\tilde{\Omega}}(\mathcal{M})$ using Definition 2.1.

1. Solve NLAV problem (10) with $\tilde{\Omega}$, $\mathcal{C}_{\tilde{\Omega}}(\mathcal{M})$ and b , and calculate the residual r based on equation (14b).

2. Construct the suspect-subgraph $(\mathcal{R}^N \setminus \mathcal{R}^L)$.

3. Set $r^t \leftarrow r$.

while $\|r^t\|_2 > \delta$ **do**

$\Omega^t \leftarrow \tilde{\Omega}$.

for line $l \in (\mathcal{R}^N \setminus \mathcal{R}^L)$ **do**

 Update Ω^t to $\Omega^{t'}$ by changing the on/off status of l .

 Re-solve (10) with $\Omega^{t'}$, $\mathcal{C}_{\Omega^{t'}}(\mathcal{M})$ and b to obtain the outputs \bar{v}_*^{update} and r^{update}

if $\|r^{update}\|_2 < \|r^t\|_2$ **then**

 Add l to \mathcal{D}_L and set $\tilde{\Omega} \leftarrow \Omega^{t'}$, $r^t \leftarrow r^{update}$.

end if

end for

end while

4. Return \bar{v}_*^{update} and \mathcal{D}_L

3.6 Unpenalized NLAV estimator and unique solution

After all the topological errors have been detected and fixed, a final state estimation based on the correct network topology can be performed. However, this does not necessarily guarantee a recovery of the true state \bar{z} . In this subsection, we disregard the regularization term M_0 for simplicity and call this the *unpenalized NLAV* problem (in other words, we set M_0 to 0). Without prior knowledge of the state, designing a favorable M_0 penalty term could be difficult, in which case setting M_0 to zero makes logical sense. Theorem 3.3 provides a sufficient condition under which the *unpenalized NLAV* problem has a unique solution. Since without M_0 , the state estimation error bound provided in Theorem 3.1 is no longer valid, Theorem 3.3 also provides a new bound.

Definition 3.3. Given a system model Ω and a set of measurements \mathcal{M} , define the linear map $\mathcal{A}^\Omega : \mathbb{R}^{n \times n} \rightarrow \mathbb{R}^m$ as

$$\mathcal{A}^\Omega(X) = [\langle M_1(\Omega), X \rangle \cdots \langle M_m(\Omega), X \rangle]^T \quad (21)$$

Theorem 3.3. Given the true network model Ω and the measurement set $\mathcal{M} = \{1, \dots, m\}$, let \mathcal{A}^Ω be the mapping as defined in Definition 3.3. Then, \bar{v}^* obtained from solving the

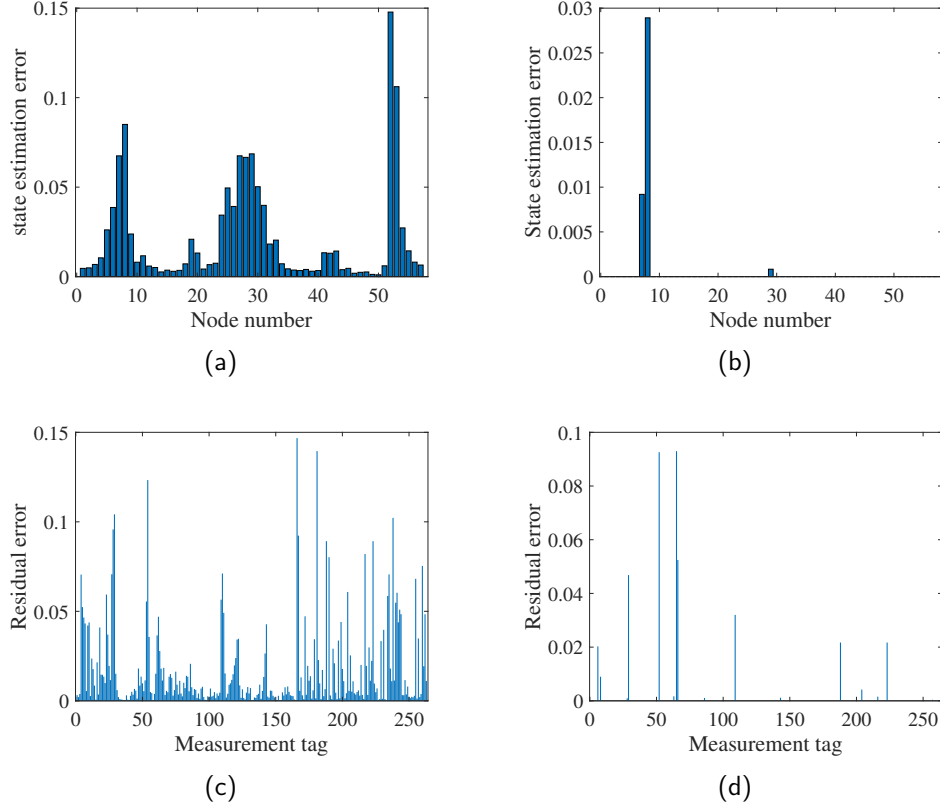


Figure 3: Noiseless state estimation error for (a) NLS, (b) NLAV; and residuals for (c) NLS, (d) NLAV. Note that in (c) and (d), the x -axis shows the measurement tag, which is not the same as the node or line number due to a random selection of line measurements.

NLAV problem (10) with $M_0 = 0$ satisfies:

$$\|\bar{v}_* \bar{v}_*^T - \bar{z} \bar{z}^T\|_F \leq \frac{2}{t} \|\eta\|_1 \quad (22)$$

where t is defined as the optimal objective value of the following optimization problem:

$$\begin{aligned} & \min_{K \in \mathbb{S}^n} \|\mathcal{A}^\Omega(K)\|_2 \\ & \text{s.t. } \text{rank}(K) = 2, \|K\|_F = 1 \end{aligned} \quad (23)$$

It is straightforward to verify that $t > 0$ if and only if there does not exist any set of noiseless measurements for the model Ω that leads to non-unique exact solutions. In other words, if $t > 0$, any global optimal of the NLAV is the true state that we wish to find (note that this applies when all topological errors have been detected and fixed). Therefore, t can be viewed as a quantification of the measurements' quality for finding a unique solution of the over-determined power flow equations. In addition, if $t > 0$, then

condition(18) is implied.

Recently, there has been some study on the connection between the property of *no spurious local minima* and the *restricted isometry property* (RIP). A linear map $\mathcal{A} : \mathbb{R}^{n \times n} \rightarrow \mathbb{R}^m$ is said to satisfy (r, δ_r) -RIP with constant $0 \leq \delta_r < 1$ if there exists $p > 0$ such that for all rank- r matrices X : $(1 - \delta_r)\|X\|_F^2 \leq \frac{1}{p}\|\mathcal{A}(X)\|^2 \leq (1 + \delta_r)\|X\|_F^2$. If \mathcal{A} satisfies $(2r, \delta_{2r})$ -RIP with $\delta_{2r} < 1$, then finding a global optimum constitutes exact recovery of the state [29]. However, this does not exclude the existence of *spurious local minima* (local minima that are not globally optimal), which can be problematic when using local search algorithms. In order to guarantee no spurious local minima, \mathcal{A} suffices to satisfy $(2r, \delta_{2r})$ -RIP with $\delta_{2r} < 0.2$, which is a strict condition [28]. A milder condition on RIP for structured mappings (such as power subsystems) has been developed in [41]. The parameter t introduced above is clearly related to the RIP constant. In fact, $t > 0$ is equivalent to having $\delta_{2r} < 1$, which implies that there is a unique global solution.

4 Simulation Results

In order to evaluate the efficacy of the proposed *NLAV* algorithm for detecting topological errors, this section presents numerical simulations on the IEEE 57-bus system. To run the simulations, we use MATPOWER data along with the MATLAB *fmincon* function as the local search algorithm.

4.1 Simulation setup

In this study we focus on two types of topological errors. **Type I error** is when a transmission line is switched off in the true system while it is switched on in the hypothetical model that is accessible to the power system operator; **Type II error** is when a branch is switched on in the true model while it is switched off in the hypothetical model. Our numerical evaluations consist of multiple cases where we vary the number of erroneous lines and the percentage of line measurements that are available. The procedure of running the simulations is as follows: (1) For a given number of erroneous lines and line measurement percentage, we run 20 simulations; (2) In each simulation the erroneous lines are randomly chosen and checked to ensure that they satisfy the system's observability and that they do not share common buses; (3) The type of topological error is also randomly assigned to each selected erroneous line; (4) In all simulations full nodal measurements (p_k, q_k and $|v_k|$) are considered; (5) The line measurements are randomly selected from the intact lines and no measurements are taken from the erroneous ones; (6) To generate a legitimate state, we assume that the voltage magnitudes are close to unity and the angles are small.

In order to assess the performance of the algorithm, we calculate the true/false positive rates and the suspect rate as:

$$\text{True positive rate} = |\mathcal{D}_L \cap \Xi|/|\Xi| \quad (24a)$$

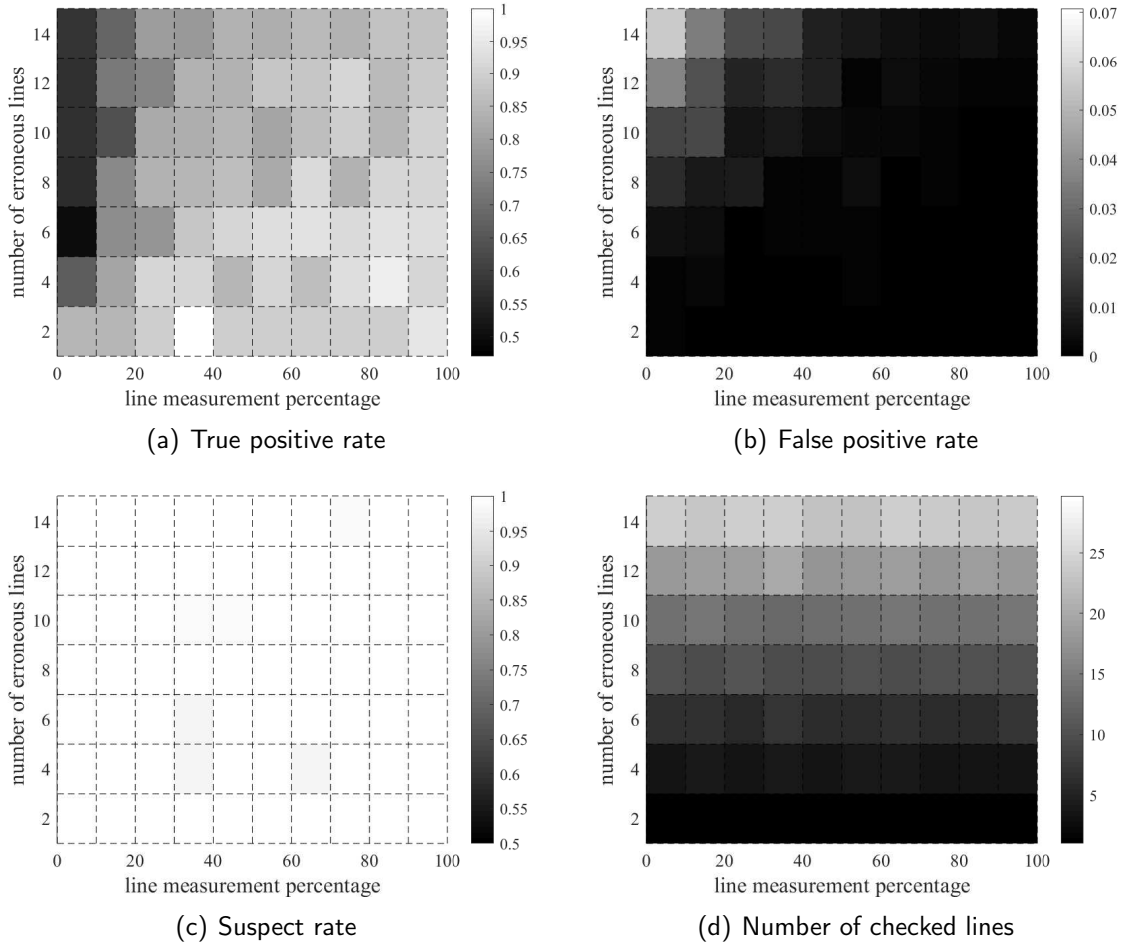


Figure 4: Simulation results on the IEEE 57-bus system. Each value represents the average over 20 simulations.

$$\text{False positive rate} = |\mathcal{D}_L \cap \Xi^c|/|\Xi| \quad (24b)$$

$$\text{Suspect rate} = |(\mathcal{R}_N \setminus \mathcal{R}^L) \cap \Xi|/|\Xi| \quad (24c)$$

Finally, we also report the number of lines that the algorithm checks before termination, which is simply the cardinality of the set $(\mathcal{R}_N \setminus \mathcal{R}^L)$.

4.2 Example: Sparse residuals for NLAV

Before analyzing the bulk of simulations data, we focus on a single example to graphically illustrate the ideas discussed in Section 3. This example is under a scenario with two erroneous lines (lines 8 and 67) and 30% line measurements. Figures 3(a) and 3(c) show the state estimation errors and residuals of *NLS* when topological errors exist. It follows from these plots that there is a lack of sparsity pattern, and the high peaks are not even

associated with the end points of the *erroneous* lines. This implies that one needs to search over all possible combinations of lines to find the erroneous ones, which is numerically intractable for large systems. In contrast, the state estimation errors and the residuals after the first run of the *NLAV* are shown in Figure 3(b) and 3(d). The highest peaks of the residual vector in this plot correspond to the nodes/lines that are directly connected to the erroneous lines. This implies that the erroneous lines can be found by searching over only the lines that are associated with the highest peaks of the residual vector. By doing so, as stated in Algorithm 1, both erroneous lines are correctly detected without any false positive detection. In the following subsection, we present a summary of the extensive simulations conducted on the IEEE 57-bus system.

4.3 57-bus system

For the 57-bus system, we consider $\{1, 3, \dots, 15\}$ as the discretized range for the possible number of erroneous lines and $\{0\%, 10\%, 20\%, \dots, 100\%\}$ as the discretized range for the possible line measurement percentage. Combining these two sets gives the total of 88 scenarios for this system.

Figure 4 shows heat maps of the performance statistics for the above-mentioned 88 scenarios. Figure 4(c) shows that an erroneous line is in the suspect subgraph with high probability. In fact, all of the values are above 0.98, which illustrates that the assumptions made in Theorem 3.2 are reasonable. Figure 4(a) implies that Algorithm 1 is able to detect most of the erroneous lines given a sufficient number of measurements, and Figure 4(b) indicates that there is close to zero false positives. We can also see that detecting topological errors becomes more difficult as the number of such errors grows. However, note that the number of lines that need to be checked grows only linearly with respect to the number of erroneous lines. More specifically, Figure 4(d) shows that the number of lines to be checked is approximately twice the number of erroneous lines. These results imply that the proposed algorithm is capable of accurately detecting topological errors and therefore provides a tool for robust state estimation if the number of measurements is large enough.

5 Conclusion

This paper proposes a new technique to solve the state estimation problem for power systems in the presence of a modest number of topological errors and to detect such modeling errors. The developed method minimizes a nonconvex function of the ℓ_1 -norm of the state estimation residual errors plus a convex quadratic penalty term. It is shown that, under mild conditions, the proposed method can efficiently detect the topological errors by searching over the lines of a (small) suspect-subgraph of the network inferred by the solution of the estimator. Two upper bounds are derived on the estimation errors, and the results are demonstrated on a benchmark system.

6 Appendix

6.1 Proof of Theorem 1

Before going into the proof, we impose the following two conditions for M_0 :

Assumption 1. *The regularizer matrix M_0 satisfies the following properties:*

1. $M_0 \succeq 0$
2. $M_0 \cdot \mathbf{1} = 0$

Also, we define the set of erroneous measurements:

Definition 6.1. *Define $\mathcal{N} \in \mathcal{M}$ as the set of indices of the measurements that correspond to the erroneous lines.*

Consider the NLAV problem (10). One can create lower and upper bounds on the optimal objective value as follows:

$$\begin{aligned}
& \bar{v}_*^T \bar{M}_0 \bar{v}_* + \rho \sum_{j=1}^m |\bar{v}_*^T \bar{M}_j(\tilde{\Omega}) \bar{v}_* - \bar{z}^T \bar{M}_j(\Omega) \bar{z}| - \rho \sum_{j=1}^m |\eta_j| \\
& \stackrel{(a)}{\leq} \bar{v}_*^T \bar{M}_0 \bar{v}_* + \rho \sum_{j=1}^m |\bar{v}_*^T \bar{M}_j(\tilde{\Omega}) \bar{v}_* - \bar{z}^T \bar{M}_j(\Omega) \bar{z} - \eta_j| \\
& \stackrel{(b)}{\leq} \bar{z}^T \bar{M}_0 \bar{z} + \rho \sum_{j=1}^m |\bar{z}^T \bar{M}_j(\tilde{\Omega}) \bar{z} - \bar{z}^T \bar{M}_j(\Omega) \bar{z} - \eta_j| \\
& \stackrel{(c)}{\leq} \bar{z}^T \bar{M}_0 \bar{z} + \rho \sum_{j \in \mathcal{N}} |\bar{z}^T \bar{M}_j(\tilde{\Omega}) \bar{z} - \bar{z}^T \bar{M}_j(\Omega) \bar{z}| + \rho \sum_{j=1}^m |\eta_j|
\end{aligned}$$

where (a) is due to the triangle inequality and (b) is due to the optimality of v_* . The equality (c) follows from $\bar{M}_j(\tilde{\Omega}) = \bar{M}_j(\Omega)$ whenever $j \notin \mathcal{N}$. Combining the above lower and upper bounds leads to

$$\begin{aligned}
& \bar{v}_*^T \bar{M}_0 \bar{v}_* - \bar{z}^T \bar{M}_0 \bar{z} + \rho \sum_{j=1}^m |\bar{v}_*^T \bar{M}_j(\tilde{\Omega}) \bar{v}_* - \bar{z}^T \bar{M}_j(\Omega) \bar{z}| \\
& \leq \rho \sum_{j \in \mathcal{N}} |\bar{z}^T \bar{M}_j(\tilde{\Omega}) \bar{z} - \bar{z}^T \bar{M}_j(\Omega) \bar{z}| + 2\rho \sum_{j=1}^m |\eta_j|
\end{aligned} \tag{25}$$

By adding and subtracting $\bar{z}^T \bar{M}_j(\tilde{\Omega}) \bar{z}$ in the absolute value of the left-hand side, one can

write:

$$\begin{aligned}
& \bar{v}_*^T \bar{M}_0 \bar{v}_* - \bar{z}^T \bar{M}_0 \bar{z} + \rho \sum_{j=1}^m |\bar{v}_*^T \bar{M}_j(\tilde{\Omega}) \bar{v}_* - \bar{z}^T \bar{M}_j(\tilde{\Omega}) \bar{z}| \\
& \leq 2\rho \left\{ \sum_{j \in \mathcal{N}} |\bar{z}^T (\bar{M}_j(\tilde{\Omega}) - \bar{M}_j(\Omega)) \bar{z}| + \sum_{j=1}^m |\eta_j| \right\} = 2g(\bar{z}, \eta, \rho) \tag{26}
\end{aligned}$$

Now, consider the following optimization problem that serves as a tool for deriving a lower bound:

$$\min_y \bar{v}_*^T \bar{M}_0 \bar{v}_* - \bar{z}^T \bar{M}_0 \bar{z} + \rho \sum_{j=1}^m |\bar{v}_*^T \bar{M}_j(\tilde{\Omega}) \bar{v}_* - \bar{z}^T \bar{M}_j(\tilde{\Omega}) \bar{z}|$$

Here y is a fictitious variable with a dimension of choice, and we call the objective of the above problem as f . By introducing a new variable $t \in \mathbb{R}^m$, an equivalent formulation can be written as

$$\begin{aligned}
& \min_t \bar{v}_*^T \bar{M}_0 \bar{v}_* - \bar{z}^T \bar{M}_0 \bar{z} + \rho \sum_{j=1}^m t_j \\
& \text{s.t.} \quad \bar{v}_*^T \bar{M}_j(\tilde{\Omega}) \bar{v}_* - \bar{z}^T \bar{M}_j(\tilde{\Omega}) \bar{z} \leq t_j, \quad \forall j \in \mathcal{M} \\
& \quad \quad -\bar{v}_*^T \bar{M}_j(\tilde{\Omega}) \bar{v}_* + \bar{z}^T \bar{M}_j(\tilde{\Omega}) \bar{z} \leq t_j, \quad \forall j \in \mathcal{M}
\end{aligned} \tag{27}$$

Let p_j^+ 's and p_j^- 's be the nonnegative Lagrange multipliers for the first and second sets of constraints. The Lagrangian can be written as

$$\begin{aligned}
\mathcal{L}(t, p^+, p^-) &= \bar{v}_*^T \bar{M}_0 \bar{v}_* - \bar{z}^T \bar{M}_0 \bar{z} + \sum_{j=1}^m (\rho - p_j^+ - p_j^-) t_j \\
& \quad + \sum_{j=1}^m \{(p_j^+ - p_j^-) (\bar{v}_*^T \bar{M}_j(\tilde{\Omega}) \bar{v}_* - \bar{z}^T \bar{M}_j(\tilde{\Omega}) \bar{z})\}
\end{aligned} \tag{28}$$

By defining $d(p^+, p^-) = \min_t \mathcal{L}(t, p^+, p^-)$ and noting that $p_j^+ + p_j^- = \rho$ for every $j \in \mathcal{M}$ at optimality, we have

$$d(p^+, p^-) = \bar{v}_*^T \left(\bar{M}_0 + \sum_{j=1}^m (p_j^+ - p_j^-) \bar{M}_j(\tilde{\Omega}) \right) \bar{v}_* - \bar{z}^T \left(\bar{M}_0 + \sum_{j=1}^m (p_j^+ - p_j^-) \bar{M}_j(\tilde{\Omega}) \right) \bar{z} \tag{29}$$

Note that $d(p^+, p^-)$ gives a lower bound on f . By assumption, there exists a dual certificate $\mu \in \mathbb{R}^m$. We can find a set of vectors p_*^+ and p_*^- such that they satisfy the previous constraint $p_*^+ + p_*^- = \rho \cdot \mathbf{1}$ and also a new constraint $p_*^+ - p_*^- = \mu$. Then,

$d(p_*^+, p_*^-)$ also gives a lower bound to f . Using the fact that $H_\mu^{\tilde{\Omega}} z = 0$ and defining $X = \bar{v}_* \bar{v}_*^T$, we can establish the following:

$$d(p_*^+, p_*^-) = \bar{v}_*^T H_\mu^{\tilde{\Omega}} \bar{v}_* - \bar{z}^T H_\mu^{\tilde{\Omega}} \bar{z} = \text{Tr}\{H_\mu^{\tilde{\Omega}} \bar{v}_* \bar{v}_*^T\} = \text{Tr}\{H_\mu^{\tilde{\Omega}} X\} \quad (30)$$

The rest of the proof can be adopted from [45] (Appendix, Proof of Theorem 2). Consider an eigen-decomposition of $H_\mu^{\tilde{\Omega}} = U \Lambda U^T$, where $\Lambda = \text{diag}(\lambda_{2n-1}, \dots, \lambda_1)$ such that $\lambda_{2n-1} \geq \dots \geq \lambda_1$ and U is a unitary matrix whose columns are the corresponding eigenvectors. Define

$$\check{X} := \begin{bmatrix} \tilde{X} & \tilde{x} \\ \tilde{x}^T & \alpha \end{bmatrix} = U^T X U \quad (31)$$

where \tilde{X} is the $(2n-2)$ th-order leading principle submatrix of \check{X} , \tilde{x} is the $(2n-2) \times 1$ leftover vector and α is a scalar. It is known that

$$\text{Tr}(H_\mu^{\tilde{\Omega}} X) = \text{Tr}(U \Lambda U^T U \check{X} U^T) = \text{Tr}(\Lambda \check{X}) \geq \lambda_2(H_\mu^{\tilde{\Omega}}) \text{Tr}(\tilde{X}) \quad (32)$$

Combining (32) and (26) leads to

$$\text{Tr}(\tilde{X}) \leq 2 \cdot g(\bar{z}, \eta, \rho) / \lambda_2(H_\mu^{\tilde{\Omega}}) \quad (33)$$

Define $\tilde{z} = \bar{z} / \|\bar{z}\|_2$ and $\tilde{v}_* = \bar{v}_* / \|\bar{v}_*\|_2$. Since $H_\mu^{\tilde{\Omega}}$ is positive-semidefinite and the eigenvector corresponding to the smallest eigenvalue (i.e. zero) is \bar{z} , the matrix X can be decomposed as

$$X = U \check{X} U^T = \begin{bmatrix} \tilde{U} & \tilde{z} \end{bmatrix} \begin{bmatrix} \tilde{X} & \tilde{x} \\ \tilde{x}^T & \alpha \end{bmatrix} \begin{bmatrix} \tilde{U}^T \\ \tilde{z}^T \end{bmatrix} = \tilde{U} \tilde{X} \tilde{U}^T + \tilde{U} \tilde{x} \tilde{z}^T + \tilde{z} \tilde{x}^T \tilde{U}^T + \alpha \tilde{z} \tilde{z}^T \quad (34)$$

Since $\check{X} \succeq 0$, Schur complement dictates the relationship $\tilde{X} - \alpha^{-1} \tilde{x} \tilde{x}^T \succeq 0$. Using the fact that $\alpha = \text{Tr}(X) - \text{Tr}(\tilde{X})$, one can write

$$\|\tilde{x}\|_2^2 \leq \alpha \text{Tr}(\tilde{X}) = \text{Tr}(X) \text{Tr}(\tilde{X}) - \text{Tr}^2(\tilde{X}) \quad (35)$$

Therefore,

$$\begin{aligned} \|X - \alpha \tilde{z} \tilde{z}^T\|_F^2 &= \|\tilde{U} \tilde{X} \tilde{U}^T + \tilde{U} \tilde{x} \tilde{z}^T + \tilde{z} \tilde{x}^T \tilde{U}^T\|_F^2 \stackrel{(d)}{=} \|\tilde{U} \tilde{X} \tilde{U}^T\|_F^2 + 2\|\tilde{z} \tilde{x}^T \tilde{U}^T\|_F^2 \\ &\stackrel{(e)}{=} \|\tilde{X}\|_F^2 + 2\|\tilde{x}\|_2^2 \leq \|\tilde{X}\|_F^2 - 2\text{Tr}^2(\tilde{X}) + 2\text{Tr}(X) \text{Tr}(\tilde{X}) \\ &\stackrel{(f)}{\leq} 2\text{Tr}(X) \text{Tr}(\tilde{X}) \stackrel{(g)}{\leq} \frac{4g(\bar{z}, \eta, \rho)}{\lambda_2(H_\mu^{\tilde{\Omega}})} \text{Tr}(X) \end{aligned} \quad (36)$$

where (d) follows from the fact that $\tilde{U}^T \tilde{z} = 0$, (e) is due to $\tilde{U}^T \tilde{U} = I_{2n-2}$ and (f) comes from the fact that $\|\tilde{X}\|_F \leq \text{Tr}(\tilde{X})$. Finally, (g) results from substituting equation (33).

Plugging back in $X = \bar{v}_* \bar{v}_*^T$ yields that

$$\|X - \alpha \bar{z} \bar{z}^T\|_F^2 = \|\bar{v}_* \bar{v}_*^T - \frac{\alpha}{\|\bar{z}\|_2^2} \bar{z} \bar{z}^T\|_F^2 \leq \frac{4g(\bar{z}, \eta, \rho)}{\lambda_2(H_\mu^\Omega(\bar{M}_0))} \text{Tr}(\bar{v}_* \bar{v}_*^T) \quad (37)$$

By defining $\beta = \alpha / \|\bar{z}\|_2^2$ and realizing that $\text{Tr}(\bar{v}_* \bar{v}_*^T) = \|\bar{v}_*\|_2^2$, the above inequality reduces to

$$\|\bar{v}_* \bar{v}_*^T - \beta \bar{z} \bar{z}^T\|_F^2 \leq \frac{4g(\bar{z}, \eta, \rho)}{\lambda_2(H_\mu^\Omega(\bar{M}_0))} \|\bar{v}_*\|_2^2 \quad (38)$$

By notational simplicity, we denote $x(i)$ as the i -th element of a vector x . Notice that

$$\begin{aligned} \|\bar{v}_* \bar{v}_*^T - \beta \bar{z} \bar{z}^T\|_F &= \sqrt{\sum_{i,j} [\bar{v}_*(i) \bar{v}_*(j) - \beta \cdot \bar{z}(i) \bar{z}(j)]^2} \geq \sqrt{\sum_i [\bar{v}_*(i)^2 - \beta \cdot \bar{z}(i)^2]^2} \\ &\stackrel{(h)}{\geq} \sqrt{\sum_i [\bar{v}_*(i) - \beta \cdot \bar{z}(i)]^4} \stackrel{(i)}{\geq} \frac{1}{\sqrt{n}} \sum_i [\bar{v}_*(i) - \beta \cdot \bar{z}(i)]^2 \\ &= \frac{1}{\sqrt{n}} \|\bar{v}_* - \beta \cdot \bar{z}\|_2^2 \end{aligned} \quad (39)$$

where (h) and (i) are due to Cauchy-Schwarz and Holder's inequality, respectively. Now combining this inequality with (38) leads to

$$\|\bar{v}_* - \beta \cdot \bar{z}\|_2^2 \leq \sqrt{n} \cdot \|\bar{v}_* \bar{v}_*^T - \beta \bar{z} \bar{z}^T\|_F \leq \sqrt{\frac{4g(\bar{z}, \eta, \rho) \cdot n}{\lambda_2(H_\mu^\Omega)}} \|\bar{v}_*\|_2$$

which completes the proof.

6.2 Proof of Theorem 2

Define $N(k)$ to be the set of nodes adjacent to node k , including k itself. We will focus on a line $l \in \mathcal{E}$ that connects two nodes i and j .

(1) First, consider the case when $l \in \tilde{\mathcal{S}}^c \cap \Xi$. The fact that $l \notin \tilde{\mathcal{S}}$ implies that all nodes in the set $N(i) \cup N(j)$ are *solvable*. Also, since $l \in \Xi$, the nodal residual at nodes i and j are nonzero, which means that $i, j \in \mathcal{V}_N$. Finally, noting that $l \notin \mathcal{R}^L$ because there is no line measurement for an erroneous line, we can conclude that $l \in (\mathcal{R}^N \setminus \mathcal{R}^L)$.

(2) Second, consider the case when $l \in \tilde{\mathcal{S}}^c \cap \Xi^c$. Again, the fact that $l \notin \tilde{\mathcal{S}}$ implies that all nodes in the set $N(i) \cup N(j)$ are *solvable*. Also, since $l \in \Xi^c$, the nodal residuals at nodes i and j are zero, and the line residuals on line l is zero. Therefore, we can conclude that $l \notin (\mathcal{R}^N \cup \mathcal{R}^L)$.

(3) Third, consider the case when $l \in \tilde{\mathcal{S}} \cap \Xi^c$. Since $l \in \tilde{\mathcal{S}}$, at least one node in $N(i)$

and at least one node in $N(j)$ are *unsolvable*. From here, two different scenarios can happen. Scenario one is when at least one of nodes i and j is unsolvable. In this case, using the fact that there do not exist two distinct set of voltages that result in the same measurement values, we can easily conclude that $l \in \mathcal{R}^L \cap \mathcal{R}^N$. Scenario two is when both nodes i and j are solvable. In this scenario, the nodal residual at nodes i and j are nonzero but the line residual at l is zero. Therefore, $l \in (\mathcal{R}^N \setminus \mathcal{R}^L)$.

(4) Finally, consider the case when $l \in \tilde{\mathcal{S}} \cap \Xi$. Since $l \in \tilde{\mathcal{S}}$, at least one node in $N(i)$ and at least one node in $N(j)$ are *unsolvable*. Also, since $l \in \Xi$, the nodal residual at nodes i and j are nonzero, which means that $i, j \in \mathcal{V}_N$. Finally, noting that $l \notin \mathcal{R}^L$ because there is no line measurement for an erroneous line, we can conclude that $l \in (\mathcal{R}^N \setminus \mathcal{R}^L)$. From (1)–(4), we can deduce that $l \in \mathcal{R}^L \implies l \in (\Xi^c \cap \tilde{\mathcal{S}})$, which proves the first part of the theorem. Furthermore, we can see that $l \in \tilde{\mathcal{S}} \cup \Xi \implies l \in \mathcal{R}^N$. Finally, from (2) specifically, we also know that if $l \in \tilde{\mathcal{S}}^c \cap \Xi^c \implies l \notin \mathcal{R}^N$. This concludes the fact that $\mathcal{R}^N = \tilde{\mathcal{S}} \cup \Xi$.

6.3 Proof of Theorem 3

Proof. Consider equation (26) and set $\bar{M}_0 = 0$, $\rho = 1$. With some basic algebraic manipulations, one can write

$$2 \sum_{j \in N} |\bar{z}^T (\bar{M}_j(\tilde{\Omega}) - \bar{M}_j(\Omega)) \bar{z}| + 2 \sum_{j=1}^m |\eta_j| \geq \|\mathcal{A}^\Omega(\bar{v}_* \bar{v}_*^T - \bar{z} \bar{z}^T)\|_1 \geq \|\mathcal{A}^\Omega(\bar{v}_* \bar{v}_*^T - \bar{z} \bar{z}^T)\|_2$$

Therefore, if t is nonzero

$$t \cdot \|\bar{v}_* \bar{v}_*^T - \bar{z} \bar{z}^T\|_F \leq 2 \sum_{j \in N} |\bar{z}^T (\bar{M}_j(\tilde{\Omega}) - \bar{M}_j(\Omega)) \bar{z}| + 2 \sum_{j=1}^m |\eta_j| = 2g(\bar{z}, \eta, 1) = 2\|\eta\|_1$$

The last equality follows because all of the topological errors have been detected and fixed. This completes the proof. \square

6.4 Theorem 4 and its proof

Theorem 6.1. Denote $f^1(\cdot)$ as the objective function of an NLAV problem (i.e., equation (11)) with Ξ^1 as the set of erroneous lines and \mathcal{M} as the index set of measurements. Similarly, denote $f^2(\cdot)$ as the objective function of another NLAV problem with Ξ^2 as the set of erroneous lines and \mathcal{M} as the index set of measurements. Without loss of generality, suppose that $|\Xi^1| < |\Xi^2|$. Furthermore, assume that for any two vector of voltages, \bar{x} and \bar{y} , and a measurement index j , the following holds:

$$|\bar{x}^T \bar{M}_j(\tilde{\Omega}) \bar{x} - \bar{y}^T \bar{M}_j(\Omega) \bar{y}| > |\bar{x}^T \bar{M}_j(\Omega) \bar{x} - \bar{y}^T \bar{M}_j(\Omega) \bar{y}| \quad (40)$$

Then, $\min_{\bar{v}} f^1(\bar{v}) < \min_{\bar{v}} f^2(\bar{v})$

Proof. Let \bar{v}_1 and \bar{v}_2 be the global minimizer of $f^1(\cdot)$ and $f^2(\cdot)$, respectively. Also, let \mathcal{M}^1 and \mathcal{M}^2 be the set of measurement indices pertaining to the erroneous lines in Ξ^1 and Ξ^2 , respectively. Then, the following inequalities hold:

$$\begin{aligned}
f^2(\bar{v}_2) &= \bar{v}_2^T \bar{M}_0 \bar{v}_2 + \rho \sum_{j=1}^m |\bar{v}_2^T \bar{M}_j(\tilde{\Omega}) \bar{v}_2 - \bar{z}^T \bar{M}_j(\Omega) \bar{z}| \\
&\stackrel{(a)}{=} \bar{v}_2^T \bar{M}_0 \bar{v}_2 + \rho \sum_{j \in \mathcal{M}^2} |\bar{v}_2^T \bar{M}_j(\tilde{\Omega}) \bar{v}_2 - \bar{z}^T \bar{M}_j(\Omega) \bar{z}| + \rho \sum_{j \in \mathcal{M} \setminus \mathcal{M}^2} |\bar{v}_2^T \bar{M}_j(\Omega) \bar{v}_2 - \bar{z}^T \bar{M}_j(\Omega) \bar{z}| \\
&= \bar{v}_2^T \bar{M}_0 \bar{v}_2 + \rho \sum_{j \in \mathcal{M}^1} |\bar{v}_2^T \bar{M}_j(\tilde{\Omega}) \bar{v}_2 - \bar{z}^T \bar{M}_j(\Omega) \bar{z}| + \rho \sum_{j \in \mathcal{M} \setminus \mathcal{M}^1} |\bar{v}_2^T \bar{M}_j(\Omega) \bar{v}_2 - \bar{z}^T \bar{M}_j(\Omega) \bar{z}| \\
&+ \rho \sum_{j \in \mathcal{M}^2 \setminus \mathcal{M}^1} |\bar{v}_2^T \bar{M}_j(\tilde{\Omega}) \bar{v}_2 - \bar{z}^T \bar{M}_j(\Omega) \bar{z}| - \rho \sum_{j \in \mathcal{M}^2 \setminus \mathcal{M}^1} |\bar{v}_2^T \bar{M}_j(\Omega) \bar{v}_2 - \bar{z}^T \bar{M}_j(\Omega) \bar{z}| \\
&\stackrel{(b)}{\geq} f^1(\bar{v}_1) + \rho \sum_{j \in \mathcal{M}^2 \setminus \mathcal{M}^1} |\bar{v}_2^T \bar{M}_j(\tilde{\Omega}) \bar{v}_2 - \bar{z}^T \bar{M}_j(\Omega) \bar{z}| - \rho \sum_{j \in \mathcal{M}^2 \setminus \mathcal{M}^1} |\bar{v}_2^T \bar{M}_j(\Omega) \bar{v}_2 - \bar{z}^T \bar{M}_j(\Omega) \bar{z}| \\
&\stackrel{(c)}{>} f^1(\bar{v}_1)
\end{aligned}$$

where (a) follows from the fact that $\bar{M}_j(\tilde{\Omega}) = \bar{M}_j(\Omega)$ if $j \notin \mathcal{M}^2$, (b) follows from the fact that \bar{v}_1 is the global minimum of $f^1(\cdot)$ and (c) follows from the assumption made in equation (40). \square

Bibliography

- [1] J. D. Glover, M. S. Sarma, and T. Overbye, *Power System Analysis and Design*, 5th ed. Cengage Learning, 2012.
- [2] I. Dobson, B. A. Carreras, and D. E. Newman, "Probabilistic load-dependent cascading failure with limited component interactions," in *Proceedings of the International Symposium on Circuits and Systems*, 2004.
- [3] K. Clements and P. Davis, "Detection and identification of topology errors in electric power systems," *IEEE Transactions on Power Systems*, vol. 3, 1988.
- [4] Y. Zhang, R. Madani, and J. Lavaei, "Conic relaxations for power system state estimation with line measurements," *IEEE Transactions on Control of Network Systems*, vol. 5, pp. 1193–1205, september 2018.
- [5] D. P. Bertsekas, *Nonlinear Programming*, 3rd ed. Athena Scientific, 2016.

- [6] R. Madani, J. Lavaei, and R. Baldick, "Convexification of power flow equations for power systems in presence of noisy measurements," *IEEE Conference on Decision and Control (CDC)*, pp. 1–8, 2015.
- [7] Y. Zhang, R. Madani, and J. Lavaei, "Conic relaxations for power system state estimation with line measurements," *arXiv preprint arXiv:1704.00133*, pp. 1–14, 2017.
- [8] F. C. Schweppe and J. Wildes, "Power system static-state estimation, Part I: Exact model," *IEEE Transactions on Power Apparatus and Systems*, pp. 120–125, 1970.
- [9] F. C. Schweppe, "Power system static-state estimation, Part III: Implementation," *IEEE Transactions on Power Apparatus and Systems*, pp. 130–135, 1970.
- [10] A. MONTICELLI, "Electric power system state estimation," *Proceedings of the IEEE*, vol. 88, 2000.
- [11] Y. Lin and A. Abur, "Lsmr: An iterative algorithm for sparse least-squares problems," *SIAM Journal on Scientific Computing*, vol. 33, 2011.
- [12] I. DAUBECHIES, R. DEVORE, M. FORNASIER, and C. S. GUNTURK, "Iteratively reweighted least squares minimization for sparse recovery," *Communications on Pure and Applied Mathematics*, vol. 63, 2009.
- [13] R. Chartrand and W. Yin, "Iteratively reweighted algorithms for compressive sensing," in *IEEE International Conference on Acoustics, Speech and Signal Processing, 2008. ICASSP 2008*.
- [14] R. Zhang, J. Lavaei, and R. Baldick, "Spurious critical points in power system state estimation," in *Hawaii International Conference on System Sciences*, 2018.
- [15] R. Zhang, J. Lavaei, and R. Baldick, "Spurious local minima in power system state estimation," to appear in *IEEE transactions on control of network systems (TCNS)*, 2019. Preprint available online at http://lavaei.ieor.berkeley.edu/SE_2018_1.pdf, 2018.
- [16] R. Ge, J. D. Lee, and T. Ma, "Matrix completion has no spurious local minimum," in *Advances in Neural Information Processing Systems (NIPS)*, 2016.
- [17] C. Jozs, R. Zhang, Y. Ouyang, J. Lavaei, and S. Sojoudi, "A theory on the absence of spurious solutions for nonconvex and nonsmooth optimization," *Thirty-second annual conference on Neural Information Processing Systems (NIPS)*, 2018.
- [18] M. Korkali and A. Abur, "Robust fault location using least-absolute-value estimator," *IEEE Transactions on power systems*, vol. 28, pp. 4384–4392, 2013.
- [19] Y. Lin and A. Abur, "Robust state estimation against measurement and network parameter errors," *IEEE Transactions on power systems*, 2018.

- [20] B. Donmez and A. Abur, "Sparse estimation based external system line outage detection," in *Power Systems Computation Conference (PSCC)*, 2016.
- [21] K. A. Clements and A. S. Costa, "Topology error identification using normalized lagrange multipliers," *IEEE Transactions on power systems*, vol. 13, 1998.
- [22] Y. Lin and A. Abur, "A computationally efficient method for identifying network parameter errors," in *Innovative Smart Grid Technologies Conference (ISGT)*. IEEE, 2016.
- [23] Y. Weng, M. D. Ilic, Q. Li, and R. Negi, "Convexification of bad data and topology error detection and identification problems in ac electric power systems," *IET Generation, Transmission & Distribution*, vol. 9, pp. 2760–2767, 2015.
- [24] H. Sehwal and I. Dobson, "Locating line outages in a specific area of a power system with synchrophasors," in *North American Power Symposium (NAPS)*. Champaign, IL, USA: IEEE, 2012.
- [25] E. M. Lourenco, A. J. A. S. Costa, K. A. Clements, and R. A. Cernev, "A topology error identification method directly based on collinearity tests," *IEEE Transactions on power systems*, vol. 21, 2006.
- [26] E. M. Lourenco, A. J. A. S. Costa, and K. A. Clements, "Bayesian-based hypothesis testing for topology error identification in generalized state estimation," *IEEE Transactions on power systems*, vol. 19, 2004.
- [27] D. Singh, J. P. Pandey, and D. S. Chauhan, "Topology identification, bad data processing, and state estimation using fuzzy pattern matching," *IEEE Transactions on power systems*, vol. 20, 2005.
- [28] R. Ge, C. Jin, and Y. Zheng, "No spurious local minima in nonconvex low rank problems: A unified geometric analysis," *International Conference on Machine Learning*, pp. 1233–1242, 2017.
- [29] B. Recht, M. Fazel, and P. Parrilo, "Guaranteed minimum-rank solutions of linear matrix equations via nuclear norm minimizations," *Siam review*, vol. 52, pp. 471–501, 2010.
- [30] W.W.Kotiuga and M.Vidyasagar, "Bad data rejection properties of weighted least absolute value techniques applied to static state estimation," *IEEE Transactions on Power Apparatus and Systems*, vol. 101, pp. 844–853, 1982.
- [31] M. Göl and A. Abur, "Lav based robust state estimation for systems measured by pmus," *IEEE Transactions on Smart Grid*, vol. 5, pp. 1808–1814, 2014.
- [32] P. Rousseeuw and A. Leroy, *Robust regression and outlier detection*. John Wiley and Sons, 1987.

- [33] L. Mili, V. Phaniraj, and P. Rousseeuw, "Least median of squares estimation in power systems," *IEEE PES Summer Meeting*, pp. 493–497, 1990.
- [34] M. Celik and A. Abur, "A robust wlav state estimator using transformations," *IEEE Transactions on Power Systems*, vol. 7, pp. 106–113, 1992.
- [35] L. Mili, M. Cheniae, N. Vichare, and P. Rousseeuw, "Robust state estimation of power systems," *IEEE Transactions on Circuits and Systems*, vol. 41, pp. 349–358, 1994.
- [36] M. Fiedler, "Algebraic connectivity of graphs," *Czechoslovak Math*, pp. 298–305, 1973.
- [37] R. Diestel, *Graph Theory*. Springer, 2006.
- [38] S. Park, R. Mohammadi-Ghazi, and J. Lavaei, "Topology error detection and robust state estimation using nonlinear least absolute value," *2019 American Control Conference*, 2019.
- [39] —, "Topology error detection and robust state estimation using nonlinear least absolute value," *archived and available at http://lavaei.ieor.berkeley.edu/SE_TC_1_2018.pdf*, 2018.
- [40] G.R.Krumpholz, K.A.Clements, and P.W.Davis, "Power system observability: A practical algorithm using network topology," *IEEE Transactions IEEE Transactions on Power Apparatus and Systems*, pp. 1534–1542, 1980.
- [41] I. Molybog, S. Sojoudi, and J. Lavaei, "No spurious solutions in non-convex matrix sensing: structure compensates for isometry," *preprint available at https://lavaei.ieor.berkeley.edu/SRIP_2019_1.pdf*, 2019.

Chapter III

Uniqueness of Power Flow Solutions Using Monotonicity and Network Topology

1 Introduction

The AC power flow equations fundamentally underpin every aspect of power systems: from day-to-day operations in contingency analysis, security-constrained dispatch of electricity markets and yearly capacity planning for peak load, to decades-long transmission expansion and renewable integration. The purpose of AC power flow problem is to solve for the complex voltages, described by their magnitudes and phase angles, given a power system set-point. The power flow equations are nonlinear, and may admit multiple solutions. In the past, the conventional wisdom was to assume that the solution becomes unique by restricting it to “realistic” or “physically realizable” values. However, various examples in the literature show that multiple solutions may persist even after restricting either voltage magnitudes or phase angle differences to “physically realizable” values [6], [7], [5, Section IV]. For the former, we present an example in Section 5 where multiple solutions exist despite having fixed voltage magnitudes for all buses. For the latter, it is possible to construct a two-bus example — one slack bus and one PQ bus — that admits a high-voltage solution within standard operating limits, and another low-voltage solution with a large phase angle difference of 49.9 degrees that is still below the steady-state limit of 90 degrees [1]. Therefore, in principle, system operators may encounter operating points that are very different from what they had expected. In order to avoid these situations, it is important to understand whether or not there is a unique “physically realizable” power flow solution for real-world power systems. The goal of this paper is to develop sufficient conditions on top of the “realism” that will guarantee a unique solution to the AC power flow equations.

1.1 Monotonicity between phase angles and power flow

Mathematical tools that are often used to prove uniqueness results include the fixed point theorem with contraction mapping and the inverse function theorem. In this paper, we use the notion of monotonicity to prove uniqueness of the power flow solution under certain conditions. The results that we present stem from a simple idea that is best explained via an example. Consider a two-bus, lossless one-line system, with the line reactance X .

Voltage magnitude and angle are specified at one of the buses ("slack bus"), whereas real power injection and voltage magnitude are specified at the other bus ("PV bus"). Then, the power transfer between the two buses is given with respect to the two voltage magnitudes $|v_1|, |v_2|$ and the angular difference $\theta_1 - \theta_2$ as a sinusoid:

$$P = |v_1| \cdot |v_2| \cdot \sin(\theta_1 - \theta_2) / X.$$

Even in this simple toy example, we can see that the power flow solutions are not unique: every value of P satisfying $|P| < |v_1| \cdot |v_2| / X$ can be attained by two choices of $\theta_1 - \theta_2$. However, if we restrict $\theta_1 - \theta_2$ to take on what we will call *physically realizable* values within the steady-state stability limit of $|\theta_1 - \theta_2| < \pi/2$, then the solution becomes unique. Indeed, this follows from the fact that P is *monotonically increasing* with respect to $\theta_1 - \theta_2$ within this range. Formally, if we define $f(x) = (|v_1| \cdot |v_2| / X) \sin x$ as the power flow function and $\Omega = [-\pi/2, +\pi/2]$ as the range of acceptable values for x , then the strictly increasing property of f guarantees the following inequality:

$$(f(x) - f(y))(x - y) > 0 \quad \forall x \neq y, \quad x, y \in \Omega.$$

The inequality forces the nonlinear equation $f(x) = P$ to have no more than one solution $x \in \Omega$, because a different $y \in \Omega$ satisfying $f(y) = P$ would contradict the inequality. Hence, the phase angles θ_1 and θ_2 can be uniquely determined (up to an absolute phase shift) given a value of P within the realizable range $|P| < |v_1| \cdot |v_2| / X$. This paper extends this idea to an arbitrary power network using a multi-dimensional generalization of the monotonicity property.

1.2 Main results

The major contribution of this paper is the identification of sufficient conditions under which the power flow equations have a unique "realistic" solution. For the remainder of the paper, we focus on the relationship between voltage angle differences and real power injections, referred to as the $P - \Theta$ problem in the literature [3]. Analogous to the two-bus case, a set of phase angles are *physically realizable* for a lossless system if the angular difference across every line lies within the stability limit of $\pi/2$. Under the constraint that phase angles are *physically realizable* and smaller than a certain limit that depends on the network topology, we extend the notion of monotonicity that was illustrated for the earlier two-bus example to high-dimensional networks. The contributions of this paper are summarized below:

- We show that all acyclic networks have at most one $P - \Theta$ power flow solution under certain conditions on voltage angles. Furthermore, the set of feasible real power injections (for non-slack buses) on these graphs is a convex set.
- We show that cyclic networks cannot have multiple distinct $P - \Theta$ power flow solutions under certain conditions on voltage angles. These conditions can be checked

offline and provide a certificate for ruling out multiple solutions. The certificate is easier to satisfy for graphs with smaller *maximal girth*.

- We show that the uniqueness of $P-\Theta$ power flow solutions is preserved under series-parallel reduction. A natural corollary to this is that power systems with *Generalized Series-Parallel graphs* have at most one $P-\Theta$ power flow solution under some angle conditions. Loosely speaking, these are graphs that can be constructed entirely out of series and parallel terminal connections in circuit theory, plus dangling vertices. Any tree or cycle graph is a Generalized Series-Parallel graph.

The implication of these results for classical power flow analysis is that, under the conditions specified above, the problem has a unique physically realizable solution if the phasor voltage magnitudes are fixed. This occurs, for example, if all buses except the slack bus are modeled as PV buses. In practice, tightly controlled voltage magnitudes are enforced by operating limits, and are usually achieved through the availability of dispersed and controllable reactive sources. The assumption is commonly used in the power industry and is implicit in the DC power flow equations.

1.3 Related work

The paper [22] is one of the first to study the solution set of the power flow equations, which contrary to the conjecture at that time constructed an example showing the general non-uniqueness of decoupled power flow solutions. A more thorough study was later presented in the paper [10], which derived the estimate number of solutions and characterized the stability region for the power flow problem. However, the results are limited to lossless transmission networks consisting of only PV buses. Soon after, [8] formulated the coupled power flow equations in rectangular coordinates and described a set of linear necessary conditions for the solution of the power flow problem, which helped systematically investigate the problem feasibility. Subsequently, researchers have tried to explicitly characterize conditions under which the power flow solution exists and is unique. For example, the work [9] derived conditions under which the reactive power-voltage problem has a unique solution under decoupling assumptions. Then, [3] extended these results by deriving conditions for the real power-phase angle problem under the same decoupling assumptions. Note that in this paper, we consider the real power-phase angle problem as in [3], but discard the decoupling assumptions because it fails to accurately capture the true physics when transmission lines are not purely inductive. Furthermore, we consider a general lossy network.

Researchers have also observed that information about the topology of the power system network can be utilized to derive stronger results. Without making decoupling assumptions, the paper [6] investigated the number of power flow solutions in a radial network and showed that, for practical system parameters, the solution always exists and is unique. The results were extended to unbalanced three-phase distribution networks in [11]. Adding to these results, the work in [31] shows that several algorithms, using

the fixed-point, convex relaxation and the energy function approaches, converge to the unique high-voltage solution for radial networks. In the more recent study [13], the authors studied the power flow problem and its relationship to optimization in tree networks by mainly analyzing the injection region of the power network. While these results are limited to tree graphs, our current work characterizes a wider class of topologies under which the power flow solution is unique. Finally, the work in [2] used the network topology to upper bound the number of power flow solutions.

The most widely used tool to prove existence and uniqueness of power flow solutions is the fixed point technique. The work [23] was the first to apply the fixed point technique developed for nonlinear circuits to power flow. In [4] and [12], a fixed point formulation of the power flow problem was used to specify a domain around a feasible point and derive sufficient conditions for a unique solution. In the recent works [24] and [25], the authors developed a new fixed point formulation of the lossless power flow equations that includes both PQ and PV buses, and for radial networks derived network parametric conditions that guarantee the existence and uniqueness of a high-voltage solution. Extensions of the conditions to multi-phase distribution systems appear in [35] and new sufficient conditions using a fixed point technique on the complex domain appear in [34].

Moving away from fixed point techniques, the work [14] developed a semidefinite programming based procedure to characterize the domain of voltages over which the power flow operator is monotone. In a similar but different spirit, this paper utilizes monotonicity to rule out multiple solutions. Furthermore, we take advantage of the network topology information to derive less conservative sufficient conditions. The recent work [32] presents a unifying framework for network problems on the n -torus while introducing the concept of *winding cell* that is used to partition solutions. The framework can be applied to the AC power flow problem under the lossless setting and their monotonicity assumptions share close resemblance to our approach. In this work, we provide a more general result on arbitrary networks with losses.

The remainder of this paper is organized as follows. Section 2 lays out the basic notations used in this paper. In Section 2.1, we define the $P - \Theta$ power flow problem formulation. Section 4 establishes the condition under which strict monotonicity holds over a single line and presents favorable properties that arise from the monotonicity. The properties are used to prove that there is at most one power flow solution for acyclic networks. Section 5 extends this result to general cyclic networks. We present additional (voltage) angular conditions under which cyclic graphs cannot have multiple distinct power flow solutions. This condition is closely related to the *maximal girth* of the underlying graph. Section 6 shows that series-parallel reduction on a graph preserves the uniqueness of power flow solutions, and arrive at the conclusion that *Generalized Series-Parallel* networks have at most one solution under additional angle constraints. Section 7 develops a linear-time algorithm for a subset of *Generalized Series-Parallel* graphs. Finally, Section 8 provides numerical and simulation results that support the ideas developed in the paper. All the proofs will be delineated in the Appendix.

2 Notations

We start with some mathematical notations. For a given vector x , let x_k denote its k -th element. When notation is overloaded, $x(k)$ will sometimes take on the role of x_k . The symbol \mathbf{j} denotes the unit imaginary number. The notations $(\cdot)^T$ and $(\cdot)^H$ denote the transpose and Hermitian transpose of a matrix, respectively. For a complex number z , $|z|$ denotes its magnitude and for a set X , the symbol $|X|$ denotes its cardinality. $\Re(\cdot)$ denotes the real part of a given argument.

Power system topology is specified by an undirected graph $\mathbb{G} = (\mathbb{V}, \mathbb{E})$ and we assume that this graph is simple and connected. For an undirected graph $\mathbb{G} = (\mathbb{V}, \mathbb{E})$, \mathbb{V} is the set of vertices (buses) and $\mathbb{E} \subseteq \mathbb{V} \times \mathbb{V}$ is the set of undirected edges (lines). If the edges of an undirected graph are weighted with the weights captured by a set \mathbb{W} , then the graph is represented as $\mathbb{G} = (\mathbb{V}, \mathbb{E}, \mathbb{W})$. For a directed graph (digraph) $\mathbb{D} = (\mathbb{V}, \tilde{\mathbb{E}}, \mathbb{W})$, $\tilde{\mathbb{E}} \subseteq \mathbb{V} \times \mathbb{V}$ denotes the set of directed edges. The undirected edge e connecting two vertices k and ℓ is denoted by a set notation $e = \{k, \ell\}$, whereas $a = (k, \ell)$ denotes a directed edge a coming out of vertex k and going into ℓ . Depending on the context, an edge can be denoted by either e or $\{k, \ell\}$. The same goes for directed edges. The series element of the equivalent Π -model of each line $\{k, \ell\}$ is modeled by admittance $G_{k\ell} - \mathbf{j}B_{k\ell}$, where $G_{k\ell}, B_{k\ell} \geq 0$. Let d denote the vector of degrees, where its k -th element $d(k)$ stands for the degree of vertex $k \in \mathbb{V}$. Similarly, limited to directed graphs, let d^+ and d^- denote the vectors of out-degrees and in-degrees, respectively. Moreover, let $\mathbb{G}[\mathbb{V}']$ and $\mathbb{E}[\mathbb{V}']$ denote the subgraph and edge-subset of \mathbb{G} that are induced by a given vertex set $\mathbb{V}' \subseteq \mathbb{V}$, respectively. The symbol $\mathbf{1}$ is the vector of ones. Finally, K_n denotes the complete graph on n vertices.

3 P-Theta problem formulation

As mentioned in the introduction, we focus our attention to the relationship between the voltage phasor angles and the real power injections. To this end, we will study the mapping from angles to real powers. Let the slack bus (also the reference bus) be indexed by 1, unless defined otherwise. Let $v \in \mathbb{C}^n$ be the vector of complex bus voltages. The complex voltage at bus k can be expressed in polar form, $v_k = |v_k|e^{\mathbf{j}\theta_k}$, where $|v_k|$ and θ_k denote the voltage magnitude and phase angle at bus k , respectively. For convenience, we also define $\theta_{k\ell} = \theta_k - \theta_\ell$ to be the angle difference across line $\{k, \ell\}$.

The $P - \Theta$ power flow problem assumes that all buses except the slack bus are PV buses. This means that the voltage magnitudes $V = (|v_1|, \dots, |v_n|)^T$ are fixed at all buses, and the net real power injections are fixed at all buses except the slack bus. We denote the specified real power injection vector as $P = (p_2, \dots, p_n)^T$. The unknown variable is $\Theta = (\theta_2, \dots, \theta_n)^T$ because bus 1 is the reference bus and θ_1 is fixed at zero. Although the voltage magnitudes are considered fixed at all buses, we make no assumption about their particular values. For example, the magnitude could be low as in the two-bus example mentioned in Section 1. Finally, assuming that the shunt elements of the model

have zero real part, we can neglect the admittance of the shunt elements without loss of generality. That is, we assume that the shunt elements are purely reactive.

Let $i \in \mathbb{C}^n$ be the vector of complex currents, where i_k is the total current flowing out of bus k into the rest of the network. Given a complex admittance matrix $Y \in \mathbb{C}^{n \times n}$, the equation $i = Yv$ holds due to Ohm's law and Kirchoff's Current Law. Furthermore, the complex power injected at bus k is equal to $s_k = p_k + \mathbf{j}q_k = v_k i_k^H$ where p_k and q_k denote the net real and reactive power injections at bus k , respectively. Therefore, we can write the equation for the real power injections as: $p_k = \Re\{(Yv)_k^H v_k\}$. Since voltage magnitudes are known parameters, the injection vector P is only a function of Θ and we can define the following injection operator that describes the $P - \Theta$ problem.

Definition 3.1. Define $\hat{P}_k : \mathbb{R}^{n-1} \rightarrow \mathbb{R}$ as the map from the vector of phasor angles to the real power injection at bus k :

$$\hat{P}_k(\Theta) = \Re\{(Yv)_k^H v_k\}. \quad (41)$$

Moreover, define the injection operator $\hat{P} : \mathbb{R}^{n-1} \rightarrow \mathbb{R}^{n-1}$ as

$$\hat{P}(\Theta) = [\hat{P}_2(\Theta), \dots, \hat{P}_n(\Theta)]. \quad (42)$$

The goal of the $P - \Theta$ problem is, given $P \in \mathbb{R}^{n-1}$, to find $\Theta \in \mathbb{R}^{n-1}$ such that $\hat{P}(\Theta) = P$.

4 Acyclic Networks

In this section, we derive conditions under which the $P - \Theta$ problem has at most one solution for a power system represented by an acyclic graph. In particular, a straightforward generalization of the elementary angle assumption that is necessary for a single line network to have at most one solution is sufficient for any acyclic network to have at most one solution.

4.1 Single line properties

We begin the analysis with a single line. Consider any line $\{k, \ell\} \in \mathbb{E}$ and the real power flow from bus k to bus ℓ , denoted by $p_{k\ell}$. Elementary calculations show that:

$$p_{k\ell} = G_{k\ell}(|v_k|^2 - |v_k| \cdot |v_\ell| \cos \theta_{k\ell}) + B_{k\ell} |v_k| \cdot |v_\ell| \sin \theta_{k\ell} \quad (43)$$

Therefore, given the line properties and the voltage magnitude at both ends, the flow $p_{k\ell}$ depends only on the voltage angle difference $\theta_{k\ell}$. Hereby, we define the function $\hat{p}_{k\ell}(\cdot)$

for every $\{k, \ell\} \in \mathbb{E}$ such that $p_{k\ell} = \hat{p}_{k\ell}(\theta_{k\ell})$. Taking the derivative

$$\frac{\partial \hat{p}_{k\ell}}{\partial \theta_{k\ell}}(\theta_{k\ell}) = G_{k\ell}|v_k| \cdot |v_\ell| \cdot \sin \theta_{k\ell} + B_{k\ell}|v_k| \cdot |v_\ell| \cdot \cos \theta_{k\ell}$$

concludes that $p_{k\ell}$ is monotonically increasing in $\theta_{k\ell}$ if:

$$G_{k\ell}|v_k| \cdot |v_\ell| \cdot \sin \theta_{k\ell} + B_{k\ell}|v_k| \cdot |v_\ell| \cdot \cos \theta_{k\ell} \geq 0.$$

A strict inequality of the above equation is obtained if:

$$-\tan^{-1}(B_{k\ell}/G_{k\ell}) < \theta_{k\ell} < \pi - \tan^{-1}(B_{k\ell}/G_{k\ell}).$$

Similarly, $p_{\ell k}$ is strictly monotonically decreasing in $\theta_{k\ell}$ if:

$$\tan^{-1}(B_{k\ell}/G_{k\ell}) - \pi < \theta_{k\ell} < \tan^{-1}(B_{k\ell}/G_{k\ell}).$$

Combining these observations, both $p_{k\ell}$ and $p_{\ell k}$ are strictly monotonic functions of $\theta_{k\ell}$ as long as:

$$|\theta_{k\ell}| < \tan^{-1}(B_{k\ell}/G_{k\ell}), \quad (44)$$

which corresponds to the region of steady-state stability of the line $\{k, \ell\}$ considered individually. We refer to $\tan^{-1}(B_{k\ell}/G_{k\ell})$ as the steady-state stability limit for line $e = \{k, \ell\} \in \mathbb{E}$ and will restrict attention to angles that satisfy (44) for each line $\{k, \ell\}$ in the system. In what follows, we will give the definitions on the *set of allowable angles* and *set of allowable injections*.

Definition 4.1. For a power system $\mathbb{G} = (\mathbb{V}, \mathbb{E})$, let $\mathbb{G} = (\mathbb{V}, \mathbb{E}, \mathbb{W})$ indicate a weighted version of the power system network. For each line $e = \{k, \ell\} \in \mathbb{E}$, there is a corresponding angle limit (weight) $w_{k\ell} \in \mathbb{W}$ such that $w_{k\ell} < \tan^{-1}(B_{k\ell}/G_{k\ell})$. Note that $w_{k\ell}$ can be written in an equivalent notation, w_e . The set \mathbb{W} is called the ‘set of allowable limits.’ The ‘set of allowable angles’ for a power system $\mathbb{G} = (\mathbb{V}, \mathbb{E}, \mathbb{W})$ is defined as:

$$\Theta(\mathbb{G}) = \{\Theta \in \mathbb{R}^{n-1} : \theta_1 = 0 \text{ and } |\theta_{k\ell}| < w_{k\ell} \forall \{k, \ell\} \in \mathbb{E}\}.$$

Furthermore, for a given $\Theta \in \Theta(\mathbb{G})$, define $\mathcal{P}(\mathbb{G}, \Theta) \in \mathbb{R}^{n-1}$ to be the vector of net injections (at all buses except for the slack bus) realized by Θ . We define $\mathcal{P}(\mathbb{G}, \Theta(\mathbb{G})) \subseteq \mathbb{R}^{n-1}$ to be the set of all possible net injections for allowable angles and refer to it as the “set of allowable injections.”

We acknowledge that there is no one-to-one correspondence between the notion of stability of a line considered individually in isolation and the *steady-state and transient stability* of an actual power system, particularly where there are additional control feedback loops such as “power system stabilizers.” However, limiting angles to satisfy (44) results in some convenient properties of power flow solutions. These properties are explained in the following lemma:

Lemma 4.1. Define $\underline{p}_{k\ell} = \hat{p}_{k\ell}(-\omega_{k\ell})$ and $\bar{p}_{k\ell} = \hat{p}_{k\ell}(\omega_{k\ell})$. Then for each $p_{k\ell} \in (\underline{p}_{k\ell}, \bar{p}_{k\ell})$ there exists a unique $\theta_{k\ell}$ with $|\theta_{k\ell}| < \omega_{k\ell}$ such that $p_{k\ell} = \hat{p}_{k\ell}(\theta_{k\ell})$. In fact, there is an explicit expression for the solution $\theta_{k\ell}$:

$$\theta_{k\ell} = \hat{\theta}_{k\ell}(p_{k\ell}) = \sin^{-1} \left(\frac{p_{k\ell} - G_{k\ell}|v_k|^2}{|v_k| \cdot |v_\ell| Z_{k\ell}} \right) - \gamma_{k\ell} \quad (45)$$

where $Z_{k\ell} = \sqrt{G_{k\ell}^2 + B_{k\ell}^2}$ and $\gamma_{k\ell} = \tan^{-1}(-G_{k\ell}/B_{k\ell})$. Furthermore, if we define $\hat{r}_{k\ell}(\cdot) = \hat{p}_{k\ell}(-\hat{\theta}_{k\ell}(\cdot))$, then

$$p_{\ell k} = \hat{r}_{k\ell}(p_{k\ell}) \quad (46)$$

where $\hat{r}_{k\ell}$ is a strictly decreasing function.

Previously, we established that $\hat{p}_{k\ell}(\cdot)$ is a strictly increasing function of $\theta_{k\ell}$ over the range $|\theta_{k\ell}| < \omega_{k\ell}$. By using the Browder–Minty theorem in its proof, Lemma 4.1 states that the inverse of the function $\hat{p}_{k\ell}(\cdot)$ is well-defined. In fact, the inverse function $\hat{\theta}_{k\ell}(\cdot)$ is also an increasing function, of $p_{k\ell}$ over $(\underline{p}_{k\ell}, \bar{p}_{k\ell})$. Moreover, given $p_{k\ell} \in (\underline{p}_{k\ell}, \bar{p}_{k\ell})$, there is a uniquely determined corresponding value for the flow $p_{\ell k}$ coming from the opposite direction. This enables us to express $p_{\ell k}$ as a well-defined function of $p_{k\ell}$ as in (46).

4.2 Tree networks

In this subsection, we build on the results for a single line to prove uniqueness of the $P - \Theta$ power flow problem for tree networks. We also show that the *set of allowable injections* is a convex set. Although a tree network is not realistic for transmission systems, this will provide important results that will be used for the general case of a mesh. Some of the results that we mention here are already well known in the existing literature. However, we organize the proof of this existing result around the monotonicity property, with the goal of generalizing the arguments to mesh networks.

We will write $\mathbb{T} \subseteq \mathbb{V} \times \mathbb{V}$ for a collection of lines that form a tree and consider power systems with graphs $\mathbb{G} = (\mathbb{V}, \mathbb{T}, \mathbb{W})$. Recall that the reference/slack bus is indexed by 1. A key observation about tree topology is that for any bus $k \in \mathbb{V}$ there is a unique path $E_k \subseteq \mathbb{T}$ of successive lines between bus k and bus 1, which we consider to be the root of the tree. Define the “distance” $c(k)$ between bus k and bus 1 to be the number of lines in the unique path E_k between bus k and bus 1 in \mathbb{T} . We define $E_1 = \emptyset$ and $c(1) = 0$. Generically, results for such networks could be proved by beginning with leaves and proceeding towards bus 1 by using an induction argument on the decreasing distance to bus 1. By following such approach, the next theorem can be obtained.

Theorem 4.2. Suppose that the power system $\mathbb{G} = (\mathbb{V}, \mathbb{T}, \mathbb{W})$ has a tree topology. Then,

1. For each $P \in \mathcal{P}(\mathbb{G}, \Theta(\mathbb{G}))$, there is a unique $\Theta \in \Theta(\mathbb{G})$ such that $P = \hat{P}(\Theta)$.
2. $\mathcal{P}(\mathbb{G}, \Theta(\mathbb{G}))$ is a convex set.

Note that by Part 1 of Theorem 4.2, for a given power system \mathbb{G} with a tree topology, there is a well-defined function $\hat{\Theta}$ such that for each $P \in \mathcal{P}(\mathbb{G}, \Theta(\mathbb{G}))$, the unique value $\Theta \in \Theta(\mathbb{G})$ with the property $P = \hat{P}(\Theta)$ satisfies $\Theta = \hat{\Theta}(P)$. That is, $\hat{\Theta}(\bullet)$ is the inverse of $\hat{P}(\Theta)$.

5 Cyclic Networks

For networks with cycles, restricting the voltage angles to the *set of allowable angles* is not enough to guarantee that the $P - \Theta$ problem has at most one solution. Hence, we begin this section by analyzing a simple example on a cycle to illustrate the need for additional conditions on voltage angles in guaranteeing a unique solution.

In Fig. 5, we have a six-bus lossless network where all the real power injections are set to be zero. Under this setting, we can see that there are at least two solutions: one with zero flow in all lines and another one with a nonzero flow around the cycle, corresponding to a $\pi/3$ angle difference across each line. This example is similar to the one in [22] and is essentially due to the fact that the sum of angle differences from bus 1 to bus 6 (i.e. $\theta_{12} + \theta_{23} + \theta_{34} + \theta_{45} + \theta_{56}$) is less than $-\pi$ and therefore becomes equivalent to $\pi/3 \pmod{2\pi}$, allowing a positive amount of power to flow from bus 1 to bus 6 and then back to bus 1. In this example, if the absolute value of $\theta_{12} + \theta_{23} + \theta_{34} + \theta_{45} + \theta_{56}$ were to be restricted below π , there would be no possibility of multiple solutions. We state this formally in the following lemma.

Lemma 5.1. *Consider a power network $\mathbb{G} = (\mathbb{V}, \mathbb{E}, \mathbb{W})$ with $\mathbb{V} = \{1, \dots, N\}$ and $\mathbb{E} = \{\{1, 2\}, \dots, \{N-1, N\}, \{N, 1\}\}$. For every $P \in \mathcal{P}(\mathbb{G}, \Theta(\mathbb{G}))$ there is a unique solution $\Theta \in \Theta(\mathbb{G})$ such that $P = \hat{P}(\Theta)$ if:*

$$\omega_{12} + \omega_{23} + \dots + \omega_{N-1, N} < \pi/2. \quad (47)$$

Lemma 5.1 applies to only a single cycle network. However, this will be extended to any arbitrary network below. The main idea behind the development of this result is to associate a digraph to every possible distinct solution based on its deviation from a baseline solution. We call two solutions distinct if every two corresponding elements of these solutions are different. If an angle constraint similar to equation (47) is met for every such digraph (named the residual-digraph), then there cannot be multiple distinct power flow solutions (i.e., distinctly unique). In this section, we prove results on distinct uniqueness, but the same methodology can also be readily used to prove results on uniqueness (in the common sense) by substituting the digraph with a hybrid graph that contains both directed and undirected edges. In addition, if there are two non-distinct solutions, then one can delete the edges with the same flows in the two solutions and then compensate for the nodal injections at the endpoints of all such removed edges in order to arrive at a subgraph that has two distinct solutions. In other words, having only unique distinct solutions for the subgraphs of the network implies the uniqueness of the solution for the original network. As a result, we only focus on studying distinct solutions in this section.

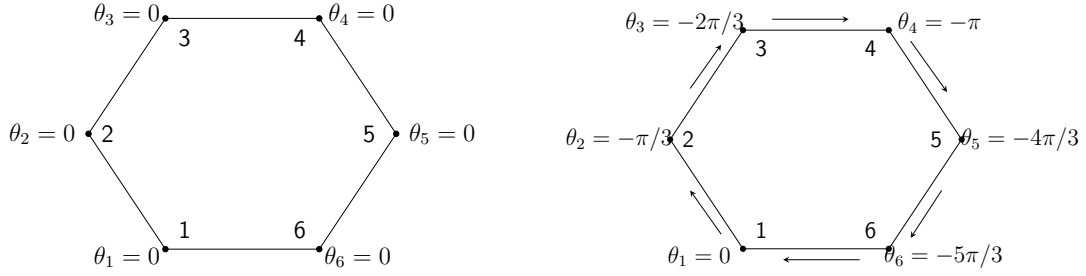


Figure 5: Cycle example showing multiple solutions. The two graphs show two different solutions that satisfy the power flow equations. In the top solution, there is no flow going around the cycle. In the bottom solution, there is a clockwise flow going around the cycle.

For the rest of this paper, we also assume that the digraphs under consideration do not have self-loops. Furthermore, in order to satisfy the power balance equations, there must be at least one incoming and one outgoing edge at each non-slack bus of the residual-digraph. This merits introducing the concept of *feasible orientation*, which we define below.

Definition 5.1. (*Feasible Orientation*) Consider a general power network $\mathbb{G} = (\mathbb{V}, \mathbb{E}, \mathbb{W})$. Let $\mathbb{D} = (\mathbb{V}, \tilde{\mathbb{E}}, \mathbb{W})$ be a digraph that is created by assigning a specific orientation $\tilde{\mathbb{E}}$ to the original undirected edges \mathbb{E} of graph \mathbb{G} . The digraph \mathbb{D} is called a ‘feasible orientation’ of the underlying undirected graph if:

$$d^+(k) \geq 1, d^-(k) \geq 1 \quad \forall k \in \mathbb{V} \setminus \{1\}$$

The set of all feasible orientations for graph \mathbb{G} is called the ‘set of feasible orientations’ and is denoted by $\mathcal{D}_f(\mathbb{G})$.

The condition in Definition 5.1 simply requires that each bus have in-degree and out-degree greater than or equal to one. Now, we are ready to state the theorem that generalizes Lemma 5.1. From here on, we will use the word ‘vertex’ more often in place of the word ‘bus.’

Theorem 5.2. Consider an arbitrary power network $\mathbb{G} = (\mathbb{V}, \mathbb{E}, \mathbb{W})$. Suppose that for every feasible orientation $\mathbb{D} \in \mathcal{D}_f(\mathbb{G})$, there exists a directed cycle \mathbb{C} with its vertex set denoted as $\mathbb{V}_{dc} = \{u(1), \dots, u(|\mathbb{V}_{dc}|)\} \subseteq \mathbb{V}$ such that

$$\sum_{i=1}^{|\mathbb{V}_{dc}|-1} \omega_{u(i), u(i+1)} < \pi/2. \quad (48)$$

Then, for each $P \in \mathcal{P}(\mathbb{G}, \Theta(\mathbb{G}))$ there cannot be multiple distinct solutions satisfying $P = \hat{P}(\Theta)$.

Note that condition (48) becomes less restrictive if there exists a short directed cycle for every *feasible orientation* of the underlying graph. In the graph theory literature, the length of the smallest directed cycle of digraph \mathbb{D} is called the *girth* of \mathbb{D} , which we denote by $\delta(\mathbb{D})$. Therefore, to rephrase the earlier statement, having a small *girth* for all of the possible *feasible orientations* is crucial. This calls for a new notion of *maximal girth* of an undirected graph, in addition to the *girth*, which we define below.

Definition 5.2. For a given undirected graph \mathbb{G} , define the ‘maximal girth’ $\Delta(\mathbb{G})$ as follows:

$$\Delta(\mathbb{G}) = \max_{\mathbb{D} \in \mathcal{D}_f(\mathbb{G})} \delta(\mathbb{D}) \quad (49)$$

Corollary 5.3. Given an arbitrary power network $\mathbb{G} = (\mathbb{V}, \mathbb{E}, \mathbb{W})$, suppose that

$$\omega_{k\ell} < \frac{\pi}{2 \cdot (\Delta(\mathbb{G}) - 1)} \quad \forall \{k, \ell\} \in \mathbb{E}. \quad (50)$$

Then, for each $P \in \mathcal{P}(\mathbb{G}, \Theta(\mathbb{G}))$ there cannot be multiple distinct solutions satisfying $P = \hat{P}(\Theta)$.

Note that for cyclic networks, $\mathcal{P}(\mathbb{G}, \Theta(\mathbb{G}))$ is in general a nonconvex set, and there have been recent works that address the issue via convex restrictions [36]. So far, we have shown that finding a directed cycle satisfying condition (48) for all feasible orientations corresponds to certifying that the $P - \Theta$ problem cannot have multiple distinct solutions. Furthermore, Corollary 5.3 has introduced the concept of *maximal girth* to show that if the *allowable limits* are uniformly less than the upper-bound in (50), then the $P - \Theta$ problem cannot have multiple distinct solutions. The smaller the value of $\Delta(\mathbb{G})$, the more freedom there is for angle differences over lines. The question arises as to whether we can calculate or upper-bound $\Delta(\mathbb{G})$. For the example in Fig. 5, it is relatively easy to see that $\Delta(\mathbb{G}) = 6$. However, for a graph with m edges, the number of *feasible orientations* is on the order of 2^m , and calculating or even proving an upper-bound on $\Delta(\mathbb{G})$ is a difficult task. Most of the existing results provide bounds that are on the order of n/s where s is the minimum out-degree of a digraph [27], which is not useful for our purpose since $s = 1$ for *feasible orientations*.

Here, we upper-bound the *maximal girth* by using another property of the underlying undirected graph, namely the length of its longest chordless cycle, which we denoted by $\kappa(\mathbb{G})$. The basic idea behind the proof is that any directed cycle with a chord can be further decomposed into two cycles, one of which is again a directed cycle. The formal statement with its proof is provided in Lemma 10 of the Appendix. With this upper-bound on *maximal girth*, condition (50) can be substituted by the following new condition:

$$\omega_{k\ell} < \frac{\pi}{2 \cdot (\kappa(\mathbb{G}) - 1)} \quad \forall \{k, \ell\} \in \mathbb{E} \quad (51)$$

A major benefit of this result comes from the fact that $\kappa(\mathbb{G})$ can be computed in a relatively straightforward fashion. For the example in Fig. 5, the value of $\kappa(\mathbb{G})$ is equal

to the value of $\Delta(\mathbb{G})$. The procedure for the computation of $\kappa(\mathbb{G})$ and its values for several IEEE test cases are reported in Section 8.2. For complete graphs, $\kappa(\mathbb{G}) = 3$ because all vertices are connected by an edge. In connection with Corollary 5.3, this implies that complete graphs cannot have multiple distinct solutions if angle differences are restricted below $\pi/4$, which is often the case in real-world power operations due to security considerations. It is acknowledged, however, that power system graphs are not in practice complete graphs and are, in fact, sparse.

6 Series-Parallel Reduction

This section shows that under the assumption that voltage angles lie within the *allowable limits*, the uniqueness of $P - \Theta$ problem solutions is preserved under *series-parallel reduction*, with appropriate updates on the *set of allowable limits*, namely \mathbb{W} . These updates are involved with the *dangling vertex*, *highway-path* and *parallel edges* of the graph, which will be explained in detail throughout the section. We conclude the section with a recognition that all graphs that are reducible (via series-parallel reduction) to a K_2 have a unique power flow solution if the updated *allowable limit* on the remaining single line is less than $\pi/2$. These graphs turn out to be equivalent to a group of graphs called *Generalized Series-Parallel (GSP)* that includes any tree or cycle graph. In fact, every outer-planar graph is *GSP* [20]. This result has practical implications because real-world transmission and distribution systems are not far away from this type of topology. We begin by defining *series-parallel reduction* and *GSP* graphs. As detailed in [20], one of the equivalent definitions of a *GSP* graph is as follows:

Definition 6.1. *A graph is a Generalized Series-Parallel (GSP) graph if it can be reduced to a single edge graph (K_2) by a sequence of the following three operations:*

1. *Replacement of a pair of parallel edges with a single edge that connects their common endpoints.*
2. *Replacement of a pair of edges incident to a vertex of degree 2 with a single edge.*
3. *Deletion of a dangling (degree 1) vertex.*

Any sequence of these three operations will be called a "series-parallel reduction".

To help visualize how the three operations work, in Fig. 6, we illustrate a reduction example on the IEEE 14-bus network. Starting from the original network (a), the graph is subsequently reduced to (d) via a sequence of series-parallel reductions. Going from (a) to (b) represents an example of operation 3, where the dangling vertex (numbered by 8 in the figure) is deleted. The process from (b) to (c) is an example of operation 2, where two edges incident to a vertex of degree 2 is replaced by a single edge. Finally, the process from (c) to (d) is an example of operation 1, where two parallel edges are replaced by a single edge.

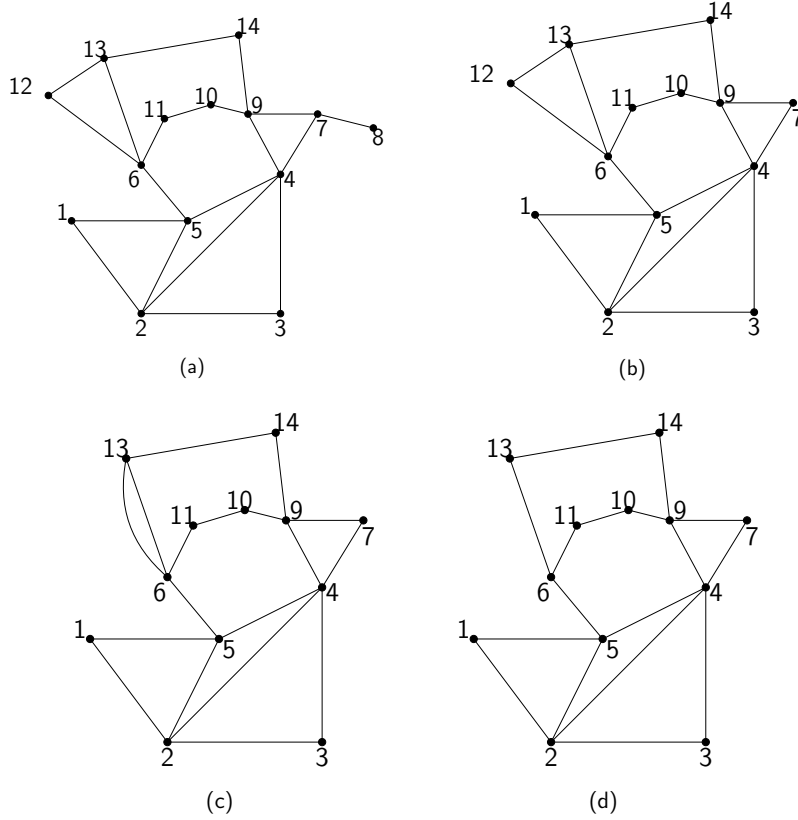


Figure 6: A simple diagram illustrating a sequence of series-parallel reductions for the IEEE 14-bus system.

It turns out that the analysis of conditions (48–51) for the original power network can be performed on a “series-parallel reduced” network that could be far smaller than the original graph. Let us revisit the example in Fig. 6. In the original network (a), edge $\{7, 8\}$ cannot be part of any cycle because vertex 8 has degree 1. Therefore, this edge can be omitted from the analysis of directed cycles. In network (b), edges $\{6, 12\}$ and $\{12, 13\}$ have to be either both part of a cycle or both not part of any cycle. Therefore, the two edges can be replaced by a single edge $\{6, 13\}$ with a new *allowable limit*, $\tilde{\omega}_{6,13} = \omega_{6,12} + \omega_{12,13}$. A similar implication follows if we replace the two parallel edge in (c), connecting vertex 6 and 13, by a single edge with a new *allowable limit* that is of maximum value among the replaced edges. Before we present the formal statement of this observation, we define what a *highway-path* is below.

Definition 6.2. An induced path \mathbb{P} of \mathbb{G} with vertex set

$$\mathbb{V}^h = \{s, u^h(1), u^h(2), \dots, u^h(H), t\} \quad (52)$$

from vertex s to vertex t is called a *highway-path* if:

$$d(u^h(i)) = 2 \quad \forall i \in \{1, \dots, H\} \quad (53)$$

and $u^h(i)$ is a *non-slack vertex* for every $i \in \{1, \dots, H\}$.

Note that a single edge is also considered a *highway-path*. By building on the previous observations and using the above definition, we show that the problem of determining the uniqueness of the power flow solutions for the original meshed network can be reduced to determining the uniqueness of solutions on a smaller graph that excludes a *dangling vertex*, a *highway-path* or a *parallel edge*.

Theorem 6.1. Consider a power network $\mathbb{G} = (\mathbb{V}, \mathbb{E}, \mathbb{W})$.

1. If \mathbb{G} contains two parallel edges $e_1, e_2 \in \mathbb{E}$ both connecting the same pair of vertices, define

$$\begin{aligned} \bar{\mathbb{V}} &= \mathbb{V}, \quad \bar{\mathbb{E}} = \mathbb{E} \setminus \{e_2\}, \\ \bar{\mathbb{W}} &= \{\bar{w}_e \mid \bar{w}_e = w_e, \forall e \in \bar{\mathbb{E}} \setminus \{e_1\}, \bar{w}_{e_1} = \max\{w_{e_1}, w_{e_2}\}\} \end{aligned}$$

2. If \mathbb{G} contains a *highway-path* \mathbb{P} , let \mathbb{V}^h be the vertex set of \mathbb{P} as described in (52). Define

$$\begin{aligned} \bar{\mathbb{V}} &= \mathbb{V} \setminus \{u^h(1), \dots, u^h(H)\}, \quad \bar{\mathbb{E}} = \mathbb{E}[\bar{\mathbb{V}}] \cup \{\{s, t\}\}, \\ \bar{\mathbb{W}} &= \{\bar{w}_e \mid \bar{w}_e = w_e, \forall e \in \mathbb{E}[\bar{\mathbb{V}}], \bar{w}_{s,t} = \sum_{e \in \mathbb{E}[\mathbb{V}^h]} \omega_e\} \end{aligned}$$

3. If \mathbb{G} contains a *dangling (degree 1) vertex* u , define

$$\bar{\mathbb{V}} = \mathbb{V} \setminus \{u\}, \quad \bar{\mathbb{E}} = \mathbb{E}[\bar{\mathbb{V}}], \quad \bar{\mathbb{W}} = \{\bar{w}_e \mid \bar{w}_e = w_e, \forall e \in \bar{\mathbb{E}}\}$$

Let the reduced graph \mathbb{G}^r be defined by $\mathbb{G}^r = (\bar{\mathbb{V}}, \bar{\mathbb{E}}, \bar{\mathbb{W}})$. Then, the $P - \Theta$ power flow problem for the original graph \mathbb{G} has at most one solution if condition (50) is satisfied for \mathbb{G}^r .

Theorem 6.1 implies that deleting the graph's *dangling vertex*, or contracting multiple edges that are connected in series, or eliminating one of the two parallel edges do not influence the uniqueness of power flow solutions as long as the *set of allowable limits* \mathbb{W} is updated appropriately. One major advantage of Theorem 6.1 is that the analyses pertaining to *directed cycles*, *maximal girth* and *longest chordless cycle* introduced in Section 5 can now be applied to a smaller reduced network. For instance, checking condition (48) is time-dependent on the number of vertices, edges, and simple cycles of a graph. As the graph becomes larger, this computation can be daunting since the number of simple cycles can grow exponentially in the number of vertices. The effect of series-parallel reduction on several IEEE test cases is illustrated in Section 8.1.

Finally, it is no coincidence that these three reduction procedures are equivalent to the three operations that are allowed and required to turn a *GSP* graph into a K_2 graph (see Definition 6.1). In other words, any *GSP* graph can be reduced to a single line after undergoing a sequence of reduction procedures delineated in Theorem 6.1. The absence of cycles suggests that Theorem 5.2 is unnecessary in this case, and warrants a simpler result, which is given as a corollary below. The corollary states that the $P - \Theta$ problem on *GSP* graphs has at most one solution if the final updated *allowable limit* for the reduced single line is less than $\pi/2$.

Corollary 6.2. *Suppose that the power system $\mathbb{G} = (\mathbb{V}, \mathbb{E}, \mathbb{W})$ has a *GSP* topology. Let $\mathbb{L} = (\bar{\mathbb{V}}, \bar{\mathbb{E}}, \bar{\mathbb{W}})$ be a K_2 graph (containing the slack bus) that is series-parallel reduced from \mathbb{G} , where $\bar{\mathbb{W}} = \{\omega\}$ represents the ‘allowable limit’ on the remaining line that is updated according to the procedures in Theorem 6.1. If $\omega < \pi/2$, then there is a unique $\Theta \in \Theta(\mathbb{G})$ such that $P = \hat{P}(\Theta)$ for each $P \in \mathcal{P}(\mathbb{G}, \Theta(\mathbb{G}))$.*

7 Algorithm

In this section, we design an algorithm for finding the unique solution of the $P - \Theta$ problem when the graph has a *GSP* structure. In general, the $P - \Theta$ equations constitute a system of nonlinear equations and are prone to complex and chaotic behavior. Conventional algorithms such as Newton’s method may fail to converge when a bad initial guess is provided or if the system is close to its security margins. In the special case where the injection operator $\hat{P}(\Theta)$ is strictly monotone, leading to a unique (if there exists) $P - \Theta$ problem solution, a fixed point iteration approach will converge to the correct solution with a convergence rate that depends on the monotonicity constant and Lipschitz constant of the operator in question. However, requiring the injection operator to be monotonic over a feasible region is quite restrictive. In our case, the uniqueness of the $P - \Theta$ power flow problem for *GSP* graphs emerges from a repetitive reduction process of the network and its flow set in a parameterized way that is not amenable to conventional numerical methods. The power flow algorithm that we propose for the *GSP* networks, therefore, will emulate this reduction process.

7.1 Linear-time algorithm

We begin with a simple example illustrating the idea behind the algorithm. Fig. 7 shows a *GSP* network with four buses and five lines, where bus 1 is the slack bus as usual. Let $\mathbb{W} = \{\omega_{1,2}, \omega_{2,3}, \omega_{1,3}, \omega_{1,4}, \omega_{3,4}\}$ denote the *set of allowable limits* for this network. Suppose that the assumption in Corollary 6.2 is met, meaning that the network can be reduced to a single edge connecting vertices 1 and 4 via series-parallel reduction and the updated *allowable limit* for that edge is less than $\pi/2$. More specifically, this means that $\bar{\omega}_{1,4} < \pi/2$, where $\bar{\omega}_{1,4}$ equals the left-hand side of the following expression:

$$\max \left\{ \omega_{1,4}, \max \{ \omega_{1,2} + \omega_{2,3}, \omega_{1,3} \} + \omega_{3,4} \right\} < \pi/2 \quad (54)$$

Now, set the variable x to represent the real power flow from vertex 1 to vertex 2, i.e. $x = p_{12}$. Due to power balance at each vertex and the fact that vertex 2 has a degree of two, p_{23} is an increasing function with respect to x . Furthermore, due to Lemma 4.1 and the allowable angle assumptions that we made, this means that θ_{12} and θ_{23} are also increasing functions of p_{12} . It follows that $\theta_{13} = \theta_{12} + \theta_{23}$ is also an increasing function of x . Finally, due to the assumption on $\bar{\omega}_{1,4}$ in (54), we know that $\omega_{1,3} < \frac{\pi}{2}$, which implies that p_{13} is an increasing function of θ_{13} and also of x .

Similarly, the flow variables expressed as bold arrows in Fig. 7 are all monotonically increasing with respect to x . Furthermore, once x is known, all the other flow variables can be calculated sequentially. We will call this flow variable x the *primary flow*. This sequential process is illustrated below:

1. Set $\mathbf{x} = x^0$.
2. Calculate: $\mathbf{p}_{23} = p_2 - \hat{r}_{12}(x)$
3. Calculate θ_{12} and θ_{23} . Then, add them up to obtain θ_{13} .
4. Calculate $\mathbf{p}_{13} = \hat{p}_{13}(\theta_{13})$.
5. Calculate: $\mathbf{p}_{34} = p_3 - \hat{r}_{23}(p_{23}) - \hat{r}_{13}(p_{13})$.
6. Calculate: $\mathbf{p}_{41} = p_4 - \hat{r}_{34}(p_{34})$.

These steps will be embedded in the algorithm proposed in this section. Each iteration of the algorithm will involve the above calculation of the flow variables, followed by an update on the value of the *primary flow*. Notice that at each step of the process, all the necessary information is already calculated in the preceding steps. Also, none of the steps involves solving a separate optimization problem and just requires simple algebraic calculations. Before delving into the full algorithm, we introduce a concept of *outer-cycles*.

Definition 7.1. *An induced cycle \mathbb{C} of \mathbb{G} is called an outer-cycle if the following two conditions are met:*

1. \mathbb{C} contains two highway-paths such that the union of the two paths is \mathbb{C} and the intersection is $\{s, t\}$. One of the paths (arbitrarily chosen), denoted by \mathbb{S}^p , will be called the *principal-path* and has vertex set \mathbb{V}^p . The other path, named \mathbb{S}^a , will be called the *auxiliary-path* and has vertex set \mathbb{V}^a . Let the vertex sets be denoted as follows:

$$\mathbb{V}^p = \{s, u^p(1), u^p(2), \dots, u^p(N), t\} \quad (55)$$

$$\mathbb{V}^a = \{s, u^a(1), u^a(2), \dots, u^a(M), t\} \quad (56)$$

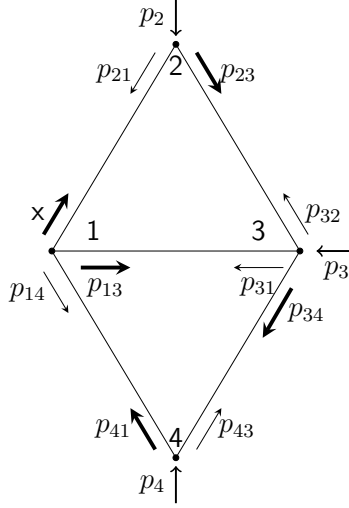


Figure 7: A two-cycle network sharing an edge

2. All the vertices except for s and t have degree 2 and are non-slack buses.

The concept of an *outer-cycle* is useful because it corresponds to a cycle that is reduced via a combination of operations 1 and 2 of the series-parallel reduction (Definition 6.1). For example, in Fig. 6, the outer-cycle with vertices $\{6, 12, 13\}$ is reduced as it is transformed from sub-figure (b) to (d). The order in which outer-cycles and dangling vertices are deleted essentially define the series-parallel reduction. In our algorithm, it also corresponds to the order in which the flows are calculated starting from the *primary flow*. Theorem 7.1 states that for a subset of *GSP* graphs, the exemplary steps above can work and the $P - \Theta$ power flow problem can be solved in linear time. Here, we will use the notation $\mathbb{G} \rightarrow \mathbb{G}^r$ to signify the series-parallel reduction from graph \mathbb{G} to \mathbb{G}^r .

Theorem 7.1. For Corollary 6.2, suppose that $\mathcal{O} = \{\mathbb{C}_1, \dots, \mathbb{C}_R\}$ is the sequence of outer-cycles reduced in the process $\mathbb{G} \rightarrow \mathbb{L}$. Let \mathbb{E}_j denote the edge set for cycle \mathbb{C}_j . Then, there is a linear-time algorithm with complexity $O(|\mathbb{E}| \cdot \log(1/\epsilon))$ to find the unique solution of the $P - \Theta$ power flow problem, given a desired precision level ϵ , if the following condition holds:

$$\left| \left(\bigcup_{i < j} \mathbb{E}_i \right) \cap \mathbb{E}_j \right| \leq 1 \quad \forall j = \{1, \dots, R\} \quad (57)$$

The linear-time algorithm is given in Algorithm 1. The algorithm makes use of the fact that for each line, there is one direction for which the flow increases with respect to the *primary flow* and another for which the flow decreases with respect to the *primary flow*. Let \mathcal{F}^+ denote the set of ordered pair of indices (k, ℓ) such that $p_{k\ell}$ is monotonically increasing with respect to the *primary flow*. Also, for notation reasons, let $p(k, \ell)$ also denote the flow from bus k to ℓ in addition to $p_{k\ell}$. Below, we define a type of projection operator Π that allows the iterative sequence to stay in the *allowable sets* arising from our angle difference assumptions. Here, x^{iter} denotes the iter^{th} iteration value of the *primary*

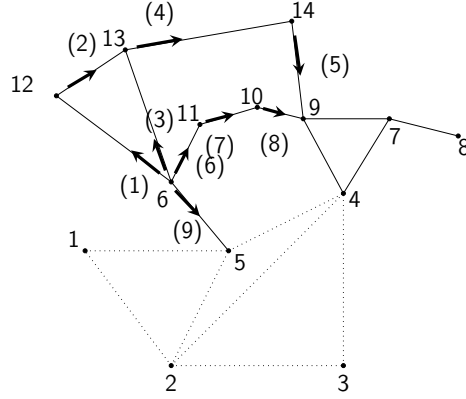


Figure 8: A simple diagram of the IEEE 14-bus system. Buses are marked in plain numbers, while the flow variables are marked in parenthesized numbers in the order in which they are calculated in Algorithm 1. Nodal real power injections are not shown in order to simplify the diagram.

flow x . Furthermore, we make use of several MATLAB functions: *break* means to break out of all the for-loops, and *find*($A == a$) returns the index of an array A for which the value is equal to a .

$$\Pi(x^{\text{iter}}, p_{kl}) = \begin{cases} x^{\text{iter}+1} = \frac{x + x^{\text{iter}}}{2} \text{ and break} & \text{if } p_{kl} \geq \bar{p}_{kl} \\ x^{\text{iter}+1} = \frac{x^{\text{iter}} + \bar{x}}{2} \text{ and break} & \text{if } p_{kl} \leq \underline{p}_{kl} \\ \theta_{kl} = \hat{\theta}_{kl}(p_{kl}) & \text{otherwise} \end{cases}$$

Each iteration of Algorithm 1 involves calculating all the flows in the set \mathcal{F}^+ based on the current value of the *primary flow*. This process is done sequentially in the same order in which the original graph is reduced to the final K_2 graph. Based on these values, the *primary flow* is updated by the bisection method until the solution is found. In Section 8.3, a set of representative numerical examples are generated and the performance of this proposed algorithm is illustrated.

7.2 Graphs that do not satisfy the assumption in Theorem 7.1

Theorem 7.1 states that if a power system network with *GSP* topology satisfies (57), then the power flow problem can be solved efficiently. Equation (57) essentially requires that any chordless cycle can only share at most one edge with all the previous reduced cycles. Obviously, this result weakens once the assumption is not met. We will illustrate the difficulties that arise using the IEEE 14-bus system, which has a *GSP* topology but does not satisfy (57).

Consider the system drawn in Fig. 8 and notice that $p_{6,12}$ is selected as the *primary flow*. Given the *primary flow* value, the flows (2)–(5) can be easily calculated as delineated in

Section 7.1. The first difficulty arises when trying to calculate the next unknown, flow (6). This is because the assumption of Theorem 7.1 breaks down: cycle $\{6, 13, 14, 9, 10, 11, 6\}$ and cycle $\{5, 6, 11, 10, 9, 4, 5\}$ share three edges. Therefore, even though we know $\theta_{6,9}$ from the previous calculations, i.e. by doing $\theta_{69} = \hat{\theta}_{6,13}(p_{6,13}) + \hat{\theta}_{13,14}(p_{13,14}) + \hat{\theta}_{14,9}(p_{14,9})$, finding flow (6) requires solving an additional implicit function. Noting that $p_{11,10} = P_{11} - \hat{r}_{6,11}(p_{6,11})$ and $p_{10,9} = P_{10} - \hat{r}_{11,10}(p_{11,10}) = P_{10} - \hat{r}_{11,10}(P_{11} - \hat{r}_{6,11}(p_{6,11}))$, the implicit function to be solved is:

$$\begin{aligned} & \hat{\theta}_{6,11}(p_{6,11}) + \hat{\theta}_{11,10}(P_{11} - \hat{r}_{6,11}(p_{6,11})) \\ & + \hat{\theta}_{10,9}(P_{10} - \hat{r}_{11,10}(P_{11} - \hat{r}_{6,11}(p_{6,11}))) = \theta_{6,9} \end{aligned}$$

where the only variable is now $p_{6,11}$. This equation is monotonically increasing in $p_{6,11}$ and can be solved in $\log(1/\epsilon)$. After having found the value for flow (6), flows (7)–(9) can be found by simple arithmetic calculations. Similarly, $p_{9,7}$ can be found by solving another monotonic implicit function. This is because the nodal injection at bus 8 gives a unique $p_{7,8}$ that acts as an additional negative injection at bus 7. After this, $p_{9,4}$ and $p_{7,4}$ can be calculated by explicit arithmetic equations. The next difficulty arises after these steps. At this point, buses 5 and 4 both have three lines where the flows are unknown, which means that there is no easy way to calculate the remaining flow variables of the network. The only thing left to do is to solve a sub-problem on a subsystem of the original network, which is depicted in Fig. 8 as dotted lines. For this sub-problem, it is important to update the original nodal real power injections at bus 5, namely P_5 , by $P_5 - \hat{r}_{6,5}(p_{6,5})$. Likewise, the original nodal real power injections at bus 9, namely P_9 , by $P_9 - \hat{r}_{10,9}(p_{10,9}) - \hat{r}_{14,9}(p_{14,9})$. Also, update injection at bus 4 in a similar manner. Now, observe that this subsystem satisfies all the assumptions made in Theorem 7.1 and hence the sub-problem can be solved in linear time.

The example above illustrates the fact that violating the assumptions corresponds to an increase in the algorithm's complexity. Suppose that the original graph \mathbb{G} can be divided into two subgraphs: the first part containing all the difficulties and the second part satisfying the assumptions made in Theorem 7.1. Then, the complexity of the algorithm will become $\mathcal{O}(\{m_1 c_1 \log(1/\epsilon)\} \cdot m_2 \log(1/\epsilon)) = \mathcal{O}(c_1 m_1 m_2 \log^2(1/\epsilon))$ where m_i 's are the number of edges for each subgraph and c_1 is the number of additional implicit functions that have to be solved for the first subgraph.

8 Numerical and simulation results

In this section, we use simulation and computation to numerically verify and support the ideas that have been developed in the paper. We start with visualizing how series-parallel reduction works on actual power systems. Then, we calculate the longest chordless cycle – which provides an upper bound on *maximal girth* – of benchmark power systems. Finally, we apply Algorithm 1 to a class of networks in order to demonstrate its performance.

8.1 Series-parallel reduction of IEEE test cases

In Section 6, we introduced series-parallel reduction and showed that analyzing the uniqueness of the $P - \Theta$ problem solution can be performed on a smaller ‘series-parallel reduced’ network. In Fig. 9, we illustrate how these reductions visualize when applied to actual IEEE test cases (note that here the slack bus was not necessarily selected as bus 1). Figures 9(a) and (c) represent the graphs before the reduction and figures 9(b) and (d) represent the graphs after the series-parallel reduction. We can see that the reduced graphs are much smaller and contain the core information of the original graph. These reductions make Theorem 5.2 more practical to use because condition (48) is much easier to check on a smaller network.

	$\kappa(\mathbb{G})$	$\tilde{\kappa}(\mathbb{G})$
case5	4	4
case14	6	6
case30	11	8
case39	17	8

Table 1: Upper-bounds on maximal girth for IEEE test cases.

8.2 Calculation of $\kappa(\mathbb{G})$

In Section 5, we introduced $\kappa(\mathbb{G})$ as an upper-bound on the *maximal girth* $\Delta(\mathbb{G})$, which is computationally more tractable than $\Delta(\mathbb{G})$. To find the value of $\kappa(\mathbb{G})$, we first use a function built in Sage [33] to calculate all simple cycles of the graph, and then narrow them down to chordless cycles. Ultimately the length of the longest chordless cycle is obtained. The values are calculated for several IEEE standard test cases and reported in Table 1. A tighter bound can be found by observing that chordless cycles are not entirely immune to further decomposition. For example, consider the IEEE 39-bus network depicted in Fig. 9(c). One of the chordless cycles that are found using our implementation is $\{1, 2, 3, 4, 14, 13, 12, 11, 6, 7, 8, 9, 39, 1\}$, which has length thirteen (note that this is not the longest chordless cycle). This is a chordless cycle because there is no edge directly connecting any two vertices of the cycle. However, as we can observe from Fig. 10, this cycle can be further partitioned into three smaller chordless cycles by the three edges in its interior. Furthermore, depending on the orientation of these three edges, at least one of the three smaller cycles is again a directed cycle if the big cycle is oriented. The tighter bound achieved from this process is denoted by $\tilde{\kappa}(\mathbb{G})$ and also reported in Table 1. Now, Corollary 5.3 can be used to study when the power flow equations have a unique solution.

8.3 Performance of linear-time algorithm

In order to verify the effectiveness of the proposed algorithm, we analyze its performance along with the performance of Newton-Raphson method as a standard algorithm used to solve power-flow in practice. To implement this standard algorithm, we use the MAT-POWER [30] *runpf* function with the ‘Newton-Raphson (NR)’ option. Furthermore, in

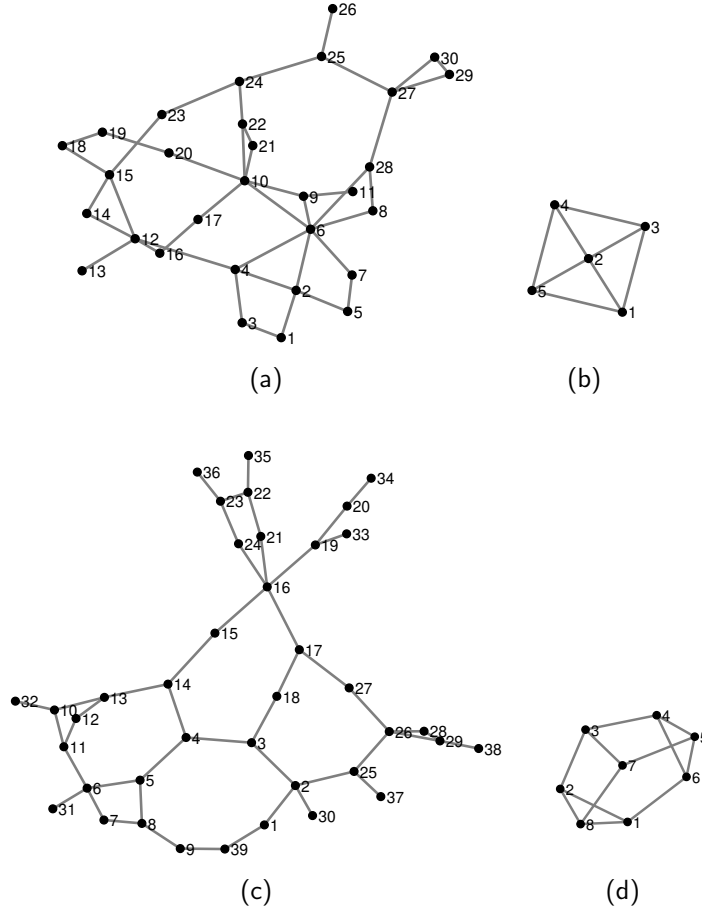


Figure 9: (a) IEEE 30-bus system before reduction, (b) IEEE 30-bus system after reduction, (c) IEEE 39-bus system before reduction, and (d) IEEE 39-bus system after reduction.

order to satisfy the assumptions in equation (57), we create a class of triangulated networks of varying sizes (see Appendix J. for figure) using the MATPOWER casefile format (mpc). The *allowable set of angles* is enforced by setting the 12th and 13th columns of the field "branch" in the casefile to the *steady-state stability limit* (refer to Definition 4.1). Note that the matpower-NR algorithm cannot enforce additional angle constraints, such as (54), whereas Algorithm 1 does by design. Note that matpower-NR can be modified to incorporate these constraints if we formulate the power flow problem as an optimal power flow (OPF) problem, but then this becomes a constrained nonconvex optimization problem which introduces its own difficulties and is not the subject of this paper (even finding a feasible point to such optimization problem is a challenge). The following steps describe the experiments:

- 1) Generate a random Θ^* that belongs to the set $\Theta(\mathbb{G})$. This is the true set of angles that we wish to recover via the above algorithms.

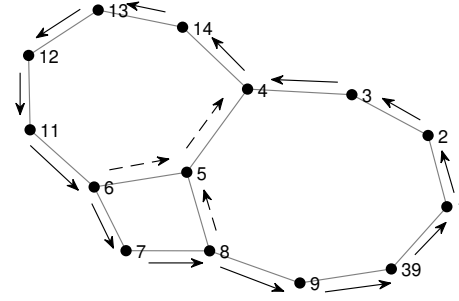


Figure 10: Further decomposition of a directed chordless cycle. The solid arrows represent the original directed chordless cycle. The dotted arrows represent a possible orientation of the three edges that lie in the interior of the cycle.

- 2) Calculate the real power injection vector P , using Θ^* .
- 3) Taking P as input, solve the $P - \Theta$ power flow problem using both Algorithm 1 and matpower-NR method. The voltage angles retrieved from each algorithm are denoted by Θ^1 and Θ^{NR} , respectively.
- 4) Calculate the errors $\|\Theta^1 - \Theta^*\|_2$ and $\|\Theta^{NR} - \Theta^*\|_2$.

For the initial point that is provided to the MATPOWER solvers, we generate a random point around the true solution via $\Theta^{init} = \Theta^* + \Theta^{noise}$, where Θ^{noise} is a random vector whose elements are independent and normally distributed with mean μ . For the initialization of Algorithm 1, a random value is chosen between the minimum and maximum allowable real power flow. In order to highlight the performance of the two algorithms as the initial point deviates away from the true solution, we test three different values of $\mu = \{0.1, 1, 10\}$. The experiments are performed on an increasing number of buses and 20 independent simulations are carried out for each fixed network.

Fig. 11 shows the results of these experiments. The top three figures plot the average 2-norm error (for varying values of μ) and the bottom three figures plot the average solver time (for varying values of μ) as a function of the network size. From the top three figures, it can be observed that matpower-NR performs relatively well and is able to recover Θ^* when the initial point is close enough to Θ^* . However, as Θ^{init} deviates further away from Θ^* , matpower-NR fails to reliably recover Θ^* . In fact, for most cases with initial values far from the true solution, the matpower-NR algorithm does not even converge within the maximum iteration limit. For $\mu = 10$, the matpower-NR method successfully converged for only 36 out of the 400 simulations. Fig. 12 plots the errors for these 36 convergent cases. It can be seen that several of these display high errors despite the successful convergence, implying that the algorithm converged to a different solution. Furthermore, it is demonstrated that Algorithm 1 does not converge to any of these different solutions and is capable of recovering Θ^* irrespective of the initial point or the number of buses. Finally, from the bottom three figures, we can observe that the

solving time for Algorithm 1 has a very slow growth in the size of the network and therefore can be used to solve large-scale problems. Note that Algorithm 1 was implemented in MATLAB with no strenuous efforts at optimizing the solving time and the purpose of Fig. 11 is only to demonstrate linear-time complexity of the proposed algorithm.

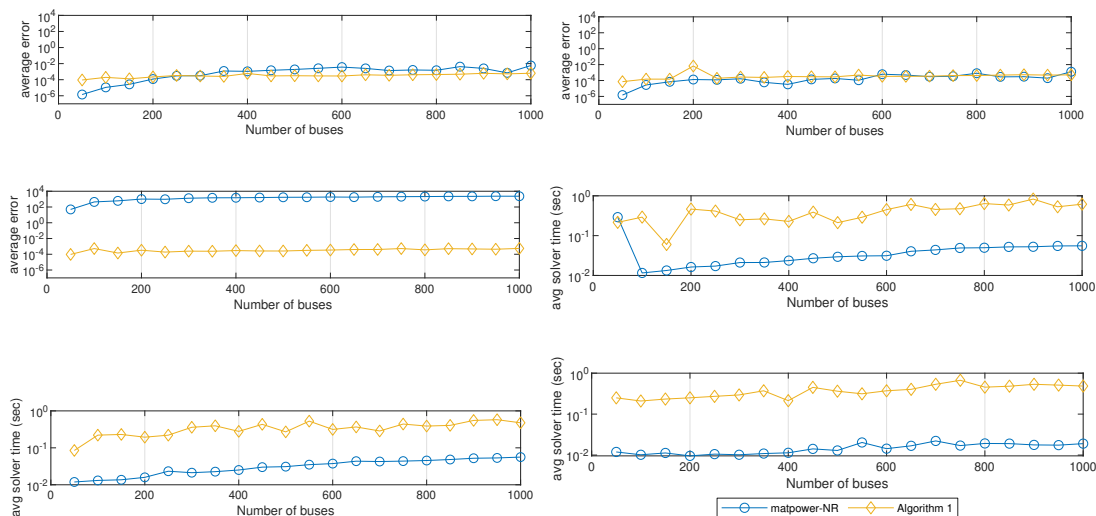


Figure 11: Comparison of average errors and solving times for Algorithm1 and matpower-NR. The first three figures plot the average error for different values of $\mu = 0.1, 1, 10$ (from top to bottom). The last three figures plot the average solving time for different values of $\mu = 0.1, 1, 10$ (from top to bottom)

9 Conclusion

In this paper, we establish sufficient conditions for the uniqueness of power flow solutions (if it exists) in an AC power system via the monotonic relationship between real power flows and voltage phase angles. We extend a simple observation made for a single line network – that angle differences bounded by their stability limit will give monotonicity and uniqueness – to the general network with multiple lines. More specifically, we prove that the $P - \Theta$ power flow problem has at most one solution for any acyclic or *GSP* graphs. These conditions guarantee the uniqueness of power flow solution, if it exists. In addition, for arbitrary power networks, we show that multiple distinct solutions cannot exist under the assumption that angle differences across the lines are bounded by some limit related to the maximal girth of the network. It is also shown that the series-parallel reduction on a graph does not alter the uniqueness of $P - \Theta$ problem solutions and therefore the analysis for a large network can be performed on a much smaller “reduced” network. Finally, we develop a efficient algorithm for a subset of the *GSP* graphs that work reliably, irrespective of the initial point.

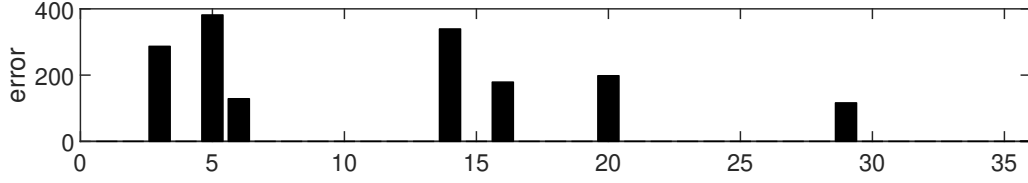


Figure 12: Errors for the 36 (out of 400) simulations when matpower-NR converged successfully for $\mu = 10$.

10 Appendix

10.1 Proof of Lemma 4.1

proof. The equation for the real power flow from node k to node ℓ over line $\{k, \ell\}$ is given in equation (43). After combining the cosine and sine functions into one sine function, we obtain a simpler equation for both flows:

$$p_{k\ell} = G_{k\ell}|v_k|^2 + |v_k| \cdot |v_\ell| Z_{k\ell} \sin(\theta_{k\ell} + \gamma_{k\ell}) \quad (58)$$

With a simple rearrangement:

$$\sin(\theta_{k\ell} + \gamma_{k\ell}) = \frac{p_{k\ell} - G_{k\ell}|v_k|^2}{|v_k| \cdot |v_\ell| Z_{k\ell}} \quad (59)$$

Using the assumption made on the angle differences and the definition of $\gamma_{k\ell}$, we deduce the following bounds on $\theta_{k\ell} + \gamma_{k\ell}$:

$$\begin{aligned} \theta_{k\ell} + \gamma_{k\ell} &\geq -\tan^{-1}(B_{k\ell}/G_{k\ell}) + \tan^{-1}(-G_{k\ell}/B_{k\ell}) \\ &= -\left(\frac{\pi}{2} - \tan^{-1}(G_{k\ell}/B_{k\ell})\right) - \tan^{-1}(G_{k\ell}/B_{k\ell}) = -\frac{\pi}{2} \\ \theta_{k\ell} + \gamma_{k\ell} &\leq \tan^{-1}(B_{k\ell}/G_{k\ell}) + \tan^{-1}(-G_{k\ell}/B_{k\ell}) \\ &= \frac{\pi}{2} - 2 \tan^{-1}(G_{k\ell}/B_{k\ell}) \leq \frac{\pi}{2} \end{aligned}$$

In summary, the angle $\theta_{k\ell} + \gamma_{k\ell}$ belongs to the range $[-0.5\pi, 0.5\pi]$ and therefore there exists a unique value of $\theta_{k\ell} + \gamma_{k\ell}$ that satisfies equation (59), leading to a unique value of $\theta_{k\ell}$. To prove the second part of the lemma, recall that the equation for the real power flow from node k to node ℓ over line $\{k, \ell\}$ is given in equation (43). Similarly, the real power flow in the opposite direction (from node ℓ to k) is given by:

$$p_{\ell k} = G_{k\ell}(|v_\ell|^2 - |v_k| \cdot |v_\ell| \cos \theta_{k\ell}) - B_{k\ell}|v_k| \cdot |v_\ell| \sin \theta_{k\ell} \quad (60)$$

After combining the cosine and sine functions into one sine function, we arrive at a simpler equation similar to equation (58):

$$p_{\ell k} = G_{k\ell}|v_\ell|^2 - |v_k| \cdot |v_\ell| Z_{k\ell} \sin(\theta_{k\ell} - \gamma_{k\ell}) \quad (61)$$

Furthermore, we can derive bounds on $\theta_{k\ell} - \gamma_{k\ell}$ similar to those on $\theta_{k\ell} + \gamma_{k\ell}$ shown above:

$$\begin{aligned} \theta_{k\ell} - \gamma_{k\ell} &\geq -\tan^{-1}(B_{k\ell}/G_{k\ell}) - \tan^{-1}(-G_{k\ell}/B_{k\ell}) \\ &= -\frac{\pi}{2} + 2 \tan^{-1}(-G_{k\ell}/B_{k\ell}) \geq -\frac{\pi}{2} \\ \theta_{k\ell} - \gamma_{k\ell} &\leq \tan^{-1}(B_{k\ell}/G_{k\ell}) - \tan^{-1}(-G_{k\ell}/B_{k\ell}) \\ &= \left(\frac{\pi}{2} - \tan^{-1}(G_{k\ell}/B_{k\ell})\right) + \tan^{-1}(G_{k\ell}/B_{k\ell}) = \frac{\pi}{2} \end{aligned}$$

Therefore, taking note of the fact that $\theta_{k\ell} + \gamma_{k\ell}$ and $\theta_{k\ell} - \gamma_{k\ell}$ are bounded by $[-0.5\pi, 0.5\pi]$, $p_{k\ell}$ and $p_{\ell k}$ are increasing and decreasing functions of $\theta_{k\ell}$, respectively. It can be concluded that $p_{\ell k}$ is a decreasing function of $p_{k\ell}$ for $p_{k\ell} \in (\underline{p}_{k\ell}, \bar{p}_{k\ell})$.

10.2 Proof of Theorem 4.2

(a) Let $P \in \mathcal{P}(\mathbb{G}, \Theta(\mathbb{G}))$. We show by construction that the specification of P uniquely determines $\Theta \in \Theta(\mathbb{G})$ such that $P = \hat{P}(\Theta)$. Note that since the power system has a tree topology, there is a unique path E_k between any bus k and bus 1 (consisting of successive lines) and that the distance $c(k)$ is therefore well-defined. Let $\bar{c} = \max_{k \in \mathbb{V}} c(k)$. We prove the result by using an induction argument on the decreasing distance \hat{c} . That is, the induction starts at $\hat{c} = \bar{c}$ and then considers successively smaller values of \hat{c} .

First, consider the case with distance $\hat{c} = \bar{c}$. Consider each bus k with $c(k) = \bar{c}$. Note that each such bus k is a leaf of the tree and that the injection p_k at this bus equals $p_{k\ell}(\theta_{k\ell})$, where $\{k, \ell\} \in \mathbb{T}$ is the unique line connected to bus k and $\theta_{k\ell}$ is the angle difference across this line. By Lemma 4.1, this means that p_k uniquely determines $\theta_{k\ell}$. Consequently, we can also evaluate $p_{\ell k}(-\theta_{k\ell})$, i.e., the power flow from bus ℓ into the line at the other end.

Now, suppose that for each bus k with $c(k) = \hat{c}$, we have that the injections p_k for each bus $k \in \mathbb{V} \setminus \{1\}$ with $c(k) \geq \hat{c}$ uniquely determines $\theta_{k\ell}$, where $\{k, \ell\} \in \mathbb{T}$ is the unique line connected to bus k such that $c(\ell) = c(k) - 1 = \hat{c} - 1$. Consider any bus k' with $c(k') = \hat{c} - 1$ and suppose that $\{k', \ell'\} \in \mathbb{T}$ is the unique line connected to bus k' such that $c(\ell') = c(k') - 1 = \hat{c} - 2$. By power balance at bus k' , $p_{k',\ell'}(\theta_{k',\ell'})$ equals the injection $p_{k'}$ minus the sum of the flows onto each other line $\{k', \ell''\}$ incident to bus k' . However, by assumption, $c(\ell'') \geq \hat{c}$ and so the flow on each such line $\{k', \ell''\}$ is uniquely determined by the injections p_k for each bus with $c(k) \geq \hat{c}$. In turn, this means that the flow $p_{k',\ell'}(\theta_{k',\ell'})$ and the corresponding angle $\theta_{k',\ell'}$ are both uniquely determined by $p_{k'}$ together with the injections p_k for each bus with $c(k) \geq \hat{c}$. That is, the angle $\theta_{k',\ell'}$ and the flow $p_{k',\ell'}(\theta_{k',\ell'})$ are uniquely determined by the injections p_k for each bus with

$c(k) \geq \hat{c} - 1$.

The induction continues to the root of the tree; that is, to bus 1. Hence, for all $\{k, \ell\} \in \mathbb{T}$, the injections p_k for each bus $k \in \mathbb{V}$ uniquely determines both $p_{k\ell}(\theta_{k\ell})$ and the corresponding angle $\theta_{k\ell}$ and $p_{\ell k}(-\theta_{k\ell})$. Now, note that the angle $\theta_1 = 0$. Therefore, since each angle difference is uniquely specified, this means that the corresponding angles are also uniquely determined. As a result, there is a unique $\Theta \in \Theta(\mathbb{G})$ such that $P = \hat{P}(\Theta)$.

(b) Suppose that $P^a, P^b \in \mathcal{P}(\mathbb{G}, \Theta(\mathbb{G}))$, with the corresponding flows also labeled by superscript a and b , and let $\lambda \in [0, 1]$ be given. Let $\Theta^a, \Theta^b \in \Theta(\mathbb{G})$ be the unique angles satisfying $P^a = \mathcal{P}(\mathbb{G}, \Theta^a)$ and $P^b = \mathcal{P}(\mathbb{G}, \Theta^b)$. Consider the injection $P^* = \lambda P^a + (1 - \lambda)P^b$. To prove convexity of $\mathcal{P}(\mathbb{G}, \Theta(\mathbb{G}))$, it is enough to show that $P^* \in \mathcal{P}(\mathbb{G}, \Theta(\mathbb{G}))$, which will involve constructing an angle $\Theta^* \in \Theta(\mathbb{G})$ such that $P^* = \mathcal{P}(\mathbb{G}, \Theta^*)$. By a similar argument to Part 1, first consider injections at buses k with $c(k) = \bar{c}$ and let $\{k, \ell\} \in \mathbb{T}$ be the unique line connected to bus k . Note that, by definition, $P_k^* = \lambda P_k^a + (1 - \lambda)P_k^b$ and therefore the corresponding flow $p_{k\ell}^*$ is the convex combination of the corresponding injections. In other words,

$$\begin{aligned} p_{k\ell}^* &= P_k^* \\ &= \lambda P_k^a + (1 - \lambda)P_k^b, \text{ by definition of } P_k^*, \\ &= \lambda p_{k\ell}(\theta_{k\ell}^a) + (1 - \lambda)p_{k\ell}(\theta_{k\ell}^b) \end{aligned}$$

The first and third equations come from the fact that $\{k, \ell\} \in \mathbb{T}$ is the unique line connected to bus k . Now, note that the values of flows $p_{k\ell}(\theta_{k\ell}^a)$ and $p_{k\ell}(\theta_{k\ell}^b)$ belong to $[\underline{p}_{k\ell}, \bar{p}_{k\ell}]$, which is a convex set. Thus, we also have that $p_{k\ell}^* \in [\underline{p}_{k\ell}, \bar{p}_{k\ell}]$. Therefore, there exists a unique $|\theta_{k\ell}^*| \leq \tan^{-1}(B_{k\ell}/G_{k\ell})$ such that $p_{k\ell}^* = p_{k\ell}(\theta_{k\ell}^*)$. We proceed as in Part 1 by using an induction argument on the decreasing distance \hat{c} . That is, the induction starts at \hat{c} and shows that for each $\{k, \ell\} \in \mathbb{T}$, the corresponding angle difference $\theta_{k\ell}^*$ with injections P^* satisfies $|\theta_{k\ell}^*| \leq \tan^{-1}(B_{k\ell}/G_{k\ell})$. Proceeding to bus 1, and again noting that $\theta_1 = 0$ is specified, it can be concluded that there is a uniquely defined $\Theta^* \in \Theta(\mathbb{G})$ such that $P^* = \mathcal{P}(\mathbb{G}, \Theta^*)$. Therefore, $\mathcal{P}(\mathbb{G}, \Theta(\mathbb{G}))$ is convex.

10.3 Lemma 10.1 and its proof

For each pair of vertices $k, \ell \in \mathbb{V}$, we define $\hat{\Theta}_{k\ell} = \hat{\Theta}_k - \hat{\Theta}_\ell$. Note that we do not require that $\{k, \ell\} \in \mathbb{T}$ in the definition of $\hat{\Theta}_{k\ell}$ and in the next lemma:

Lemma 10.1. *Suppose that the power system $\mathbb{G} = (\mathbb{V}, \mathbb{T})$ has a tree topology. Then, for each $k \in \mathbb{V} \setminus \{1\}$ and $\ell \in \mathbb{V}$ and for each $P \in \mathcal{P}(\mathbb{G}, \Theta(\mathbb{G}))$, we have $\frac{\partial \hat{\Theta}_{k\ell}}{\partial p_k}(P) \geq 0$.*

proof. Consider the path E_k from bus k to bus 1 and the path E_ℓ from bus ℓ to bus 1. Note that $\hat{\Theta}_k = \sum_{(k', \ell') \in E_k} \hat{\Theta}_{k'\ell'}$ and $\hat{\Theta}_\ell = \sum_{(k', \ell') \in E_\ell} \hat{\Theta}_{k'\ell'}$, because $\theta_1 = 0$. Moreover, $\hat{\Theta}_{k\ell} = \sum_{(k', \ell') \in E_k} \hat{\Theta}_{k'\ell'} - \sum_{(k', \ell') \in E_\ell} \hat{\Theta}_{k'\ell'}$. Now, observe that changes in injection at bus k can only affect flows, and therefore angle differences, in the path between bus k and

bus 1. Moreover, changes in flows and angles differences in the common part of the path $E_k \cap E_\ell$ affect the angle at both buses k and ℓ equally. Define $E_{k\ell} = E_k \setminus (E_k \cap E_\ell)$. That is, $E_{k\ell}$ is the path from bus k to the bus that is common to both E_k and E_ℓ and furthest from bus 1. Then:

$$\frac{\partial \hat{\Theta}_{k\ell}}{\partial p_k}(P) = \sum_{(k', \ell') \in E_{k\ell}} \frac{\partial \hat{\Theta}_{k'\ell'}}{\partial p_k}(P).$$

We now observe that the relationship between injection at bus k and angle differences at lines in this path $E_{k\ell}$ are all monotonic. That is, $\frac{\partial \hat{\Theta}_{k\ell}}{\partial p_k}(P) \geq 0$. According to Lemma 10.1, we can see that the angle difference between any non-slack bus k and any other bus ℓ is a monotonically increasing function of the real power injection at bus k when the injection vector P is within the *set of allowable injections*.

10.4 Proof of Lemma 5.1

Suppose that there are two distinct vectors of voltage angles, $\Theta^*, \Theta^{**} \in \Theta(\mathbb{G})$ that satisfy the power flow equations. Without loss of generality, assume that $\theta_{12}^{**} > \theta_{12}^*$. Then, due to power balance at buses $2, \dots, N$ and Assumption 4.1, a simple induction argument shows that

$$\theta_{i,i+1}^{**} - \theta_{i,i+1}^* > 0 \quad \forall i = \{1, \dots, N\}, \quad (62)$$

where bus $N + 1$ is again bus 1. Furthermore, we have that

$$\theta_{i,i+1}^{**} - \theta_{i,i+1}^* < \pi \quad \forall i = \{1, \dots, N\}, \quad (63)$$

which can be shown using the same logic followed to derive equation (67). Finally, by definition,

$$\theta_{1,N}^{**} - \theta_{1,N}^* = \sum_{i=1}^{N-1} (\theta_{i,i+1}^{**} - \theta_{i,i+1}^*) > 0 \quad (64)$$

and also,

$$\begin{aligned} \theta_{1,N}^{**} - \theta_{1,N}^* &= \sum_{i=1}^{N-1} (\theta_{i,i+1}^{**} - \theta_{i,i+1}^*) \leq \sum_{i=1}^{N-1} |\theta_{i,i+1}^{**} - \theta_{i,i+1}^*| \\ &\leq \sum_{i=1}^{N-1} (|\theta_{i,i+1}^{**}| + |\theta_{i,i+1}^*|) \\ &< \sum_{i=1}^{N-1} \omega_{i,i+1}^{**} + \sum_{i=1}^{N-1} \omega_{i,i+1}^* < \pi. \end{aligned}$$

This is a contradiction to equation (63) and therefore there cannot be two distinct solutions.

10.5 Proof of Theorem 5.2

In order to prove by contraction, suppose that there are two distinct solutions to the power flow problem, denoted as Θ^* , $\Theta^{**} \in \Theta(\mathbb{G})$. Now, we define a digraph $\mathbb{D}^r(\mathbb{G}) = \mathbb{D}^r(\mathbb{V}, \mathbb{A}^r)$ where the direction of each directed edge in \mathbb{A}^r is based on the difference (residual) between these two solutions. Hereby, we define the residual incidence matrix L^r for $\mathbb{D}^r(\mathbb{G})$ below:

$$L^r(a, k) = \begin{cases} -1 & \text{if } a = (k, \ell) \in \mathbb{A}^r \text{ and } \theta_{k,\ell}^{**} > \theta_{k,\ell}^* \\ 1 & \text{if } a = (\ell, k) \in \mathbb{A}^r \text{ and } \theta_{k,\ell}^{**} > \theta_{k,\ell}^* \\ 1 & \text{if } a = (k, \ell) \in \mathbb{A}^r \text{ and } \theta_{k,\ell}^{**} < \theta_{k,\ell}^* \\ -1 & \text{if } a = (\ell, k) \in \mathbb{A}^r \text{ and } \theta_{k,\ell}^{**} < \theta_{k,\ell}^* \end{cases} \quad (65)$$

Note that because of power balance at each node, this orientation has to be a *Feasible Orientation*. By assumption, for this fixed feasible orientation $\mathbb{D}^r(\mathbb{G}) \in \mathcal{D}_f(\mathbb{G})$, there exists a directed cycle \mathbb{C} satisfying the inequality in (48). Without loss of generality, assume that $\theta_{u(1),u(2)}^{**} > \theta_{u(1),u(2)}^*$. Then, because \mathbb{C} is a directed cycle, it holds that

$$\theta_{u(i),u(i+1)}^{**} - \theta_{u(i),u(i+1)}^* > 0 \quad \forall i = \{1, \dots, N\}, \quad (66)$$

where the $(N + 1)^{\text{th}}$ bus is again the 1^{st} bus. Furthermore,

$$\theta_{u(i),u(i+1)}^{**} - \theta_{u(i),u(i+1)}^* < \pi \quad \forall i = \{1, \dots, N\}, \quad (67)$$

which is due to the following inequalities:

$$\begin{aligned} \theta_{u(i),u(i+1)}^{**} - \theta_{u(i),u(i+1)}^* &\leq |\theta_{u(i),u(i+1)}^{**} - \theta_{u(i),u(i+1)}^*| \\ &\leq |\theta_{u(i),u(i+1)}^{**}| + |\theta_{u(i),u(i+1)}^*| < 2 \cdot \omega_{u(i),u(i+1)} < \pi \end{aligned}$$

However, by definition,

$$\begin{aligned}
\theta_{u(1),u(N)}^{**} - \theta_{u(1),u(N)}^* &= \sum_{i=1}^{N-1} (\theta_{u(i),u(i+1)}^{**} - \theta_{u(i),u(i+1)}^*) \\
&\leq \sum_{i=1}^{N-1} |\theta_{u(i),u(i+1)}^{**} - \theta_{u(i),u(i+1)}^*| \\
&\leq \sum_{i=1}^{N-1} |\theta_{u(i),u(i+1)}^{**}| + \sum_{i=1}^{N-1} |\theta_{u(i),u(i+1)}^*| \\
&< \sum_{i=1}^{N-1} \omega_{u(i),u(i+1)} + \sum_{i=1}^{N-1} \omega_{u(i),u(i+1)} < \pi
\end{aligned}$$

which is a contradiction to equations (66) and (67). Therefore, there cannot be two distinct vectors $\Theta^*, \Theta^{**} \in \Theta(\mathbb{G})$ that satisfy $P = \hat{P}(\Theta)$.

10.6 Proof of Theorem 5.3

Suppose that equation (50) is satisfied. In other words, to restate the equation here,

$$\omega_{kl} < \frac{\pi}{2 \cdot (\Delta(\mathbb{G}) - 1)} \quad \forall \{k, \ell\} \in \mathbb{E}. \quad (68)$$

Defining $\omega_{kl}^{max} = \max_{\{k, \ell\} \in \mathbb{E}} \omega_{kl}$, we also have that

$$\omega_{kl}^{max} < \frac{\pi}{2 \cdot (\Delta(\mathbb{G}) - 1)} \quad \forall \{k, \ell\} \in \mathbb{E}. \quad (69)$$

Multiplying both sides of the equation by $(\Delta(\mathbb{G}) - 1)$ yields

$$(\Delta(\mathbb{G}) - 1) \cdot \omega_{kl}^{max} < \frac{\pi}{2}. \quad (70)$$

Now, using the definition of $\Delta(\mathbb{G})$, the following holds true for every $\mathbb{D} \in \mathcal{D}_f(\mathbb{G})$:

$$(\delta(\mathbb{D}) - 1) \cdot \omega_{kl}^{max} < \frac{\pi}{2}. \quad (71)$$

Since $\delta(\mathbb{D})$ represents the length of the smallest directed cycle of \mathbb{D} , let us denote this smallest directed cycle by \mathbb{C} and its vertex set by $\mathbb{V}_{dc} = \{u(1), \dots, u(|\mathbb{V}_{dc}|)\} \subseteq \mathbb{V}$. Then, the above inequality becomes equivalent to the following:

$$(|\mathbb{V}_{dc}| - 1) \cdot \omega_{kl}^{max} < \frac{\pi}{2}. \quad (72)$$

This implies that

$$\sum_{i=1}^{|\mathbb{V}_{dc}|-1} \omega_{u(i),u(i+1)} < \frac{\pi}{2}. \quad (73)$$

Therefore, we have satisfied condition (48) of Theorem 5.2 and as a result can conclude that for each $P \in \mathcal{P}(\mathbb{G}, \Theta(\mathbb{G}))$ there cannot be multiple distinct solutions for the $P = \hat{P}(\Theta)$ problem.

10.7 Lemma 10.2 and its proof

Lemma 10.2. *For a given graph $\mathbb{G} = (\mathbb{V}, \mathbb{E})$, the following inequality holds:*

$$\Delta(\mathbb{G}) \leq \kappa(\mathbb{G}) \quad (74)$$

Proof. Consider an arbitrary *feasible orientation* on graph \mathbb{G} , and denote it as $\mathbb{D} = (\mathbb{V}, \mathbb{A})$. We will first show that the shortest directed cycle in \mathbb{D} must be chordless. Recall that because the feasible orientation enforces every vertex to have at least one incoming arc and one outgoing arc, there always exists a sequence of arcs in \mathbb{D} that form a directed cycle. To put this in another way, there is at least one directed cycle in $\mathbb{D}(\mathbb{G})$. Let us call the shortest of these directed cycles, \mathbb{C}^0 and denote its vertices using the ordered set $\{u(1), \dots, u(N)\}$. In other words, $(u(i), u(i+1)) \in \mathbb{A} \forall i \in \{1, \dots, N-1\}$ and $(u(N), u(1)) \in \mathbb{A}$. In order to prove by contradiction, assume that \mathbb{C}^0 contains a chord with two endpoints $u(k), u(\ell)$ and $k < \ell$. Then, this chord divides \mathbb{C}^0 into two cycles \mathbb{C}^1 and \mathbb{C}^2 such that the symmetric difference of the two becomes \mathbb{C}^0 . Depending on whether $(u(k), u(\ell)) \in \mathbb{A}$ or $(u(\ell), u(k)) \in \mathbb{A}$, exactly one of \mathbb{C}^1 and \mathbb{C}^2 again becomes a directed cycle. This is a contradiction to \mathbb{C}^0 being the shortest directed cycle. So far, we have established that the shortest directed cycle of a given digraph is a chordless cycle of its underlying undirected graph \mathbb{G} . It follows naturally that the length of this shortest directed cycle is less than the length of the longest chordless cycle in \mathbb{G} :

$$\delta(\mathbb{D}) \leq \kappa(\mathbb{G}) \text{ for any } \mathbb{D} \in \mathcal{D}_f(\mathbb{G})$$

Taking the maximum over $\mathbb{D} \in \mathcal{D}_f(\mathbb{G})$ on both sides of the inequality and using the definition of *maximal girth* in (49), we arrive at the desired conclusion.

10.8 Proof of Theorem 6.1

(a) Consider a graph $\mathbb{G} = (\mathbb{V}, \mathbb{E}, \mathbb{W})$ with a dangling vertex k . See Figure 14 for an example, where $k = 1$ is the dangling vertex. By definition, vertex k cannot be part of any cycle. Therefore, if there exists a directed cycle \mathbb{C} that satisfies condition (50) for $\mathbb{G}^r = (\bar{\mathbb{V}}, \bar{\mathbb{E}}, \bar{\mathbb{W}})$, the same cycle also satisfies condition (50) for $\mathbb{G} = (\mathbb{V}, \mathbb{E}, \mathbb{W})$.

(b) Consider a graph $\mathbb{G} = (\mathbb{V}, \mathbb{E}, \mathbb{W})$ with a highway-path. See Figure 15 for an example, where the vertex set $\{1, 2, 3, 4\}$ specify the highway-path. Denote the vertex

set of the highway-path \mathbb{P} as the following:

$$\mathbb{V}^h = \{s, u^h(1), u^h(2), \dots, u^h(H), t\} \quad (75)$$

For $\mathbb{G}^r = (\bar{\mathbb{V}}, \bar{\mathbb{E}}, \bar{\mathbb{W}})$, suppose that condition (50) is satisfied for a directed cycle \mathbb{C}^r that includes the edge $\{s, t\}$. This implies that for $\mathbb{G} = (\mathbb{V}, \mathbb{E}, \mathbb{W})$, condition (50) is satisfied for a directed cycle \mathbb{C} that includes the edges $\{s, u^h(1)\}, \{u^h(1), u^h(2)\}, \dots, \{u^h(H-1), u^h(H)\}$ and $\{u^h(H), t\}$. This is because the edges in a highway-path must either all be part of a cycle or all not be part of any cycle.

(c) Consider a graph $\mathbb{G} = (\mathbb{V}, \mathbb{E}, \mathbb{W})$ with a pair of parallel edges e_1 and e_2 , both connecting the two end-points s and t . For $\mathbb{G}^r = (\bar{\mathbb{V}}, \bar{\mathbb{E}}, \bar{\mathbb{W}})$, suppose that condition (50) is satisfied for a directed cycle \mathbb{C}^r that includes the edge $\{s, t\}$. This implies that for $\mathbb{G} = (\mathbb{V}, \mathbb{E}, \mathbb{W})$, condition (50) is satisfied for a directed cycle \mathbb{C} that either (i) includes only edge e_1 but not e_2 , (ii) includes only edge e_2 but not e_1 , or (iii) includes both edges e_1 and e_2 .

10.9 Proof of Theorem 7.1

We prove that there is a linear-time algorithm by construction. Denote the vertex set of the auxiliary path of the j^{th} outer-cycle by:

$$\mathbb{V}_j^a = \{s_j, u_j^a(1), u_j^a(2), \dots, u_j^a(N_j), t_j\}$$

Set the *primary flow* to be $p(s_j, u_j^a(1))$ and initialize its value to be the average-value of the range

$$[p(s_j, u_j^a(1)), \bar{p}(s_j, u_j^a(1))]$$

. Here, we again abuse some notation so that $p(k, \ell)$ denotes the real power flow from vertex k to ℓ . Then, because all of the intermediate nodes $u_j^a(1), \dots, u_j^a(N_j)$ have degree two, the subsequent flows on the auxiliary path can be calculated by simple arithmetic. Furthermore, due to the *allowable angle* assumption, we can uniquely determine the angle difference across every edge that is part of the auxiliary path. Summing them up will also provide the value for θ_{s_j, t_j} . Also, because of the assumption made in (57), the principal path consists of a single edge. The flow on this edge can be calculated by using the previously calculated θ_{s_j, t_j} . Finally, note that the flows that we calculated so far are all increasing functions of the *primary flow*. This process can be repeated for all outer-cycles in \mathcal{O} until the last cycle \mathbb{C}_R . For \mathbb{C}_R , instead of calculating θ_{s_R, t_R} and then using it to calculate $p(s_R, t_R)$, do the following: $p(s_R, t_R) = p_{t_R} - p(u_R(N_R), t_R)$. Finally, calculate all the angle differences using these flow values and add them around the cycle. If the angle sum is greater than zero, reduce the range of the *primary flow* to $[p(s_j, u_j^a(1)), p(s_j, u_j^a(1))]$ and restart the process; otherwise, if the angle sum is greater than zero, reduce the range of the *primary flow* to $[p(s_j, u_j^a(1)), \bar{p}(s_j, u_j^a(1))]$ and restart the process. We repeat this process until the range is less than ϵ . Calculating all flows

takes $O(|\mathbb{E}|)$ time and this is repeated for $\log(1/\epsilon)$ times if we want ϵ -accuracy. This concludes the proof.

10.10 Additional Figures

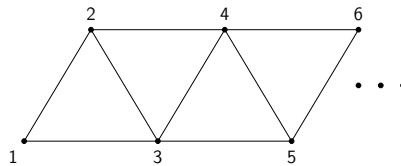


Figure 13: A test network consisting of triangles

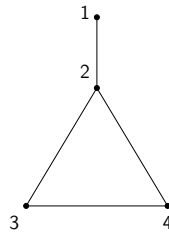


Figure 14: A simple graph with dangling vertex

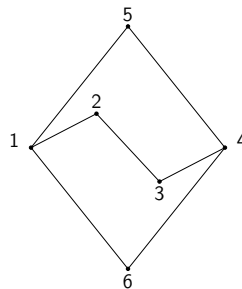


Figure 15: A simple graph with multiple edges in series

Bibliography

- [1] T. Overbye, "Lecture Notes: ECEN 460 power systems operation and control," 2017, available from: <https://overbye.engr.tamu.edu/course-2/ecen460fa2017/lecture-notes/>.

- [2] T. Chen and D. Mehta, "On the network topology dependent solution count of the algebraic load flow equations," *IEEE Transactions on Power Systems*, vol. 33, no. 2, pp. 1451–1460, March 2018, available from: <https://arxiv.org/pdf/1512.04987.pdf>.
- [3] M. Ilic, "Network theoretic conditions for existence and uniqueness of steady state solutions to electric power circuits," in *Proceedings of the IEEE International Symposium on Circuits and Systems*, 1992.
- [4] C. Wang, A. Bernstein, J.-Y. Le Boudec, and M. Paolone, "Explicit conditions on existence and uniqueness of load-flow solutions in distribution networks," *IEEE Transactions on Smart Grid*, vol. 9, no. 2, pp. 953–962, March 2018.
- [5] H. D. Nguyen and K. S. Turitsyn, "Appearance of multiple stable load flow solutions under power flow reversal conditions," in *Proceedings of the IEEE PES General Meeting, National Harbor, MD*, July 2014, available from: <https://arxiv.org/pdf/1404.6591.pdf>.
- [6] H.-D. Chiang and M. E. Baran, "On the existence and uniqueness of load flow solution for radial distribution power networks," *IEEE Transactions on Circuits and Systems*, vol. CAS-37, no. 3, pp. 410–416, March 1990.
- [7] I. A. Hiskens and R. J. Davy, "Exploring the power flow solution space boundary," *IEEE Transactions on Power Systems*, vol. 16, no. 3, pp. 389–395, August 2001.
- [8] F. Galiana, "Analytical investigation of the power flow equations," 1983, pp. 411–415.
- [9] J. Thorp, D. Schulz, and M. Ilic-Spong, "Reactive power-voltage problem: conditions for the existence of solution and localized disturbance propagation," *International Journal of Electrical and Power Energy Systems*, vol. 9, pp. 66–74, January 1986.
- [10] A. Araposthatis, S. Sastry, and P. Varaiya, "Analysis of power-flow equation," *International Journal of Electrical and Power Energy Systems*, vol. 3, pp. 115–126, July 1981.
- [11] K. Miu and H.-D. Chiang, "Existence, uniqueness, and monotonic properties of the feasible power flow solution for radial three-phase distribution networks," *IEEE Transactions on Circuits and Systems*, vol. 47, pp. 1502–1514, October 2000.
- [12] S. Z. S. Bolognani, "On the existence and linear approximation of the power flow solution in power distribution networks," *IEEE Transactions on Power Systems*, vol. 31, pp. 163–172, January 2016.
- [13] J. Lavaei, D. Tse, and B. Zhang, "Geometry of power flows in tree networks," *IEEE Transactions on Power Systems*, vol. 31, pp. 163–172, January 2016.

- [14] K. Dvijotham, S. Low, and M. Chertkov, "Solving the power flow equations: a monotone operator approach," *archived and available at <https://arxiv.org/pdf/1506.08472.pdf>*, 2015.
- [15] E. Ryu and S. Boyd, "A primer on monotone operator methods," *Applied and Computational Mathematics*, vol. 15, no. 1, pp. 3–43, 2016.
- [16] R. Phelps, *Convex Functions, Monotone Operators and Differentiability*, 2nd ed. Springer, 1993.
- [17] H. Bauschke and P. Combettes, *Convex analysis and monotone operator theory in hilbert spaces*, 2nd ed. Springer, 2011.
- [18] R. Baldick, *Applied Optimization: Formulation and Algorithms for Engineering Systems*. Cambridge: Cambridge University Press, 2006.
- [19] S. Park, R. Y. Zhang, R. Baldick, and J. Lavaei, "Monotonicity between phase angles and power flow and its implications for the uniqueness of solutions," *52nd Hawaii International Conference on System Sciences (HICSS)*, 2019.
- [20] N. Korneyenko, "Combinatorial algorithms on a class of graphs," *Discrete Applied Mathematics*, vol. 54, pp. 215–217, 1994.
- [21] Y. Nesterov and L. Scriali, "solving strongly monotone variational and quasi-variational inequalities," *archived and available at <https://ssrn.com/abstract=970903orhttp://dx.doi.org/10.2139/ssrn.970903>*, 2006.
- [22] A.J.Korsak, "On the question of uniqueness of stable load-flow solutions," *IEEE Transactions on Power Apparatus and Systems*, vol. PAS-91, no. 3, pp. 1093–1100, May 1972.
- [23] F.F.Wu, "Theoretical study of the convergence of the fast decoupled load flow," *IEEE Transactions on Power Apparatus and Systems*, vol. PAS-96, no. 1, pp. 268–275, January 1977.
- [24] J. W. Simpson-Porco, "A theory of solvability for lossless power flow equations – part I: Fixed-point power flow," *IEEE Transactions on Control of Network Systems*, vol. 5, no. 3, pp. 1361–1372, September 2018.
- [25] —, "A theory of solvability for lossless power flow equations – part II: Conditions for radial networks," *IEEE Transactions on Control of Network Systems*, vol. 5, no. 3, pp. 1373–1385, September 2018.
- [26] J. Bermond, A. Germa, M. Heydemann, and D. Sotteau, "Girth in digraphs," *Graph Theory*, vol. 4, no. 3, pp. 337–341, 1980.

- [27] V. Chvátal and E. Szemerédi, "Short cycles in directed graphs," *Journal of Combinatorial Theory, Series B*, vol. 35, no. 3, pp. 323–327, 1983.
- [28] R. Zimmerman, C. Murillo-Sanchez, and R. Thomas, "Matpower: Steady-state operations, planning and analysis tools for power systems research and education," *IEEE Transactions on Power Systems*, vol. 26, no. 1, pp. 12–19, 2011.
- [29] K. Dvijotham, E. Mallada, and J. Simpson-Porco, "High-voltage solution in radial power networks: existence, properties, and equivalent algorithms," *IEEE Control Systems Letters*, vol. 1, no. 2, pp. 322–327, October 2017.
- [30] S. Jafarpour, E. Huang, K. Smith, and F. Bullo, "Flow and elastic networks on the n-torus: geometry, analysis, and computation," 2019, available online at <https://arxiv.org/pdf/1901.11189.pdf>.
- [31] T. S. Developers, "Sagemath, the Sage Mathematics Software System (Version 8.9)," 2019, available online at <https://www.sagemath.org>.
- [32] B. Cui and X. A. Sun, "Solvability of power flow equations through existence and uniqueness of complex fixed point," 2019, available online at <https://arxiv.org/pdf/1904.08855.pdf>.
- [33] A. Bernstein, C. Wang, E. Dall'Anese, J.-Y. L. Boudec, and C. Zhao, "Load-flow in multiphase distribution networks: Existence, uniqueness, non-singularity and linear models," *IEEE Transactions on Power Systems*, vol. 33, no. 6, pp. 5832–5843, April 2018.
- [34] D. Lee, H. D. Nguyen, K. Dvijotham, and K. Turitsyn, "Convex restriction of power flow feasible sets," 2019, available online at <https://arxiv.org/pdf/1803.00818.pdf>.

Algorithm 1: Linear-time GSP algorithm

Initialize: Set $\epsilon, \delta^0 > \epsilon, P$ and $\text{iter} = 0$

Delete dangling vertex k and add injection value of $-\hat{r}_{k,\ell}(p_k)$ to its unique adjacent bus ℓ : $P_\ell = P_\ell - \hat{r}_{k,\ell}(p_k)$. Do this for all dangling vertices.

Set reduction order: Find the sequence of outer-cycles that are eliminated during the sp-reduction process. $\Rightarrow \mathcal{O} = \{\mathbb{C}_1, \dots, \mathbb{C}_R\}$

For each cycle $\mathbb{C}_j \in \mathcal{O}$: set the principal (\mathbb{S}_j^p) and auxiliary (\mathbb{S}_j^a) paths of \mathbb{C}_j so that \mathbb{S}_j^p be the path with one edge.

Order the vertices in \mathbb{S}_j^a as $\mathbb{V}_j^a = \{u_j^a(1), \dots, u_j^a(M_j)\}$ so that $(u_j^a(1), u_j^a(2)) \in \mathcal{F}^+$.

Set primary flow x to represent $p(u_1^a(1), u_1^a(2))$. Then, **do**

$\bar{x} = \bar{p}(u_1^a(1), u_1^a(2)), \underline{x} = \underline{p}(u_1^a(1), u_1^a(2)), x^0 = \frac{1}{2}(\bar{x} + \underline{x}), u_0^a(1) = u_1^a(1)$

while $|\delta^{\text{iter}}| > \epsilon$ **do**

for $j=1:R$ **do**

$z = \text{find}(\mathbb{V}_j^a == u_{j-1}^a(1))$

for $f = 1 : z-1$ **do**

$k = u_j^a(z - f), \ell = u_j^a(z - f + 1), q = u_j^a(z - f + 2),$

$p(k, \ell) = \hat{r}_{k,\ell}(P_\ell - p(\ell, q)), \Pi(x^{\text{iter}}, p(k, \ell))$

end

for $f = z : M_j-2$ **do**

$k = u_j^a(f + 1), \ell = u_j^a(f + 2), q = u_j^a(f),$

$p(k, \ell) = P_k - \hat{r}_{q,k}(p(q, k)) \Pi(x^{\text{iter}}, p(k, \ell))$

end

$w_j = \sum_{k=1}^{M_j-1} \theta_{u_j^a(k), u_j^a(k+1)}, p(u_j^a(1), u_j^a(M_j)) = \hat{p}_{u_j^a(1), u_j^a(M_j)}(w_j),$

$P_{u_j^a(1)} = P_{u_j^a(1)} - p(u_j^a(1), u_j^a(2)),$

$P_{u_j^a(M_j)} = P_{u_j^a(M_j)} + p(u_j^a(M_j - 1), u_j^a(M_j))$

Delete dangling vertex k , and add injection value of $-\hat{r}_{k,\ell}(p_k)$ to its unique adjacent bus ℓ : $P_\ell = P_\ell - \hat{r}_{k,\ell}(p_k)$

end

$p(u_R^a(M_R), u_R^a(1)) = P_{u_R^a(M_R)} - p(u_R^a(M_R - 1), u_R^a(M_R))$

$\Pi(x^{\text{iter}}, p(u_R^a(M_R), u_R^a(1))), \delta^{\text{iter}} = w_R + \theta_{u_R^a(M_R), u_R^a(1)}$

if $\delta^{\text{iter}} > 0$ **then**

$\bar{x} = x^{\text{iter}}, x^{\text{iter}+1} = \frac{1}{2}(\bar{x} + \underline{x})$

else

$\underline{x} = x^{\text{iter}}, x^{\text{iter}+1} = \frac{1}{2}(\bar{x} + \underline{x})$

end

$\text{iter} = \text{iter} + 1$

end

Chapter IV

Uniqueness of Power Flow Solutions Using Graph-theoretic Notions

1 Introduction

The AC power flow problem plays a crucial role in various aspects of power systems, e.g., the daily operations in contingency analysis and security-constrained dispatch of electricity markets. In essence, the goal of the AC power flow problem is to solve for the complex voltage of each bus that determines the power system set-point. However, the presence of sinusoidal functions in the AC power flow equations makes it difficult to analytically solve the equations, if not impossible. Moreover, the periodicity of sinusoidal functions destroys the uniqueness of the AC power flow solution, even when either voltage magnitudes or phase angle differences are limited to the “physically realizable” regime [28, 6, 7, 5]. Hence, unexpected operating points may appear for some system conditions and can jeopardize the normal operations of power systems. Conditions that ensure the existence of a unique “physically realizable” power flow solution are important but not fully understood.

For a special case of the AC power flow problem, the uniqueness property of the P - Θ power flow problem [3] has been studied in [28]. In the P - Θ power flow problem, the magnitude of the complex voltage at each node is given and the objective is to find a set of voltage phases such that the power flow equations are satisfied. The “physically realizable” constraint requires that the angular difference across every line lies within the stability limit of $\pi/2$ for lossless networks. Sufficient conditions (on the angular differences) that depend on the topological properties of the power network are established in [28]. Specifically, the authors proposed the notion of monotone regime and an upper bound on the angular differences based on the power network topology, which together can ensure the uniqueness of solutions. However, due to the nonlinear property of sinusoidal functions and the low-rank structure of angular differences, it is unclear to what extent the sufficient conditions given in [28] are necessary.

The goal of this paper is to provide more general necessary and sufficient conditions for the uniqueness, using the notion of maximal eye defined in Section 3 and the notion of maximal girth introduced in [28]. The paper also designs algorithms to compute these graph-theoretic parameters.

1.1 Main results

In this paper, we extend the uniqueness theory of P - Θ power flow problem proposed in [28]. We focus on the uniqueness of the power flow problem in a stronger sense and derive general necessary and sufficient conditions that *depend only on the choice of the monotone regime and network topology*. Under certain circumstances, the general conditions can be simplified to obtain tighter sufficient conditions. In addition, some algorithms for computing the maximal eye and the maximal girth of undirected graphs are proposed. A reduction method is designed to reduce the size of graphs and accelerate the computation process. More specifically, the contributions of this paper are three-folds:

- We extend the uniqueness theory of P - Θ problem to a stronger sense. In [28], two solutions for cyclic graphs are treated as different if all phase angle vectors are different (this is referred to as weak uniqueness). In contrast, in this paper, we consider the uniqueness in the usual sense, i.e., two solutions are different if they are different in at least one phase angle (this is referred to as strong uniqueness). A constant called the maximal eye is developed to classify all network topology that ensure strong uniqueness. Numerical results show that the maximal eye gives more reasonable constraints compared to its counterpart for weak uniqueness, which is known as the maximal girth. Moreover, for 2-vertex-connected Series-Parallel graphs, we prove that the maximal eye is equal to the maximal girth.
- We propose general necessary and sufficient conditions for both the strong and the weak uniqueness. The conditions are derived by Farka's Lemma, which gives the dual problem with simpler solutions. Sufficient conditions for the weak uniqueness in [28] and their counterparts for the strong uniqueness are derived directly from the general conditions. In the special case when the power network is a single cycle or is lossless, stronger necessary and sufficient conditions that do not contain sinusoidal functions are derived.
- Finally, we develop a reduction method, named the SSPR method, that can accelerate the computation of the maximal eye and the maximal girth. The SSPR method is proved to reduce 2-vertex-connected Series-Parallel graphs to a single line, independent of the choice of the slack bus. The relationship between the maximal eye (girth) of graphs before and after the reduction is unveiled. When applying the SSPR method to real-world examples, the maximal eye is usually not changed over the reduction process, while the maximal girth is already computed during the reduction process. We also design search-based algorithms for computing the maximal eye and the maximal girth, which are able to compute the exact value for graphs with up to 100 nodes before reduction.

In summary, this paper constitutes a substantial generalization of the uniqueness theory in [28]. A stronger notion of uniqueness is proposed and general necessary and sufficient conditions are proposed. These two combined provides a tool for analyzing large-scale

power networks and enables a deeper understanding of the uniqueness of the P - Θ power flow problem.

1.2 Related work

The study of solutions to the power flow problem has a long history dating back to [22], which gave an example showing the general non-uniqueness of solutions for the power flow problem. Then, the number of solutions of the power flow problem was estimated in [10], which also characterized the stability region for the power flow problem. However, these early works only considered lossless transmission networks consisting of PV buses. Under the assumption that resistive losses are negligible, conditions for the existence and uniqueness of both real power-phase (P - Θ) problem, and reactive power-voltage (Q - V) problem were derived in [9, 3].

In another line of work, the topology structure of the power network was also considered to derive stronger conditions for the uniqueness. The number of solutions was estimated for radial networks in [6, 11], and later for general networks. Moreover, a more recent work [31] gave several algorithms to compute the unique high-voltage solution. In this paper, we consider the P - Θ problem [3] for general lossy power networks and utilize the topology information. We refer to [28] for a more detailed review of the existing literature.

The fixed-point technique is often used for proving the existence and uniqueness of equations. For the power flow problem, the fixed-point technique was first utilized in [23] and was further developed by several works [12, 4, 24, 25, 35, 34]. Another more recently applied approach is to treat the P - Θ power flow problem as a rank-1 matrix sensing problem and solve its convex relaxation counterpart [44, 45]. The work [14] also considered the domain of voltages over which the power flow operator is monotone. However, the relation between the rank-1-constrained problem and its convexification is not clear for general power networks.

The work [32] presented a unifying framework for network problems on the n -torus. The framework applies to the AC power flow problem when the power networks are lossless. The idea of considering the regime when the power flow on each line is monotone was extended to lossy power networks in [28]. The regime where the power flow on a line increases monotonically with the angle difference across the line – called the monotone regime in this paper – was proposed. In [28], it was also shown that the solution of P - Θ problem is unique under the assumption that angle differences across the lines are bounded by some limit related to the maximal girth of the network [46].

The existing algorithms in the literature cannot be directly used to compute maximal eye (introduced in Section 3) or maximal girth. A related problem is computing the maximal chordless cycle as an upper bound to these parameters. The computation of maximal chordless cycles was proved to be \mathcal{NP} -complete in [43]. Efficient algorithms for enumerating chordless cycles were proposed in [41, 42] and both take linear time to enumerate a single chordless cycle. The algorithms for enumerating maximal chordless cycles can be easily modified to compute the minimal chordless cycle containing a given

edge. Series-parallel reduction method was introduced as an alternative definition of Generalized Series-Parallel (GSP) graphs in [20]. Under the assumption that the slack bus is the last bus to be reduced, all GSP graphs can be reduced to a single line [28]. However, whether the series-parallel reduction method can still reduce GSP graphs without the assumption on the slack bus is not known. In this paper, we show that 2-vertex-connected³ Series-Parallel graphs can be reduced to a single line without the assumption.

1.3 Notations

We start with some mathematical notations. We use $\mathbb{N}, \mathbb{Z}, \mathbb{R}, \mathbb{C}$ to denote the set of all natural numbers, integers, real numbers and complex numbers, respectively. We denote $[n] := \{1, \dots, n\}$ for any $n \in \mathbb{N}$. The symbol \mathbf{j} denotes the unit imaginary number. The notations $(\cdot)^T$ and $(\cdot)^H$ denote the transpose and Hermitian transpose of a matrix, respectively. For a complex number z , $|z|$ denotes its magnitude and for a set X , the symbol $|X|$ denotes its cardinality. $\Re(\cdot)$ denotes the real part of a given scalar or matrix.

For an undirected graph, the set of vertices and the set of edges are denoted as \mathbb{V} and \mathbb{E} , respectively. If the edges of an undirected graph are weighted with the weights captured by a matrix $W \in \{\pm 1\}^{|\mathbb{V}| \times |\mathbb{V}|}$, then the graph is represented as $(\mathbb{V}, \mathbb{E}, W)$. For a directed graph $(\mathbb{V}, \mathbb{E}, A)$, the matrix $A \in \mathbb{R}^{|\mathbb{V}| \times |\mathbb{V}|}$ gives the orientation of each line. The undirected edge connecting two vertices k and ℓ is denoted by a set notation $\{k, \ell\}$, whereas (k, ℓ) denotes a directed edge coming out of vertex k and going into ℓ . For parallel edges, we use $\{k, \ell, i\}$ to represent different edges connecting k and ℓ , where $i \in \mathbb{Z}_+$ is the index of each parallel edge.

A power network $\mathbb{G} = (\mathbb{V}, \mathbb{E}, Y)$ consists of two parts: the underlying undirected graph (\mathbb{V}, \mathbb{E}) and the complex admittance matrix $Y \in \mathbb{C}^{n \times n}$, where n is the number of vertices in the underlying graph. The underlying graph is assumed to be a simple and connected graph. The set of vertices \mathbb{V} and the set of edges \mathbb{E} correspond to the set of buses and the set of lines of the power network. The series element of the equivalent Π -model of each line $\{k, \ell\}$ is modeled by admittance $Y_{k\ell} = G_{k\ell} - \mathbf{j}B_{k\ell}$, where $G_{k\ell}, B_{k\ell} \geq 0$.

We denote $\mathbf{v} \in \mathbb{C}^n$ as the vector of complex bus voltages. The complex voltage at bus k can be written in the polar form using its magnitude and phase angle $v_k = |v_k|e^{\mathbf{j}\Theta_k}$ for all $k \in [n]$, where $|v_k| \in \mathbb{R}$ and $\Theta_k \in \mathbb{R}$ denote the voltage magnitude and phase angle, respectively. We denote $\Theta_{k\ell} := \Theta_k - \Theta_\ell \in [-\pi, \pi)$ as the phase difference modulus by 2π for all $\{k, \ell\} \in \mathbb{E}$. In the rest of the paper, we use the corresponding values in $[-\pi, \pi)$ for phase differences.

1.4 Paper organization

The remainder of this paper is organized as follows. Section 2 gives the necessary background knowledge about the P - Θ power flow problem and the existing uniqueness theory for the P - Θ problem. The notions of strong uniqueness and weak uniqueness are also

³A graph is called 2-vertex-connected if it is connected after the deletion of any single vertex.

introduced. In Section 3, we propose the general analysis framework of the uniqueness theory that only depends on the monotone regime and the topological structure. We show that necessary and sufficient conditions can be fully characterized by a feasibility problem, which has fewer variables than the P - Θ problem. Sufficient conditions for uniqueness are derived and it is shown that the uniqueness conditions in [28] follow as a natural corollary. Then, we consider three special cases in Section 4 by assuming specific topological structures for the underlying graph or a specific monotone regime. In these special cases, the necessary and sufficient conditions are simplified and the intricate sinusoidal functions are avoided in the verification of those conditions. Furthermore, the sufficient conditions proposed in Section 3 are proved to be tight when no information beyond the monotone regime and the topological structure is available. Finally, a reduction method and search-based algorithms for computing the maximal girth and maximal eye are given in Section 5. Proofs are delineated in the technical report [29].

2 Preliminaries

2.1 P - Θ problem formulation

As mentioned in the introduction, we focus our attention to the P - Θ problem, which describes the relationship between the voltage phasor angles and the real power injections. We assume that the slack bus and the reference bus are bus 1, and that all other buses except the slack bus are PV buses. Recall that the following injection operator describes the P - Θ problem, where the shunt elements are assumed to be purely reactive.

Definition 2.1. Define $\hat{P}_k : \{0\} \times \mathbb{R}^{n-1} \rightarrow \mathbb{R}$ as the map from the vector of phasor angles to the real power injection at bus k :

$$\hat{P}_k(\Theta) := \Re\{(Yv)_k^H v_k\} \quad \forall \Theta \in \{0\} \times \mathbb{R}^{n-1}.$$

Moreover, define the injection operator $\hat{P} : \{0\} \times \mathbb{R}^{n-1} \rightarrow \mathbb{R}^{n-1}$ as

$$\hat{P}(\Theta) := [\hat{P}_2(\Theta), \dots, \hat{P}_n(\Theta)].$$

The goal of the P - Θ problem is, given $P \in \mathbb{R}^{n-1}$, to find the voltage phasor angles $\Theta \in \{0\} \times \mathbb{R}^{n-1}$ such that

$$\hat{P}(\Theta) = P. \tag{76}$$

2.2 Monotone regime and allowable sets

We are interested in the uniqueness property of the solution to problem (76). In general, the number of solutions to problem (76) is hard to estimate because of the periodic behavior of sinusoidal functions, especially when there is no symmetrical structure in the

power network. Thus, we limit the phase angle vectors to the monotone regime, within which the real power flow from bus k to bus ℓ increases monotonically with respect to the phase difference $\Theta_{k\ell}$ for each line $\{k, \ell\} \in \mathbb{E}$. The monotone regime is defined in [28] as follows.

Definition 2.2. *The **monotone regime** of a power network $(\mathbb{V}, \mathbb{E}, Y)$ is the set*

$$\{\Theta \in \mathbb{R}^n \mid \Theta_1 = 0, \Theta_{k\ell} \in [-\gamma_{k\ell}, \gamma_{k\ell}], \forall \{k, \ell\} \in \mathbb{E}\},$$

where $\gamma_{k\ell} := \tan^{-1}(B_{k\ell}/G_{k\ell}) \in [0, \pi/2]$ for all $\{k, \ell\} \in \mathbb{E}$.

Restricting the voltage phase angle vectors to the monotone regime is necessary for the uniqueness of solution to problem (76) and facilitates the theoretical analysis. The constraint that the angular difference across every line lies within the stability limit of $[-\gamma_{k\ell}, \gamma_{k\ell}]$ is equivalent to the steady-state stability limit if each line is considered individually. As shown in [28], the phase angle vectors of leaf buses except the slack bus are uniquely determined by the phase angle vectors of non-leaf buses in the monotone regime. Hence, we assume that all vertices in the underlying graph except vertex 1 have degree at least 2.

Assumption 2. *The graph (\mathbb{V}, \mathbb{E}) is connected. All vertices except vertex 1 in the graph (\mathbb{V}, \mathbb{E}) have degree at least 2.*

We focus on finding a neighborhood of a solution in which there is no other solution to the P - Θ problem. The neighborhood is defined as follows.

Definition 2.3. *The set of **allowable perturbations** is defined as*

$$\mathcal{W} := \{\omega_{k\ell} \geq 0 \mid \forall \{k, \ell\} \in \mathbb{E}\}.$$

Suppose that Θ is a solution to the $P - \Theta$ problem in the monotone regime. Then, the set of **neighboring phases** is defined as

$$\begin{aligned} \mathcal{N}(\mathbb{G}, \Theta, \mathcal{W}) &:= \{\tilde{\Theta} \in \mathbb{R}^n \mid \tilde{\Theta}_1 = 0, \\ &\tilde{\Theta}_{k\ell} \in [-\gamma_{k\ell}, \gamma_{k\ell}] \cap [\Theta_{k\ell} - \omega_{k\ell}, \Theta_{k\ell} + \omega_{k\ell}], \forall \{k, \ell\} \in \mathbb{E}\}. \end{aligned}$$

We note that $\tilde{\Theta}_{k\ell}$ refers to the value of $\tilde{\Theta}_k - \tilde{\Theta}_\ell$ modulo 2π . Without loss of generality, we assume that $\omega_{k\ell} \leq 2\gamma_{k\ell}$ for all $\{k, \ell\} \in \mathbb{E}$, since the width of the monotone regime is $2\gamma_{k\ell}$ and setting $\omega_{k\ell} > 2\gamma_{k\ell}$ will not enlarge the set of neighboring phases compared to setting $\omega_{k\ell} = 2\gamma_{k\ell}$.

It is desirable to analyze the uniqueness of the solution in the neighborhood $\mathcal{N}(\mathbb{G}, \Theta, \mathcal{W})$. In [28], the authors considered the *set of allowable angles*, which is defined as

$$\{\tilde{\Theta} \in \mathbb{R}^n \mid \tilde{\Theta}_1 = 0, \tilde{\Theta}_{k\ell} \in [-\omega_{k\ell}/2, \omega_{k\ell}/2], \forall \{k, \ell\} \in \mathbb{E}\}.$$

Note that the set of allowable angles is a special case of the set of allowable perturbations, since any two phase vectors in the set of allowable angles are in the corresponding sets of neighboring phases of each other. In this paper, we use the *set of allowable perturbations* but the sufficient conditions we derive can be naturally applied to using the *set of allowable phases*.

2.3 Notions of weak and strong uniqueness

Informally, we say that the P - Θ problem (76) has a unique solution Θ under the allowable perturbation set \mathcal{W} , if there exists at most one solution in the set $\mathcal{N}(\mathbb{G}, \Theta, \mathcal{W})$. We give two different definitions of uniqueness. Firstly, we introduce the uniqueness in the weak sense.

Definition 2.4. *We say that a solution Θ to the P - Θ problem (76) is **weakly unique** with the given set of allowable perturbations \mathcal{W} , if for any solution $\tilde{\Theta} \in \mathcal{N}(\mathbb{G}, \Theta, \mathcal{W})$, there exists a line $\{k, \ell\} \in \mathbb{E}$ such that $\Theta_{k\ell} = \tilde{\Theta}_{k\ell}$.*

In other words, two solutions are different according to Definition 2.4 if and only if they have different phase differences for every line. Next, we extend the definition of weak uniqueness to a stronger sense that is also more useful and usual.

Definition 2.5. *We say that a solution Θ to the P - Θ problem (76) is **strongly unique** with the given set of allowable perturbations \mathcal{W} , if for any solution $\tilde{\Theta} \in \mathcal{N}(\mathbb{G}, \Theta, \mathcal{W})$ and any $\{k, \ell\} \in \mathbb{E}$, we have $\Theta_{k\ell} = \tilde{\Theta}_{k\ell}$.*

In other words, two solutions are different according to Definition 2.5 if and only if the phase differences are different on at least one line. We mention that two different solutions to problem (76) according to Definition 2.5 correspond to two different solutions to problem (76) according to Definition 2.4 for a “power sub-network”. To understand this, suppose that Θ^1 and Θ^2 are two different solutions according to Definition 2.5 and let $\Delta_{k\ell} := \Theta_{k\ell}^1 - \Theta_{k\ell}^2$ be the difference between the solutions on each line $\{k, \ell\} \in \mathbb{E}$. If $\Delta_{k\ell} = 0$ for some line $\{k, \ell\} \in \mathbb{E}$, then we can create another power system by removing the line $\{k, \ell\}$ such that Θ_1 and Θ_2 become the solutions to the new power system. This can be achieved by adding a generator or a load at bus k that matches the power flow from ℓ to k and adding a generator or a load at bus ℓ that matches the power flow from k to ℓ . Note that the original solutions Θ^1 and Θ^2 still solve the power flow equations for the sub-network with some generators or loads added and the line removed. We can repeat this process until the difference $\Delta_{k\ell}$ becomes nonzero for all remaining lines $\{k, \ell\}$. If some bus becomes a singleton, we can omit it since it does not affect the uniqueness of power flow solutions. If the slack bus becomes a singleton, we can choose another arbitrary bus as the new slack bus, since the real power injection is the same for both solutions at PV buses. Now, the two solutions are different according to Definition 2.4 on the “power sub-network” of the original power network. Hence, the strong uniqueness can be implied if we ensure the weak uniqueness on all “possible sub-networks”.

3 Uniqueness Theory for General Graphs

In this section, we derive necessary and sufficient conditions on the set of allowable perturbations \mathcal{W} such that the solution to problem (76) becomes strongly or weakly unique. In particular, we aim to analyze *the impact of the power system topology and the size of the monotone regime* on the uniqueness property. Namely, given the topological structure and the monotone regime, we aim to find conditions on \mathcal{W} such that the uniqueness of solutions holds. To achieve this, we need to derive conditions under which all power networks with the same topological structure and monotone regime have unique solutions. To formalize the problem, we fix the underlying graph (\mathbb{V}, \mathbb{E}) and the angles specifying the monotone regime $\Gamma := \{\gamma_{k\ell} \in (0, \pi/2] \mid \{k, \ell\} \in \mathbb{E}\}$. We define the set of possible admittances with the same monotone regime as

$$\mathcal{S}(\gamma) := \{(C \cos(\gamma), C \sin(\gamma)) \mid C > 0\} \quad \forall \gamma \in [0, \pi/2].$$

The set of complex admittance matrices with the same monotone regime is defined as

$$\begin{aligned} \mathcal{Y}(\mathbb{V}, \mathbb{E}, \Gamma) := \{Y \text{ is an admittance matrix} \mid \\ Y_{k\ell} = G_{k\ell} - \mathbf{j}B_{k\ell}, (G_{k\ell}, B_{k\ell}) \in \mathcal{S}(\gamma_{k\ell}), \{k, \ell\} \in \mathbb{E}\}. \end{aligned}$$

Then, we define the set of power networks with the same topological structure and same monotone regime as

$$\mathcal{G}(\mathbb{V}, \mathbb{E}, \Gamma) := \{\mathbb{G} = (\mathbb{V}, \mathbb{E}, Y) \mid Y \in \mathcal{Y}(\mathbb{V}, \mathbb{E}, \Gamma)\},$$

or simply \mathcal{G} if there is no confusion about \mathbb{V} , \mathbb{E} and Γ . Hence, the problem under study in this paper can be stated as follows:

- What are the necessary conditions and sufficient conditions on the allowable perturbations \mathcal{W} such that the solution to problem (76) is unique within the set of allowable perturbations for any power network $\mathbb{G} \in \mathcal{G}$?

The necessary conditions and the sufficient conditions provide two sides on the uniqueness theory. The sufficient conditions give a guarantee for the uniqueness of solutions for any single power network with the given topological structure and monotone regime, while the necessary conditions bound the optimal conditions we can derive only using the knowledge of topological structure and monotone regime. We first give an equivalent characterization of strong and weak uniqueness.

Lemma 3.1. (Necessary and Sufficient Conditions for Uniqueness) *Given the set of power networks $\mathcal{G}(\mathbb{V}, \mathbb{E}, \Gamma)$ and the set of allowable perturbations \mathcal{W} , the following two statements are equivalent:*

- 1) *For any power network $\mathbb{G} \in \mathcal{G}(\mathbb{V}, \mathbb{E}, \Gamma)$ and any power injection $P \in \mathbb{R}^{|\mathbb{V}|-1}$ such that problem (76) is feasible in the monotone regime, the solution to problem (76) in the monotone regime is strongly unique in $\mathcal{N}(\mathbb{G}, \Theta, \mathcal{W})$.*

- 2) For any power network $\mathbb{G} \in \mathcal{G}(\mathbb{V}, \mathbb{E}, \Gamma)$ and any two phase angle vectors Θ^1, Θ^2 in the monotone regime with the property $\Theta^2 \in \mathcal{N}(\mathbb{G}, \Theta^1, \mathcal{W})$, there exists a vector $\mathbf{y} \in \mathbb{R}^{|\mathbb{V}|}$ such that $y_1 = 0$ and

$$\begin{aligned} \sin(\gamma_{k\ell} + \Theta_{k\ell}^1/2 + \Theta_{k\ell}^2/2) \cdot y_k & \quad (77) \\ & \geq \sin(\gamma_{k\ell} - \Theta_{k\ell}^1/2 - \Theta_{k\ell}^2/2) \cdot y_\ell \\ & \quad \forall \{k, \ell\} \in \mathbb{E} \quad \text{s.t. } \Theta_{k\ell}^1 - \Theta_{k\ell}^2 > 0, \end{aligned}$$

where at least one of the inequalities above is strict.

The equivalence between statements 1 and 2 still holds true even after replacing strong uniqueness with weak uniqueness in statement 1, provided that the phase angle vector Θ^2 in statement 2 is required to satisfy $\Theta_{k\ell}^1 \neq \Theta_{k\ell}^2$ for all $\{k, \ell\} \in \mathbb{E}$.

Intuitively, the above lemma studies the uniqueness of solutions through its dual form. The dual form is preferred since the dual problem has fewer variables and its solution is easier to construct. We then derive several sufficient conditions using Lemma 3.1. We first show that we only need to verify statement 2 in Lemma 3.1 for two phase angle vectors Θ^1 and Θ^2 that induce a (weakly) feasible orientation, which we will define below. We define the orientation induced by two phase angle vectors.

Definition 3.1. Suppose that Θ^1 and Θ^2 are two phase angle vectors of the graph. Then, we define the **induced orientation** of $\Delta := \Theta^1 - \Theta^2$ as $A_{k\ell} := \text{sign}(\Delta_{k\ell})$ for all $\{k, \ell\} \in \mathbb{E}$, where the sign function $\text{sign}(\cdot)$ is defined as

$$\text{sign}(x) := \begin{cases} +1 & \text{if } x > 0 \\ 0 & \text{if } x = 0 \\ -1 & \text{if } x < 0 \end{cases}.$$

In the definition of induced orientations, we assign one of the three directions $+1, -1, 0$ to each edge. The first two directions are “normal” directions for directed graphs. An edge with direction $+1$ or -1 is called a **normal edge**. Edges with direction 0 are viewed as an undirected edge and reachable in both directions. In addition, edges with direction 0 are not considered when computing the in-degree and the out-degree. We only need to consider orientations induced by two different phase angle vectors Θ^1, Θ^2 such that $\hat{P}(\Theta^1) = \hat{P}(\Theta^2)$. However, a precise characterization of those orientations is difficult and we consider a larger set that contains those orientations.

Definition 3.2. An orientation assigned to an undirected graph is called a **feasible orientation** if all edges are normal and each vertex except vertex 1 has nonzero in-degree and out-degree.

According to the analysis in [28], the induced orientation of two solutions Θ^1 and Θ^2 in the monotone regime that are different according to Definition 2.4 must be a feasible

orientation. Then, we give the definition of weakly feasible orientations as the counterpart for strong uniqueness.

Definition 3.3. *An orientation assigned to an undirected graph is called a **weakly feasible orientation** if two properties are satisfied: (i) there exists at least one normal edge, and (ii) the in-degree and the out-degree of any vertex except vertex 1 are both zero or both nonzero.*

Edges with direction 0 are lines with the same angular difference in two phase angle vectors. By the same discussion as in Section 2, we can view a weakly feasible orientation as a feasible orientation for the sub-graph that only has normal edges. The next lemma shows that we only need to consider weakly feasible orientations or feasible orientations when checking the conditions in statement 2 of Lemma 3.1.

Lemma 3.2. *If two different phase angle vectors $\Theta^1 - \Theta^2$ in the monotone regime satisfy $\Theta^2 \in \mathcal{N}(\mathbb{G}, \Theta^1, \mathcal{W})$ and the induced orientation of $\Theta^1 - \Theta^2$ is not weakly feasible, then there exists a vector $\mathbf{y} \in \mathbb{R}^{|\mathcal{V}|}$ such that statement 2 of Lemma 3.1 holds. The result holds true for the weak uniqueness property as well, provided that the induced orientation of Θ^1, Θ^2 is not a feasible orientation.*

Combining Lemmas 3.1 and 3.2, we obtain sufficient conditions for strong uniqueness and weak uniqueness.

Theorem 3.3. (Sufficient Conditions for Uniqueness) *Given the set of allowable perturbations \mathcal{W} , suppose that for any two different phase angle vectors Θ^1 and Θ^2 in the monotone regime satisfying $\Theta_2 \in \mathcal{N}(\mathbb{G}, \Theta^1, \mathcal{W})$, the induced orientation of $\Theta^1 - \Theta^2$ is not a weakly feasible orientation. Then, the solution to problem (76) is strongly unique for all power networks in \mathcal{G} . The result holds true for the weak uniqueness as well, provided that the induced orientation of $\Theta^1 - \Theta^2$ is not a feasible orientation.*

The sufficient condition given above is a generalization of Theorem 4 in [28], which ensures the weak uniqueness of solutions in the set of allowable phases. Using Theorem 3.3, we can derive a corollary similar to Theorem 4 in [28].

Corollary 3.4. *Consider an arbitrary set of allowable perturbations \mathcal{W} . The solution to problem (76) in the monotone regime is strongly unique for any power network $\mathbb{G} \in \mathcal{G}$ if for any weakly feasible orientation of the underlying graph (\mathbb{V}, \mathbb{E}) , there exists a directed cycle (k_1, \dots, k_t) containing at least one normal edge such that the allowable perturbations satisfy the inequality*

$$\sum_{\{k_i, k_{i+1}\} \text{ is normal}} \omega_{k_i k_{i+1}} < 2\pi,$$

where $k_{t+1} := k_1$. The same result holds true for the weak uniqueness if we substitute weakly feasible orientations with feasible orientations.

Now, we consider a special case where all constants $\omega_{k\ell}$ in the set of allowable perturbations are equal, i.e., there exists a constant $\omega \geq 0$ such that the set of allowable perturbation is

$$\mathcal{W}_\omega := \{\omega_{k\ell} = \omega, \forall \{k, \ell\} \in \mathbb{E}\}.$$

The problem we consider in this case is:

- What is the sufficient condition on ω such that the solution to problem (76) is unique with the allowable perturbation set \mathcal{W}_ω ?

We derive an upper bound on the constant ω to guarantee the uniqueness. We first define the maximal eye and the maximal girth of an undirected graph.

Definition 3.4. Consider an undirected graph (\mathbb{V}, \mathbb{E}) . For any weakly feasible orientation assigned to the graph (\mathbb{V}, \mathbb{E}) , we define the minimal length of directed cycles that contain at least one normal edge as the **size of eye** of this orientation, where edges with direction 0 are considered as bi-directional edges. We define the **maximal eye** of the graph (\mathbb{V}, \mathbb{E}) as the maximum of the size of eye over all possible weakly feasible orientations. We denote the maximal eyes of the graph (\mathbb{V}, \mathbb{E}) , a power network \mathbb{G} and a group of power networks \mathcal{G} as $e(\mathbb{V}, \mathbb{E})$, $e(\mathbb{G})$ and $e(\mathcal{G})$, respectively.

Remark 1. There always exists a directed cycle containing normal edges when the underlying graph is under a weakly feasible orientation. To understand this, we first choose an arbitrary normal edge $(k_1, k_2) \in \mathbb{E}$. Since the vertex k_2 has nonzero in-degree, it also has nonzero out-degree. Hence, there exists another vertex k_3 such that $(k_2, k_3) \in \mathbb{E}$. Continuing this procedure will result in the existence of a vertex k_t such that $v_t = k_s$ for some $s < t$. This generates a directed cycle $(k_s, k_{s+1}, \dots, k_{t-1})$ containing only normal edges. Hence, the size of eye is well-defined.

The counterpart of the maximal eye, known as the maximal girth, is defined in [28] and we restate the definition below.

Definition 3.5. Consider an undirected graph (\mathbb{V}, \mathbb{E}) . For any feasible orientation assigned to the underlying graph (\mathbb{V}, \mathbb{E}) , we define the minimal size of directed cycles as the **girth** of this feasible orientation. We define the **maximal girth** of the graph (\mathbb{V}, \mathbb{E}) as the maximum of the girth over all feasible orientations. We denote the maximal girths of the graph (\mathbb{V}, \mathbb{E}) , a power network \mathbb{G} and a group of power networks \mathcal{G} as $g(\mathbb{V}, \mathbb{E})$, $g(\mathbb{G})$ and $g(\mathcal{G})$, respectively.

Remark 2. Similar to the discussion in Remark 1, there exists at least one directed cycle when the graph is under a feasible orientation. The maximal eye can be equivalently defined as the maximum of the maximal girth over all sub-graphs that do not have degree-1 vertices.

We provide an upper bound for ω using the maximal eye and the maximal girth, which follows from Corollary 3.4.

Corollary 3.5. *If the inequality*

$$\omega_{k\ell} < \frac{2\pi}{e(\mathcal{G})} \quad \forall \{k, \ell\} \in \mathbb{E}, \quad (78)$$

is satisfied, then the solution to problem (76) in the monotone regime is strongly unique for any power network $\mathbb{G} \in \mathcal{G}$. The same result holds true for weak uniqueness, provided that $e(\mathcal{G})$ in (78) is substituted by $g(\mathcal{G})$.

In Section 5, we design search-based algorithms to calculate the maximal eye and the maximal girth. However, computing the maximal eye or the maximal girth is challenging for graphs with more than 100 nodes. Hence, we seek upper bounds and lower bounds for the maximal eye and the maximal girth. In this paper, we obtain a simple upper bound for both the maximal girth and the maximal eye. We define $\kappa(\mathbb{G})$ and $\kappa(\mathcal{G})$ as the sizes of the longest chordless cycles of the underlying graph of the power network \mathbb{G} and any power network in the power network class \mathcal{G} , respectively. The upper bound on the maximal girth and eye will be provided below.

Theorem 3.6. *For any power network \mathbb{G} , it holds that*

$$g(\mathbb{G}) \leq e(\mathbb{G}) \leq \kappa(\mathbb{G}) \quad (79)$$

and that $g(\mathcal{G}) \leq e(\mathcal{G}) \leq \kappa(\mathcal{G})$.

We note that although computing the longest chordless cycle is \mathcal{NP} -complete [43], the computation of the longest chordless cycle is faster than the computation of the maximal eye and the maximal girth in practice.

4 Uniqueness Theory for Three Special Cases

In this section, we consider three special cases. For each case, the power network either has a special topological structure or a special monotone regime. In the first two cases, the underlying graph of the power network is a single cycle or a 2-vertex-connected Series-Parallel (SP) graph. When the underlying graph is a single cycle, the sufficient conditions in Corollary 3.4 are also necessary. If the underlying graph is a 2-vertex-connected SP graph, we prove that the sufficient conditions for the weak uniqueness in Corollary 3.5 also ensure the strong uniqueness. In the last case, the power network is assumed to be lossless. In this case, the monotone regime of each line reaches the maximum possible size $[-\pi/2, \pi/2]$. Sinusoidal functions can then be avoided in statement 2 of Lemma 3.1, and therefore the verification of conditions is easier.

4.1 Single cycles

We first consider the case when the underlying graph (\mathbb{V}, \mathbb{E}) is a single cycle. We first show that the weak uniqueness is equivalent to the strong uniqueness in this case.

Lemma 4.1. *Suppose that the underlying graph is a single cycle with the edges $(1, 2), (2, 3), \dots, (n, 1)$. Then, given the set of allowable perturbations \mathcal{W} , the solution to problem (76) in the monotone regime is weakly unique if and only if it is strongly unique.*

Next, we prove that the sufficient conditions derived in Corollary 3.4 are also necessary for a single cycle with non-trivial monotone regime.

Theorem 4.2. *Suppose that the underlying graph is a single cycle with the edges $(1, 2), (2, 3), \dots, (n, 1)$, and that the set of allowable perturbations satisfies $0 < \omega_{i,i+1} \leq \gamma_{i,i+1}$ for all $i \in [n]$, where $\gamma_{n,n+1} := \gamma_{n,1}$ and $\omega_{n,n+1} := \omega_{n,1}$. The solution to problem (76) in the monotone regime is strongly unique for any power network $\mathbb{G} \in \mathcal{G}(\mathbb{V}, \mathbb{E}, \Gamma)$ and any power injection $P \in \mathbb{R}^{n-1}$ that makes problem (76) feasible if and only if the set of allowable perturbations \mathcal{W} satisfies*

$$\sum_{i=1}^n \omega_{i,i+1} < 2\pi,$$

where $\omega_{n,n+1} := \omega_{n,1}$.

In contrast to requiring $\omega_{i,i+1} > 0$ in the above theorem, the condition that $\omega_{i,i+1} = 0$ for some i is sufficient but not necessary for the uniqueness of solutions. Under this condition, two solutions Θ^1 and Θ^2 in the monotone regime such that $\Theta^2 \in \mathcal{N}(\mathbb{G}, \Theta^1, \mathcal{W})$ must satisfy $\Theta_{i,i+1}^1 = \Theta_{i,i+1}^2$. Hence, any solution is strongly unique with this set of allowable perturbations. However, by Theorem 4.2, this condition is not necessary for the uniqueness of solutions.

4.2 Series-Parallel graphs

In this subsection, we consider another special class of graphs, namely, the 2-vertex-connected SP graphs. The objective is to find an upper bound on the constant ω to guarantee that the solution to problem (76) is unique. Corollary 3.5 shows that the solution is strongly unique if $\omega < 2\pi/e(\mathbb{G})$ and is weakly unique if $\omega < 2\pi/g(\mathbb{G})$. However, for a 2-vertex-connected SP graph, we can prove a stronger theorem. We first prove that the maximal eye is equal to the maximal girth for a 2-vertex-connected SP graph. The main tool is the ear decomposition of an undirected graph [38].

Definition 4.1. *An ear of an undirected graph (\mathbb{V}, \mathbb{E}) is a simple path or a single cycle. An ear decomposition of an undirected graph (\mathbb{V}, \mathbb{E}) , denoted as $\mathcal{D} := (L_0, \dots, L_{r-1})$, is a partition of \mathbb{E} into an ordered sequence of ears such that one or two endpoints of each ear L_k are contained in an earlier ear, i.e., an ear L_ℓ with $\ell < k$, and the internal vertices of each ear do not belong to any earlier ear. We call \mathcal{D} a **proper ear decomposition** if each ear L_k is a simple path for all $k = 1, \dots, r-1$. A **tree ear decomposition** is a proper ear decomposition in which the first ear is a single edge and for each subsequent ear L_k , there is a single ear L_ℓ with $\ell < k$, such that both endpoints of L_k lie on L_ℓ . A **nested ear decomposition** is a tree ear decomposition such that, within each ear L_ℓ ,*

the set of pairs of endpoints of other ears L_k that lie within L_ℓ forms a set of nested intervals.

The following theorem in [39] provides an equivalent characterization of 2-vertex-connected SP graphs through the ear decomposition.

Theorem 4.3. *A 2-vertex-connected graph is series-parallel if and only if it has a nested ear decomposition.*

With the help of the nested ear decomposition, we will prove that the maximal girth is equal to the maximal eye for 2-vertex-connected SP graphs. The intuition behind the proof is that we first choose two vertices as the “source” and the “sink” for the power flow network, and then assign a normal direction to each edge with direction 0 according to the directed path that contains this edge and goes from the “source” to the “sink”. This makes the first inequality in (79) holds as equality.

Lemma 4.4. *Suppose that (\mathbb{V}, \mathbb{E}) is a 2-vertex-connected SP graph. Then, the following equality holds true:*

$$g(\mathbb{V}, \mathbb{E}) = e(\mathbb{V}, \mathbb{E}).$$

Therefore, combining the above lemma with Corollary 3.5, we obtain a stronger sufficient condition for 2-vertex-connected SP graphs. This result implies that the sufficient conditions for the weak uniqueness in Corollary 3.5 also guarantee the strong uniqueness.

Theorem 4.5. *Suppose that the underlying graph (\mathbb{V}, \mathbb{E}) is a 2-vertex-connected SP graph. The solution to problem (76) is strongly unique for any power network $\mathbb{G} \in \mathcal{G}$ in the monotone regime if*

$$\omega < \frac{2\pi}{g(\mathcal{G})}.$$

4.3 Lossless networks

Finally, we consider the case when the power network is lossless, namely, when $\gamma_{k\ell} = \pi/2$ for all $\{k, \ell\} \in \mathbb{E}$. In this case, we prove that the strong uniqueness holds if and only if there does not exist another solution in the set of neighboring phases such that the induced orientation has strictly more strongly connected components than weakly connected components. This results makes it possible to avoid nonlinear sinusoidal functions in statement 2 of Lemma 3.1, and therefore the uniqueness of solutions becomes easier to verify. We first define the sub-graph induced by two phase angle vectors.

Definition 4.2. *Suppose that Θ^1 and Θ^2 are two different phase angle vectors, and that the orientation A is the induced orientation of $\Theta^1 - \Theta^2$. Then, the **induced sub-graph** of $\Theta^1 - \Theta^2$ is constructed as a directed sub-graph of $(\mathbb{V}, \mathbb{E}, A)$ by first deleting all edges with direction 0 and then deleting all degree-1 vertices.*

In what follows, we establish a necessary and sufficient condition for the uniqueness of the solution that does not contain sinusoidal functions.

Theorem 4.6. *Consider a that the set of allowable perturbations \mathcal{W} . If the monotone regime satisfies $\gamma_{k\ell} = \pi/2$ for all $\{k, \ell\} \in \mathbb{E}$, then the following two statements are equivalent:*

- 1) *For any power network $\mathbb{G} \in \mathcal{G}(\mathbb{V}, \mathbb{E}, \Gamma)$ and any power injection $P \in \mathbb{R}^{|\mathbb{V}|-1}$ such that problem (76) is feasible, the solution to problem (76) in the monotone regime is strongly unique in $\mathcal{N}(\mathbb{G}, \Theta, \mathcal{W})$.*
- 2) *For any power network $\mathbb{G} \in \mathcal{G}(\mathbb{V}, \mathbb{E}, \Gamma)$ and any two phase angle vectors Θ^1 and Θ^2 in the monotone regime with the property $\Theta^2 \in \mathcal{N}(\mathbb{G}, \Theta^1, \mathcal{W})$, the induced sub-graph of $\Theta^1 - \Theta^2$ has strictly more strongly connected components than weakly connected components.*

The equivalence between statements 1 and 2 still holds true even after replacing strong uniqueness with weak uniqueness in statement 1, provided that the phase angle vectors Θ^2 in statement 2 is required to satisfy $\Theta_{k\ell}^1 \neq \Theta_{k\ell}^2$ for all $\{k, \ell\} \in \mathbb{E}$.

The result of the above theorem is stronger than the sufficient conditions in Theorem 3.3. This is because any (weakly) *infeasible* orientation has strictly more strongly connected components than weakly connected components. Hence, the sufficient conditions in Theorem 3.3 ensure that all induced orientations are (weakly) *infeasible*. Then, statement 2 of this theorem holds true and the solution becomes strongly (weakly) unique.

5 Algorithms and Numerical Results

In the preceding sections, we have shown that the maximal eye and the maximal girth play important roles in the uniqueness theory. However, computing the maximal eye or maximal girth is cumbersome for large graphs. Hence, we develop a successive reduction method to design a reduced graph, and then prove the relationship between the maximal eye or the maximal girth of the original graph and those of the reduced graph. Next, we test the performance of those algorithms on real-world problems. Search-based algorithms for computing the maximal eye and the maximal girth are given in appendix.

5.1 Successive Series-Parallel Reduction method

In this subsection, we propose a successive reduction method, named as the Successive Series-Parallel Reduction (SSPR) method, that can reduce the size of the underlying graph. for computing the maximal eye and maximal girth. The SSPR method is different from the Series-Parallel Reduction (SPR) method introduced in [28] in two aspects. First, the purpose of the SSPR method is to accelerate the computation of the maximal eye and the maximal girth, while the focus of SPR method is to facilitate the verification of uniqueness conditions. Second, we prove that all 2-vertex-connected SP graphs can be

reduced to a single edge (K_2) without making the assumption in [28] that the slack bus is the last bus to be reduced.

Before introducing the SSPR method, we extend the definition of the maximal eye and the maximal girth to weighted graphs with “multiple slack buses”. This generalized class of graphs appear during the reduction process. By defining the length of a cycle as the sum of the weights of the edges on the cycle, the maximal eye and the maximal girth can be generalized to weighted graphs. Next, we define (weakly) feasible orientations for graphs with “multiple slack buses”, namely, the slack nodes.

Definition 5.1. *For a weighted undirected graph $(\mathbb{V}, \mathbb{E}, W)$, a subset of vertices $\mathbb{V}_s \subseteq \mathbb{V}$ is called the set of **slack nodes**. An orientation A assigned to the graph is called a **weakly feasible orientation** if each edge has one of the directions $\{+1, -1, 0\}$ and each vertex not in \mathbb{V}_s either has nonzero in-degree and nonzero out-degree, or has zero in-degree and zero out-degree. An orientation A assigned to the graph is called a **feasible orientation** if each edge has one of the directions $\{+1, -1\}$ and each vertex not in \mathbb{V}_s has nonzero in-degree and nonzero out-degree.*

Now, we can define the maximal eye for graphs with slack nodes by taking the maximum of the size of eye over weakly feasible orientations. The maximal girth can be defined in a similar way. For power networks, the only slack node is the slack bus of the power network. Hence, the extended definitions of the maximal eye and the maximal girth are consistent with their original definitions. The SSPR method is based on three types of operations:

- **Type I Operation.** Replacement of a set of parallel edges with a single edge that connects their common endpoints. The weight of the new single edge is the minimum over the weights of the deleted parallel edges.
- **Type II Operation.** Replacement of the two edges incident to a degree-2 vertex with a single edge, if the vertex has exactly two neighboring vertices and is not a slack node. The weight of the new edge is the sum of the weights of the two deleted edges.
- **Type III Operation.** Deletion of a vertex that has only a single neighboring vertex. If the deleted vertex is a slack node, or if the deleted vertex has degree at least 2 for the problem of computing the maximal girth, then we define its neighboring vertex as a slack node.

The update scheme of weights and slack nodes is designed to control the change of the maximal eye or the maximal girth. The SSPR method successively reduces the size of the graph by applying Type I-III Operations; the pseudo-code of the SSPR method is given in Algorithm 2.

We note that after the reduction process, there is no parallel edge or pendant (degree-1) vertex in the reduced graph. Ignoring the weights of the edges and the set of the

Algorithm 2 Successive Series-Parallel Reduction (SSPR) method

Given: Undirected unweighted graph (\mathbb{V}, \mathbb{E}) , slack bus k

Output: Reduced undirected weighted graph $(\mathbb{V}_R, \mathbb{E}_R, W_R)$, two constants α_1, α_2 defined in Theorems 5.2 and 5.4, set of slack nodes \mathbb{V}_s .

1. Set the initial weight for each edge to be 1.

2. Set the initial set of slack nodes as $\mathbb{V}_s \leftarrow \{k\}$.

while at least one operation is implementable **do**

if Type I Operations are implementable **then**

 Implement Type I Operation.

 Update values α_1, α_2 according to their definitions in Theorems 5.2 and 5.4.

continue

end if

if Type II Operations are implementable **then**

 Implement Type II Operation.

continue

end if

if Type III Operations are implementable **then**

 Implement Type III Operation.

 Update values α_1, α_2 according to their definitions in Theorems 5.2 and 5.4.

 Update the set of slack nodes \mathbb{V}_s .

continue

end if

end while

Return reduced graph $(\mathbb{V}_R, \mathbb{E}_R, W_R)$, set of slack nodes \mathbb{V}_s and values α_1, α_2 .

slack nodes, the operations in the SSPR method can cover the operations in the classical series-parallel reduction [20], which are defined as

- **Type I' Operation.** Replacement of parallel edges with a single edge that connects their common endpoints.
- **Type II' Operation.** Replacement of the two edges incident to a degree-2 vertex with a single edge.
- **Type III' Operation.** Deletion of a pendant vertex.

Hence, the SSPR method can be viewed as a generalization of the classical series-parallel reduction.

Now, we study the maximal eye of the graph before and after the reduction. We first consider the change of the maximal eye after each operation.

Lemma 5.1. *Given a weighted undirected graph $(\mathbb{V}, \mathbb{E}, W)$, let e denote its maximal eye. Assume that one of Type I-III Operations is implemented on the graph. By denoting the new graph and its maximal eye as $(\tilde{\mathbb{V}}, \tilde{\mathbb{E}}, \tilde{W})$ and \tilde{e} , the following statements hold:*

- If Type I Operation is implemented, then

$$\tilde{e} \leq e \leq \max\{\tilde{e}, W_{max} + W_{min}\},$$

where W_{max} and W_{min} are the maximal and minimal weights of the deleted parallel edges, respectively.

- If Type II Operation is implemented, then $e = \tilde{e}$.
- If Type III Operation is implemented and the deleted vertex has degree 1, then $e = \tilde{e}$.
- If Type III Operation is implemented and the deleted vertex has degree larger than 1, then

$$e = \max\{\tilde{e}, W_{max} + W_{min}\},$$

where W_{max} and W_{min} are the maximal and minimal weights of the deleted parallel edges, respectively.

Using the above lemma, we have the following theorem.

Theorem 5.2. Given a power network with the underlying graph (\mathbb{V}, \mathbb{E}) , let e denote the maximal eye of the graph. Denote the graph after reduction and its maximal eye as $(\mathbb{V}_R, \mathbb{E}_R, W_R)$ and e_R , respectively. Then, we have

$$\max\{e_R, \alpha_2\} \leq e \leq \max\{e_R, \alpha_1, \alpha_2\},$$

where α_1 and α_2 are the maximum of $W_{max} + W_{min}$ over Type I and Type III Operations, respectively. Here, W_{max}, W_{min} are defined in Lemma 5.1. If Type I or Type III Operations is not implemented, then we set α_1 or α_2 to 0.

Similarly, we can prove the relation between the maximal girth of the original graph and that of the reduced graph. We first show the change of the maximal girth after each operation.

Lemma 5.3. Given a weighted undirected graph $(\mathbb{V}, \mathbb{E}, W)$, let g denote its maximal girth. Assume that one of Type I-III Operations is implemented on the graph. By denoting the new graph and its maximal girth of new graph as $(\tilde{\mathbb{V}}, \tilde{\mathbb{E}}, \tilde{W})$ and \tilde{g} , the following statements hold:

- If Type I Operation is implemented, then

$$\tilde{g} \leq g \leq \max\{\tilde{g}, W_{max} + W_{min}\},$$

where W_{max} and W_{min} are the maximal and minimal weights of the deleted parallel edges, respectively.

- If Type II Operation is implemented, then $g = \tilde{g}$.
- If Type III Operation is implemented and the deleted vertex has degree 1, then $g = \tilde{g}$.
- If Type III Operation is implemented, the deleted vertex is a slack node and has degree larger than 1, then

$$\tilde{g} \leq g \leq \max\{\tilde{g}, W_{max} + W_{min}\},$$

where W_{max} and W_{min} are the maximal and minimal weights of the deleted parallel edges, respectively.

- If Type III Operation is implemented, the deleted vertex is not a slack node and has degree larger than 1, then

$$g = \min\{\tilde{g}, W_{max} + W_{min}\},$$

where W_{max} and W_{min} are the maximal and minimal weights of the deleted parallel edges, respectively.

By the above lemma, the relationship between the maximal girth of the original graph and that of the reduced graph will be discovered below.

Theorem 5.4. *Given a power network with the underlying graph (\mathbb{V}, \mathbb{E}) , let g denote its the maximal girth. By denoting the graph after reduction and its maximal girth as $(\mathbb{V}_R, \mathbb{E}_R, W_R)$ and g_R , we have*

$$\min\{g_R, \alpha_2\} \leq g \leq \min\{\max\{g_R, \alpha_1\}, \alpha_2\},$$

where α_1 is the maximum of $W_{max} + W_{min}$ over Type I Operations and the second case of Type III Operations, and α_2 is the minimum of $W_{max} + W_{min}$ over the third case of Type III Operations. Here, W_{max}, W_{min} are defined in Lemma 5.1. If operations for computing α_1 or α_2 are not implemented, then we set α_1 to 0 or α_2 to $+\infty$.

Based on the numerical results in Tables 2 and II in [29] for large power networks, the values of α_1 and α_2 in Theorems 5.2 and 5.4 are usually smaller than e_R and g_R . Hence, we have the approximation

$$e \approx e_R, \quad g \approx \alpha_2. \quad (80)$$

The above relations imply that for large power networks, computing the maximal eye is equivalent to computing the maximal eye of a reduced graph, while the maximal girth is already computed during the reduction process. Finally, we prove that 2-vertex-connected SP graphs can be reduced to a single edge by the SSPR method.

Theorem 5.5. *If the underlying graph (\mathbb{V}, \mathbb{E}) of a power network is a 2-vertex-connected SP graph, then the SSPR method reduces the underlying graph to a single edge.*

For an undirected graph without slack nodes, the classical series-parallel reduction (Type I'-III' Operations) can reduce the graph to a single edge if and only if the graph is a Generalized Series-Parallel (GSP) graph [20]. We note that 2-vertex-connected SP graphs are a special class of GSP graphs and it is unclear whether the reduction guarantee for the SSPR method can be extended to any GSP graphs in the presence of slack nodes.

5.2 Numerical results

In this subsection, we verify the theoretical results of this work and test the performance of the proposed algorithms. First, we show that, using the SSPR method, the computation of the maximal eye can be reduced to a smaller graph, while the computation of the maximal girth is finished during the process of reduction. Then, we show that Corollary 3.5 gives a valid sufficient condition for strong uniqueness. We use IEEE power networks in MATPOWER [30] to perform experiments.

We first consider the computation of the maximal eye. The results are listed in Table 2. Here, we use '-' to denote the case when this value does not exist, and use 'TLE' (Time Limit Exceeded) to denote the case when the algorithm does not find any leaf node in two days. The lower bounds for the maximal eye are derived by stopping the algorithm before it terminates. It can be observed that the SSPR method can largely reduce the size of the graph, and therefore can accelerate the computing process. Moreover, the values of α_1 and α_2 are small compared to the maximal eye of the reduced graph. Hence, the approximation in equation (80) holds and the maximal eye of the original graph is equal to the maximal eye of the reduced graph. Although the algorithm achieves acceleration compared to the brute-force search method, we are only able to compute the maximal eye for graphs with up to 118 vertices. Note that since graph problems have exponential complexities, solving them for graphs having as low as 200 nodes is still beyond the current computational capabilities. However, this does not undermine the usefulness of the introduced graph parameters, since it is shown in this work that those parameters accurately decide whether the power flow problem has a unique solution.

Next, we consider the computation of the maximal girth. We use the same algorithms and the results are listed in the technical report [29]. In this case, it can be observed that α_2 is equal to 3 for large power networks. This is because the underlying graphs of large power networks considered in the table have "pendant triangles". Pendant triangles are triangles that have only one vertex connected to the rest of the graph. Furthermore, the approximation in Theorem 5.4 holds and the maximal girth of the original graph is equal to $\alpha_2 = 3$. Hence, the maximal girth can be computed during the reduction process. This shows that the conditions for the weak uniqueness is significantly loose and requiring $\omega_{k\ell}$ to be at most $2\pi/3$ for all edges $\{k, \ell\}$ is enough. However, for 2-vertex-connected SP graphs, we have shown that the maximal girth is equal to the maximal eye and the requirement for the weak uniqueness is the same as that for the strong uniqueness.

Power Network	Original Size	Reduced Size	α_1	α_2	e_R
Case 14	(14,20)	(2,1)	6	3	0
Case 30	(30,41)	(8,13)	4	3	8
Case 39	(39,46)	(8,12)	4	5	8
Case 57	(57,78)	(22,39)	4	-	23
Case 118	(118,179)	(44,83)	5	-	13
Case 300	(300,409)	(109,196)	8	4	≥ 10
Case 1354	(1354,1710)	(263,500)	9	8	TLE
Case 2383	(2383,2886)	(499,949)	11	5	TLE

Table 2: Number of vertices and edges before and after the SSPR method for maximal eye along with values computed during the reduction process.

Finally, we validate the results in Corollary 3.5, i.e., showing that there does not exist a different solution in the monotone regime with the set of allowable perturbations being $\mathcal{W}_{2\pi/e(\mathcal{G})}$. Given a power network in MATPOWER data set, we randomly generate power systems with the same network topology and monotone regime. Then, we construct several random solutions and use **MATPOWER runpf** to check if there are different solutions in the neighborhood of the constructed ground truth solution. For power systems with at most 118 buses, the ground truth solution is the only solution found in the neighborhood of the ground truth. Hence, we know the strong uniqueness holds for those power networks. More details about the experiment are given in technical report [29].

6 Conclusion

In this paper, we extend the uniqueness theory of P - Θ power flow solutions developed in [28] for an AC power system. The notion of strong uniqueness is introduced to characterize the uniqueness in the common sense. We propose a general necessary and sufficient condition for the uniqueness of the solution, which depends only on the monotone regime and the network topology. These conditions can be greatly simplified in certain scenarios. When the underlying graph of the power network is a single cycle, sufficient conditions in [28] are proved to be necessary. For 2-vertex-connected SP graphs, we show that the maximal eye is equal to the maximal girth, which means that the sufficient condition for the weak uniqueness also implies the strong uniqueness. When the power network is lossless, we derive a necessary and sufficient condition that does not contain sinusoidal functions and its sufficient part is stronger than the general sufficient conditions. A reduction method, named the SSPR method, is proposed to reduce the size of power network and accelerate the computation of the maximal eye and the maximal girth. The SSPR method is proved to reduce a 2-vertex-connected SP graph to a single edge and the relation between the graphs before and after the reduction is analyzed. Some algorithms based on the DFS method with pruning are designed to compute the maximal eye and

maximal girth.

7 Appendix

7.1 Algorithms for computing maximal eye and maximal girth

In the appendix, we propose search-based algorithms for computing the maximal eye and the maximal girth. Our approach is based on the Depth-First Search (DFS) method and utilized the pruning technique to accelerate the computing process. We first describe a common sub-procedure that will be used in both algorithms. The sub-procedure computes the minimal directed chordless cycle containing a given edge. Given a truncation length $T \geq 1$, the sub-procedure returns the truncation length if there does not exist a directed chordless cycle that contains the given edge and has length at most T . The sub-procedure is also based on the DFS method with pruning and borrows the idea of *blocking* from [40] to accelerate the searching process. The pseudo-code of the sub-procedure is listed in Algorithm 3.

The search space of the sub-procedure is the set of directed chordless paths with length at most T . When the current directed chordless path is a directed chordless cycle, the length of the cycle is recorded and the minimal length of known directed chordless cycles is updated. By searching over all chordless paths, we find the length of the minimal directed chordless cycle. The DFS method is initialized with the given edge, denoted as (k, ℓ) , and extends the directed chordless path by adding a neighbouring vertex of the end point other than k to the path. The pruning technique becomes effective and delete the end point other than k from the path if one of the following cases occurs:

- The length of the directed chordless path is larger than T or the known minimal length of directed chordless cycles;
- All neighbouring vertices have been searched or will introduce a chord if added to the path.

Using the idea of blocking, one can efficiently check whether adding a vertex to the path will introduce a chord. This approach is based on the following observation: if the path (k_1, \dots, k_t) is chordless, then any vertex k_s can only be in the neighborhood of k_{s-1}, k_{s+1} . We construct an array and, for each vertex, we record the number of vertices on the path that are in the neighborhood of the vertex. The array is updated whenever the path is updated. If there are at least two vertices on the path in the neighbourhood of a vertex not on the path, then adding the vertex to the path will introduce a chord. Hence, the cost of checking this condition for each potential vertex not on the path is a single evaluation of an array.

Algorithm 3 Truncated Minimal Chordless Cycle

Given: Directed weighted graph $(\mathbb{V}, \mathbb{E}, W)$, selected edge (k, ℓ) , truncation length T

Output: Length of minimal chordless cycle c

1. Construct the neighbourhood of each vertex $N : \mathbb{V} \mapsto 2^{\mathbb{V}}$.
2. Initialize blocked array $block[i] \leftarrow 0$ for all vertices $i \in \mathbb{V}$.
3. Set the length of minimal cycle recorded $c \leftarrow T$.
4. Set current length $L_{cur} \leftarrow W_{k\ell}$.
5. Set the path $P \leftarrow [k, \ell]$.
6. Set $block[k] \leftarrow 1, block[\ell] \leftarrow 1$.

if $L_{cur} \geq T$ **then**
 return c
end if

while the length of P is at least 2 **do**
 Get the endpoint $i \leftarrow P[-1]$.
 Increase $block$ for vertices in $N[j]$ by 1.
 Get the minimal vertex $j \in N[i]$ such that $block[j] \leq 1$ and $L_{cur} + W_{P[-1]j} < v$.
 if no such vertex j exists **then**
 Find the maximal index h such that $P[h] \notin \{k, \ell, i\}$ and $P[h+1]$ is not the
 maximal vertex in $N[P[h]]$.
 if no such h exists **then**
 break
 else
 Remove $P[h+1], \dots, P[-1]$ from path P .
 Decrease $block$ of $N[P[h]], \dots, N[P[-1]]$ by 1.
 Add the next smallest vertex in $N[P[h]]$ to P .
 Update L_{cur} to be the length of path P .
 continue
 end if
 else
 Add vertex j to P and update L_{cur} .
 if $k \in N[j]$ **then**
 Calculate length $c_{cur} \leftarrow L_{cur} + W_{jk}$.
 if $c_{cur} > 0$ **then**
 Update $c \leftarrow \min\{c, c_{cur}\}$.
 end if
 Recursion similarly as above.
 else
 continue
 end if
 end if
end while
return c

Next, we propose the algorithms for computing the maximal eye and the maximal girth. Since the algorithm of maximal girth is similar to the algorithm for maximal eye, we only present the algorithm for computing the maximal eye and offer the other one in [29]. The algorithm is also based on the DFS method with pruning, and the pseudo-code is provided in Algorithm 4. We first order all edges and gradually assign one of the directions $\{0, -1, +1\}$ to each edge following the ordering of the edges. The search space consists of the orientations for the first several edges (intermediate states) and the orientations for the entire graph (final states). One can verify that all intermediate states and final states form a trinomial⁴ tree, since each orientation for the first $k < |\mathbb{E}|$ edges leads to three different orientations for the first $k + 1$ edges. Then, the algorithm for computing the maximal eye searches in the same way as the classical DFS method on a directed tree. For each node, we consider the sub-graph consisting of those edges that have been assigned a direction. We compute the length of the minimal directed chordless cycle in the sub-graph, which contains the last edge in the sub-graph, using the sub-procedure (Algorithm 3). The truncation length can be decided as follows. Since a DFS method is implemented on a trinomial tree, there exists a directed path from the root node of the trinomial tree to the current node. The truncation length can be chosen as the minimal length computed on the preceding nodes of the path. When the search reaches a leaf node, we obtain an orientation for the entire graph, and the size of the eye becomes the minimal length on the path to the root node. By searching over all leaf nodes, we find the maximal eye. Similarly, one can use the pruning technique to reduce the search space. The current node is pruned if it can not be extended to a weakly feasible orientation for the entire graph, or the size of the eye of the sub-graph is smaller than the known maximal size of the eye.

⁴A directed tree is called a trinomial tree if there is a root node and each non-leaf node has exactly three descendant nodes.

Algorithm 4 Algorithm for Computing The Maximal Eye

Given: Undirected weighted graph $(\mathbb{V}, \mathbb{E}, W)$, slack bus k

Output: Maximal eye e

1. Set the maximal eye $e \leftarrow 0$.
2. Assign an order to the set of edges \mathbb{E} and denote edges as $\{k_1, \ell_1\}, \dots, \{k_m, \ell_m\}$.
3. Initialize the set of edges $\mathbb{E}_0 \leftarrow \{\{k_1, \ell_1\}\}$.
4. Initialize the set of orientations $A_{k_1, \ell_1} \leftarrow -1$.

loop

Check the weak feasibility with current orientation.

if weak feasibility fails **then**

Get the maximal index j such that $A_{k_j, \ell_j} \neq 1$.

if no such j exists **then**

break

else

Remove $\{k_{j+1}, \ell_{j+1}\}, \dots, \{k_m, \ell_m\}$ from \mathbb{E}_0 .

Change orientation $A_{k_j, \ell_j} \leftarrow A_{k_j, \ell_j} + 1$.

continue

end if

end if

Compute the size of eye e_{cur} under \mathbb{E}_0 and A using Algorithm 3. The truncation length is set to be the size of eye of the precedent state.

if $e_{cur} < e$ **then**

Recursion in the same way.

end if

Get the next edge $\{k_i, \ell_i\}$ that is not in \mathbb{E}_0 .

if no such edge **then**

Update $e \leftarrow \max\{e, e_{cur}\}$.

Recursion in the same way.

else

Add the next edge $\{k_i, \ell_i\}$ that is not in \mathbb{E}_0 .

Assign $A_{k_j, \ell_j} \leftarrow -1$.

continue

end if

end loop

return e

7.2 Proof of Lemma 3.1

Proof. We only prove the strong uniqueness part since the proof for weak uniqueness is similar. For a given power network, we define the real power flow along the line $\{k, \ell\} \in \mathbb{E}$

from bus k in the direction of bus ℓ as

$$\tilde{p}_{k\ell}(\Theta) := -G_{k\ell}|v_k||v_\ell|\cos(\Theta_{k\ell}) + B_{k\ell}|v_k||v_\ell|\sin(\Theta_{k\ell}).$$

By definition, it follows that

$$\hat{P}_k(\Theta) = \sum_{\ell:\{k,\ell\}\in\mathbb{E}} \tilde{p}_{k\ell}(\Theta) \quad \forall k \in \mathbb{V}.$$

Proof of sufficiency We first show by contradiction that statement 2 of the lemma is sufficient for statement 1. In particular, suppose that statement 2 holds, but the solution is not strongly unique for some graph $\mathbb{G} \in \mathcal{G}$ and some real power injection P while problem (76) is feasible. Then, there exist two different phase angle vectors Θ^1, Θ^2 such that $\Theta^2 \in \mathcal{N}(\mathbb{G}, \Theta^1, \mathcal{W})$ and $\hat{P}(\Theta^1) = \hat{P}(\Theta^2)$. For each line $\{k, \ell\} \in \mathbb{E}$, there exists a constant $C_{k\ell} > 0$ such that

$$B_{k\ell} = C_{k\ell} \sin(\gamma_{k\ell}), \quad G_{k\ell} = C_{k\ell} \cos(\gamma_{k\ell}).$$

We calculate the change of power flow from k to ℓ as

$$\begin{aligned} \tilde{p}_{k\ell}(\Theta^1) - \tilde{p}_{k\ell}(\Theta^2) &= -G_{k\ell}|v_k||v_\ell|[\cos(\Theta_{k\ell}^1) - \cos(\Theta_{k\ell}^2)] + B_{k\ell}|v_k||v_\ell|[\sin(\Theta_{k\ell}^1) - \sin(\Theta_{k\ell}^2)] \\ &= -C_{k\ell} \cos(\gamma_{k\ell})|v_k||v_\ell|[\cos(\Theta_{k\ell}^1) - \cos(\Theta_{k\ell}^2)] + C_{k\ell} \sin(\gamma_{k\ell})|v_k||v_\ell|[\sin(\Theta_{k\ell}^1) - \sin(\Theta_{k\ell}^2)] \\ &= (-\cos(\gamma_{k\ell})[\cos(\Theta_{k\ell}^1) - \cos(\Theta_{k\ell}^2)] + \sin(\gamma_{k\ell})[\sin(\Theta_{k\ell}^1) - \sin(\Theta_{k\ell}^2)]) \cdot |v_k||v_\ell|C_{k\ell} \\ &= 2[\cos(\gamma_{k\ell}) \sin(\Theta_{k\ell}^1/2 + \Theta_{k\ell}^2/2) + \sin(\gamma_{k\ell}) \cos(\Theta_{k\ell}^1/2 + \Theta_{k\ell}^2/2)] \cdot \sin(\Delta_{k\ell}/2)|v_k||v_\ell|C_{k\ell} \\ &= 2 \sin(\gamma_{k\ell} + \Theta_{k\ell}^1/2 + \Theta_{k\ell}^2/2) \cdot \text{sign}(\sin(\Delta_{k\ell}/2)) \cdot |\sin(\Delta_{k\ell}/2)||v_k||v_\ell|C_{k\ell} \\ &:= \delta_{k\ell} \cdot |\sin(\Delta_{k\ell}/2)v_kv_\ell|C_{k\ell}, \end{aligned}$$

where

$$\begin{aligned} \Delta_{k\ell} &:= \Theta_{k\ell}^1 - \Theta_{k\ell}^2, \\ \delta_{k\ell} &:= 2 \sin(\gamma_{k\ell} + \Theta_{k\ell}^1/2 + \Theta_{k\ell}^2/2) \text{sign}(\sin(\Delta_{k\ell}/2)). \end{aligned} \tag{81}$$

Note that the third equality in (81) is due to the following triangular identities:

$$\begin{aligned} \cos(\eta) - \cos(\varphi) &= -2 \sin[(\eta - \varphi)/2] \sin[(\eta + \varphi)/2], \\ \sin(\eta) - \sin(\varphi) &= 2 \sin[(\eta - \varphi)/2] \cos[(\eta + \varphi)/2]. \end{aligned}$$

Since $\hat{P}_k(\Theta^1) = \hat{P}_k(\Theta^2)$ for all $k \neq 1$, we obtain

$$\hat{P}_k(\Theta^1) - \hat{P}_k(\Theta^2) = \sum_{\ell:\{k,\ell\}\in\mathbb{E}} [\tilde{p}_{k\ell}(\Theta^1) - \tilde{p}_{k\ell}(\Theta^2)] = \sum_{\ell:\{k,\ell\}\in\mathbb{E}} \delta_{k\ell} \cdot |\sin(\Delta_{k\ell}/2)v_kv_\ell|C_{k\ell} = 0$$

for all $k \neq 1$. Let the set \mathbb{E}_0 be the subset of edges such that $\Delta_{k\ell} \neq 0$ for all $\{k, \ell\} \in \mathbb{E}_0$; we assign an order to elements in \mathbb{E}_0 . Define the matrix $M \in \mathbb{R}^{|\mathbb{V}| \times |\mathbb{E}_0|}$ and the vector $\mathbf{g} \in \mathbb{R}^{|\mathbb{E}_0|}$ as

$$M_{ki} := \delta_{k\ell}, \quad M_{\ell i} := \delta_{\ell k}, \quad \mathbf{g}_i := |\sin(\Delta_{k\ell}/2)v_k v_\ell| C_{k\ell},$$

where $\{k, \ell\}$ is the i -th edge in the set \mathbb{E}_0 . Since $\Delta_{k\ell} \neq 0$ for all $\{k, \ell\} \in \mathbb{E}_0$ and $\Delta_{k\ell} \leq 2\gamma_{k\ell} \leq \pi$, it holds that

$$|\sin(\Delta_{k\ell}/2)| > 0 \quad \forall \{k, \ell\} \in \mathbb{E}_0.$$

Then, the vector \mathbf{g} is a solution to the linear feasibility problem

$$\text{find } \mathbf{x} \in \mathbb{R}^{|\mathbb{E}_0|} \quad \text{s.t. } (M\mathbf{x})_{2:|\mathbb{V}|} = 0, \quad \mathbf{x} > 0.$$

where $(y)_{i:j} := (y_i, y_{i+1}, \dots, y_j)$ includes the i -th to the j -th entries of the vector y and inequality $x > 0$ means that $x_k > 0$ holds for all entries of the vector x . The notation $x \geq 1$ is defined in the same way. The above feasibility problem is equivalent to

$$\text{find } \mathbf{x} \in \mathbb{R}^{|\mathbb{E}_0|} \quad \text{s.t. } (M\mathbf{x})_{2:|\mathbb{V}|} = 0, \quad \mathbf{x} \geq 1.$$

Then, by Farka's Lemma, the dual feasibility problem

$$\text{find } \mathbf{y} \in \mathbb{R}^{|\mathbb{V}|} \quad \text{s.t. } M^T \mathbf{y} \geq 0, \quad \mathbf{1}^T M^T \mathbf{y} > 0, \quad y_1 = 0$$

is infeasible. However, the conditions in the dual problem are the same as the conditions in statement 2 of Lemma 3.1. This contradicts the claim in statement 2 that there exists a vector \mathbf{y} satisfying these conditions. Thus, statement 1 must hold true.

Proof of necessity Next, we again show by contradiction that statement 2 of the lemma is necessary for statement 1. Assume that statement 1 holds true, and that there exist two different phase angle vectors Θ^1, Θ^2 in the monotone regime such that $\Theta^2 \in \mathcal{N}(\mathbb{G}, \Theta^1, \mathcal{W})$ while there does not exist \mathbf{y} satisfying the conditions in statement 2. We define \mathbb{E}_0 as the set of edges such that $\Delta_{k\ell} \neq 0$, where $\Delta_{k\ell} := \Theta_{k\ell}^1 - \Theta_{k\ell}^2$ for all $\{k, \ell\} \in \mathbb{E}_0$. We construct the matrix $M \in \mathbb{R}^{|\mathbb{V}| \times |\mathbb{E}_0|}$ as

$$M_{ki} := \delta_{k\ell}, \quad M_{\ell i} := \delta_{\ell k},$$

where $\{k, \ell\}$ is the i -th edge in the set \mathbb{E}_0 and

$$\delta_{k\ell} := \sin(\gamma_{k\ell} + \Theta_{k\ell}^1/2 + \Theta_{k\ell}^2/2) \text{sign}(\sin(\Delta_{k\ell}/2)).$$

By the same analysis, the conditions in statement 2 turn out to be equivalent to the feasibility of the linear feasibility problem

$$\text{find } \mathbf{y} \in \mathbb{R}^{|\mathbb{V}|} \quad \text{s.t. } M^T \mathbf{y} \geq 0, \quad \mathbf{1}^T M^T \mathbf{y} > 0, \quad y_1 = 0.$$

By our assumption, the above problem is infeasible. By Farka's Lemma, there exists a solution $\mathbf{g} \in \mathbb{R}^{|\mathbb{E}_0|}$ to the feasibility problem

$$\text{find } \mathbf{x} \in \mathbb{R}^{|\mathbb{E}_0|} \quad \text{s.t. } (M\mathbf{x})_{2:|V|} = 0, \quad \mathbf{x} \geq 1$$

and also to the feasibility problem

$$\text{find } \mathbf{x} \in \mathbb{R}^{|\mathbb{E}_0|} \quad \text{s.t. } (M\mathbf{x})_{2:|V|} = 0, \quad \mathbf{x} > 0.$$

We define the matrix $C \in \mathbb{R}^{|\mathbb{V}| \times |\mathbb{V}|}$ as

$$C_{k\ell} := |\sin(\Delta_{k\ell}/2)v_k v_\ell|^{-1} \mathbf{g}_i \quad \forall \{k, \ell\} \in \mathbb{E}_0,$$

where $\{k, \ell\}$ is the i -th edge in the set \mathbb{E}_0 , and

$$C_{k\ell} := 1 \quad \forall \{k, \ell\} \in \mathbb{E} \setminus \mathbb{E}_0, \quad C_{k\ell} := 0 \quad \forall \{k, \ell\} \notin \mathbb{E}.$$

By the definition, it follows that $C_{k\ell} > 0$ for all $\{k, \ell\} \in \mathbb{E}$. We construct a graph \mathbb{G} with the complex admittance matrix

$$Y_{k\ell} := C_{k\ell} \cos(\gamma_{k\ell}) - \mathbf{j} C_{k\ell} \sin(\gamma_{k\ell}) \quad \forall \{k, \ell\} \in \mathbb{E}.$$

Then, for all $k \neq 1$, we have

$$\begin{aligned} \hat{P}_k(\Theta^1) - \hat{P}_k(\Theta^2) &= \sum_{\ell: \{k, \ell\} \in \mathbb{E}} [\tilde{p}_{k\ell}(\Theta^1) - \tilde{p}_{k\ell}(\Theta^2)] \\ &= \sum_{\ell: \{k, \ell\} \in \mathbb{E}} \delta_{k\ell} \cdot |\sin(\Delta_{k\ell}/2)v_k v_\ell| C_{k\ell} = (M\mathbf{g})_k = 0. \end{aligned}$$

This implies that Θ^1 and Θ^2 are both solutions to problem (76) in the monotone regime when the real power injection is

$$P := \hat{P}(\Theta^1).$$

This contradicts statement 1 that the solution is strongly unique for any real power injection. Hence, the conditions in statement 2 must be satisfied. \square

7.3 Proof of Lemma 3.2

Proof. We only prove the strong uniqueness part since the proof for weak uniqueness is similar. Since the induced orientation A is not a weakly feasible orientation, there exists

a vertex $i \neq 1$ such that it has nonzero out-degree and zero in-degree, or it has nonzero in-degree and zero out-degree. Without loss of generality, assume that the vertex i has nonzero out-degree and zero in-degree. We prove that the i -th unit vector $\mathbf{y} := \mathbf{e}_i$ satisfies the conditions in statement 1 of Lemma 3.1. It is straightforward that $y_1 = 0$. We only need to show that the inequalities in (77) hold and at least one of them is strict. We consider any edge (k, ℓ) such that $\Delta_{k\ell} > 0$. First, if $k \neq i$ and $\ell \neq i$, then both sides of the inequality (77) are zero. Next, if $k \neq i$ and $\ell = i$, then the condition $\Delta_{ki} > 0$ implies that $A_{ki} = +1$, which contradicts the assumption that i has zero in-degree. Finally, if $k = i$ and $\ell \neq i$, the goal is to prove that

$$\sin(\gamma_{i\ell} + \Theta_{i\ell}^1/2 + \Theta_{i\ell}^2/2) \cdot y_i > \sin(\gamma_{i\ell} - \Theta_{i\ell}^1/2 - \Theta_{i\ell}^2/2) \cdot y_\ell.$$

Since $y_i = 1$ and $y_\ell = 0$, the above inequality is equivalent to

$$\sin(\gamma_{i\ell} + \Theta_{i\ell}^1/2 + \Theta_{i\ell}^2/2) > 0.$$

Recalling the assumption that $\Theta_{i\ell}^1$ and $\Theta_{i\ell}^2$ are in the monotone regime $[-\gamma_{i\ell}, \gamma_{i\ell}]$, one can write

$$\gamma_{i\ell} + \Theta_{i\ell}^1/2 + \Theta_{i\ell}^2/2 \in [0, 2\gamma_{i\ell}] \subset [0, \pi].$$

Hence, it is enough to show that

$$\gamma_{i\ell} + \Theta_{i\ell}^1/2 + \Theta_{i\ell}^2/2 \in (0, 2\gamma_{k\ell}) \subset (0, \pi).$$

If $\gamma_{i\ell} + \Theta_{i\ell}^1/2 + \Theta_{i\ell}^2/2 = 0$, then it holds that

$$\Theta_{i\ell}^1 = \Theta_{i\ell}^2 = -\gamma_{i\ell}.$$

This contradicts the inequality $\Delta_{i\ell} = \Theta_{i\ell}^1 - \Theta_{i\ell}^2 > 0$. If $\gamma_{i\ell} + \Theta_{i\ell}^1/2 + \Theta_{i\ell}^2/2 = 2\gamma_{k\ell}$, then it holds that

$$\Theta_{i\ell}^1 = \Theta_{i\ell}^2 = \gamma_{i\ell},$$

which also contradicts the inequality $\Delta_{i\ell} > 0$. Combining the two cases, we obtain that $\sin(\gamma_{i\ell} + \Theta_{i\ell}^1/2 + \Theta_{i\ell}^2/2) > 0$ and the inequality

$$\sin(\gamma_{i\ell} + \Theta_{i\ell}^1/2 + \Theta_{i\ell}^2/2) \cdot y_i > \sin(\gamma_{i\ell} - \Theta_{i\ell}^1/2 - \Theta_{i\ell}^2/2) \cdot y_\ell.$$

holds strictly. It follows that $\mathbf{y} = \mathbf{e}_i$ satisfies the conditions in statement 2 of Lemma 3.1. \square

7.4 Proof of Corollary 3.4

Proof. We only prove the strong uniqueness part since the proof for weak uniqueness is similar. Suppose that Θ^1 and Θ^2 are two solutions to problem (76) in the monotone regime such that $\Theta^2 \in \mathcal{N}(\mathbb{G}, \Theta^1, \mathcal{W})$. Using the results of Theorem 3.3, we only need to

show that the induced orientation of $\Theta^1 - \Theta^2$ is not weakly feasible. Assume conversely that the induced orientation A is a weakly feasible orientation. Then, by hypothesis, there exists a directed cycle (k_1, \dots, k_t) containing at least one normal edge such that

$$\sum_{k_i k_{i+1} \text{ is normal}} \omega_{k_i k_{i+1}} < 2\pi, \quad (82)$$

where $k_{t+1} := k_1$. We denote $\Delta_{k\ell} := \Theta_{k\ell}^1 - \Theta_{k\ell}^2$ and it follows that

$$\begin{aligned} 0 < \Delta_{k_i k_{i+1}} &\leq \omega_{k_i k_{i+1}} & \forall i \text{ s.t. } \{k_i, k_{i+1}\} \text{ is normal,} \\ \Delta_{k_i k_{i+1}} &= 0 & \forall i \text{ s.t. } \{k_i, k_{i+1}\} \text{ is not normal,} \end{aligned} \quad (83)$$

where the right part of the first inequality is because $\Theta^2 \in \mathcal{N}(\mathbb{G}, \Theta^1, \mathcal{W})$. Combining inequalities (82) and (83) yields that

$$0 < \sum_{i=1}^t \Delta_{k_i k_{i+1}} = \sum_{k_i k_{i+1} \text{ is normal}} \Delta_{k_i k_{i+1}} \leq \sum_{k_i k_{i+1} \text{ is normal}} \omega_{k_i k_{i+1}} < 2\pi. \quad (84)$$

However, by the definition of $\Delta_{k\ell}$ and $\Theta_{k\ell}$, one can write

$$\sum_{i=1}^t \Delta_{k_i k_{i+1}} = \sum_{i=1}^t \Theta_{k_i k_{i+1}}^1 - \sum_{i=1}^t \Theta_{k_i k_{i+1}}^2 = \sum_{i=1}^t \left[\Theta_{k_i}^1 - \Theta_{k_{i+1}}^1 \right] - \sum_{i=1}^t \left[\Theta_{k_i}^2 - \Theta_{k_{i+1}}^2 \right] = 0,$$

where the second last equality is the congruence relation module 2π and the last equality is because (k_1, \dots, k_t) is a cycle. This contradicts equation (84). Thus, the induced orientation is not a weakly feasible orientation and the strong uniqueness holds. \square

7.5 Proof of Theorem 3.6

Proof. To prove the first inequality, we only need to notice that any feasible orientation is also a weakly feasible orientation and the size of eye is equal to the girth when all edges are normal.

Then, we consider the second inequality. Assume conversely that the maximal eye is attained by a directed cycle with chords in the weakly feasible orientation A . Without loss of generality, assume that the directed cycle $(1, \dots, t)$ attains the maximal eye *with fewest chords*, where $t \geq e(\mathbb{G})$ and $\{1, i\} \in \mathbb{E}$ is a chord for some $i \in \{3, \dots, t-1\}$. We consider four different cases:

1. $A_{1,i} = 0$: Consider the directed cycle

$$(1, i, i+1, \dots, t),$$

which has at most $e(\mathbb{G})$ normal edges and strictly fewer chords than $(1, \dots, t)$. This

contradicts the assumption that the cycle $(1, \dots, t)$ is a directed cycle that attains the size of eye with fewest chords.

2. $A_{1,i} = +1$: and there exists at least one normal edge among $\{1, 2\}, \dots, \{i-1, i\}$:
The directed cycle

$$(1, i, i+1, \dots, t)$$

has at most $e(\mathbb{G})$ normal edges and strictly fewer chords than $(1, \dots, t)$. This also contradicts the assumption on $(1, \dots, t)$.

3. $A_{1,i} = +1$ and edges $\{1, 2\}, \dots, \{i-1, i\}$ are not normal: Consider the directed cycle

$$(1, i, i-1, \dots, 2),$$

which has exactly one normal edge and strictly fewer chords. By the definition of the maximal eye, we know $e(\mathbb{G}) \geq 1$ and the cycle $(1, i, i-1, \dots, 2)$ has at most $e(\mathbb{G}) \geq 1$ normal edges. Hence, this contradicts the assumption on $(1, \dots, t)$.

4. $A_{1,i} = -1$: Consider the orientation \tilde{A} defined as

$$\tilde{A}_{k\ell} := -A_{k\ell} \quad \forall \{k, \ell\} \in \mathbb{E}$$

and use the discussion in the first three cases.

Combining the above four cases concludes that the maximal eye of the power network \mathbb{G} must be attained by a chordless cycle. Hence, the maximal eye is upper bounded by the longest chordless cycle. \square

7.6 Proof of Lemma 4.1

Proof. By the definition of strong uniqueness and weak uniqueness, if a solution to problem (76) is strongly unique, then it is also weakly unique. We only need to consider the other direction. Assume conversely that there exists a solution Θ^1 in the monotone regime that is weakly unique but not strongly unique. Then, there exists another solution $\Theta^2 \in \mathcal{N}(\mathbb{G}, \Theta^1, \mathcal{W})$ that is different from Θ^1 according to Definition 2.5. Then, the phase difference of some line is different for the two solutions. Considering the power injection balance at each bus, we know that the phase difference is different at all lines.

This means that the two solutions Θ^1 and Θ^2 are different according to Definition 2.4, which contradicts the assumption that Θ^1 is weakly unique. \square

7.7 Proof of Theorem 4.2

Proof. The sufficient part is proved in Corollary 3.4 and we only prove the necessary part. In this proof, bus $n + 1$ is defined as bus 1. We assume that

$$\sum_{i=1}^n \omega_{i,i+1} \geq 2\pi$$

We construct a power network $\mathbb{G} \in \mathcal{G}$ and power injection P such that there exist two different solutions Θ^1, Θ^2 in the monotone regime and $\Theta^2 \in \mathcal{N}(\mathbb{G}, \Theta^1, \mathcal{W})$. Without loss of generality, assume that

$$\sum_{i=1}^n \omega_{i,i+1} = 2\pi.$$

This is because the construction for

$$\tilde{W} := \left\{ \frac{2\pi}{\sum_{j=1}^n \omega_{j,j+1}} \cdot \omega_{i,i+1} : i \in [n] \right\}.$$

also works for the original $W = \{\omega_{i,i+1} : i \in [n]\}$ if $\sum_{j=1}^n \omega_{j,j+1} \geq 2\pi$. We define two phase angle vectors as

$$\begin{aligned} \Theta_1^1 &:= 0, & \Theta_i^1 &:= \sum_{j=2}^i \omega_{j,j+1} \quad \forall i \in \{2, \dots, n\}, \\ \Theta_i^2 &:= 0 \quad \forall i \in [n]. \end{aligned}$$

Then, it follows that

$$\Theta_{i,i+1}^1 = \omega_{i,i+1}, \quad \Theta_{i,i+1}^2 = 0 \quad \forall i \in [n],$$

which means that Θ^1 and Θ^2 are both in the monotone regime. Since $\omega_{i,i+1}, \gamma_{i,i+1} \in (0, \pi/2]$, we know that $\gamma_{i,i+1} + \omega_{i,i+1} \in (0, \pi]$ and therefore, by the monotonicity of $\cos(\cdot)$ in $[0, \pi]$, we have

$$\cos(\gamma_{i,i+1} + \omega_{i,i+1}) < \cos(\gamma_{i,i+1}).$$

For each line $\{i, i + 1\}$, we define the positive constant

$$C_{i,i+1} := |v_i v_{i+1}|^{-1} [-\cos(\gamma_{i,i+1} + \omega_{i,i+1}) + \cos(\gamma_{i,i+1})]^{-1}$$

and the complex admittance

$$B_{i,i+1} := \sin(\gamma_{i,i+1})C_{i,i+1}, \quad G_{i,i+1} := \cos(\gamma_{i,i+1})C_{i,i+1}.$$

We use $\tilde{p}_{i,i+1}(\Theta)$ to denote the real power flow from bus i to bus $i + 1$ given the phase angle vectors Θ . Then, we can calculate that

$$\begin{aligned}
\tilde{p}_{i,i+1}(\Theta^1) - \tilde{p}_{i,i+1}(\Theta^2) &= -G_{i,i+1}|v_i v_{i+1}|[\cos(\Theta_{i,i+1}^1) - \cos(\Theta_{i,i+1}^2)] \\
&\quad + B_{k\ell}|v_i v_{i+1}|[\sin(\Theta_{i,i+1}^1) - \sin(\Theta_{i,i+1}^2)] \\
&= -\cos(\gamma_{i,i+1})C_{i,i+1}|v_i v_{i+1}|[\cos(\omega_{i,i+1}) - 1] \\
&\quad + \sin(\gamma_{i,i+1})C_{i,i+1}|v_i v_{i+1}|\sin(\omega_{i,i+1}) \\
&= C_{i,i+1}|v_i v_{i+1}| \cdot [-\cos(\gamma_{i,i+1} + \omega_{i,i+1}) + \cos(\gamma_{i,i+1})] = 1.
\end{aligned}$$

It follows that

$$\begin{aligned}
\hat{P}_i(\Theta^1) - \hat{P}_i(\Theta^2) &= [\tilde{p}_{i-1,i}(\Theta^1) - \tilde{p}_{i-1,i}(\Theta^2)] - [\tilde{p}_{i,i+1}(\Theta^1) - \tilde{p}_{i,i+1}(\Theta^2)] \\
&= 1 - 1 = 0.
\end{aligned}$$

If we choose $P := \hat{P}(\Theta^1)$, then Θ^1 and Θ^2 are two different solutions to problem (76) in the monotone regime such that $\Theta^2 \in \mathcal{N}(\mathbb{G}, \Theta^1, \mathcal{W})$ and that the strong uniqueness does not hold. \square

7.8 Proof of Lemma 4.4

Proof. For the notational simplicity, we denote the maximal eye and the maximal girth of the graph $(\mathbb{V}, \mathbb{E}, W)$ as e and g , respectively. Since the graph is 2-vertex-connected, there does not exist a degree-1 vertex.

By Lemmas 5.1 and 5.3, Type II Operations do not change the maximal eye and the maximal girth of the graph. Moreover, the graph has a nested ear decomposition $\{L_0, L_1, \dots, L_{r-1}\}$ by Theorem 4.3. Hence, we can assume that there is no degree-2 vertex except the slack bus. Assume conversely that graph $(\mathbb{V}, \mathbb{E}, W)$ is the 2-vertex-connected SP graph with minimal number of ears such that $e > g$. We will show that there must exist another graph with fewer ears in the ear decomposition and $e > g$. This will lead to a contradiction with our assumption that this graph has the minimal number of ears. If the graph has at most two ears, then the graph is a single line of a cycle and we know $e = g$. Hence, there exist at least three ears in the graph $(\mathbb{V}, \mathbb{E}, W)$.

Step 1 In this step, we prove that the graph has a pair of parallel edges that contains a leaf ear, which we will define below. Since a nested ear decomposition is also a tree decomposition, we can assign a directed tree structure to ears in the decomposition. Here, we call an ear L_k a **descendant ear** of L_ℓ if L_k is a descendant node of L_ℓ on the directed tree, or equivalently, both endpoints of ear L_k are on L_ℓ and at least one of them is different from the endpoints of L_ℓ . We also call ear L_ℓ the **precedent ear** of L_k . For any ear L_ℓ , we say that ear L_k is a **smallest descendant ear** of L_ℓ if L_k is a descendant ear of L_ℓ and there does not exist another ear L_i such that L_i is also

a descendant ear of L_ℓ and the interval formed by the endpoints of L_i on L_ℓ is a strict subset of the interval formed by the endpoints of L_k . We note that each ear may have multiple smallest descendant ears. We say that an ear is a **leaf ear** if it is the smallest descendant ear of some ear and has no descendant ear. We denote the set of leaf ears as \mathcal{L} . Considering the directed tree structure of the ear decomposition, we know that the set \mathcal{L} is not empty.

Suppose that L_k is a leaf ear with the endpoints k_1, k_2 and that L_ℓ is the precedent ear of L_k . Since we have deleted all degree-2 vertices except the slack bus, ear L_k is either a single line $\{k_1, k_2\}$ or two edges $\{k_1, k_3\}$ and $\{k_2, k_3\}$ connecting the endpoints to the slack bus k_3 . Similarly, the path connecting the two endpoints of L_k on the precedent ear L_ℓ , which we denote as P_k , is either a single line or contains the slack bus. Considering the ear L_k and the path P_k , there are two cases: two parallel edges with endpoints $\{k_1, k_2\}$, or one is a single line and the other is two edges with the slack bus. If the first case occurs, we have a pair of parallel edges containing a leaf ear. Now, we consider the second case. If we exchange the two paths, i.e., let P_k be a leaf ear and L_k be a path on the precedent ear, then the structure of nested ear decomposition is not changed. Hence, without loss of generality, assume that L_k is a single line and P_k contains the slack bus. If there exists an ear L_j different from L_ℓ that also contains leaf ears, then by the uniqueness of slack bus, the first case occurs for leaf ears on ear L_j .

Hence, we simply need to consider the case when L_ℓ is the only ear that contains leaf ears. We consider the root ear L_0 . By the definition of tree ear decomposition, we know that L_0 is a single line; let ℓ_1, ℓ_2 be the two endpoints of L_0 . Since all vertices except the slack bus have degree at least 3 and the slack bus is not an endpoint of ears, both ℓ_1 and ℓ_2 have degree at least 3. This implies that the root ear L_0 has at least 2 descendant ears and all descendant ears have endpoints ℓ_1, ℓ_2 . Let $L_{k_1}, L_{k_2}, \dots, L_{k_m}$ be the descendant ears of L_0 . For each L_{k_i} , we define a sub-graph of $(\mathbb{V}, \mathbb{E}, W)$ consisting of ear L_0 and ears that are descendant nodes of L_{k_i} in the directed tree of ears. We can verify that each sub-graph also has a nested ear decomposition and therefore contains at least one leaf ear, which implies that ear L_ℓ belongs to all sub-graphs. On the other hand, due to the tree structure, the intersection of two different sub-graphs is ear L_0 and is not a leaf ear. Hence, the leaf ears in different sub-graphs are different and $L_\ell = L_0$. It follows that all descendant ears of L_0 are leaf ears and they form at least a pair of parallel edges containing a leaf ear.

Step 2 In this step, we construct a nested ear decomposition of the graph $(\mathbb{V}, \mathbb{E}, W)$ such that there exists a pair of parallel edges that contains the root ear L_0 and that all edges are ears in the ear decomposition. According to Step 1, there exists a pair of parallel edges that contains a leaf ear. We denote the leaf ear in the pair of parallel edges as L_k . We consider the (undirected) cycle containing L_0 and L_k . Suppose that the cycle has a non-empty edge intersection with ears L_{k_0}, \dots, L_{k_t} , where $k_0 = 0, k_t = k$ and $L_{k_{s+1}}$ is a descendant ear of L_{k_s} for $s = 0, 1, \dots, t-1$. Notice that the endpoints of each ear L_{k_s} are on the cycle. Now, we construct a new nested ear decomposition $\tilde{L}_0, \dots, \tilde{L}_{m-1}$

such that $L_k = \tilde{L}_0$ is the root ear. We define $\tilde{L}_0 := L_k$ and \tilde{L}_k as the remaining part of the cycle. For ears L_{k_s} with $1 \leq s \leq t-1$, we define \tilde{L}_{k_s} as the ear L_{k_s} with edges on the cycle deleted. For ears that do not intersect with the cycle, we define $\tilde{L}_i := L_i$. It is desirable to show that with the new set of ears still forms a nested ear decomposition. To this end, we analyze three cases:

- **Case I.** First, it can be verified that ears $\tilde{L}_{k_1}, \dots, \tilde{L}_{k_{t-1}}$ are nested ears on \tilde{L}_{k_t} . Hence, ears $\tilde{L}_{k_0}, \dots, \tilde{L}_{k_t}$ still form a nesting structure.
- **Case II.** Next, we consider an ear $\tilde{L}_i = L_i$ that is not changed and has both endpoints on L_{k_s} for some $s \in \{0, 1, \dots, t-1\}$. Since $L_{k_{s+1}}$ is a descendant ear on L_{k_s} , by the definition of nested ear decomposition, we know that the endpoints of \tilde{L}_i are either both on \tilde{L}_{k_s} or both on \tilde{L}_{k_t} . For the first case, L_i is an ear on \tilde{L}_{k_s} and ears on \tilde{L}_{k_s} have the same nesting structure as L_{k_s} . For the second case, both endpoints of \tilde{L}_i locate on \tilde{L}_{k_t} and are nested between the endpoints of \tilde{L}_{k_s} and $\tilde{L}_{k_{s-1}}$. We note that for the case when $s = 0$, both endpoints are equal to the endpoints of L_0 and they form the smallest possible interval on \tilde{L}_{k_t} . Hence, ears on \tilde{L}_{k_t} also have a nested structure.
- **Case III.** Finally, we consider ears that are not changed and do not have endpoints on L_{k_s} for any $s = 0, \dots, t$. These ears still form a nested structure on the original precedent ear and the nested ear decomposition structure is not changed.

Combining the above three cases concludes that the new set of ears is also a nested ear decomposition. Moreover, the topological structure of the graph is not changed. Hence, in the new ear decomposition, the root ear $\tilde{L}_0 = L_k$ has parallel edges. Finally, we observe that the parallel edges of the root ear are also ears in the ear decomposition.

Step 3 Suppose that the maximal eye is achieved by the weakly feasible orientation A . In this step, we show that we can modify A such that each edge with direction 0 is incident to a degree-0 vertex and the size of eye is not changed. Here, the degree is calculated for the directed graph with orientation A and all edges with orientation 0 are not counted towards the degree. We define a partition of vertices as

$$\begin{aligned}\mathbb{V}_1 &:= \{k \in \mathbb{V} \mid \deg(k) > 0 \text{ or } k \text{ is the slack bus}\}, \\ \mathbb{V}_2 &:= \{k \in \mathbb{V} \mid \deg(k) = 0 \text{ and } k \text{ is not the slack bus}\}\end{aligned}$$

and a partition of edges as

$$\begin{aligned}\mathbb{E}_1 &:= \{\{k, \ell\} \in \mathbb{E} \mid A_{k\ell} \in \{+1, -1\}\}, \\ \mathbb{E}_2 &:= \{\{k, \ell\} \in \mathbb{E} \mid A_{k\ell} = 0, k \in \mathbb{V}_1 \text{ and } \ell \in \mathbb{V}_1\}, \\ \mathbb{E}_3 &:= \{\{k, \ell\} \in \mathbb{E} \mid A_{k\ell} = 0, k \in \mathbb{V}_2 \text{ or } \ell \in \mathbb{V}_2\}.\end{aligned}$$

Then, the objective is to show that there exists a weakly feasible orientation such that the size of eye is still e and the set \mathbb{E}_2 is empty. For any edge $\{k, \ell\} \in \mathbb{E}_2$, we can arbitrarily assign direction $+1$ or -1 to the edge and the orientation is still weakly feasible. This is because for vertices in \mathbb{V}_1 , the requirement on in-degree and out-degree is satisfied by other edges. More specifically, if the degree of k or ℓ is nonzero, then by the definition of weakly feasible orientation, the vertex already has nonzero in-degree and out-degree. Otherwise, if k or ℓ is the slack bus, then the in-degree and out-degree can be arbitrary. Thus, we can arbitrarily assign directions $+1$ or -1 to all edges in \mathbb{E}_2 and the new orientation is still weakly feasible. We define a new orientation as

$$\begin{aligned}\tilde{A}_{k\ell} &:= \begin{cases} +1 & \text{if } k > \ell \\ -1 & \text{otherwise} \end{cases} \quad \forall \{k, \ell\} \in \mathbb{E}_2, \\ \tilde{A}_{k\ell} &:= A_{k\ell} \quad \forall \{k, \ell\} \in \mathbb{E}_1 \cup \mathbb{E}_3.\end{aligned}$$

We prove that with orientation \tilde{A} , the size of eye is not changed. Let (k_1, \dots, k_t) be a directed cycle in the graph with orientation \tilde{A} . If some edges of this cycle are in $\mathbb{E}_1 \cup \mathbb{E}_3$, then this cycle also exists in the graph with A . By assigning directions ± 1 to edges with direction 0, the lengths of the cycles are not decreased and therefore the length of (k_1, \dots, k_t) is at least e under the orientation \tilde{A} .

If all edges of this cycle are in \mathbb{E}_2 , then we choose the minimal index in $\{k_1, \dots, k_t\}$, which is assumed to be k_1 without loss of generality. By the definition of \tilde{A} , the edge $\{k_1, k_2\}$ has orientation $\tilde{A}_{k_1 k_2} = -1$, which contradicts the fact that (k_1, \dots, k_t) is a directed cycle with \tilde{A} . Combining the above two cases, it can be inferred that the size of eye with orientation \tilde{A} is at least e . On the other hand, e is defined to be the maximal eye. Hence, the size of eye with orientation \tilde{A} is equal to e .

Step 4 In this step, we prove that the maximal eye is equal to the maximal girth. Suppose that the maximal eye is achieved by the weakly feasible orientation A and orientation A satisfies the conditions in Steps 2-3. We consider the set of parallel edges containing the root ear, which we denote as $\{k, \ell, 1\}, \dots, \{k, \ell, t\}$ for some $t \geq 2$. We analyze two different cases:

- **Case I.** If there exists at least one parallel edge having direction 0, then by the conditions in Step 3, we know that at least one of the endpoints k, ℓ has degree 0. This means that all parallel edges have direction 0. We construct another graph $(\tilde{\mathbb{V}}, \tilde{\mathbb{E}}, \tilde{W})$, where the parallel edges $\{k, \ell, 1\}, \dots, \{k, \ell, t\}$ are substituted by a single edge $\{k, \ell\}$ and the weight of the new edge is the minimal weight among all parallel edges, i.e.,

$$\tilde{W}_{k\ell} := \min_{s \in [t]} W_{k,\ell,s}.$$

Other edges are the same as those in the original graph. We construct a weakly

feasible orientation \tilde{A} for the new graph. For the edge $\{k, \ell\}$, we define

$$\tilde{A}_{k\ell} := 0.$$

For other edges, we define

$$\tilde{A}_{k_1\ell_1} := A_{k_1\ell_1} \forall \{k_1, \ell_1\} \in \mathbb{E} \setminus \{\{k, \ell, 1\}, \dots, \{k, \ell, t\}\}.$$

Since the orientations \tilde{A} and A have the same degree at each node, \tilde{A} also becomes weakly feasible. Moreover, the size of eye of the graph with \tilde{A} is also equal to e , which implies that the maximal eye of the new graph \tilde{e} is at least e . Since the new graph $(\tilde{\mathbb{V}}, \tilde{\mathbb{E}}, \tilde{W})$ has $t - 1$ fewer ears, the induction assumption implies that the maximal girth of the new graph \tilde{g} satisfies

$$\tilde{g} = \tilde{e} \geq e.$$

Hence, we can choose a feasible orientation \tilde{A}^g such that the girth is equal to \tilde{g} . Now, we extend the feasible orientation \tilde{A}^g to be a feasible orientation of the original graph $(\mathbb{V}, \mathbb{E}, W)$. We define

$$A_{k_1\ell_1}^g := \tilde{A}_{k_1\ell_1}^g \forall \{k_1, \ell_1\} \in \mathbb{E} \setminus \{\{k, \ell, 1\}, \dots, \{k, \ell, t\}\}$$

and

$$A_{k,\ell,s}^g := \tilde{A}_{k\ell}^g \quad \forall s \in [t].$$

Since the in-degree and out-degree at points k, ℓ are still nonzero for the orientation A^g , it can be concluded that A^g is a feasible orientation for the original graph. Moreover, the girth of the original graph with orientation A^g is equal to \tilde{g} . It follows that the maximal girth g is at least $\tilde{g} \geq e$. This contradicts the assumption that $e > g$.

- **Case II.** Next, we consider the case when all parallel edges $\{k, \ell, 1\}, \dots, \{k, \ell, t\}$ are normal edges. In this case, the goal is to construct a feasible orientation with the same size of eye by assigning directions to edges with direction 0. We first construct a feasible orientation \tilde{A} . Assume that $L_0 = \{k, \ell, 1\}$ is the root ear, and define

$$\tilde{A}_{k,\ell,1} := A_{k,\ell,1}, \quad \tilde{A}_{k,\ell,s} := -A_{k,\ell,1} \quad \forall s \in \{2, \dots, t\}.$$

Then, we inductively define the directions of other ears using the directed tree structure of ears. For any ear L_k that has been assigned a direction, we assign its descendant ear L_ℓ with the parallel direction as the path formed by the endpoints of L_ℓ on L_k . In this way, the orientation \tilde{A} is defined for all ears and the definition is unique because of the directed tree structure. Considering the structure of the nested ear decomposition, we also know that all directed cycles in orientation \tilde{A}

must contain the root ear. In addition, the orientation \tilde{A} is feasible. This is because all internal vertices of ears have nonzero in-degree and nonzero out-degree. The only vertices that are not internal vertices of ears are the endpoints of the root ear. For the endpoints of the root ear, they also have nonzero in-degree nonzero and out-degree by the definition of directions on parallel edges. Hence, the constructed orientation \tilde{A} is feasible.

We then define an orientation that combines orientations A and \tilde{A} as follows:

$$A_{k\ell}^g := \begin{cases} A_{k\ell} & \text{if } A_{k\ell} \in \{+1, -1\} \\ \tilde{A}_{k,\ell} & \text{if } A_{k\ell} = 0, \end{cases} \quad \forall \{k, \ell\} \in \mathbb{E}.$$

We prove that A^g is a feasible orientation and the girth of orientation A^g is at least e . For any vertex k that has a nonzero degree in orientation A , the vertex k has nonzero in-degree and out-degree by the definition of weakly feasible orientation. Hence, the vertex k also has nonzero in-degree and out-degree in the new orientation. If the vertex has degree 0 in the orientation A , then all edges incident to the vertex k has the same direction as in \tilde{A} . Since the orientation \tilde{A} is feasible, the vertex k has nonzero in-degree and nonzero out-degree in the new orientation A^g . Combining the two cases, it can be concluded that the orientation A^g is feasible. Now, we estimate the girth of orientation A^g . We consider any directed cycle C in A^g . If the cycle C has normal edges in the original orientation A , then the length of cycle C is not decreased in the new orientation and therefore is at least e . If the cycle C does not have normal edges in the original orientation A , then all edges of C have the same direction as in \tilde{A} and therefore is also a cycle in \tilde{A} . This implies that the root ear L_0 is on the cycle C . However, the root ear is a normal edge in orientation \tilde{A} and this contradicts the assumption that none of the edges of the cycle C are normal. Thus, the girth of A^g is at least e . On the other hand, the girth of a feasible orientation is bounded by the maximal girth g . This contradicts the assumption that $e > g$.

Combining the above two cases and using the induction method, it can be concluded that the maximal eye of a 2-vertex-connected SP graph is equal to its maximal girth. \square

7.9 Proof of Theorem 4.6

Proof. We only prove the strong uniqueness part since the proof for the weak uniqueness is similar. We only need to show that statement 2 of this theorem holds if and only if statement 2 of Lemma 3.1 holds.

Proof of sufficiency We assume conversely that there exist two sets of phase angle vectors Θ^1 and Θ^2 satisfying statement 2 of Lemma 3.1 such that the induced sub-graph of $\Theta^1 - \Theta^2$ denoted as $(\mathbb{V}_0, \mathbb{E}_0, A_0)$ has the same number of strongly connected components and weakly connected components.

Let \mathbf{y} be a vector that satisfies conditions in statement 2 of Lemma 3.1. We prove that if vertices k and ℓ are in the same connected component, then $y_k = y_\ell$. By the definition of strongly connected components, there exist directed paths from k to ℓ and from ℓ to k . We first consider the directed path from k to ℓ , which we denote as $(k, k_1, \dots, k_t, \ell)$. Considering the edge $\{k, k_1\}$ and inequality (77), one can write

$$\sin(\pi/2 + \Theta_{k,k_1}^1/2 + \Theta_{k,k_1}^2/2) \cdot y_k \geq \sin(\pi/2 - \Theta_{k,k_1}^1/2 - \Theta_{k,k_1}^2/2) \cdot y_{k_1}. \quad (85)$$

By the same analysis in Lemma 3.2, the condition $\Delta_{k,k_1} > 0$ implies that $\Theta_{k,k_1}^1/2 + \Theta_{k,k_1}^2/2 \in (-\pi/2, \pi/2)$, which leads to

$$\sin(\pi/2 + \Theta_{k,k_1}^1/2 + \Theta_{k,k_1}^2/2) = \sin(\pi/2 - \Theta_{k,k_1}^1/2 - \Theta_{k,k_1}^2/2) > 0. \quad (86)$$

Combining the relations in (85) and (86), we obtain $y_k \geq y_{k_1}$. Considering edges $\{k_1, k_2\}, \dots, \{k_n, \ell\}$ and using the same analysis, we have

$$y_k \geq y_{k_1} \geq y_{k_2} \geq \dots \geq y_{k_t} \geq y_\ell,$$

and therefore $y_k \geq y_\ell$. Similarly, the existence of a directed path from y_ℓ to y_k implies that $y_\ell \geq y_k$. Combining the two directions, we obtain $y_k = y_\ell$. If we further assume $\{k, \ell\} \in \mathbb{E}_0$ and $\Delta_{k\ell} > 0$, then the relation in (86) implies that inequality (77) holds with equality for $\{k, \ell\}$. By the definition of weakly connected components, there does not exist any edge in \mathbb{E}_0 connecting different connected components. Hence, the endpoints of all edges in \mathbb{E}_0 are in the same connected component and therefore inequality (77) holds with equality for all $\{k, \ell\} \in \mathbb{E}_0$ such that $\Delta_{k\ell} > 0$. Finally, by the definition of induced sub-graph, \mathbb{E}_0 contains all edges $\{k, \ell\} \in \mathbb{E}$ such that $\Delta_{k\ell} > 0$. It follows that inequality (77) holds with equality for all $\{k, \ell\} \in \mathbb{E}$ such that $\Delta_{k\ell} > 0$. This contradicts statement 2 of Lemma 3.1 that there exists at least one strict inequality in the set of inequalities (77). Hence, statement 2 of this theorem holds.

Proof of necessity Assume that the conditions in statement 2 of this theorem hold. We denote the strongly connected components as $\mathcal{C}_1, \dots, \mathcal{C}_m$. Now, we define a tree structure for the set $\{\mathcal{C}_1, \dots, \mathcal{C}_m\}$. For two different strongly connected components \mathcal{C}_s and \mathcal{C}_t , if there exists a directed path from \mathcal{C}_s to \mathcal{C}_t , we define a directed edge from \mathcal{C}_t to \mathcal{C}_s . Considering all strongly connected components pairs, we obtain a directed graph with the vertex set $\{\mathcal{C}_1, \dots, \mathcal{C}_m\}$. By the definition of strongly connected components, we know that there does not exist directed cycle in this directed graph and therefore this directed graph is a directed tree. Using the directed tree structure, we can choose m real numbers c_1, \dots, c_m such that if there exists a directed path from \mathcal{C}_t to \mathcal{C}_s , then it holds that $c_t > c_s$. Moreover, if vertex 1 belongs to some strongly connected component \mathcal{C}_s , then we can shift c_t for all $t \in [m]$ such that $c_s = 0$ and the relation between all c_t 's is not changed. If vertex 1 does not belong to any strongly connected component, we do not change the value of c_t .

We construct a vector $\mathbf{y} \in \mathbb{R}^{|\mathbb{V}|}$ by

$$y_k := \begin{cases} c_s & \text{if } k \text{ is in } \mathcal{C}_s \\ 0 & \text{if } k \in \mathbb{V} \setminus \mathbb{V}_0. \end{cases}$$

Note that the set of strongly connected components gives a disjoint partition of the set \mathbb{V}_0 . Hence, the vector \mathbf{y} is well-defined. By the choice of $\{c_1, \dots, c_m\}$, the vector \mathbf{y} satisfies $y_1 = 0$. Suppose that the edge $\{k, \ell\}$ belongs to \mathbb{E} and $\Delta_{k\ell} > 0$. We verify that inequality (77) holds for $\{k, \ell\}$, namely,

$$\sin(\pi/2 + \Theta_{k\ell}^1/2 + \Theta_{k\ell}^2/2) \cdot y_k \geq \sin(\pi/2 - \Theta_{k\ell}^1/2 - \Theta_{k\ell}^2/2) \cdot y_\ell.$$

Recalling that the relation (86) holds for all $\{k, \ell\}$ such that $\Delta_{k\ell} > 0$, we only need to verify

$$y_k \geq y_\ell \quad \forall \{k, \ell\} \in \mathbb{E}_0 \quad \text{s.t. } \Delta_{k\ell} > 0. \quad (87)$$

By the definition of induced sub-graph, the condition $\Delta_{k\ell} > 0$ implies that $\{k, \ell\} \in \mathbb{E}_0$. Thus, vertices k and ℓ must belong to certain strongly connected components. If k and ℓ belong to the same strongly connected component \mathcal{C}_s , then $y_k = y_\ell = c_s$ and inequality (87) holds. Otherwise, we assume that k and ℓ belong to two different strongly connected components \mathcal{C}_s and \mathcal{C}_t , respectively. Since (k, ℓ) is a directed path from \mathcal{C}_s to \mathcal{C}_t , one can write

$$y_k = c_s > c_t = y_\ell$$

and inequality (87) holds strictly. By the assumption that there are strictly more strongly connected components than weakly connected components, there exists at least one edge $\{k, \ell\} \in \mathbb{E}_0$ such that k and ℓ belong to different strongly connected components. Without loss of generality, assume that $\Delta_{k\ell} > 0$. Then, the inequality (87), or equivalently the inequality (77), holds strictly for $\{k, \ell\}$. This shows that \mathbf{y} is a vector that satisfies conditions in statement 2 of Lemma 3.1. \square

7.10 Proof for Successive Series-Parallel Reduction Method

7.11 Proof of Lemma 5.1

Proof. We prove the four claims separately.

Type I Operation We first consider the inequality on the right. We denote the two endpoints as k, ℓ and the parallel edges connecting them as $\{k, \ell, 1\}, \dots, \{k, \ell, t\}$ for some $t \geq 2$. Without loss of generality, assume that the weights of parallel edges satisfy

$$W_{min} = W_{k,\ell,1} \leq \dots \leq W_{k,\ell,t} = W_{max}.$$

Suppose that the maximal eye of graph $(\mathbb{V}, \mathbb{E}, W)$ is achieved by the weakly feasible orientation A . If there exist different directions among these parallel edges when orientation A is assigned, then we choose the first edge $\{k, \ell, 1\}$ and another edge $\{k, \ell, s\}$ such that the direction of $\{k, \ell, s\}$ is different from the direction of $\{k, \ell, 1\}$. Hence, $\{k, \ell, 1\}$ and $\{k, \ell, s\}$ form a directed cycle and two edges have different directions. Then, at least one edge is a normal edge, i.e., an edge with direction $+1$ or -1 . The weight of the cycle is bounded by $W_{k,\ell,1} + W_{k,\ell,s} \leq W_{max} + W_{min}$. Thus, it holds that $e \leq W_{max} + W_{min}$ in this case. Otherwise, assume that all parallel edges have the same direction when orientation A is assigned. Considering a directed cycle that contains the edge $\{k, \ell, s\}$ for some $s \in \{2, \dots, t\}$, we can substitute the edge $\{k, \ell, s\}$ with edge $\{k, \ell, 1\}$ and the length of the directed cycle is not increased. Hence, if we delete edges $\{k, \ell, 2\}, \dots, \{k, \ell, t\}$, the size of eye is not changed. On the other hand, the deletion of edges $\{k, \ell, 2\}, \dots, \{k, \ell, t\}$ is equivalent to the Type I Operation on the set of parallel edges $\{k, \ell, 1\}, \dots, \{k, \ell, t\}$. Hence, we obtain $e = \tilde{e}$ in this case. Combining the two cases, it follows that $e \leq \max\{\tilde{e}, W_{max} + W_{min}\}$.

We now prove the inequality on the left. Suppose that the maximal eye of the new graph $(\tilde{\mathbb{V}}, \tilde{\mathbb{E}}, \tilde{W})$ is achieved by the weakly feasible orientation \tilde{A} . By the definition of Type I Operations, the weight $\tilde{W}_{k,\ell}$ is equal to the weight $W_{k,\ell,1}$. We consider the inverse operation of Type I Operation. Namely, we add parallel edges $\{k, \ell, s\}$ with weight $W_{k,\ell,s}$ to the new graph and define the direction $\tilde{A}_{k,\ell,s} := \tilde{A}_{k,\ell,1}$ for all $s \in \{2, \dots, t\}$. Then, the orientation \tilde{A} becomes a weakly feasible orientation for the original graph. By the discussion for the inequality on the right, the inverse operation will not change the size of eye. Therefore, we have a weakly feasible orientation for $(\mathbb{V}, \mathbb{E}, W)$ and the size of eye is \tilde{e} , which implies that $e \geq \tilde{e}$.

Type II Operation We consider the case when a Type II Operation is implemented. We denote the deleted degree-2 vertex as k . By the definition of Type II Operations, vertex k has two neighbouring vertices and we denote the two neighbouring vertices as $\ell_1 \neq \ell_2$. If A is a weakly feasible orientation for $(\mathbb{V}, \mathbb{E}, W)$, then the direction $A_{\ell_1,k}$ must be equal to the direction A_{k,ℓ_2} . Hence, treating the two edges $\{\ell_1, k\}$ and $\{k, \ell_2\}$ as a single edge with weight $W_{\ell_1,k} + W_{k,\ell_2}$ will not change the size of eye. Noticing that the claim is true for any weakly feasible orientation A , we know that $e = \tilde{e}$.

Type III Operation with a pendant vertex Removing a pendant vertex will not affect the maximal eye, since any directed cycle does not contain pendant vertices. Thus, we conclude that $e = \tilde{e}$.

Type III Operation with a non-pendant vertex Finally, we consider the case when the deleted vertex has degree at least 2. We denote the deleted vertex as k and denote the only neighbouring vertex as ℓ . The parallel edges connecting k and ℓ are denoted as $\{k, \ell, 1\}, \dots, \{k, \ell, t\}$ for some $t \geq 2$. Similar to the Type I Operation case, assume that

the weights of parallel edges satisfy

$$W_{min} = W_{k,\ell,1} \leq \dots \leq W_{k,\ell,t} = W_{max}.$$

We can split the deletion of vertex k into two operations. We first substitute parallel edges $\{k, \ell, 1\}, \dots, \{k, \ell, t\}$ with a single edge $\{k, \ell\}$ with weight $W_{k,\ell,1}$. Then, we delete the pendant vertex k . The two operations can be viewed as Type I and Type III Operations, respectively. Using the results in the first case and the third case, one can write

$$\tilde{e} \leq e \leq \max\{\tilde{e}, W_{max} + W_{min}\}.$$

Hence, it remains to prove that $e \geq W_{max} + W_{min}$. We can construct a weakly feasible orientation such that size of eye is $W_{max} + W_{min}$. Specifically, we define

$$A_{k,\ell,s} := +1 \quad \forall s \in \{1, \dots, t-1\}, \quad A_{k,\ell,t} := -1$$

and all other edges are assigned the direction 0. Then, vertices k and ℓ have nonzero in-degree and out-degree, while other vertices have zero in-degree and out-degree. Hence the orientation A is weakly feasible. Now, consider directed cycles with at least one normal edge. Since parallel edges $\{k, \ell, 1\}, \dots, \{k, \ell, t\}$ are the only normal edges, the directed cycle must contain at least one of these parallel edges. Using the facts that ℓ is the only neighbouring vertex of k and directed cycles do not have repeated vertices, vertices k and ℓ are the only two vertices of the directed cycle. Hence, the size of eye should be the the minimal length of such directed cycles, which is $W_{k,\ell,1} + W_{k,\ell,t} = W_{max} + W_{min}$. Thus, it follows that $e \geq W_{max} + W_{min}$.

Combining the two parts yields that $e = \max\{\tilde{e}, W_{max} + W_{min}\}$. \square

7.12 Proof of Lemma 5.3

Proof. The first three claims can be proved in the same way as Lemma 5.1 and we only prove the last two claims. We denote the deleted vertex as k and its only neighboring vertex as ℓ . The parallel edges connecting k and ℓ are denoted as $\{k, \ell, 1\}, \dots, \{k, \ell, t\}$ for some $t \geq 2$. Without loss of generality, assume that the weights of parallel edges satisfy

$$W_{min} = W_{k,\ell,1} \leq \dots \leq W_{k,\ell,t} = W_{max}.$$

Type III Operation for slack node We first consider the case when the deleted vertex is a slack node. By discussing whether parallel edges $\{k, \ell, 1\}, \dots, \{k, \ell, t\}$ have the same direction as in the first claim in Lemma 5.1, it holds that $g \leq \max\{\tilde{g}, W_{max} + W_{min}\}$.

We prove the other inequality $\tilde{g} \leq g$ by constructing a feasible orientation A such that the girth is \tilde{g} . Suppose that the maximal girth of the new graph $(\tilde{V}, \tilde{E}, \tilde{W})$ is achieved by the feasible orientation \tilde{A} . We define directions for deleted parallel edge such that the orientation \tilde{A} becomes a feasible orientation of the original graph (V, E, W) . We note

that, by the definition of Type III Operations, the vertex ℓ is a slack node in the new graph and it may not satisfy the condition on in-degree and out-degree. If the vertex ℓ in the new graph with orientation \tilde{A} has nonzero in-degree, then we define

$$\tilde{A}_{k,\ell,s} := -1 \quad \forall s \in \{1, \dots, t\}.$$

Then, the vertex ℓ has both nonzero in-degree and nonzero out-degree. Since the vertex k is a slack node, the orientation \tilde{A} becomes a feasible orientation for the original graph $(\mathbb{V}, \mathbb{E}, W)$. By the construction of \tilde{A} , the vertex k only has nonzero in-degree and therefore there does not exist any directed cycle containing parallel edges $\{k, \ell, 1\}, \dots, \{k, \ell, t\}$. It follows that the girth is not changed and is equal to \tilde{g} . If the vertex ℓ in the new graph with orientation \tilde{A} has nonzero out-degree, then we can similarly define

$$\tilde{A}_{k,\ell,s} := +1 \quad \forall s \in \{1, \dots, t\}.$$

The orientation \tilde{A} also becomes a feasible orientation for the original graph and the girth is \tilde{g} . Combining the two cases concludes that $e \geq \tilde{g}$.

Type III Operation for non-slack node We then consider the case when the deleted vertex is not a slack node. Suppose that the maximal girth of the original graph $(\mathbb{V}, \mathbb{E}, W)$ is achieved by the feasible orientation A . Since the vertex k has nonzero in-degree and nonzero out-degree, there must exist different directions among parallel edges $\{k, \ell, 1\}, \dots, \{k, \ell, t\}$. Hence, by the same analysis as the first claim in Lemma 5.1, it holds that $g \leq W_{max} + W_{min}$. Now, we consider restricting the orientation A to the new graph $(\tilde{\mathbb{V}}, \tilde{\mathbb{E}}, \tilde{W})$. Since the vertex ℓ is a slack node in the new graph and the orientation A is not changed for other vertices, the orientation A becomes a feasible orientation for the new graph. Then, by the definition of the maximal girth, there exists a directed cycle in the new graph with length at most \tilde{g} . Hence, we conclude that $g \leq \tilde{g}$. Combining the two inequalities, it follows that $g \leq \min\{\tilde{g}, W_{max} + W_{min}\}$.

Now, it remains to prove $g \geq \min\{\tilde{g}, W_{max} + W_{min}\}$. Suppose that the maximal girth of the new graph $(\tilde{\mathbb{V}}, \tilde{\mathbb{E}}, \tilde{W})$ is achieved by the feasible orientation \tilde{A} . We extend the orientation \tilde{A} to be an orientation for the original graph by defining

$$A_{k,\ell,s} := +1 \quad \forall s \in \{1, \dots, t-1\}, \quad A_{k,\ell,t} = -1.$$

Since both vertices k, ℓ have nonzero in-degree and nonzero out-degree and the orientation at other vertices is not changed, the orientation A becomes a feasible orientation for the original graph. Now, we calculate the girth of the original graph. For any directed cycle that does not contain parallel edges $\{k, \ell, 1\}, \dots, \{k, \ell, t\}$, it is also a directed cycle in the new graph and has length at least \tilde{g} . For any directed cycle that contains at least one of those parallel edges, vertices k and ℓ are the only two vertices of the directed cycle, since there does not exist repeated vertices on directed cycles. Hence, the length of the directed cycle is at least $W_{k,\ell,1} + W_{k,\ell,t} = W_{max} + W_{min}$. Combining the two cases yields that the

girth is at least $\min\{\tilde{g}, W_{max} + W_{min}\}$ and therefore $g \geq \min\{\tilde{g}, W_{max} + W_{min}\}$. \square

7.13 Proof of Theorem 5.5

Proof. We prove that Type I-II Operations are enough for reducing a 2-vertex-connected SP graph to a single edge. Since Type I-II Operations do not introduce new slack nodes, there exists at most one slack node in the graph throughout the reduction process. By the assumption that the graph is a 2-vertex-connected SP graph, Theorem 4.3 implies that there exists a nested ear decomposition (L_0, \dots, L_{r-1}) of the graph. We use the induction method on the number of ears in the ear decomposition. If there are only one ear or two ears in the ear decomposition, then the result holds trivially. We assume that any 2-vertex connected SP graphs with at most $r - 1$ ears in the ear decomposition can be reduced to a single edge with Type I-II Operations.

Now, we consider the case when there are r ears in the ear decomposition. We first implement Type II Operations until there is no degree-2 vertices except the slack bus. Since Type II Operations will not change the structure of the nested ear decomposition, the new graph still has a nested ear decomposition with at most r ears in the decomposition. By the first step in the proof of Theorem 4.4, there exists a set of parallel edges containing the root ear or a leaf ear. We analyze two different cases:

Case I Assume that there exists a set of parallel edges containing a leaf ear. We denote the leaf ear as $L_s = \{k, \ell\}$. Let L_t be the precedent ear of L_t . Then, then set of parallel ears consists of the segment $\overline{k\ell}$ on ear L_t and leaf ears on L_t . We can apply a Type I Operation to substitute the set of parallel edges with a single edge. We can view the new edge as the segment $\overline{k\ell}$ on ear L_t . Then, at least leaf ear is deleted and the new graph has a nested ear decomposition with at most $r - 1$ ears. By the induction assumption, the new graph can be reduced to a single edge with Type I-II Operations. Thus, the original graph can be reduced to a single edge with Type I-II Operations.

Case II Assume that there exists a set of parallel edges containing the root ear. Then by the same construction in the second step in the proof of Theorem 4.4, we can change the root ear to a leaf ear. Hence, we obtain a set of parallel edges containing a leaf ear and we can apply the discussion in Case I.

Combining the two cases, it follows that the result is true when there are r ears in the ear decomposition. By the induction method, the result is true for any $r \geq 1$ and the SSPR method can reduce a 2-vertex-connected SP graph to a single edge. \square

7.14 Numerical results of SSPR method for computing the maximal girth

Power Network	Original Size	Reduced Size	α_1	α_2	g_R
Case 14	(14,20)	(2,1)	6	3	0
Case 30	(30,41)	(9,14)	4	3	3
Case 39	(39,46)	(10,14)	4	3	3
Case 57	(57,78)	(22,39)	4	-	23
Case 118	(118,179)	(44,83)	5	-	4
Case 300	(300,409)	(110,197)	8	3	≥ 7
Case 1354	(1354,1710)	(271,509)	9	3	≥ 3
Case 2383	(2383,2886)	(500,950)	11	3	≥ 3

Table 3: Number of vertices and edges before and after the SSPR method for maximal girth along with values computed during the reduction process.

7.15 Algorithm for Computing The Maximal Girth

Algorithm 5 Algorithm for computing the maximal girth

Given: Undirected weighted graph $(\mathbb{V}, \mathbb{E}, W)$, slack bus k

Output: Maximal girth g

1. Set the maximal girth $g \leftarrow 0$.

2. Assign an order to the set of edges \mathbb{E} and denote edges as $\{k_1, \ell_1\}, \dots, \{k_m, \ell_m\}$.
Initialize the set of edges.

$\mathbb{E}_0 \leftarrow \{\{k_1, \ell_1\}\}$.

Initialize the set of orientations $A_{k_1, \ell_1} \leftarrow -1$.

loop

Check the feasibility with current orientation.

if feasibility fails **then**

Get the maximal index j such that $A_{k_j, \ell_j} \neq 1$.

if no such j exists **then**

break

else

Remove $\{k_{j+1}, \ell_{j+1}\}, \dots, \{k_m, \ell_m\}$ from \mathbb{E}_0 .

Change orientation $A_{k_j, \ell_j} \leftarrow -A_{k_j, \ell_j}$.

continue

end if

end if

Compute the girth g_{cur} under \mathbb{E}_0 and A using Algorithm 3. The truncation length is set to be the girth of the precedent state.

if $g_{cur} < g$ **then**

Recursion in the same way.

end if

Get the next edge $\{k_i, \ell_i\}$ that is not in \mathbb{E}_0 .

if no such edge **then**

Update $g \leftarrow \max\{g, g_{cur}\}$.

Recursion in the same way.

else

Add the next edge $\{k_i, \ell_i\}$ that is not in \mathbb{E}_0 .

Assign $A_{k_j, \ell_j} \leftarrow -1$.

continue

end if

end loop

return g

7.16 More details and results of numerical experiments

We give a more detailed description of the experiment that verifies the uniqueness condition in Corollary 3.5. A random power flow set point is generated by first choosing a random vector of voltages. The voltage magnitudes and angles are randomly sampled from a uniform distribution ranging from user-set min/max values.

$$|v_i^0| \sim U(V_{min}, V_{max}) \text{ for all } i \in \mathbb{V}$$

$$|\Theta_i^0| \sim U(\Theta_{min}, \Theta_{max}) \text{ for all } i \in \mathbb{V}$$

The voltage angles are rejected and discarded if they do not belong to the monotone regime. A new random sample is chosen until the angles belong to the the monotone regime. Finally, once we have a voltage profile belonging to the monotone regime, we use the information to calculate the real power injections, P^0 . The values of $|v^0|$ and P^0 are provided as an input to the power flow algorithm. Note that Θ^0 is always a solution to the P - Θ problem $\hat{P}(\Theta) = P^0$. In this sense, we refer to Θ^0 the ground truth solution. There are usually other solutions and the goal of this experiment is to analyze where those other solutions are with respect to the ground truth solution.

In order to explore different parts of the solution space, we randomly sample an initial point around the ground truth Θ^0 and provide it to MATPOWER. The current setting is to consider a normal distribution around the ground truth, with some specified standard deviation. Intuitively, if the random initial point is close enough to the ground truth solution, then the algorithm will converge to the ground truth solution. However, if we start the algorithm with a suitably far initial point, then the power flow algorithms may converge to a different solution. Note that initializing too far way can lead to convergence issues of the algorithm.

Next, we define a metric that can capture the distance between two solutions of the P - Θ problem. Consider a solution of the P - Θ problem, Θ^i , where i corresponds to the random initialization number ($i \in \mathcal{R} = \{1, \dots, 10,000\}$). Let Θ_k^i denote the voltage angle at bus k for the i -th experiment. We define $\text{dist}(\Theta^i)$ to be the distance between the particular solution Θ^i and the ground truth solution, characterized in terms of their angle differences:

$$\text{dist}(\Theta^i) = \max_{(k,\ell) \in \mathbb{E}} |\Theta_{k,\ell}^i - \Theta_{k,\ell}^0|$$

Now, define $\text{dist}^m(\mathbb{G})$ to be the smallest nonzero distance among all solutions in the monotone region for a given power system \mathbb{G} . The symbol \mathcal{M} represents the set of indices i such that the solution Θ^i belongs to the monotone region defined in the paper:

$$\text{dist}^m(\mathbb{G}) = \min_{i \in \mathcal{M} \cap \mathcal{R}} \text{dist}(\Theta^i) \quad \text{s.t. } \text{dist}(\Theta^i) \neq 0.$$

As a specific scenario, we consider the case when all the line properties are the same and the voltage magnitudes are fixed to be one. In other words, $V_{max} = V_{min} = 1$. Furthermore, the lines are close to being lossless. We note that when we experimented with

(significantly) lossy lines, different solutions were not found within the monotone region. The values of $\text{dist}(\Theta^i)$ and dist^m are calculated for different networks and are summarized in Table 4. The last column shows the upper bound on the allowable perturbations used in Corollary 3.5. In order to validate our theoretical results, it suffices to observe that dist^m is greater than the values in the final column.

Power Networks	dist^m	$2\pi/e$
Case 14	∞	∞
Case 30	71.8	45
Case 39	53.8	45
Case 57	37.8	15.7
Case 118	66.1	27.7

Table 4: Distance measure for different test cases.

Bibliography

- [1] T. Overbye, "Lecture Notes: ECEN 460 power systems operation and control," 2017, available from: <https://overbye.engr.tamu.edu/course-2/ecen460fa2017/lecture-notes/>.
- [2] T. Chen and D. Mehta, "On the network topology dependent solution count of the algebraic load flow equations," *IEEE Transactions on Power Systems*, vol. 33, no. 2, pp. 1451–1460, March 2018, available from: <https://arxiv.org/pdf/1512.04987.pdf>.
- [3] M. Ilic, "Network theoretic conditions for existence and uniqueness of steady state solutions to electric power circuits," in *Proceedings of the IEEE International Symposium on Circuits and Systems*, 1992.
- [4] C. Wang, A. Bernstein, J.-Y. Le Boudec, and M. Paolone, "Explicit conditions on existence and uniqueness of load-flow solutions in distribution networks," *IEEE Transactions on Smart Grid*, vol. 9, no. 2, pp. 953–962, March 2018.
- [5] H. D. Nguyen and K. S. Turitsyn, "Appearance of multiple stable load flow solutions under power flow reversal conditions," in *Proceedings of the IEEE PES General Meeting, National Harbor, MD*, July 2014, available from: <https://arxiv.org/pdf/1404.6591.pdf>.
- [6] H.-D. Chiang and M. E. Baran, "On the existence and uniqueness of load flow solution for radial distribution power networks," *IEEE Transactions on Circuits and Systems*, vol. CAS-37, no. 3, pp. 410–416, March 1990.

- [7] I. A. Hiskens and R. J. Davy, "Exploring the power flow solution space boundary," *IEEE Transactions on Power Systems*, vol. 16, no. 3, pp. 389–395, August 2001.
- [8] F. Galiana, "Analytical investigation of the power flow equations," 1983, pp. 411–415.
- [9] J. Thorp, D. Schulz, and M. Ilic-Spong, "Reactive power-voltage problem: conditions for the existence of solution and localized disturbance propagation," *International Journal of Electrical and Power Energy Systems*, vol. 9, January 1986.
- [10] A. Araposthatis, S. Sastry, and P. Varaiya, "Analysis of power-flow equation," *International Journal of Electrical and Power Energy Systems*, vol. 3, pp. 115–126, July 1981.
- [11] K. Miu and H.-D. Chiang, "Existence, uniqueness, and monotonic properties of the feasible power flow solution for radial three-phase distribution networks," *IEEE Transactions on Circuits and Systems*, vol. 47, pp. 1502–1514, October 2000.
- [12] S. Z. S. Bolognani, "On the existence and linear approximation of the power flow solution in power distribution networks," *IEEE Transactions on Power Systems*, vol. 31, pp. 163–172, January 2016.
- [13] J. Lavaei, D. Tse, and B. Zhang, "Geometry of power flows in tree networks," *IEEE Transactions on Power Systems*, vol. 31, pp. 163–172, January 2016.
- [14] K. Dvijotham, S. Low, and M. Chertkov, "Solving the power flow equations: a monotone operator approach," *archived and available at <https://arxiv.org/pdf/1506.08472.pdf>*, 2015.
- [15] E. Ryu and S. Boyd, "A primer on monotone operator methods," *Applied and Computational Mathematics*, vol. 15, no. 1, pp. 3–43, 2016.
- [16] R. Phelps, *Convex Functions, Monotone Operators and Differentiability*, 2nd ed. Springer, 1993.
- [17] H. Bauschke and P. Combettes, *Convex analysis and monotone operator theory in hilbert spaces*, 2nd ed. Springer, 2011.
- [18] R. Baldick, *Applied Optimization: Formulation and Algorithms for Engineering Systems*. Cambridge: Cambridge University Press, 2006.
- [19] S. Park, R. Y. Zhang, R. Baldick, and J. Lavaei, "Monotonicity between phase angles and power flow and its implications for the uniqueness of solutions," *52nd Hawaii International Conference on System Sciences (HICSS)*, 2019.
- [20] N. Korneyenko, "Combinatorial algorithms on a class of graphs," *Discrete Applied Mathematics*, vol. 54, pp. 215–217, 1994.

- [21] Y. Nesterov and L. Scrimali, “solving strongly monotone variational and quasi-variational inequalities,” *archived and available at <https://ssrn.com/abstract=970903>* or <http://dx.doi.org/10.2139/ssrn.970903>, 2006.
- [22] A.J.Korsak, “On the question of uniqueness of stable load-flow solutions,” *IEEE Transactions on Power Apparatus and Systems*, vol. PAS-91, no. 3, pp. 1093–1100, May 1972.
- [23] F.F.Wu, “Theoretical study of the convergence of the fast decoupled load flow,” *IEEE Transactions on Power Apparatus and Systems*, vol. PAS-96, no. 1, pp. 268–275, January 1977.
- [24] J. W. Simpson-Porco, “A theory of solvability for lossless power flow equations – part I: Fixed-point power flow,” *IEEE Transactions on Control of Network Systems*, vol. 5, no. 3, pp. 1361–1372, September 2018.
- [25] —, “A theory of solvability for lossless power flow equations – part II: Conditions for radial networks,” *IEEE Transactions on Control of Network Systems*, vol. 5, no. 3, pp. 1373–1385, September 2018.
- [26] J. Bermond, A. Germa, M. Heydemann, and D. Sotteau, “Girth in digraphs,” *Graph Theory*, vol. 4, no. 3, pp. 337–341, 1980.
- [27] V. Chvátal and E. Szemerédi, “Short cycles in directed graphs,” *Journal of Combinatorial Theory, Series B*, vol. 35, no. 3, pp. 323–327, 1983.
- [28] S. Park, R. Y. Zhang, J. Lavaei, and R. Baldick, “Uniqueness of power flow solutions using monotonicity and network topology,” *to appear in IEEE Transactions on Control of Network Systems*, 2020, available online at https://lavaei.ieor.berkeley.edu/Mono_PF_2019_1.pdf.
- [29] H. Zhang, S. Park, J. Lavaei, and R. Baldick, “Uniqueness of power flow solutions using graph-theoretic notions,” 2020, available online at https://lavaei.ieor.berkeley.edu/Eye_PF_2020_1.pdf.
- [30] R. Zimmerman, C. Murillo-Sanchez, and R. Thomas, “Matpower: Steady-state operations, planning and analysis tools for power systems research and education,” *IEEE Transactions on Power Systems*, vol. 26, no. 1, pp. 12–19, 2011.
- [31] K. Dvijotham, E. Mallada, and J. Simpson-Porco, “High-voltage solution in radial power networks: existence, properties, and equivalent algorithms,” *IEEE Control Systems Letters*, vol. 1, no. 2, pp. 322–327, October 2017.
- [32] S.Jafarpour, E. Huang, K. Smith, and F.Bullo, “Flow and elastic networks on the n-torus: geometry, analysis, and computation,” 2019, available online at <https://arxiv.org/pdf/1901.11189.pdf>.

- [33] T. S. Developers, "Sagemath, the Sage Mathematics Software System (Version 8.9)," 2019, available online at <https://www.sagemath.org>.
- [34] B. Cui and X. A. Sun, "Solvability of power flow equations through existence and uniqueness of complex fixed point," 2019, available online at <https://arxiv.org/pdf/1904.08855.pdf>.
- [35] A. Bernstein, C. Wang, E. Dall'Anese, J.-Y. L. Boudec, and C. Zhao, "Load-flow in multiphase distribution networks: Existence, uniqueness, non-singularity and linear models," *IEEE Transactions on Power Systems*, vol. 33, no. 6, pp. 5832–5843, April 2018.
- [36] D. Lee, H. D. Nguyen, K. Dvijotham, and K. Turitsyn, "Convex restriction of power flow feasible sets," 2019, available online at <https://arxiv.org/pdf/1803.00818.pdf>.
- [37] S. Park, R. Y. Zhang, J. Lavaei, and R. Baldick, "Uniqueness of power flow solutions using monotonicity and network topology," *IEEE Transactions on Control of Network Systems*, 2019.
- [38] D. Eppstein, "Parallel recognition of series-parallel graphs," *Information and Computation*, vol. 98, no. 1, p. 41–55, 1992.
- [39] S. Khuller, "Ear decompositions," *SIGACT News*, vol. 20, no. 1, p. 128, 1989.
- [40] J. C. Tiernan, "An efficient search algorithm to find the elementary circuits of a graph," *Communications of the ACM*, vol. 13, no. 12, pp. 722–726, 1970.
- [41] E. S. Dias, D. Castonguay, H. Longo, and W. A. R. Jradi, "Efficient enumeration of chordless cycles," *arXiv preprint arXiv:1309.1051*, 2013.
- [42] T. Uno and H. Satoh, "An efficient algorithm for enumerating chordless cycles and chordless paths," in *International Conference on Discovery Science*. Springer, 2014, pp. 313–324.
- [43] M. R. Garey and D. S. Johnson, *Computers and intractability*. freeman San Francisco, 1979, vol. 174.
- [44] R. Madani, J. Lavaei, and R. Baldick, "Convexification of power flow problem over arbitrary networks," in *2015 54th IEEE Conference on Decision and Control (CDC)*. IEEE, 2015, pp. 1–8.
- [45] Y. Zhang, R. Madani, and J. Lavaei, "Conic relaxations for power system state estimation with line measurements," *IEEE Transactions on Control of Network Systems*, vol. 5, no. 3, pp. 1193–1205, 2017.
- [46] S. Pemmaraju and S. Skiena, *Computational Discrete Mathematics: Combinatorics and Graph Theory with Mathematica®*. Cambridge university press, 2003.

Chapter V

An Efficient Homotopy Method for Solving the Post-contingency Optimal Power Flow to Global Optimality

1 Introduction

Optimal power flow (OPF) is a fundamental tool for power system network analysis, where the goal is to find a low-cost production of the committed generating units while satisfying the technical constraints of the system [73]. The main challenges in solving the OPF arise from the fact that it is a nonconvex optimization problem on a large-scale network that must be solved every few minutes. In order to overcome these challenges, the common practice in the electric power industry is to use a linearized approach called the DC-OPF approximation [74, 75], as opposed to the original AC-OPF problem. However, such methods simplify important aspects of the power flow physics and cannot guarantee attaining any optimal solution of the original problem. Improvements in interior-point methods have also provided an effective tool for solving the OPF problem, but they only guarantee convergence to a locally optimal solution [76, 77, 78]. Despite its difficulty, finding a global optimum for a large-scale OPF problem modeled with AC power flow equations is crucial for the reliable and efficient operation of power systems.

Initiated by the work [10], conic optimization has been extensively studied in recent years and proven to be a powerful technique for solving OPF to global or near-global optimality. The paper [10] has indeed shown that a semidefinite programming (SDP) relaxation is able to find a global minimum of OPF for a large class of practical systems, and [11] has discovered that the success of this method is related to the underlying physics of power systems. [9] and [8] have developed different sufficient conditions under which the SDP relaxation provides zero duality gap. Moreover, [7] has found an upper bound on the the rank of the minimum-rank solution of the SDP relaxation, which is leveraged in [6] to find a near globally optimal solution of OPF via a penalized SDP technique in the case where the SDP relaxation fails to work. These ideas have been refined in many papers to improve the relaxations via branch-and-cut approaches, conic hierarchies, and valid inequalities [5, 4, 3, 12]. In order to tackle the computational burden of solving large-scale SDP relaxations, the authors of [79] proposed strong second-order

cone programming (SOCP) relaxations, which produce high-quality feasible solutions for the AC-OPF problem in a short amount of time. The reader is referred to the survey paper [47] for more details.

Recently, there has been elevated interest in studying the robust operations of power systems that can withstand element failures (contingencies) in the network. Power operators are required to solve the *security-constrained* OPF (SCOPF) instead of an idealistic OPF problem [90, 68]. SCOPF is formulated by adding extra constraints to the classic OPF discussed above. These constraints impose additional limits on line flows and nodal voltages for a predetermined set of post-contingency configurations. In other words, SCOPF can be regarded as a more conservative version of the classic OPF that leads to a higher level of system security. This means that SCOPF inherits the challenges of classic OPF and furthermore, invites new challenges. It has been shown in [6] that SDP relaxations are able to obtain high-quality solutions of SCOPF. However, since SCOPF is a gigantic problem with an enormous number of variables, conic relaxations and even simple local search methods may be ineffective for real-world systems [63]. There are two primary methods to address the huge size of the SCOPF problem. One approach is to reduce the number of contingencies to a subset of binding contingencies that will lead to the same solution as the full set of contingencies [64, 65, 91]. If the number of binding contingencies is not sufficiently small enough to satisfy computational requirements, then we must make use of the second method, which is to simplify the SCOPF formulation. There have been many proposed methods to simplify the model of post-contingency states in SCOPF, such as Benders decomposition, linearization of the power flow equations, Lagrangian relaxation, and network compression [66, 67, 89, 69]. These contingency selection, approximation, and decomposition techniques can be combined to generate heuristic solutions to large-scale SCOPF problems, as in [83, 84]. Additionally, recent research has applied approaches from distributed control, stochastic programming, and machine learning to solve the SCOPF problem [85, 86, 87, 88].

The outputs of such methods include the optimal (or approximately optimal) values of the pre-contingency operating variables and possibly feasible values for the post-contingency variables for each contingency. The major drawback is that the post-contingency variables are not optimized with respect to each corresponding contingency configuration to minimize the violation of the constraints in case there is no feasible operating point. Currently, there is a rather limited literature that attempts to optimize the post-contingency settings. In the classic work [68], the optimal post-contingency actions were modelled as sub-problems and explicitly included in the SCOPF formulation. In order to overcome the complexity of this two-level optimization problem, an algorithm based on Bender's decomposition was developed, for which convergence is not guaranteed for general nonconvex problems. More recently, the work in [80] proposed an approach to determine an optimal combination of preventive and corrective actions taking into the account the system dynamics, while [70] introduced a hybrid computational strategy to solve the pre-contingency and post-contingency OPF problems. To the best of our knowledge, none of the previous works have ventured into finding the global optimum of each

of the post-contingency OPF problems (from here on called ‘contingency-OPF’), mainly because applying a computationally burdensome algorithm (such as SDP) to each of the contingency scenarios is unrealistic.

Nevertheless, it is important to find a globally optimal solution because local solutions can be much more costly. In this paper, we develop a computationally efficient homotopy method to improve the quality of the contingency-OPF solution. Constraint violations in the case of a contingency are very expensive to deal with, and under our formulation, a global solution corresponds to the minimum violation. Instead of solving for the solution to a contingency-OPF problem directly, we generate and solve (using local search algorithms) a series of intermediate optimization problems wherein we gradually remove a set of components of the power system. We show that the effectiveness of homotopy to find a global solution of the contingency-OPF problem is dependent on the homotopy path, and therefore, we characterize desirable homotopy paths. In doing so, we prove that the contingency-OPF generically has a unique global minimum. Furthermore, we prove that the complexity of implementing such homotopy scheme is on the order of solving $O(\log(1/\epsilon))$ convex quadratic optimization problems.

The remainder of the paper is organized as follows. In Section 2, we provide a literature review on homotopy methods and explain how it relates to our approach. In Section 3, we present the formulation of the two-stage Security-constrained Optimal Power Flow that can be decomposed into the base-OPF and contingency-OPF. Next, in Section 4, we introduce the homotopy method that connects contingency-OPF to base-OPF via parametrization. In Section 5, we develop theoretical results to characterize cases when homotopy will lead to a global solution of the deformed problem. Finally, in Section 6 we implement the homotopy method on actual test cases and verify its effectiveness. The proofs and additional simulation results appear in the Appendix.

1.1 Notations

The symbol \mathbb{R}^N denotes the space of N -dimensional real vectors and $(\cdot)^T$ denotes the transpose of a matrix. $\text{Re}\{\cdot\}$ and $\text{Im}\{\cdot\}$ denote the real and imaginary parts of a given scalar or matrix. The symbol $|\cdot|$ is the absolute value operator if the argument is a scalar, vector, or matrix; otherwise, it is the cardinality of a measurable set. Given a function $f(x, \cdot)$, $\nabla_x f(x, \cdot)$ and $\nabla_x^2 f(x, \cdot)$ denote the Jacobian and Hessian of f with respect to x , respectively. The symbol \odot denotes the elementwise multiplication between two vectors. Let $\mathbf{1}_n$ and $\mathbf{0}_n$ denote the n -dimensional vectors of ones and zeros, respectively. Furthermore, $\mathbf{1}_n^k$ denotes an n -dimensional vector of ones except for the k -th element that is zero. The imaginary unit is denoted by $\mathbf{j} = \sqrt{-1}$. Let the power network be defined by a graph $\mathcal{G}(\mathcal{V}, \mathcal{E})$, where \mathcal{V} is the node set and \mathcal{E} is the edge set. For notational simplicity, we assume that there is one generator at each node, but this formulation is easily generalizable to the case when there are multiple generators at each node (the case with no generator at a bus can be modeled by setting the upper and lower bounds on generation to zero). Each node $i \in \mathcal{V}$ has an associated complex voltage v_i , a fixed demand $P_i^d + \mathbf{j}Q_i^d$, and

an unknown generation $p_i^g + \mathbf{j}q_i^g$, and we assume that the nodal shunt admittance is zero. The complex voltage v_i can be expressed in polar form, $v_i = |v_i|e^{\mathbf{j}\theta_i}$, where $|v_i|$ and θ_i denote the voltage magnitude and phase angle at bus i , respectively. With a slight abuse of notation, $|v|$ denotes the vector of all voltage magnitudes. In addition, we define $\theta_{ij} = \theta_i - \theta_j$. The set of neighboring nodes of node i is denoted by $\mathcal{N}(i)$. Each line connecting two nodes i and j is represented by a standard Π -model with a series admittance $y_{ij} = g_{ij} + \mathbf{j}b_{ij}$ and a shunt admittance $y_{ij}^{\text{sh}} = g_{ij}^{\text{sh}} + \mathbf{j}b_{ij}^{\text{sh}}$. Then, the nodal admittance matrix Y is defined as

$$Y_{ij} = \begin{cases} \sum_{k \in \mathcal{N}(i)} y_{ik} + \frac{1}{2}y_{ik}^{\text{sh}} & \text{for } j = i \\ -y_{ij} & \text{for } j \in \mathcal{N}(i) \\ 0 & \text{otherwise} \end{cases} \quad (88)$$

whose (i, j) element is denoted as $Y_{ij} = G_{ij} + \mathbf{j}B_{ij}$. Finally, p_{ij} and q_{ij} are the real and reactive power flows from bus i to j , respectively.

2 Homotopy for Optimization

Homotopy methods have been used to improve the convergence of optimization problems. The benefit of homotopy methods compared to other iterative methods is that homotopy methods may yield global rather than local convergence. These methods are most useful for problems where convergence to a global solution is heavily dependent on a good initial point, which can be hard to obtain. More recently, probability-one homotopy methods have been applied to solving optimization problems, such as optimal control [36, 34] and statistical learning [33]. Typically, the homotopy methods in optimization focus on parametrizing the first-order optimality conditions [13, 32] or the objective function ([17, 15]). Homotopy methods have also been applied in the field of power systems, primarily to solve the power flow (PF) problem for cases that do not converge [14, 31, 18, 16, 39].

While convergence to a global minimum with probability one is guaranteed for a convex optimization problem [17], this is generally not true for nonconvex problems. In order to understand when homotopy can be effective in finding a global solution for nonconvex optimization, we explore a minimization problem of the form: $\min_x f(x)$ where $f : \mathbb{R}^n \rightarrow \mathbb{R}$ is a nonconvex function of $x \in \mathbb{R}^n$. This problem is named (P^o) . Note that the function $f(\cdot)$ can incorporate exact/inexact penalty functions to enforce constraints on x , implying that this formulation is general for both unconstrained and constrained optimization [46]. We refer to (P^o) as the “base-case” problem. A deformed version of the base-case, which is also a nonconvex minimization problem, is denoted by (P^f) and defined as $\min_x \tilde{f}(x)$. For our application, (P^o) corresponds to the base-OPF problem and (P^f) corresponds to the contingency-OPF problem (the definition of these two problems are provided in the next section). We consider two possible methods for solving the deformed problem that are based on local search algorithms:

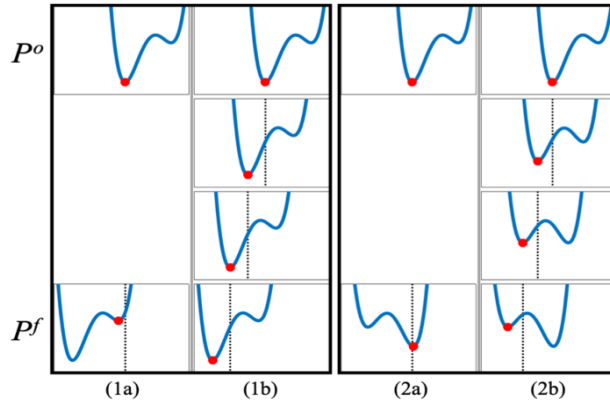


Figure 16: Evaluating the performance of homotopy on one-dimensional unconstrained minimization problems. The figure compares two different samples (1) and (2), with two different methods (a) and (b). The dotted lines show how the solution from the previous iteration is used in local search algorithms to solve the next problem. The red dots show the solution at each iteration using the position of the dotted lines as the initial point. For the one-shot method (a), the solution of P^o is used as the initial point for P^f . For the homotopy method (b), the base problem P^o is gradually transformed to P^f over three iterations, updating the initial point as the solution to the previous problem.

- a) *One-shot method*: Use the solution of P^o as the initial point for any descent numerical algorithm to solve P^f .
- b) *Homotopy method*: Generate a (discretized) homotopy map from P^o to P^f . Use the solution of P^o as the initial point, but update it at each step of the homotopy by solving an intermediate problem using local search that is initialized at the solution of the previous step. A linear (non-discretized) homotopy map can be defined as:
$$P(\lambda) = \min_x \left\{ \lambda \tilde{f}(x) + (1 - \lambda) f(x) \right\}, \quad 0 \leq \lambda \leq 1,$$
with the property that $P(0) = P^o$ and $P(1) = P^f$.

Depending on $f(x)$ and $\tilde{f}(x)$, homotopy may or may not lead to better results than solving the deformed problem in one shot. In Figure 16, we see an example where homotopy is effective in finding the global minimum of a deformed problem and another example where it leads to a non-global local minimum. Knowing when homotopy will be effective is highly dependent on understanding how the shape of the function changes from the base-case to the deformed problem. In the current literature, there is a lack of theoretical results to characterize the performance of homotopy in finding a global optimum. While [17] presents algorithms that make use of homotopy to solve nonconvex, unconstrained minimization problems, these algorithms are similar to other stochastic search methods in that they do not guarantee convergence to the global minimum.

3 Formulation of Two-stage Security-constrained Optimal Power Flow

In this section, we present the mathematical formulation of the two-stage security-constrained OPF which is decomposed into the base-OPF and the contingency-OPF. The base-OPF resembles the conventional SCOPF that finds a base-case operational point which is robust against potential contingencies. The contingency-OPF focuses on a single contingency and attempts to find an adjusted operating point that minimizes constraint violations.

3.1 Base-case Optimal Power Flow

Recall that the *classic* optimal power flow problem (without security considerations) minimizes operating costs subject to technical limits, such as the power flow equations and explicit bounds on variables. The decision variables $x = (|v|, \theta, p^g, q^g) \in \mathbb{R}^{4|\mathcal{V}|}$ represent the vector of voltage magnitudes, voltage phase angles, real power generations and reactive power generations, corresponding to the pre-contingency base-case configuration of the network.

Now, suppose that there is a set of possible contingencies, namely \mathcal{K} , where each contingency corresponds to a line or generator outage. Each contingency $k \in \mathcal{K}$ introduces a new set of variables x^k , and therefore, for a network with $|\mathcal{V}|$ buses and $|\mathcal{K}|$ contingencies, the SCOPF problem will involve optimizing over $4|\mathcal{V}|(|\mathcal{K}|+1)$ scalar variables. The contingencies also add operational constraints of their own. In addition, there are physical limitations on how the post-contingency network can adapt from the base-case, and these limits are added as constraints that are functions of the base-case variables.

Since this extremely high-dimensional problem is cumbersome to solve, in practice the contingency constraints are approximated via methods such as LODF and PTDF [43]. In essence, this approximates the contingency variable x^k as a function of the base-case variable x . Therefore, post-contingency equality constraints for contingency k are approximated by a composite function of the form $h_k(x) \triangleq t_k(a_k(x))$, where $a_k(x)$ represents the control actions that are taken in the event of a contingency. The same goes for post-contingency inequality constraints, represented by $g_k(x)$.

Finally, another important consideration is how SCOPF performs when the problem is infeasible. Therefore, we model some operational limits using soft constraints with extra variables that capture the amount of violation. The objective function that is minimized is the sum of real power generation costs in the base-case as well as a weighted sum of equality constraint violation penalties in the contingencies. The standard optimization

form is presented below:

$$\begin{aligned}
 \text{[base-OPF]} \quad & \min_{x, \{\sigma_k\}} && f(x) + \sum_{k=1}^{|\mathcal{K}|} \phi_k(\sigma_k) \\
 & \text{s.t.} && h(x) = 0, \quad g(x) \leq 0 \\
 & && h_k(x) = \sigma_k, \quad g_k(x) \leq 0, \quad \forall k \in \{1, \dots, |\mathcal{K}|\}
 \end{aligned} \tag{89}$$

where $\phi_k(\cdot)$ represents the penalty functions for the violations. We denote this problem as the base-OPF.

3.2 Post-contingency Optimal Power Flow

The base-OPF solves for the base-case operating point by taking into account the possible failures in the network. In the process, it approximates the relationship between the contingency operation point x^k and the base-case operating point x . However, it does not actually solve for the optimal x^k 's. Therefore, for each contingency we propose to solve a contingency-OPF problem to find the best operating point for the specific contingency scenario, given the base solution.

We model a contingency, such as a line or generator outage, by changing the system parameters from their base values. For example, a line outage physically means that power cannot flow over that connection, which can be modeled by setting the resistance of the line to infinity or its conductance to zero. In the event of a line outage, the power is re-routed through other paths and therefore the amount of loss in the system changes. However, the difference in loss is small enough such that there is often no need for additional participation from other generators, unlike in the scenario of a generator outage. Therefore, we fix the real power generation to be equal to the base-case values and solve for the remaining variables such that the violations for the bus balance equations are small and spread out as much as possible (note that the proposed method can handle generator participation, if needed). This is because a large concentrated violation in a few buses can result in serious issues for the power network, whereas small power mismatches can be taken care of by real-time feedback controllers. Taking these into consideration,

each contingency-OPF under study is given as

$$\begin{aligned}
& \min_{|v|, \theta, q^g, \sigma^p, \sigma^q} \quad \phi(\sigma^p, \sigma^q) \\
& \text{s.t.} \quad P_i^g - \sum_{j=1}^{|\mathcal{V}|} |v_i| |v_j| (\tilde{G}_{ij} \cos \theta_{ij} + \tilde{B}_{ij} \sin \theta_{ij}) = P_i^d + \sigma_i^p \quad \forall i \in \mathcal{V} \\
& \quad q_i^g - \sum_{j=1}^{|\mathcal{V}|} |v_i| |v_j| (\tilde{G}_{ij} \sin \theta_{ij} - \tilde{B}_{ij} \cos \theta_{ij}) = Q_i^d + \sigma_i^q \quad \forall i \in \mathcal{V} \quad (90) \\
& \quad |v_i| = |v_i|^{base} \quad \forall i \in \mathcal{V} \setminus \mathcal{V}^q \\
& \quad Q_i^{min} \leq q_i^g \leq Q_i^{max} \quad \forall i \in \mathcal{V} \\
& \quad V_i^{min} \leq |v_i| \leq V_i^{max} \quad \forall i \in \mathcal{V}^q \\
& \quad |\theta_i - \theta_j| \leq \Theta_{ij}^{max} \quad \forall (i, j) \in \mathcal{E}
\end{aligned}$$

Here, \mathcal{V}^q is the set of buses that hit their upper or lower reactive power generation bounds in the base-case, and $|v_i|^{base}$ is the voltage magnitude of bus i in the base-case. The notations \tilde{G}_{ij} and \tilde{B}_{ij} reflect the potential change in the admittance matrix from the base-case values $Y_{ij} = G_{ij} + \mathbf{j}B_{ij}$. Note that real power generation is now a fixed parameter obtained from a solution of the base-OPF and therefore has been denoted by capital P^g . In the above formulation, constraints on the power flow over transmission lines are modeled as constraints on the angle differences between buses, which is a common practice [7]. However, the proposed method is general and can accommodate other types of line flow constraints.

For generator outage contingencies, there is an additional aspect to consider. A generator outage corresponds to setting the real power generation at that generator to zero. However, in order to compensate for the lost generation, the system operator needs to increase the power generation at other generators that participate in the outage response. The above framework is general enough to incorporate this difference: simply set $P^g = P^{g,f}$ and $\tilde{G}_{ij} = G_{ij}$, $\tilde{B}_{ij} = B_{ij}$ for all $(i, j) \in \mathcal{E}$, where $P^{g,f}$ is the new setpoint for the real power generation. Denoting $x = [|v|, \theta, q^g, \sigma^p, \sigma^q]$ as the combined variable, contingency-OPF in a standard optimization form would be:

$$\begin{aligned}
& \text{[contingency-OPF]} \quad \min_x \quad f(x) \\
& \quad \text{s.t.} \quad h(x) = 0, \quad g(x) \leq 0
\end{aligned} \quad (91)$$

Note that $f(\cdot)$ is not the same objective function used for the base-OPF but merely a simplified notation for $\phi(\sigma^p, \sigma^q)$. With no loss of generality, we focus on the case when $\phi(\sigma^p, \sigma^q) = \sum_i \{c_i^p (\sigma_i^p)^2 + c_i^q (\sigma_i^q)^2\}$, where c_i^p and c_i^q are cost coefficients. Similarly, $h(\cdot)$ is not the same as the constraint functions used for the base-OPF.

If the optimal objective value of the contingency-OPF is zero, it means that the solution of the base-case could be modified to stay feasible in case of the contingency. However,

the primary focus of this paper is on hard instances with a nonzero optimal cost, meaning that some of the constraints must be violated to accommodate the outage. In these cases, since taking corrective actions to deal with nodal power violations is expensive, it is essential to find a global solution.

4 Methods

In the following subsections, we present a homotopy method that parametrizes the contingency-OPF to model a gradual line or a generator outage.

4.1 Homotopy Method for a Line Outage

In order to solve the contingency-OPF problem, we propose a homotopy method that gradually changes certain parameters of the problem from the base-OPF, rather than abruptly changing the structure of the network. For a line outage contingency, we introduce an aggregate homotopy parameter $\lambda = [\gamma, \beta, \gamma^{\text{sh}}, \beta^{\text{sh}}]$ corresponding to the series admittance and the shunt admittance, where $\gamma, \beta, \gamma^{\text{sh}}, \beta^{\text{sh}} \in \mathbb{R}^{|\mathcal{E}|}$. To be more precise, we parametrize the admittance in the contingency-OPF as follows:

$$y_{ij}(\lambda) = g_{ij}\gamma_{ij} + \mathbf{j}b_{ij}\beta_{ij} \quad \forall (i, j) \in \mathcal{E} \quad (92a)$$

$$y_{ij}^{\text{sh}}(\lambda) = g_{ij}^{\text{sh}}\gamma_{ij}^{\text{sh}} + \mathbf{j}b_{ij}^{\text{sh}}\beta_{ij}^{\text{sh}} \quad \forall (i, j) \in \mathcal{E} \quad (92b)$$

which creates a family of OPF problems, named H_λ , written in the standard form of:

$$\begin{array}{ll} \left[\begin{array}{l} \text{homotopy-OPF} \\ H_\lambda \end{array} \right] & \begin{array}{l} \min_x \quad f(x, \lambda) \\ \text{s.t.} \quad h(x, \lambda) = 0, \quad g(x, \lambda) \leq 0 \end{array} \end{array} \quad (93)$$

Now, let $\ell \in \mathcal{E}$ be a line that connects buses i and j , and consider a contingency scenario in which the line ℓ is out. Notice that $\lambda^o = [\mathbf{1}_{|\mathcal{E}|}, \mathbf{1}_{|\mathcal{E}|}, \mathbf{1}_{|\mathcal{E}|}, \mathbf{1}_{|\mathcal{E}|}]$ corresponds to the original network before the line outage, and $\lambda^f = [\mathbf{1}_{|\mathcal{E}|}^\ell, \mathbf{1}_{|\mathcal{E}|}^\ell, \mathbf{1}_{|\mathcal{E}|}^\ell, \mathbf{1}_{|\mathcal{E}|}^\ell]$ corresponds to the post-contingency network after the line outage. By varying λ from λ^o to λ^f , the homotopy map allows us to create fictitious power networks that constitute a series of intermediate OPF problems.

4.2 Homotopy Method for a Generator Outage

For a generator outage, our proposed homotopy map gradually decreases the real power generation at the generators that are out and gradually increases the real power generation at the generators participating in the contingency response. For the simplicity of presentation, consider contingencies associated with a single generator (generator k) outage. This is common practice in power systems and is referred to as the $N - 1$ criterion. Yet,

note that the proposed method can easily be extended to multiple generator outages and is incorporated in Algorithm 7.

Let $P^{g,o} \in \mathbb{R}^{|\mathcal{V}|}$ be the real power generated at all generators in the base-case. Using the participation factors of generators that are still active in the contingency, we can compute $P^{g,f} \in \mathbb{R}^{|\mathcal{V}|}$, the real power generated at all generators after the contingency. Since generator k is down in this contingency scenario, $P_k^{g,f} = 0$. One possible method to choose the participation factors that determine $P^{g,f}$ is provided in the Appendix. Similar to what we did for line outage contingencies, we introduce an aggregate homotopy parameter $\lambda = [\gamma, \beta]$ with $\gamma, \beta \in \mathbb{R}^{|\mathcal{V}|}$ to create the following homotopy map:

$$P^g(\gamma) = P^{g,o} \odot \gamma + P^{g,f} \odot (\mathbf{1}_{|\mathcal{V}|} - \gamma) \quad (94a)$$

$$Q^d(\beta) = Q^{d,o} \odot \beta + Q^{d,f} \odot (\mathbf{1}_{|\mathcal{V}|} - \beta) \quad (94b)$$

Focusing on the first equation where we parametrize the real power generation, notice that $\lambda^o = [\mathbf{1}_{|\mathcal{V}|}, \mathbf{1}_{|\mathcal{V}|}]$ corresponds to the original network before the generator outage, and $\lambda^f = [\mathbf{0}_{|\mathcal{V}|}, \mathbf{0}_{|\mathcal{V}|}]$ corresponds to the post-contingency network after the generator outage. By varying λ from λ^o to λ^f , the homotopy map allows us to trace a gradual generator outage. Equation (94b) parametrizes the reactive power demand, and we will set the value $Q^{d,f} \simeq Q^{d,o}$. Although the justification for this extra parametrization is not clear for the moment, we will explain later that the parametrization needs to be of high enough dimension in order for the homotopy method to be effective. The series of homotopy problems have the same form as those for the line outage, given by Equation (93).

4.3 Implementation of Homotopy-OPF

The global minimum of the base-OPF is also a global minimum of H_{λ^o} because at $\lambda = \lambda^o$, the parameters of the homotopy-OPF corresponds to the pre-contingency network, for which the violations are zero. Starting with a solution to the base-OPF, we aim to iteratively solve a series of homotopy-OPF problems along a path of λ to eventually arrive at the contingency-OPF. Our implementation of solving a series of homotopy-OPF, as presented in the previous section, can be viewed as a one-parametric optimization problem by defining $\tilde{f}(x, t) = f(x, \lambda(t))$, $\tilde{h}(x, t) = h(x, \lambda(t))$ and $\tilde{g}(x, t) = g(x, \lambda(t))$, where $\lambda(t)$ is a continuous function in t such that $\lambda(0) = \lambda^o$ and $\lambda(1) = \lambda^f$. The trajectory of λ 's tracing from $\lambda(0)$ to $\lambda(1)$ is called the homotopy path. Then, the problem reduces to solving the following problem for a suitable discretized partition of t in the range $[0, 1]$, namely $0 = t^1 \leq t^2 \leq \dots \leq t^T = 1$:

$$\left[\begin{array}{c} \text{homotopy-OPF} \\ H_t \end{array} \right] \quad \begin{array}{l} \min_x \quad \tilde{f}(x, t) \\ \text{s.t.} \quad \tilde{h}(x, t) = 0, \quad \tilde{g}(x, t) \leq 0 \end{array} \quad (95)$$

We make the following assumptions for the development of the results of this section:

Algorithm 6 Homotopy-OPF for Line Outages

Given: Contingency set \mathcal{K} with line outages $L_k \subset \mathcal{E}$ for each $k \in \mathcal{K}$

Initialize: Solve base-OPF problem to find a globally optimal solution $(|v|_*, \theta_*, p_*^g, q_*^g, \{\sigma_{k*}\})$.

Formulate the contingency-OPF problem:

1. Fix real power generation to base-case solution: $P^g := p_*^g$
2. Find \mathcal{V}^q based on q_*^g .

for $k \in \mathcal{K}$ **do**

Set up homotopy-OPF family H_Λ for given line outages L_k .

Initialize $(|\tilde{v}|, \tilde{\theta}, \tilde{q}^g, \tilde{\sigma}^p, \tilde{\sigma}^q)$ as the solution of base-OPF.

for $i \in \{1, \dots, T\}$ **do**

Solve H_{Λ^i} using initial point $(|\tilde{v}|, \tilde{\theta}, \tilde{q}^g, \tilde{\sigma}^p, \tilde{\sigma}^q)$, and obtain new solution $(|v|, \theta, q^g, \sigma^p, \sigma^q)$.

Update $(|\tilde{v}|, \tilde{\theta}, \tilde{q}^g, \tilde{\sigma}^p, \tilde{\sigma}^q) \leftarrow (|v|, \theta, q^g, \sigma^p, \sigma^q)$

end for

Return $(|v|, \theta, q^g, \sigma^p, \sigma^q)$ and violation cost $\phi(\sigma^p, \sigma^q)$.

end for

- (A₁) There exists a continuous function $x^*(t) : [0, 1] \rightarrow \mathbb{R}^{5|\mathcal{V}|}$ such that $x^*(t)$ is a global minimizer for H_t . Moreover, $x^*(0)$ is unique and known.
- (A₂) There exists a neighborhood U of $\{(x^*(t), t)\} \subset \mathbb{R}^{5|\mathcal{V}|} \times [0, 1]$ such that for all $(x, t) \in U$, the functions \tilde{f} and \tilde{h} are twice continuously differentiable with respect to x .
- (A₃) Linear independence constraint qualification (LICQ) and strong second-order sufficient conditions (SSOC) are satisfied at $x^*(t)$ for every $t \in [0, 1]$.

Note that the discretization of homotopy path can also be represented by the set $\Lambda := \{\Lambda^1, \dots, \Lambda^T\}$, where $\Lambda^i = \lambda(t^i)$ for $i = 1, \dots, T$, $\Lambda^1 = \lambda(t^1) = \lambda^o$ and $\Lambda^T = \lambda(t^T) = \lambda^f$. In other words, $H_{t^i} = H_{\Lambda^i}$. The SSOC is similar to the second-order sufficient conditions for local optimality but with the addition of the strict complementary slackness condition and the linear independence of the active constraints [54]. Furthermore, Assumptions (A₂) and (A₃) together imply that the Lagrange multipliers associated with $x^*(t)$ are uniquely determined for every $t \in [0, 1]$. We will later discuss that these assumptions are mild.

To begin, the first homotopy-OPF problem H_{t^1} is initialized as the solution to the base-OPF problem. The series of homotopy-OPF problems are then solved sequentially, where the solution to the previous homotopy-OPF problem H_{t^i} is utilized as the initial point for a local search algorithm solving $H_{t^{i+1}}$. Please refer to Algorithms 6 and 7 for complete details of the method.

Algorithm 7 Homotopy-OPF for Generator Outages

Given: Contingency set \mathcal{K} with generator outages $R_k \subset \mathcal{V}$ for each $k \in \mathcal{K}$
Initialize: Solve base-OPF problem to find a globally optimal solution $(|v|_*, \theta_*, p_*^g, q_*^g, \{\sigma_{k*}\})$.
for $k \in \mathcal{K}$ **do**
 Formulate the contingency-OPF problem:
 Define P_r^g as the fixed real power generation at $r \in \mathcal{V}$
 Define ΔP_k^g as the total lost real power generation at k : $\Delta P_k^g := \sum_{r \in R_k} P_{*,r}^g$
 1. Find \mathcal{V}^q .
 2. Remove real power generation for generators in R_k : $P_r^g \leftarrow 0 \quad \forall r \in R_k$
 3. Compute participation factors α_r^g for $r \in \mathcal{V} \setminus R_k$ (see Algorithm 8 in the Appendix)
 4. Add real power generation for participating generators:
 for $r \in \mathcal{V} \setminus R_k$ **do**
 if $\alpha_r^g > 0$ **then**
 $P_r^g \leftarrow \max\{\alpha_r^g \Delta P_k^g, P_r^{max} - p_{*,r}^g\}$
 end if
 end for
 Set up homotopy-OPF family H_Λ for given generator outages R_k .
 Let $P^{g,o} := p_*^g$ and $P^{g,f} := P^g$
 Initialize $(|\tilde{v}|, \tilde{\theta}, \tilde{q}^g, \tilde{\sigma}^p, \tilde{\sigma}^q)$ as the solution of base-OPF.
 for $i \in \{1, \dots, T\}$ **do**
 Solve H_{Λ^i} using initial point $(|\tilde{v}|, \tilde{\theta}, \tilde{q}^g, \tilde{\sigma}^p, \tilde{\sigma}^q)$ and obtain new solution $(|v|, \theta, q^g, \sigma^p, \sigma^q)$
 Update $(|\tilde{v}|, \tilde{\theta}, \tilde{q}^g, \tilde{\sigma}^p, \tilde{\sigma}^q) \leftarrow (|v|, \theta, q^g, \sigma^p, \sigma^q)$
 end for
 Return $(|v|, \theta, q^g, \sigma^p, \sigma^q)$ and violation cost $\phi(\sigma^p, \sigma^q)$
end for

In this paper, we assume that the base-OPF has a unique global minimum that is available (known). The availability of a global minimum is a reasonable assumption because a good initial point is usually provided for the base-OPF, and also because more time is allocated to solving it compared to a large number of contingency-OPF problems for different outages, allowing the use of various convex relaxation techniques for the base-OPF. If the optimal violation cost for H_{λ^o} is nonzero, the global minimum will be unique with overwhelming probability. Furthermore, even if the violation cost is zero, it will immediately become nonzero during the next homotopy iteration if removing a line or generator introduces inflexibilities that the network cannot accommodate. In fact, these near-infeasible problems where a contingency will make the system "stressed" are the cases where homotopy can be useful and are the focus of this paper. Later in the paper, we will present a rigorous result showing that the uniqueness of the global minimum is a generic

property for H_λ .

5 Analysis of Homotopy Paths

In Section 2, we offered two examples of nonconvex optimization: one in which the homotopy method resulted in the global minimum and another in which the homotopy method resulted in a non-global local minimum (see Figure 16). In this section, we describe a theoretical framework that describes when homotopy can be used to obtain a global minimum. We apply this framework to analyze the performance of homotopy-OPF in finding the global solution of the contingency-OPF. The results developed in this section have implications for homotopy methods in a broad range of optimization problems.

Theorem 5.1. *Let $\bar{x}(t^i, z)$ denote the stationary point of H_{t^i} that a local search algorithm converges to when initialized at point z . Set $z^1 = x^*(t^1) := x^*(0)$ and consider the sequence of points $\{x(t^i)\}_{i=1}^T$ generated by the following update rule:*

$$x(t^i) = \bar{x}(t^i, z^i) \tag{96}$$

$$z^{i+1} = x(t^i) \tag{97}$$

Moreover, define $\Delta t := \sup_{i=1, \dots, T-1} (t^{i+1} - t^i)$. Under Assumptions (A1), (A2) and (A3), a sufficiently small Δt will ensure that $x(t^i)$ is a global minimizer of H_{t^i} for $i = 1, \dots, T$.

Theorem 5.1 states that if we can solve each H_t exactly, then a sufficiently small stepsize in the parameter t (or equivalently λ) can track the global minimizer from the base-OPF all the way to the contingency-OPF. However, an exact solution to each H_t (or equivalently H_λ) is generally unattainable in practice. Furthermore, the interplay between the accuracy of solving each H_t and the number of discretization contribute to the overall complexity of solving homotopy-OPF. We will show that it suffices to find an approximate solution with not a necessarily high accuracy. This will significantly reduce the complexity of solving the parametric homotopy-OPF.

5.1 Convergence and Complexity of Homotopy-OPF

In this subsection, we analyze the complexity of solving the contingency-OPF using the proposed homotopy method. The results here are based on a specific local search algorithm called Wilson's method. However, there are many other methods, such as Robinson's method, that can achieve the same results [71]. Let μ and ζ denote the Lagrange multipliers for the constraints $\tilde{h}(x, t) = 0$ and $\tilde{g}(x, t) \leq 0$, respectively. For every instance of H_t , we determine a local minimizer and its Lagrange multipliers, $w(t) = (x(t), \mu(t), \zeta(t))$ by using the following Wilson's method: Start with an initial point w^0 , and solve the optimization problem $W(w^k, t)$ in order to find the next iterate w^{k+1} for $k \in \{0, 1, 2, \dots\}$,

where the problem $W(w^k, t)$ is defined below.

$$W(w^k, t) : \min_x \quad \nabla_x \tilde{f}(x^k, t)^T (x - x^k) + \frac{1}{2} (x - x^k)^T \nabla_x^2 \tilde{L}(w^k, t) (x - x^k) \quad (98a)$$

$$\text{s.t.} \quad \tilde{h}_i(x^k, t) + \nabla_x \tilde{h}_i(x^k, t)^T (x - x^k) = 0, \quad \forall i \in \mathcal{I} \quad (98b)$$

$$\tilde{g}_j(x^k, t) + \nabla_x \tilde{g}_j(x^k, t)^T (x - x^k) \leq 0, \quad \forall j \in \mathcal{J} \quad (98c)$$

where \mathcal{I} and \mathcal{J} denote the set of indices for the equality constraints and inequality constraints, respectively, and $\tilde{L}(w^k, t) = \tilde{f}(x^k, t) + \sum_i \mu_i^k \tilde{h}_i(x^k, t) + \sum_i \zeta_i^k \tilde{g}_i(x^k, t)$. Furthermore, let a global minimizer of H_t and its corresponding Lagrange multipliers be denoted by $w^*(t) = (x^*(t), \mu^*(t), \zeta^*(t))$. In this problem, we solve for the optimization variable x and the Lagrange multipliers associated with (98b) and (98c) to be able to find a primal-dual solution. Let us define the function $\hat{w}(w^k, t)$ as the exact solution to $W(w^k, t)$. Then, w^{k+1} numerically approximates $\hat{w}(w^k, t)$. The process is repeated for increasing values of k until a predefined criteria is met, and the final iterate of $\{w^k\}$ is returned as an approximate solution to $w(t)$.

Theorem 5.2. *Suppose that Assumptions (A1), (A2) and (A3) hold. Consider the following algorithm for a constant number M : Given $w_0 = w^*(t^1) := (x^*(t^1), \mu^*(t^1), \zeta^*(t^1))$, compute w_i as the solution to H_{t^i} using M Wilson's iterations starting at w_{i-1} for $i = 1, \dots, T$. There exist positive constants \hat{r} and Δt such that for every sufficiently small $\epsilon > 0$, the algorithm generates points $\{w'_i\}_{i=1}^T$ with $\|w'_i - w^*(t^i)\| < \epsilon$ whenever $t^{i+1} - t^i \leq \Delta t$ for $i = 1, 2, \dots, T$, provided that M is chosen to be larger than $\log(\hat{r}/\epsilon)$. In particular, the Wilson complexity (total number of Wilson steps) of finding an almost globally optimal solution with ϵ error for H_{t^T} is $O(\log(1/\epsilon))$.*

The above theorem implies that given a global minimizer for the initial problem H_{t^1} , we can simply solve a small number of convex quadratic programs for each H_{t^i} and keep track of its global minimizers. In particular, the quadratic program (98) is convex because the SSOC holds at the global minimizers. Furthermore, the number of parameter discretizations needed is upper bounded by a constant for small values of ϵ . This result is aligned with the complexity analysis of interior-point methods [72]. More insight is provided in the proof.

Remark 3. *Our assumptions imply that H_t along $\lambda(t)$ has a unique global solution satisfying SSOC. In the next subsection, we argue that this is a reasonable assumption to make. In addition, this assumption on the global solution can be replaced by the "connectivity" of the set of all global solutions (this allows having infinitely many possible solutions for post-contingency OPF with zero violation cost). In what follows, we show that the uniqueness of the global minimum is a generic property for H_t .*

5.2 Genericity of Unique Global Minimzer with SSOC

Recall that a set $\mathbb{S} \subset \mathbb{R}^n$ has (Lebesgue) measure zero if for every $\epsilon > 0$, \mathbb{S} can be covered by a countable union of n -cubes, the sum of whose measures is less than ϵ . A property that holds except on a subset whose Lebesgue measure is zero is said to be satisfied *generically* or hold for *almost all*. In this subsection, we will show that the homotopy-OPF generically has a unique global minimizer that satisfies SSOC .

Consider the following family of problems, which adds a linear perturbation to the objective of the homotopy-OPF:

$$\begin{aligned} [H_{\lambda,\omega}] \quad & \min_{x \in \Psi} f(x, \lambda) + \omega^T x \\ & \text{s.t. } h(x, \lambda) = 0 \end{aligned} \quad (99)$$

where $f : \mathbb{R}^{5|\mathcal{V}|} \times \mathbb{R}^\ell \rightarrow \mathbb{R}$, $h : \mathbb{R}^{5|\mathcal{V}|} \times \mathbb{R}^\ell \rightarrow \mathbb{R}^{2|\mathcal{V}|}$ are smooth functions and the parameters (λ, ω) belong to an open set $\mathbb{U} \subset \mathbb{R}^\ell \times \mathbb{R}^{5|\mathcal{V}|}$. The set $\Psi \subset \mathbb{R}^{5|\mathcal{V}|}$ is defined as below:

$$\Psi = \left\{ (|v|, \theta, q^g, \sigma^p, \sigma^q) \left| \begin{array}{l} Q_i^{min} \leq q_i^g \leq Q_i^{max} \quad \forall i \in \mathcal{V} \\ V_i^{min} \leq |v_i| \leq V_i^{max} \quad \forall i \in \mathcal{V}^q \\ |\theta_i - \theta_j| \leq \Theta_{ij}^{max} \quad \forall (i,j) \in \mathcal{E} \\ |v_i| = |v_i|^{base} \quad \forall i \in \mathcal{V} \setminus \mathcal{V}^q \end{array} \right. \right\} \quad (100)$$

This formulation is possible by noticing that the inequality constraints of homotopy-OPF are independent of the parameter λ . We call this problem the extended homotopy-OPF. Here, ℓ represents the dimension of the parameter λ , which can be equal to either $4|\mathcal{E}|$ (for line contingencies) or $2|\mathcal{V}|$ (for generator contingencies). Then, using the results from [54], we can easily derive the following lemma:

Lemma 5.3. *Suppose that the following two conditions are satisfied:*

1. *The function $\lambda \rightarrow h(x, \lambda)$ is of full rank $2|\mathcal{V}|$ for all $x \in \Psi$ at every λ ⁵.*
2. *The set Ψ is a cyrtohedron and the set \mathbb{U} is an open set.*

Then, for almost all (λ, ω) except those in a set $\mathbb{U}' \subset \mathbb{U}$ of measure zero, $H_{\lambda,\omega}$ has a unique global minimizer satisfying SSOC. In fact, for every $(\lambda, \omega) \in \mathbb{U} \setminus \mathbb{U}'$, $H_{\lambda,\omega}$ cannot achieve the same objective value at any two distinct critical points.

The concept of a cyrtohedra was first introduced in [51] and it captures a class of sets whose boundaries are a union of countably many smooth manifolds pieced together. A few main examples of cyrtohedra include polyhedral convex sets, submanifolds, submanifolds with boundaries, and manifolds with corners. In our case, the set Ψ is naturally a cyrtohedra and therefore we only have to verify the first condition. The next lemma proves that the condition can be easily verified for the line outage contingency.

⁵The rank of a differentiable mapping is the rank of its Jacobian.

Lemma 5.4. Define the matrix $J = \left[\begin{array}{c|c} J^1 & 0 \\ \hline 0 & J^2 \end{array} \right] \in \mathbb{R}^{2|\mathcal{E}| \times 2|\mathcal{V}|}$ as

$$J_{(i,j),k}^1 = \begin{cases} -\frac{1}{2}g_{ij}^{sh}|v_k|^2 & \text{for } k = i \text{ or } j, j \in \mathcal{N}(i) \\ 0 & \text{otherwise} \end{cases}$$

$$J_{(i,j),k}^2 = \begin{cases} \frac{1}{2}b_{ij}^{sh}|v_k|^2 & \text{for } k = i \text{ or } j, j \in \mathcal{N}(i) \\ 0 & \text{otherwise} \end{cases}$$

where the column and row indices represent the lines and the nodes of the power system, respectively. If J has full column rank, then the function $\lambda \rightarrow h(x, \lambda)$ associated with the line outage homotopy method is of full rank $2|\mathcal{V}|$.

A similar result holds for generator outage contingencies, as shown below.

Lemma 5.5. Define the matrix $M = \left[\begin{array}{c|c} M^1 & 0 \\ \hline 0 & M^2 \end{array} \right] \in \mathbb{R}^{2|\mathcal{V}| \times 2|\mathcal{V}|}$ as

$$M_{i,j}^1 = \begin{cases} P_i^{g,o} - P_i^{g,f} & \text{for } j = i \\ 0 & \text{otherwise} \end{cases}$$

$$M_{i,j}^2 = \begin{cases} Q_i^{d,o} - Q_i^{d,f} & \text{for } j = i \\ 0 & \text{otherwise} \end{cases}$$

where both the column and row indices represent the nodes of the power system network. If M has full rank, then the function $\lambda \rightarrow h(x, \lambda)$ associated with the generator outage homotopy method is of full rank $2|\mathcal{V}|$.

The result implies that the first condition of Lemma 5.3 is satisfied if: (i) the pre-contingency real power generations and the post-contingency real power generations are different and (ii) the pre-contingency reactive power demands and the post-contingency reactive power demands are different. Note that this does not necessarily hold true because some real power generations are supposed to be fixed even after the contingency (same for reactive power demand). However, we can address this issue by allowing $P_i^{g,f}$ ($Q_i^{d,f}$) to take on a value within a small interval around $P_i^{g,o}$ ($Q_i^{d,o}$) whenever we want the two values to be close to each other.

Note that the linear perturbation term in $H_{\lambda,\omega}$ is a mathematically necessary device that allows us to prove generic uniqueness of a family of nonlinear optimization problems. Ultimately, we will only consider very small perturbations so that $H_{\lambda,\omega}$ closely resembles H_λ . Using the lemmas above, we arrive at the following corollary:

Corollary 5.6. Let $\mathbb{U}(\delta) = \{(\lambda, \omega) \mid \lambda \in \mathbb{S}, \omega \in \mathcal{B}(\delta)\}$, where \mathbb{S} is an open set such that $[0, 1]^m \subset \mathbb{S}$ and $\mathcal{B}(\delta)$ is an open n -dimensional ball around the origin with radius δ . Suppose that J and M have full column rank. Then, for every $\delta > 0$, $H_{\lambda,\omega}$ has a unique

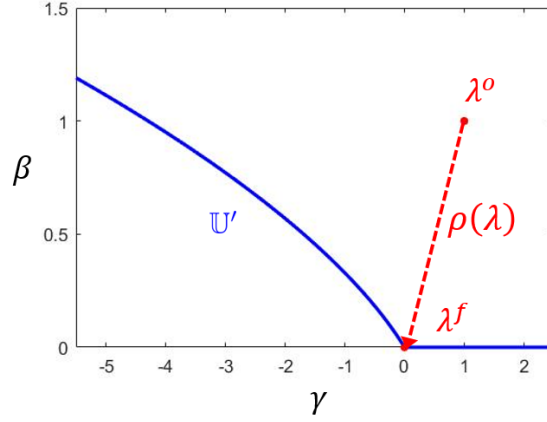


Figure 17: An example of the set \mathbb{U}' (blue) and an effective homotopy path (red) that can reach the origin without passing through a point in \mathbb{U}' .

global minimizer satisfying SSOC for all $(\lambda, \omega) \in \mathbb{U}(\delta) \setminus \mathbb{U}'(\delta)$, where $\mathbb{U}'(\delta) \subset \mathbb{U}(\delta)$ is of measure zero.

In other words, the uniqueness of a global minimizer satisfying SSOC is a generic property of H_λ , and thus supporting the assumptions made in this paper (specifically Assumptions (A1) and (A3)).

5.3 Geometry of the homotopy path: Two-bus example

In order to illustrate the previous ideas, we consider a simple homotopy-OPF example on a two-bus system. The line connecting the two buses has the admittance $y = G\gamma - \mathbf{j}B\beta$, and there is a lower bound Q^{min} on the reactive power injections at both buses. In this two-bus example, we consider the objective function $(\sigma_1^p)^2 + c(\sigma_2^p)^2$. Furthermore, assume that:

1. $|v_1| = |v_2| = 1$
2. $-\Delta' \leq \theta_1 - \theta_2 \leq \Delta'$
3. $0 < Q^{min} < q(\Delta')$

where $\Delta' = \tan^{-1}(B\beta/G\gamma)$ and $q(\cdot)$ denotes the reactive power injection as a function of solely the angle difference, which is due to the fact that voltage magnitudes are fixed. Note that the second constraint on the angle difference is reasonable for the secure operation of power systems and is also used in [8] in order to restrict the two-bus real power injection region to be the Pareto front of the original feasible region. Geometrically, the feasible set of the two-bus injection region is the Pareto front of an ellipse, which is partially removed due to the reactive power constraints (the details can be found in [8]). Let $P_i^{g,b}$ denote the real power generation at bus i obtained from the base-OPF solution. The following

lemma characterizes the set of homotopy parameters for which there are at least two global solutions.

Lemma 5.7. *Denote $\alpha = \cos^{-1}\left(\frac{-Q^{min}+B\beta}{|y|}\right)$, and define two polynomial functions of $\lambda = (\gamma, \beta)$ as follows:*

$$\Omega_1(\gamma, \beta) = \frac{2B\beta}{|y|}(B\beta \cdot \sin \alpha + \alpha \cdot G\gamma) \quad (101)$$

$$\Omega_2(\gamma, \beta) = 2G\gamma - \frac{2G\gamma}{|y|}(-G\gamma \cdot \sin \alpha + \alpha \cdot B\beta) \quad (102)$$

Then, the set of parameters leading to multiple global minimizers, \mathbb{U}' , can be characterized as:

$$\begin{aligned} \mathbb{U}' = \{ \lambda \in \mathbb{R}^2 \mid & (1 - c) \cdot \Omega_1(\gamma, \beta) \cdot \Omega_2(\gamma, \beta) \\ & - 2(P_1^{g,b} - P_1^d) \cdot \Omega_1(\gamma, \beta) + 2c(P_2^{g,b} - P_2^d) \cdot \Omega_1(\gamma, \beta) = 0 \} \end{aligned} \quad (103)$$

The set \mathbb{U}' in Lemma 5.7 for a particular instance of the example is depicted in Figure 17. As we can observe, \mathbb{U}' is a measure zero set in the two-dimensional parameter space, and it is possible to design an effective homotopy path. Note that the linear perturbation term in $H_{\lambda,\omega}$ is a mathematical device used to prove generic uniqueness of the global minimizer for a family of problems. The characterization of \mathbb{U}' in Lemma 5.7 did not require the linear perturbation. However, this means that particular instances of the example may not lead to the result that we desire. For instance, if $c = 1$ and $P_1^{g,b} - P_1^d = P_2^{g,b} - P_2^d$ in the above example, \mathbb{U}' is no longer a measure-zero set.

6 Simulations

In this section, we illustrate the success of the homotopy method in finding the global solution of the contingency-OPF. In doing so, we present simulations of different line and generator outage scenarios on various networks. We also evaluate the performance using different homotopy paths and discretizations, and verify our earlier theoretical results.

In these simulations, we consider $N - 1$ contingencies wherein there is one line or generator out as well as $N - 2$ and $N - 3$ contingencies wherein there are multiple outages. Although $N - 1$ contingencies occur more frequently in practice, $N - 2$ and $N - 3$ contingencies are catastrophic events that are worth considering as they are harder to correct. Extreme weather events, attacks, or component aging could cause these $N - k$ (where $k \geq 2$) contingency scenarios to occur [82]. Adding uncertain renewable energy sources such as wind energy to power networks increases the probability of correlated faults and thus the possibility of $N - 2$ and $N - 3$ contingencies [81]. Additionally, these multi-contingency scenarios can capture cascading failures that occur in a short window where corrective action is not possible between contingencies [81].

In order to implement the contingency-OPF within the MATPOWER format [59], we introduce virtual generators that model the violations of real and reactive power balance equations (σ^p and σ^q). Virtual generators are modelled so that they only generate or consume (virtual) power when there is a nonzero violation in the respective power balance equation. Therefore, by penalizing the virtual generation in the modified objective function, we fully implement the contingency-OPF as formulated in Section III.B. To solve each of the homotopy simulations, we use the MATPOWER Interior Point Solver (MIPS) [60].

For both line and generator outages, we solve the corresponding contingency-OPF problems via both homotopy and the one-shot method. The one-shot method uses the solution for the base-OPF as the initial point for directly solving the contingency-OPF. We compare various homotopy discretization schemes to the one-shot method. Note that the one-shot method is equivalent to solving the contingency-OPF problem via interior point methods and thus represents the current state-of-the-art.

For the line outages, we consider three different homotopy paths. If we take the line connecting buses i and j to be out, then the three homotopy paths are given by:

- Scheme 1: Uniformly decrease $(\gamma_{ij}, \beta_{ij})$ from $(1, 1) \rightarrow (0, 0)$
- Scheme 2: Decrease γ_{ij} from $1 \rightarrow 0$, then β_{ij} from $1 \rightarrow 0$
- Scheme 3: Decrease β_{ij} from $1 \rightarrow 0$, then γ_{ij} from $1 \rightarrow 0$

These schemes can be applied to multiple line outages by simultaneously modifying γ_{ij} and β_{ij} for each line $(i, j) \in \mathcal{E}$ that is out. For line outage scenarios on the 3375-bus and 3120-bus Polish networks, Figures 18 and 19 show the evolution of the violation cost over these homotopy schemes (with a 10-iteration discretization) compared to the violation cost of the one-shot method [59]. Next, we consider changing the discretization of homotopy scheme 1 in a line outage scenario. Figure 20 shows line outage scenarios on the 3375-bus and 3120-bus Polish networks using homotopy scheme 1 with a varying number of iterations [59].

For generator outages, we implement a homotopy path that decreases λ from $[\mathbf{1}_{|\mathcal{V}|}, \mathbf{1}_{|\mathcal{V}|}]$ to $[\mathbf{0}_{|\mathcal{V}|}, \mathbf{0}_{|\mathcal{V}|}]$ uniformly throughout the iterations. For this homotopy path, we also consider varying the discretization of the path. Figure 21 shows generator outage scenarios on the 89-bus and 1354-bus PEGASE networks [61, 62]. From these figures, we can see that the final violation cost obtained using the given homotopy paths can vary significantly depending on the number of iterations (i.e. $\Delta\lambda$) of homotopy-OPF.

In some of the examples from Figures 18, 20, and 22, we can see that solving the contingency-OPF problems with our homotopy method results in a lower violation cost than solving the same problems via the one-shot method. We also considered how far the bus voltages in the contingency-OPF problem were from the base-case voltages when we solved the problem with homotopy versus one-shot methods, as shown in Figure 23 and 24. The results show that with homotopy we can obtain a solution that is relatively close to

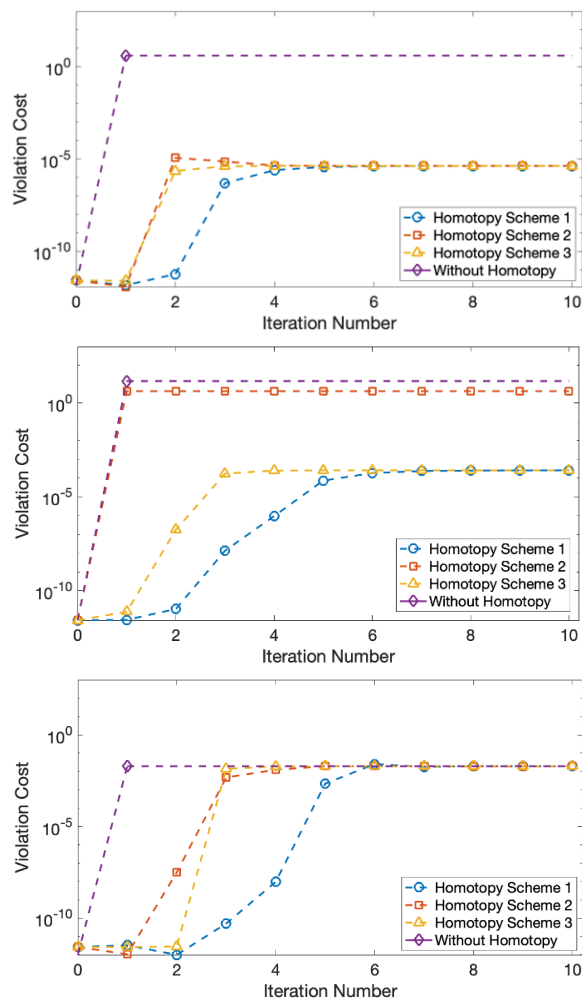


Figure 18: Performance of proposed homotopy method on the 3375-bus Polish network (case3375wp with real and reactive power demand scaled up by 10%) with single line outages. Homotopy schemes 1 through 3 are tested with 10 iterations. In the top figure (line out ID: 3596), we have a case where all three homotopy schemes outperform the one-shot method, and in the middle figure (line out ID: 3551), we have a case where only homotopy schemes 1 and 3 significantly outperform the one-shot method. In the bottom figure (line out ID: 268), we have a case where the one-shot method performs the same as all three homotopy methods. This was the most common case for our experiments on the 3375-bus network, representing about 95% of 4161 tested single line outages. While homotopy in general yielded the same solution as the one-shot method, in cases where it outperformed the one-shot method, the results were often better by a factor of 10^5 , as seen in the top two figures. Note that all solutions shown here are convergent, compared to the cases for the 3120-bus Polish network shown in Figure 19 which have some non-convergent solutions.

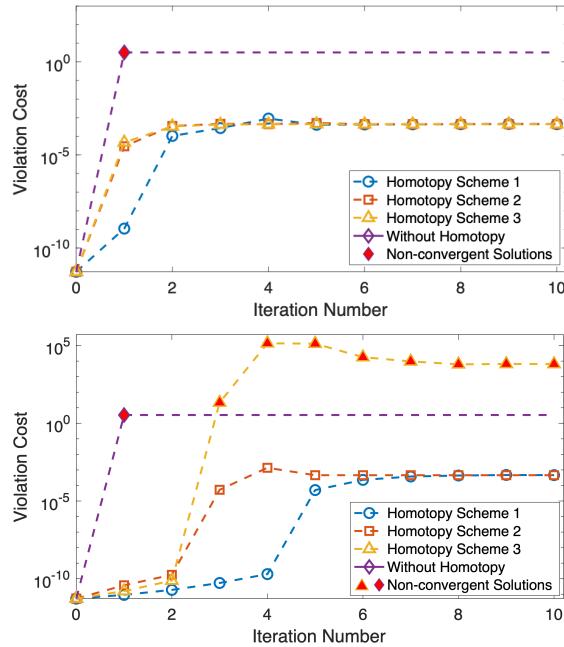


Figure 19: Performance of proposed homotopy method on the 3120-bus Polish network (case3120sp with real and reactive power demand scaled up by 10%) with a multiple line outages. Homotopy schemes 1 through 3 are tested with 10 iterations. By introducing multiple line outages, we make the contingency-OPF problem more difficult to solve, which makes it a good candidate for the proposed homotopy method. In both of these cases, homotopy schemes 1 and 2 find a convergent solution while the one-shot method does not. In the top figure, the IDs of the outed lines are 438, 439, and 3150, and in the bottom figure, the IDs of the outed lines are 2056 and 3082.

that of the base-case, while the solution obtained without homotopy can be unnecessarily far away from that of the base-case.

In other cases from Figures 19, 20, and 21, solving the contingency-OPF problems via the one-shot method results in non-convergence while the homotopy method can find a convergent solution.

In order to formally compare the performance of homotopy versus the one-shot method, we say that homotopy “outperforms” the one-shot method if either of the following are true:

1. If the homotopy scheme converges and the one-shot method does not converge.
2. If the homotopy scheme converges to a value that is better than that of the one-shot method by at least 0.01% of the optimal base-OPF cost.

For the 1354-bus PEGASE network, we tested 1, 2, and 3 line and generator outages, testing 100 simulations of each type of outage. The homotopy paths for these line and generator outages are the same as those described for the simulations in Figures 20, 21

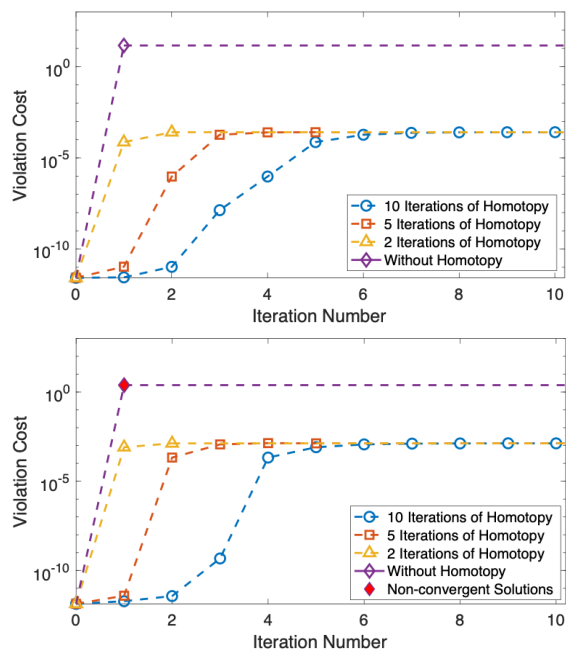


Figure 20: Performance of proposed homotopy scheme 1 tested with a varying number of iterations. The top figure shows the 3375-bus Polish network (case3375wp with real and reactive power demand scaled up by 10%) with a single line outage (line out ID: 3551). In this case, we see that the 2, 5, and 10-iteration homotopy methods converge to a solution that is much better than that obtained by the one-shot method. The bottom figure shows the 3012-bus Polish network (case3012wp with real and reactive power demand scaled up by 8%) with a single line outage (line out ID: 1604). In this case, we see that the 2, 5, and 10-iteration homotopy methods result in a convergent solution while the one-shot method does not. For both scenarios, by introducing even a 2-iteration homotopy scheme, we outperform the one-shot method.

and 22. The percent of simulations where homotopy outperformed the one-shot method is given in Table 5 for the network with base-level demand and with demand scaled up by 10%. It can be observed that for the line outage contingencies, the homotopy methods appear to be more useful when the demand is higher. This is likely because the increased demand makes the problem harder, and thus homotopy is more useful. However, the inverse appears true for the generator outage scenarios, i.e. the homotopy methods appear to be more useful when demand is at the base-level. This could be because the removal of a generator could lead to many possibilities for operating the post-contingency network in a lower demand scenario, which may introduce bad local minima.

Although the percent of simulations where homotopy outperforms the one-shot method is less than 20% for the considered cases, it is important to note that in these cases the homotopy method can lead to a significant reduction in the violation cost during a contingency scenario or to a convergent solution when the one-shot method fails to

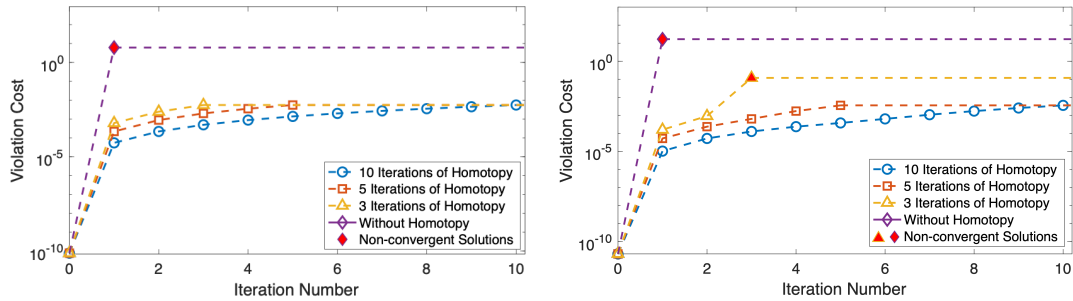


Figure 21: Performance of proposed homotopy method for generator outages. The top figure shows a 2 generator outage (generator out IDs: 4 and 7) in the 89-bus PEGASE network (case89pegase). The bottom figure shows a 1 generator outage (generator out ID: 30) in the 1354-bus PEGASE network (case1354pegase). In these cases, the homotopy method can be used to find a convergent solution when the one-shot method fails to find one.

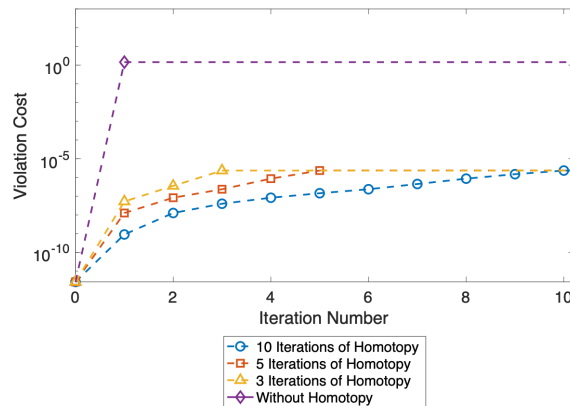


Figure 22: Performance of proposed homotopy method on the 3375-bus Polish network (case3375wp with real and reactive power demand scaled up by 10%) with a single generator outage. The figure (generator out ID: 100) shows a case where all homotopy discretization schemes result in a violation cost much lower than that obtained by the one-shot method.

converge. For the cases where the proposed homotopy method does not outperform the one-shot method, the homotopy method typically is at least as good as the one-shot method.

7 Conclusions

This paper studies the contingency-OPF problem, which is used to find an optimal operating point in the case of a line or generator outage. Unlike the base-OPF problem that is a single optimization problem, there are many contingency-OPF problems that should all be

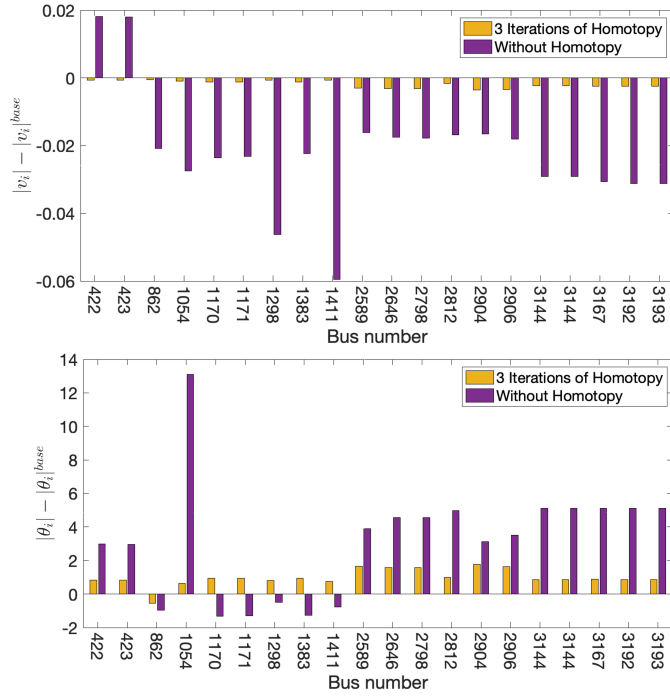


Figure 23: Comparison of solution for homotopy and one-shot methods for the 3375-bus Polish network (case3375wp with real and reactive power demand scaled up by 10%) with a single generator outage (generator out ID: 100). The twenty *generator* buses with the largest variation from the base-case voltage magnitude are shown here. In this case, all three homotopy methods converge to the same solution, as shown in Figure (22), so we only compare the solution from the 3-iteration method to that obtained by the one-shot method. For this test case, the homotopy method gradually deforms the base-case to yield a solution that is much closer to the base-case while the one-shot method yields a solution that is far from the base-case.

Table 5: Percent of simulations where 5-iteration homotopy scheme outperformed one-shot method for 1354-bus PEGASE network

Type of contingency	Base-level power demand	10% greater power demand
1 line outage	10%	12%
2 line outage	7%	12%
3 line outage	12%	15%
1 generator outage	9%	7%
2 generator outage	10%	9%
3 generator outage	17%	12%

solved in a short period of time. Recognizing that the contingency-OPF problem is a challenging variant of the classical OPF problem, we introduce a new homotopy method to find the best solution of the contingency-OPF problem. This method involves solving a series of intermediate homotopy-OPF problems using simple local search methods, and we study

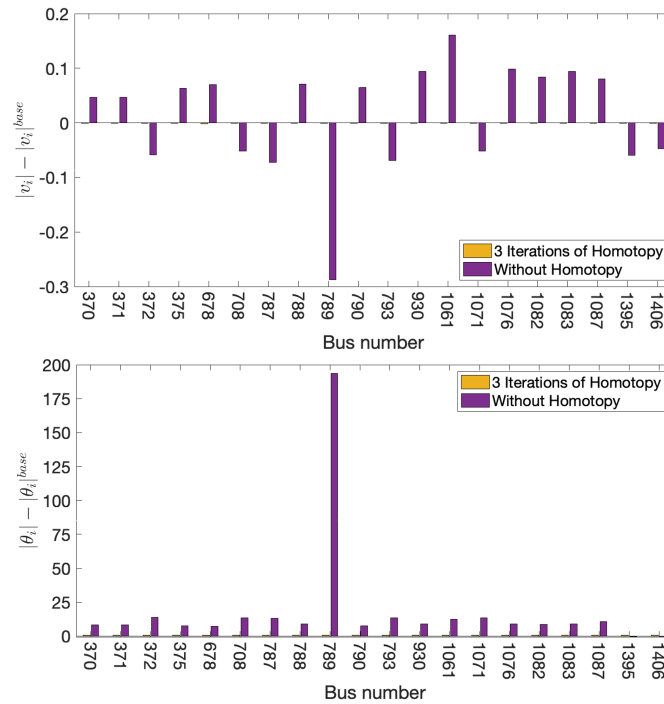


Figure 24: Comparison of solution for homotopy and one-shot methods for the 3375-bus Polish network (case3375wp with real and reactive power demand scaled up by 10%) with a single generator outage (generator out ID: 100). The twenty *load* buses with the largest variation from the base-case voltage magnitude are shown here. See Figures (22) and (23) for more details on this case.

conditions that guarantee convergence to a global solution of the contingency-OPF. We perform simulations on real-world networks and show that the proposed homotopy method can result in a lower value of the objective.

8 Appendix

8.1 Proof of Theorem 5.1

Due to the continuity of $\lambda(t)$, we can equivalently prove that a sufficiently small $\Delta\lambda$ will ensure the desired result, where $\Delta\lambda := \sup_{i=1, \dots, T-1} (\Lambda^{i+1} - \Lambda^i)$. Let x_1^* denote the unique global solution satisfying SSOC for the problem H_{Λ^1} . Using an argument relying on the implicit function theorem [55], it follows that for each (x_1^*, Λ^1) pair, there exist a neighborhood \mathbb{U}_1 around Λ^1 and a neighborhood \mathbb{X}_1 around x_1^* , and there is a differentiable function $x_1(\lambda)$ defined for $\lambda \in \mathbb{U}_1$ such that

1. $x_1(\Lambda^1) = x_1^*$
2. For each $\lambda \in \mathbb{U}_1$, $x_1(\lambda)$ is the unique point in \mathbb{X}_1 satisfying the SSOC for H_λ .

Now, suppose that $\Delta\lambda$ is small enough so that $\Lambda^2 \in \mathbb{U}_1$. Then, since $x_1(\lambda)$ is a continuous function and there is no λ on the path $\lambda(t) = 0$ such that H_λ has more than one global minimizer, $x_1(\Lambda^2)$ becomes the unique global minimizer satisfying SSOC for the next OPF problem, H_{Λ^2} . The same logic can be applied for all Λ^i , and by induction we have proved the result. \square

8.2 Proof of Theorem 5.2

We begin by defining the radius of convergence for Wilson's method for solving H_t in a neighborhood of a local minimizer $w(t)$.

Definition 8.1.

$r(t, w(t)) = \sup\{r \mid \text{for all } w^0 \text{ satisfying } \|w^0 - w(t)\| \leq r, \text{ starting Wilson's method with } w^0 \text{ provides a sequence } \{w^i\} \text{ converging to } w(t)\}$. (104)

The following lemma is a natural corollary of Theorem 3.2.1 in [71]. We do not state the proof of this lemma here but the derivation uses properties of the Wilson's method.

Lemma 8.1. *Suppose that Assumptions (A1), (A2) and (A3) hold. Then, there exists a real number $\hat{r} > 0$ such that*

$$r(t, w(t)) \geq \hat{r} \text{ for all } w(t), t \in [0, 1] \quad (105)$$

Let us consider the sequence $\{w'_i\}_{i=1}^T$ such that

$$\|w'_1 - w^*(t^1)\| < \epsilon, \quad (106)$$

$$\|w'_i - \hat{w}^M(w'_{i-1}, t)\| < \epsilon', \quad i = 2, \dots, T, \quad (107)$$

where $0 < \epsilon' \ll \epsilon$ and $\hat{w}^M(w'_k, t)$ denotes the true (or exact) KKT point after applying M Wilson's steps starting from w'_k . The choice of w'_1 satisfying (106) is possible because of the known initial global minimizer assumption in (A_1) . From the proof of Theorem 3.2.1 in [71], we also know that there is a constant $\hat{r} > 0$ such that $\|\hat{w}(w, t) - w^*(t^i)\| \leq \frac{1}{2}\|w - w^*(t^i)\|$ whenever $\|w - w^*(t^i)\| \leq \hat{r}$. Now, we choose $\epsilon > 0$ and $\eta > 0$ such that the following condition is satisfied:

$$\epsilon + \eta < \hat{r} \quad (108)$$

Due to the assumption on the continuity of the global minimizers (A_1) , there is a $\Delta t > 0$ such that

$$\|w^*(\tilde{t}) - w^*(t)\| < \eta, \quad \text{for all } \tilde{t}, t \in [0, 1] \text{ with } \|\tilde{t} - t\| \leq \Delta t \quad (109)$$

Given t^k and w'_k with $\|w'_k - w^*(t^k)\| < \epsilon$ for some $k \in \{1, \dots, T-1\}$, we obtain

$$\|w'_k - w^*(t^{k+1})\| \leq \|w'_k - w^*(t^k)\| + \|w^*(t^k) - w^*(t^{k+1})\| < \epsilon + \eta < \hat{r} \quad (110)$$

Hence, the point w'_k is in the region of convergence and therefore,

$$\|\hat{w}^M(w'_k, t) - w^*(t^{k+1})\| \leq \left(\frac{1}{2}\right)^M (\epsilon + \eta) \quad (111)$$

Furthermore, we obtain

$$\|w'_{k+1} - w^*(t^{k+1})\| \leq \|w'_{k+1} - \hat{w}^M(w'_k, t)\| + \|\hat{w}^M(w'_k, t) - w^*(t^{k+1})\| \leq \epsilon' + \left(\frac{1}{2}\right)^M (\epsilon + \eta) \quad (112)$$

To find M , we need to ensure that the equation (112) can be upper bounded by ϵ :

$$\epsilon' + \left(\frac{1}{2}\right)^M (\epsilon + \eta) \leq \epsilon \quad (113)$$

Solving for M , we obtain the condition

$$M \geq \log_2 \frac{\epsilon + \eta}{\epsilon - \epsilon'} \quad (114)$$

Noting that $\hat{r} > \epsilon + \eta$ from equation (108) and $\epsilon' \ll \epsilon$, we observe that M satisfies the condition (114) if $M \geq \log_2 \frac{\hat{r}}{\epsilon}$. We can continue this logic until $k = T-1$ and arrive at the conclusion that the number of Wilson's method that will enable the algorithm to keep track of the global minimizers is on the order of $O(\log(\hat{r}/\epsilon)) \cdot \frac{1}{\Delta t}$. Finally, we claim that $1/\Delta t$ is upper bounded by a constant for sufficiently small ϵ . This is because Δt only needs to be small enough so that η satisfies equation (108). Therefore, if we have a constant $\bar{\Delta t}$ corresponding to some value $\bar{\eta}$ satisfying the condition for a given $\bar{\epsilon}$, the same $\bar{\Delta t}$ (and equivalently $\bar{\eta}$) will satisfy the condition for any ϵ smaller than $\bar{\epsilon}$. This concludes that the overall complexity of solving homotopy-OPF is $O(\log(\hat{r}/\epsilon))$, which is

equivalent to $O(\log(1/\epsilon))$ \square

8.3 Proof of Lemma 5.3

By Proposition 4 of [54], the family of optimization problems

$$\begin{aligned} \min_{x \in \Psi} \quad & \bar{f}(x, \lambda, \omega) \\ \text{s.t.} \quad & h(x, \lambda) = 0 \end{aligned}$$

has a unique global minimizer satisfying SSOC for all parameters $(\lambda, \omega) \in \mathbb{U}$ except on a set of measure zero if (i) for all $x_1 \neq x_2$, and for all ω , the function $\omega \rightarrow \bar{f}(x_1, \lambda, \omega) - \bar{f}(x_2, \lambda, \omega)$ is of rank one at all λ , (ii) the function $\lambda \rightarrow h(x, \lambda)$ is of full rank $2|\mathcal{V}|$ for all x at every ω , and (iii) the fixed set Ψ is a cyrtohedron and \mathbb{U} is an open set. It is straightforward to check that if $\bar{f}(x, \lambda, \omega) = f(x, \lambda) + \omega^T x$, condition (i) is satisfied. Conditions (ii) and (iii) are given as assumptions, which completes the proof. \square

8.4 Proof of Lemma 5.4

The rank of the function $\lambda \rightarrow h(x, \lambda)$ is the rank of its Jacobian (w.r.t. λ). Therefore, we analyze the Jacobian of $h(x, \lambda) = h(x, [\gamma, \beta, \gamma^{\text{sh}}, \beta^{\text{sh}}])$ with respect to $[\gamma, \beta, \gamma^{\text{sh}}, \beta^{\text{sh}}]$. From Section 3.2 and 4.1, we know that h consists of two types of functions, h^1 and h^2 (corresponding to the real power flow equations and the reactive power flow equations, respectively), whose i -th elements are defined by:

$$\begin{aligned} h_i^1(x, [\gamma, \beta, \gamma^{\text{sh}}, \beta^{\text{sh}}]) &= P_i^g - P_i^d - \sigma_i^p - \sum_{j \in \mathcal{N}(i)} \frac{g_{ij}^{\text{sh}} \gamma_{ij}^{\text{sh}}}{2} |v_i|^2 \\ &\quad - \sum_{j \in \mathcal{N}(i)} g_{ij} \gamma_{ij} (|v_i|^2 - |v_i| |v_j| \cos \theta_{ij}) - b_{ij} \beta_{ij} |v_i| |v_j| \sin \theta_{ij} \end{aligned}$$

$$\begin{aligned} h_i^2(x, [\gamma, \beta, \gamma^{\text{sh}}, \beta^{\text{sh}}]) &= q_i^g - Q_i^d - \sigma_i^q + \sum_{j \in \mathcal{N}(i)} \frac{b_{ij}^{\text{sh}} \beta_{ij}^{\text{sh}}}{2} |v_i|^2 \\ &\quad + \sum_{j \in \mathcal{N}(i)} b_{ij} \beta_{ij} (|v_i|^2 - |v_i| |v_j| \cos \theta_{ij}) - g_{ij} \gamma_{ij} |v_i| |v_j| \sin \theta_{ij} \end{aligned}$$

We focus on the submatrix of the Jacobian that consists only of the derivatives of h_i^1 and h_i^2 with respect to γ^{sh} and β^{sh} (denote this as J). This is because if this submatrix has full column rank, then the full Jacobian also has full column rank. First, we notice that the Jacobian of h^1 with respect to β^{sh} and the Jacobian of h^2 with respect to γ^{sh} are equal to zero. Therefore, J can be expressed as a 2×2 block matrix of the form

$J = \left[\begin{array}{c|c} J^1 & 0 \\ \hline 0 & J^2 \end{array} \right] \in \mathbb{R}^{2|\mathcal{E}| \times 2|\mathcal{V}|}$, where J^1 corresponds to the Jacobian of h^1 with respect to γ^{sh} and J^2 corresponds to the Jacobian of h^2 with respect to β^{sh} .

For line outage contingencies, γ^{sh} and β^{sh} are parameters indexed by the line number. Hereby, let $J_{((i,j),k)}^1$ refer to the element of J^1 that is located at the (i, j) -th row and the k -th column (the row index representing the line and the column index representing the bus number). For example, $J_{((i,j),k)}^1$ denotes the partial derivative of the real power flow equation at bus k with respect to the shunt susceptance parameter at line (i, j) . The same goes for J^2 .

Then, directly from basic calculus, we can derive the following form for the matrix J :

$$J_{(i,j),k}^1 = \begin{cases} -\frac{1}{2}g_{ij}^{\text{sh}}|v_k|^2 & \text{for } k = i \text{ or } j, j \in \mathcal{N}(i) \\ 0 & \text{otherwise} \end{cases}$$

$$J_{(i,j),k}^2 = \begin{cases} \frac{1}{2}b_{ij}^{\text{sh}}|v_k|^2 & \text{for } k = i \text{ or } j, j \in \mathcal{N}(i) \\ 0 & \text{otherwise} \end{cases}$$

Therefore, if J has full column rank, so will the Jacobian of the function $\lambda \rightarrow h(x, \lambda)$, which completes the proof. \square

8.5 Proof of Lemma 5.5

Similar to the proof of Lemma 5.4, we analyze the Jacobian of $h(x, \lambda) = h(x, [\gamma, \beta])$ with respect to $[\gamma, \beta]$. From Section 3.2 and 4.1, we know that h consists of two types of functions, h^1 and h^2 (corresponding to the real power flow equations and the reactive power flow equations, respectively), whose i -th elements are defined by:

$$\begin{aligned} h_i^1(x, [\gamma, \beta]) &= P_i^{g,o}\gamma_i + P_i^{g,f}(1 - \gamma_i) - P_i^d - \sigma_i^p \\ &\quad - \sum_{j \in \mathcal{N}(i)} g_{ij}\gamma_{ij}(|v_i|^2 - |v_i||v_j|\cos\theta_{ij}) - b_{ij}\beta_{ij}|v_i||v_j|\sin\theta_{ij} \\ &\quad - \sum_{j \in \mathcal{N}(i)} \frac{g_{ij}^{\text{sh}}\gamma_{ij}^{\text{sh}}}{2}|v_i|^2 \end{aligned}$$

$$\begin{aligned} h_i^2(x, [\gamma, \beta]) &= q_i^g - Q_i^{d,o}\beta_i - Q_i^{d,f}(1 - \beta_i) - \sigma_i^q \\ &\quad + \sum_{j \in \mathcal{N}(i)} b_{ij}\beta_{ij}(|v_i|^2 - |v_i||v_j|\cos\theta_{ij}) - g_{ij}\gamma_{ij}|v_i||v_j|\sin\theta_{ij} \\ &\quad + \sum_{j \in \mathcal{N}(i)} \frac{b_{ij}^{\text{sh}}\beta_{ij}^{\text{sh}}}{2}|v_i|^2 \end{aligned}$$

First, we notice that the Jacobian of h^1 with respect to β and the Jacobian of h^2 with respect to γ are equal to zero. Therefore, M can be expressed as a 2×2 block matrix of the form $M = \left[\begin{array}{c|c} M^1 & 0 \\ \hline 0 & M^2 \end{array} \right] \in \mathbb{R}^{2|\mathcal{V}| \times 2|\mathcal{V}|}$ where M^1 corresponds to the Jacobian of h^1 with respect to γ and M^2 corresponds to the Jacobian of h^2 with respect to β .

For generator outage contingencies, γ and β are parameters indexed by the bus number (because we assume each bus has exactly one generator). Hereby, let $M_{i,j}^1$ refer to the element of M^1 that is located at the i -th row and the j -th column. In other words, $M_{i,j}^1$ denotes the partial derivative of the real power flow equation at bus i with respect to the γ parameter at bus j . The same goes for M^2 .

Then, directly from basic calculus, we can derive the following form for the matrix M :

$$M_{i,j}^1 = \begin{cases} P_i^{g,o} - P_i^{g,f} & \text{for } j = i \\ 0 & \text{otherwise} \end{cases}$$

$$M_{i,j}^2 = \begin{cases} Q_i^{d,o} - Q_i^{d,f} & \text{for } j = i \\ 0 & \text{otherwise} \end{cases}$$

Therefore, if M has full column rank, so will the Jacobian of the function $\lambda \rightarrow h(x, \lambda)$, which completes the proof. \square

8.6 Proof of Corollary 5.6

The first statement on $H_{\lambda,\omega}$ having a unique global minimizer satisfying SSOC follows directly from applying Lemma 5.3. The functions $\lambda \rightarrow h(x, \lambda)$ is of full rank $2|\mathcal{V}|$ due to Lemmas 5.4 and 5.5, and this in turn satisfies the first condition of Lemma 5.3. As discussed in Section 5, the set Ψ is a cyrtohedron, and the set \mathbb{U} is defined to be an open set for any $\epsilon > 0$ by the assumptions of this theorem. In other words, the second condition of Lemma 5.3 is also satisfied. Therefore, we can conclude that for any value of $\epsilon > 0$, $H_{\lambda,\omega}$ has a unique global minimizer satisfying SSOC for every $(\lambda, \omega) \in \mathbb{U} \setminus \mathbb{U}'$ where $\mathbb{U}' \subset \mathbb{U}$ is of measure zero.

8.7 Proof of Lemma 5.7

Let us start with the equation for the reactive power injections. Let θ_1 and θ_2 denote the voltage phasor angles at buses 1 and 2, respectively. Let the real and reactive power injections at bus i be denoted by p_i^{inj} and q_i^{inj} , respectively. In this two-bus example, we consider the objective function: $(\sigma_1^p)^2 + c(\sigma_2^p)^2$. Then after denoting $\theta = \theta_1 - \theta_2$, we have the following:

$$q_1^{\text{inj}} = B\beta - G\gamma \cdot \sin \theta - B\beta \cdot \cos \theta$$

$$q_2^{\text{inj}} = B\beta + G\gamma \cdot \sin \theta - B\beta \cdot \cos \theta$$

A lower bound of Q^{\min} on q_1^{inj} results in the following:

$$Q^{\min} \leq B\beta - G\gamma \cdot \sin \theta - B\beta \cdot \cos \theta$$

Then, after rearranging and using trigonometry, we arrive at

$$\begin{aligned} -Q^{\min} + B\beta &\geq G\gamma \cdot \sin \theta + B\beta \cdot \cos \theta \\ &= \sqrt{(G\gamma)^2 + (B\beta)^2} \cdot \cos(\theta - \Delta) \quad \text{where } \Delta = \tan^{-1}\left(\frac{G\gamma}{B\beta}\right). \end{aligned}$$

After dividing both sides by $\sqrt{(G\gamma)^2 + (B\beta)^2}$, we have

$$\cos(\theta - \Delta) \leq \frac{-Q^{\min} + B\beta}{\sqrt{(G\gamma)^2 + (B\beta)^2}}$$

which implies

$$\theta \geq \cos^{-1}\left(\frac{-Q^{\min} + B\beta}{\sqrt{(G\gamma)^2 + (B\beta)^2}}\right) + \Delta \quad \text{or} \quad \theta \leq -\cos^{-1}\left(\frac{-Q^{\min} + B\beta}{\sqrt{(G\gamma)^2 + (B\beta)^2}}\right) + \Delta \quad (115)$$

From the lower bound on q_2^{inj} , we can perform a similar derivation and arrive at

$$\theta \geq \cos^{-1}\left(\frac{-Q^{\min} + B\beta}{\sqrt{(G\gamma)^2 + (B\beta)^2}}\right) - \Delta \quad \text{or} \quad \theta \leq -\cos^{-1}\left(\frac{-Q^{\min} + B\beta}{\sqrt{(G\gamma)^2 + (B\beta)^2}}\right) - \Delta. \quad (116)$$

Therefore, combining inequalities (115) and (116) leads to

$$\theta \geq \cos^{-1}\left(\frac{-Q^{\min} + B\beta}{\sqrt{(G\gamma)^2 + (B\beta)^2}}\right) + \Delta \quad \text{or} \quad \theta \leq -\cos^{-1}\left(\frac{-Q^{\min} + B\beta}{\sqrt{(G\gamma)^2 + (B\beta)^2}}\right) - \Delta. \quad (117)$$

Furthermore, we assume that

$$-\tan^{-1}\left(\frac{B\beta}{G\gamma}\right) \leq \theta \leq \tan^{-1}\left(\frac{B\beta}{G\gamma}\right)$$

which is equivalent to

$$-\left(\frac{\pi}{2} - \Delta\right) \leq \theta \leq \left(\frac{\pi}{2} - \Delta\right) \quad (118)$$

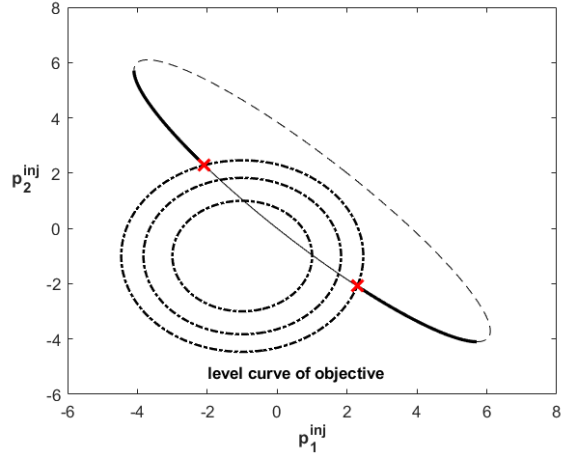


Figure 25: An example of two-bus network for which there are two global solutions to an instance of the homotopy-OPF.

Combining (117) and (118) and using the definition of α yields the final constraint on θ :

$$\alpha + \Delta \leq \theta \leq \left(\frac{\pi}{2} - \Delta\right) \quad \text{or} \quad -\left(\frac{\pi}{2} - \Delta\right) \leq \theta \leq -\alpha - \Delta. \quad (119)$$

This feasible region of θ is reflected in the feasible region of the real power injections, as shown in the bolded part of the ellipse in Figure 25. As illustrated in the figure, the two red points are real power injections, corresponding to $\theta = \alpha + \Delta$ and $\theta = -\alpha - \Delta$. Let the first red point, $(p_1^{\text{inj}}, p_2^{\text{inj}})$, be generated by $\theta = \alpha + \Delta$. Then, one can write:

$$\begin{aligned} p_1^{\text{inj}} &= G\gamma + B\beta \cdot \sin \theta - G\gamma \cdot \cos \theta \\ &= G\gamma + B\beta \cdot \sin(\alpha + \Delta) - G\gamma \cdot \cos(\alpha + \Delta) \\ &= G\gamma + B\beta \cdot (\sin \alpha \cdot \cos \Delta + \alpha \sin \Delta) - G\gamma \cdot (\alpha \cos \Delta - \sin \alpha \cdot \sin \Delta) \\ &= G\gamma + \frac{B\beta}{|y|} (B\beta \cdot \sin \alpha + \alpha \cdot G\gamma) - \frac{G\gamma}{|y|} (\alpha \cdot B\beta - G\gamma \cdot \sin \alpha) \end{aligned}$$

Similarly, if we let the second red point $(\bar{p}_1^{\text{inj}}, \bar{p}_2^{\text{inj}})$, be generated by $\theta = -\alpha - \Delta$, we have

$$\bar{p}_1^{\text{inj}} = G\gamma - \frac{B\beta}{|y|} (B\beta \cdot \sin \alpha + \alpha \cdot G\gamma) - \frac{G\gamma}{|y|} (\alpha \cdot B\beta - G\gamma \cdot \sin \alpha)$$

Moreover, note that due to symmetry, $p_2^{\text{inj}} = \bar{p}_1^{\text{inj}}$ and $\bar{p}_2^{\text{inj}} = p_1^{\text{inj}}$. Define the following two functions:

$$\begin{aligned}\Omega_1(\gamma, \beta) &\equiv p_1^{\text{inj}} - \bar{p}_1^{\text{inj}} = \frac{2B\beta}{|y|}(B\beta \cdot \sin \alpha + \alpha \cdot G\gamma), \\ \Omega_2(\gamma, \beta) &\equiv p_1^{\text{inj}} + \bar{p}_1^{\text{inj}} = 2G\gamma - \frac{2G\gamma}{|y|}(-G\gamma \cdot \sin \alpha + \alpha \cdot B\beta).\end{aligned}$$

Recall that $P_i^{\text{g,b}}$ denotes the real power generation at bus i obtained from the base-OPF solution. If the two points $(p_1^{\text{inj}}, p_2^{\text{inj}})$ and $(\bar{p}_1^{\text{inj}}, \bar{p}_2^{\text{inj}})$ are both globally optimal, their objective values must be equal. In other words,

$$(p_1^{\text{inj}} - (P_1^{\text{g,b}} - P_1^d))^2 + c(p_2^{\text{inj}} - (P_2^{\text{g,b}} - P_2^d))^2 = (\bar{p}_1^{\text{inj}} - (P_1^{\text{g,b}} - P_1^d))^2 + c(\bar{p}_2^{\text{inj}} - (P_2^{\text{g,b}} - P_2^d))^2.$$

Rearranging the terms leads to

$$(1 - c)\{(p_1^{\text{inj}})^2 - (\bar{p}_1^{\text{inj}})^2\} - 2(P_1^{\text{g,b}} - P_1^d)(p_1^{\text{inj}} - \bar{p}_1^{\text{inj}}) + 2c(P_2^{\text{g,b}} - P_2^d)(p_1^{\text{inj}} - \bar{p}_1^{\text{inj}}) = 0$$

Finally, substituting the definition of Ω_1 and Ω_2 , we arrive at

$$(1 - c) \cdot \Omega_1(\gamma, \beta) \cdot \Omega_2(\gamma, \beta) - 2(P_1^{\text{g,b}} - P_1^d) \cdot \Omega_1(\gamma, \beta) + 2c(P_2^{\text{g,b}} - P_2^d) \cdot \Omega_1(\gamma, \beta) = 0$$

This completes the proof. \square

8.8 Computation of Participation Factors for Generator Outage

During the outage of one or more generators, a collection of other generators will increase their power generation in order to respond to the outage and meet power demand. The ‘‘participation factor’’ of a generator determines the portion of the generation response that is assigned to that generator. There are a variety of ways to compute participation factors, including scaling the participation factors based on the remaining power capacity. In Algorithm 8, we present one method for computing participation factors which is based on the topology of the network, i.e. it redirects generation from the outed generators to generators that supply the same set of buses as the outed generators in the base-OPF. This method is based on the work [48]. In our simulations of generator outages, we use this method for computing participation factors with Algorithm 7.

Algorithm 8 Calculation of Participation Factors for Power Redistribution at Contingency k

Given: (i) solution to base-OPF problem $(|v|, \theta, p^g, q^g, \{\sigma_k\})$
(ii) generators out in contingency k : $R_k \subset \mathcal{V}$

Compute real power flow for all $(i, j) \in \mathcal{E}$ in the base-case:

$$p_{ij} = G_{ij}|v|_i^2 - G_{ij}|v|_i|v|_j \cos(\theta_{ij}) + B_{ij}|v|_i|v|_j \sin(\theta_{ij})$$

Generate a directed graph $\mathcal{D}(\mathcal{V}, \mathcal{A})$ based on direction of power flow: $(i, j) \in \mathcal{A}$ if $p_{ij} \geq 0$

Use shortest path algorithm to compute the domain of each generator

Group the buses supplied by the same set of generators into commons \mathcal{C} (see [48])

Use algorithm in [48] to determine the contribution C_{rj} of each generator r to common j

Remove contribution of generators that are out:

$$C_{rj} \leftarrow 0 \quad \forall r \in R_k, \forall j \in \mathcal{C}$$

Distribute lost generation over generations that supply the same common:

for $j \in \mathcal{C}$ **do**

 Define $C_j = \sum_r C_{rj}$

if $C_j \neq 0$ **then**

for $r \in \mathcal{V}$ **do**

$$C_{rj} \leftarrow C_{rj}/C_j$$

end for

end if

end for

Initialize participation factors: $\alpha_r^g = 0$ for all $r \in \mathcal{V}$

Define participation factors based on contribution to common:

for $r \in R_k$ **do**

for $j \in \mathcal{C}$ **do**

$$\alpha_t^g \leftarrow \alpha_t^g + C_{tj} \text{ for all generators } t \text{ in common } j$$

end for

end for

Normalize the participation factors α^g so that $\sum_{r \in \mathcal{V}} \alpha_r^g = 1$

Bibliography

- [1] L. T. Watson, "Numerical linear algebra aspects of globally convergent homotopy methods," *SIAM Review*, vol. 28, no. 4, pp. 529–545, December 1986.
- [2] D. K. Molzahn, F. Dörfler, H. Sandberg, S. H. Low, S. Chakrabarti, R. Baldick, and J. Lavaei, "A survey of distributed optimization and control algorithms for electric power systems," *IEEE Transactions on Smart Grid*, vol. 8, no. 6, pp. 2941–2962, 2017.

- [3] D. K. Molzahn and I. A. Hiskens, "Sparsity-exploiting moment-based relaxations of the optimal power flow problem," *IEEE Transactions on Power Systems*, vol. 30, no. 6, pp. 3168–3180, 2014.
- [4] C. Jozs, J. Maeght, P. Panciatici, J. C. Gilbert, "Application of the moment-SOS approach to global optimization of the OPF problem," *IEEE Transactions on Power Systems*, vol. 30, no. 1, pp. 463–470, 2015.
- [5] C. Chen, A. Atamtürk, and S. Oren, "A spatial branch-and-cut method for nonconvex QCQP with bounded complex variables," *Mathematical Programming*, 2016.
- [6] R. Madani, M. Ashraphijuo, and J. Lavaei, "Promises of conic relaxation for contingency-constrained optimal power flow problem," *IEEE Transactions on Power Systems*, vol. 31, no. 2, pp. 1297–1307, 2016.
- [7] R. Madani, S. Sojoudi, and J. Lavaei, "Convex relaxation for optimal power flow problem: Mesh networks," *IEEE Transactions on Power Systems*, vol. 30, no. 1, pp. 199–211, 2015.
- [8] J. Lavaei, D. Tse, and B. Zhang, "Geometry of power flows and optimization in distribution networks," *IEEE Transactions on Power Systems*, vol. 29, no. 2, pp. 572–583, 2014.
- [9] M. Farivar and S. H. Low, "Branch flow model: Relaxations and convexification—part I," *IEEE Transactions on Power Systems*, vol. 28, no. 3, pp. 2554–2564, 2013.
- [10] J. Lavaei and S. H. Low, "Zero duality gap in optimal power flow problem," *IEEE Transactions on Power Systems*, vol. 27, no. 1, pp. 92–107, 2012.
- [11] S. Sojoudi and J. Lavaei, "Physics of power networks makes hard optimization problems easy to solve," in *Power and Energy Society General Meeting*, 2012, pp. 1–8.
- [12] B. Kocuk, S. S. Dey, and X. A. Sun, "Matrix minor reformulation and SOCP-based spatial branch-and-cut method for the AC optimal power flow problem," *Mathematical Programming Computation*, vol. 10, no. 4, pp. 557–596, 2018.
- [13] L. T. Watson and R. T. Haftka, "Modern homotopy methods in optimization," *Computer Methods in Applied Mechanics and Engineering*, vol. 74, no. 3, pp. 289–305, September 1989.
- [14] H.-D. Chiang, T.-Q. Zhao, J.-J. Deng, and K. Koyanagi, "Homotopy-enhanced power flow methods for general distribution networks with distributed generators," *IEEE Transactions on Power Systems*, vol. 29, no. 1, pp. 93–100, January 2014.
- [15] H. Mobahi and J. W. Fisher III, "A theoretical analysis of optimization by Gaussian continuation," *AAAI Conference on Artificial Intelligence, North America*, February 2015.

- [16] D. Mehta, H. D. Nguyen, and K. Turitsyn, "Numerical polynomial homotopy continuation method to locate all the power flow solutions," *IET Generation, Transmission & Distribution*, vol. 10, no. 12, pp. 2972 – 2980, August 2016.
- [17] D. M. Dunlavy and D. P. O'Leary, "Homotopy optimization methods for global optimization," *Sandia National Laboratories Report*, December 2005.
- [18] S. Yu, H. D. Nguyen, and K. S. Turitsyn, "Simple certificate of solvability of power flow equations for distribution systems," *2015 IEEE Power & Energy Society General Meeting*, July 2015.
- [19] O. Alsac and B. Stott, "Optimal load flow with steady-state security," *IEEE Transactions on Power Apparatus and Systems*, vol. PAS-93, no. 3, pp. 745–751, May 1974.
- [20] B. Scott, O. Alsac, and A. J. Monticelli, "Security analysis and optimization," *Proceedings of the IEEE*, vol. 75, no. 12, pp. 1623–1644, December 1987.
- [21] M. Huneault and F. Galiana, "A survey of the optimal power flow literature," *IEEE transactions on power systems*, vol. 6, no. 2, pp. 762–770, May 1991.
- [22] Y. C. Wu, A. Debs, and R. Marsten, "A direct nonlinear predictor-corrector primal-dual interior point algorithm for optimal power flows," *IEEE transactions on power systems*, vol. 9, no. 2, pp. 876–883, May 1994.
- [23] G. Torres and V. Quintana, "An interior-point method for nonlinear optimal power flow using voltage rectangular coordinates," *IEEE transactions on power systems*, vol. 13, no. 4, pp. 1211–1218, November 1998.
- [24] J. Momoh and J. Zhu, "Improved interior point method for opf problems," *IEEE transactions on power systems*, vol. 14, no. 3, pp. 1114–1120, August 1999.
- [25] H. Wei, H. Sasaki, J. Kubokawa, and R. Yokoyama, "An interior point method for power system weighted nonlinear L_1 norm static state estimation," *IEEE transactions on power systems*, vol. 13, no. 2, pp. 617–623, May 1998.
- [26] J. Ramirez and E. Barocio, "Solving state estimation in power systems by an interior point method," *Electrical power and energy systems*, vol. 22, pp. 355–365, 2000.
- [27] X. Wang, G. Ejebe, J. Tong, and J. Waight, "Preventive/corrective control for voltage stability using direct interior point method," *Proceedings of the 20th International conference on power industry computer applications*, pp. 312–317, May 1997.
- [28] K. Karoui, L. Platbrood, H. Crisciu, and R. A. Waltz, "New large-scale security constrained optimal power flow program using a new interior point algorithm," *5th international conference on European electricity market*, June 2008.

- [29] N. Chiang and A. Grothey, "Solving security constrained optimal power flow problems by a structure exploiting interior point method," *Optimization and engineering*, vol. 16, no. 1, pp. 49–71, March 2015.
- [30] W. Qiu, A. Flueck, and F. Tu, "A new parallel algorithm for security constrained optimal power flow with a nonlinear interior point method," *IEEE power engineering society general meeting*, June 2005.
- [31] A. Pandey, M. Jereminov, M. Wagner, G. Hug, and L. Pileggi, "Robust convergence of power flow using Tx stepping method with equivalent circuit formulation," November 2017.
- [32] A. Poore and Q. Al-Hassan, "The expanded Lagrangian system for constrained optimization problems," *SIAM Journal on Control and Optimization*, vol. 26, no. 2, p. 417–427, 1988.
- [33] P. Garrigues and L. E. Ghaoui, "An homotopy algorithm for the lasso with online observations," in *Advances in Neural Information Processing Systems*, 2009, pp. 489–496.
- [34] H. Feng and J. Lavaei, "Damping with varying regularization in optimal decentralized control," 2019, available online at https://lavaei.ieor.berkeley.edu/ODC_hom_2019_2.pdf.
- [35] J. Lavaei, D. Tse, and B. Zhang, "Geometry of power flows and optimization in distribution networks," *IEEE transactions on power systems*, vol. 29, no. 2, pp. 572–583, October 2013.
- [36] D. Zigic, L. T. Watson, E. G. Collins, and D. S. Bernstein, "Homotopy approaches to the H_2 reduced order model problem," 1991.
- [37] S.-N. Chow, J. Mallet-Paret, and J. A. Yorke, "Finding zeroes of maps: Homotopy methods that are constructive with probability one," *Mathematics of Computation*, vol. 32, no. 143, pp. 887–899, July 1978.
- [38] M. B. Cain, R. P. O'Neill, and A. Castillo, "History of optimal power flow and formulations," <https://www.ferc.gov/industries/electric/indus-act/market-planning/opf-papers/acopf-1-history-formulation-testing.pdf>, December 2012.
- [39] V. Ajjarapu and C. Christy, "The continuation power flow: A tool for steady state voltage stability analysis," *IEEE Transactions on Power Systems*, vol. 7, no. 1, pp. 416–423, February 1992.
- [40] E. L. Allgower and K. Georg, "Introduction to numerical continuation methods," in *SIAM Classics in Applied Mathematics*, 2003.

- [41] L. T. Watson, "Theory of globally convergent probability-one homotopies for non-linear programming," *SIAM Journal on Optimization*, vol. 11, no. 3, p. 761–780, 2000.
- [42] S. Frank and S. Rebennack, "An introduction to optimal power flow: Theory, formulation, and examples," *IIE transactions*, vol. 48, no. 12, pp. 1172–1197, August 2016.
- [43] V. H. Hinojosa and F. Gonzalez-Longatt, "Preventive security-constrained DCOPF formulation using power transmission distribution factors and line outage distribution factors," *Energies*, vol. 11, no. 6, 2018.
- [44] B. Sturmfels, *Solving systems of polynomial equations*, 2002.
- [45] S. Park, E. Glista, J. Lavaei, and S. Sojoudi, "An efficient homotopy method for solving the post-contingency optimal power flow to global optimality," 2019, https://lavaei.ieor.berkeley.edu/SCOPF_hom_2020_1.pdf.
- [46] D. P. Bertsekas, *Nonlinear programming*. Athena scientific, 2016.
- [47] F. Zohrizadeh, C. Jozs, M. Jin, R. Madani, J. Lavaei, and S. Sojoudi, "Conic relaxations of power system optimization: Theory and algorithms," *European Journal of Operational Research*, vol. 287, no. 2, 2020.
- [48] D. Kirschen, R. Allan, and G. Strbac, "Contributions of individual generators to loads and flows," *IEEE Transactions on Power Systems*, vol. 12, no. 1, pp. 52–60, February 1997.
- [49] C. Garcia and T.Y.Li, "On the number of solutions to polynomial equations," *SIAM Journal on Numerical Analysis*, vol. 17, no. 4, pp. 540–546, August 1980.
- [50] F. Cucker and A. Corbalan, "An alternate proof of the continuity of the roots of a polynomial," *The American Mathematical Monthly*, vol. 96, no. 4, pp. 342–346, April 1989.
- [51] J. E. Spingarn, "Fixed and variable constraints in sensitivity analysis," *SIAM Journal Control and Optimization*, vol. 18, pp. 297–310, 1980.
- [52] O. Fujiwara, "Morse programs: a topological approach to smooth constrained optimization," *Mathematics of operations research*, vol. 7, no. 4, pp. 602–616, 1982.
- [53] R. Rockafellar, "Proximal subgradients, marginal values, and augmented lagrangians in nonconvex optimization," *Mathematics of operations research*, vol. 6, no. 3, pp. 424–436, 1981.

- [54] J. E. Spingarn, "Multifunctions and integrands." Springer, 1984, ch. Multifunctions associated with parametrized classes of constrained optimization problems, pp. 206–215.
- [55] A. V. Fiacco, "Sensitivity analysis for nonlinear programming using penalty methods," *Mathematical Programming*, vol. 10, pp. 287–311, 1976.
- [56] S. Park, E. Glista, J. Lavaei, and S. Sojoudi, "Homotopy method for finding the global solution of post-contingency optimal power flow," *American Control Conference*, 2020.
- [57] ———, "Homotopy method for finding the global solution of post-contingency optimal power flow," 2020, https://lavaei.ieor.berkeley.edu/SCOPF_hom_2020_1.pdf.
- [58] P. A. Parrilo, "Structured semidefinite programs and semialgebraic geometry methods in robustness and optimization," 2000, PhD thesis, <http://www.mit.edu/~parrilo/pubs/files/thesis.pdf>.
- [59] R. D. Zimmerman, C. E. Murillo-Sanchez, and R. J. Thomas, "MATPOWER: Steady-state operations, planning and analysis tools for power systems research and education," *IEEE Transactions on Power Systems*, vol. 26, no. 1, pp. 12–19, February 2011.
- [60] H. Wang, C. E. Murillo-Sánchez, R. D. Zimmerman, and R. J. Thomas, "On computational issues of market-based optimal power flow," *IEEE Transactions on Power Systems*, vol. 22, no. 3, pp. 1185–1193, August 2007.
- [61] C. Jozs, S. Fliscounakis, J. Maeght, and P. Panciatic, "AC power flow data in MATPOWER and QCQP format: iTesla, RTE snapshots, and PEGASE," available online at <http://arxiv.org/abs/1603.01533>.
- [62] S. Fliscounakis, P. Panciatici, F. Capitanescu, and L. Wehenkel, "Contingency ranking with respect to overloads in very large power systems taking into account uncertainty, preventive and corrective actions," *IEEE Transactions on Power Systems*, vol. 28, no. 4, pp. 4909 – 4917, November 2013.
- [63] F. Capitanescu, J. Martinez Ramos, P. Panciatici, D. Kirschen, A. Marano Marcolini, L. Platbrood, and L. Wehenkel, "State-of-the-art, challenges, and future trends in security constrained optimal power flow," *Electric Power Systems Research*, vol. 81, no. 8, pp. 1731 – 1741, 2011.
- [64] F. Capitanescu, M. Glavic, D. Ernst, and L. Wehenkel, "Contingency filtering techniques for preventive security-constrained optimal power flow," *IEEE Transactions on Power Systems*, vol. 22, no. 4, pp. 1690–1697, 2007.

- [65] F. Bouffard, F. Galiana, and J. Arroyo, "Umbrella contingencies in security-constrained optimal power flow," in *Proc. of the 15th Power Systems Computation Conference (PSCC)*, 2005.
- [66] Y. Li and J. D. McCalley, "Decomposed SCOPF for improving efficiency," *IEEE Transactions on Power Systems*, vol. 24, no. 1, pp. 494–495, 2009.
- [67] A. Marano-Marcolini, F. Capitanescu, J. L. Martinez-Ramos, and L. Wehenkel, "Exploiting the use of DC SCOPF approximation to improve iterative AC SCOPF algorithms," *IEEE Transactions on Power Systems*, vol. 27, no. 3, pp. 1459–1466, 2012.
- [68] A. Monticelli, M. V. F. Pereira, and S. Granville, "Security-constrained optimal power flow with post-contingency corrective rescheduling," *IEEE Transactions on Power Systems*, vol. 2, no. 1, pp. 175–180, 1987.
- [69] K. Karoui, H. Crisciu, A. Szekut, and M. Stubbe, "Large scale security constrained optimal power flow," in *Proc. of the 16th Power Systems Computation Conference (PSCC)*, 2008.
- [70] Y. Xu, Z. Y. Dong, R. Zhang, K. P. Wong, and M. Lai, "Solving preventive-corrective SCOPF by a hybrid computational strategy," *IEEE Transactions on Power Systems*, vol. 29, no. 3, pp. 1345–1355, 2014.
- [71] J. Guddat, F. Vasquez, and H.Th.Jongen, *Parametric optimization: singularities, pathfollowing and jumps*. Springer, 1990.
- [72] A. Nemirovski, "Interior point polynomial time methods in convex programming," lecture notes from Georgia Tech.
- [73] J. Carpentier, "Contribution to the economic dispatch problem," *Bulletin de la Societe Francoise des Electriciens*, vol. 3, no. 8, pp. 431–447, 1962.
- [74] A. J. Wood, B. F. Wollenberg, and G. B. Sheblé, *Power generation, operation and control*. Wiley, 2014.
- [75] A. Conejo and J. Aguado, "Multi-area coordinated decentralized DC optimal power flow," *IEEE Transactions on Power Systems*, vol. 13, no. 4, pp. 1272–1278, 1998.
- [76] G. Torres and V. Quintana, "An interior-point method for nonlinear optimal power flow using voltage rectangular coordinates," *IEEE Transactions on Power Systems*, vol. 13, no. 4, pp. 1211–1218, 1998.
- [77] R. A. Jabr, "A primal-dual interior-point method to solve the optimal power flow dispatching problem," *Optimization and Engineering*, vol. 4, pp. 309–336, 2003.

- [78] E. J.Oliveira, L. W.Oliveira, J.L.R.Pereira, L. M.Honório, I. C. Junior, and A.L.M.Marcato, "An optimal power flow based on safety barrier interior point method," *International Journal of Electrical power & energy systems*, vol. 64, pp. 977–985, 2015.
- [79] B. Kocuk, S. Dey, and X. Sun, "Strong SOCP relaxations for the optimal power flow problem," *Operations Research*, vol. 64, no. 6, pp. 1177–1196, 2016.
- [80] F. Capitanescu, T. V. Cutsem, and L. Wehenkel, "Coupling optimization and dynamic simulation for preventive-corrective control of voltage instability," *IEEE Transactions on Power Systems*, vol. 24, no. 2, pp. 796–805, 2009.
- [81] Vaiman, Bell, Chen, Chowdhury, Dobson, Hines, Papic, Miller, and Zhang, "Risk assessment of cascading outages: Methodologies and challenges," *IEEE Transactions on Power Systems*, vol. 27, no. 2, pp. 631–641, 2012.
- [82] L. A. Clarfeld, P. D. H. Hines, E. M. Hernandez, and M. J. Eppstein, "Risk of cascading blackouts given correlated component outages," *IEEE Transactions on Network Science and Engineering*, vol. 7, no. 3, pp. 1133–1144, 2020.
- [83] M. Bazrafshan, K. Baker, and J. Mohammadi, "Computationally efficient solutions for large-scale security-constrained optimal power flow," *arXiv preprint <https://arxiv.org/pdf/2006.00585.pdf>*, 2020.
- [84] I. Avramidis, F. Capitanescu, S. Karagiannopoulos, and E. Vrettos, "A novel approximation of security-constrained optimal power flow with incorporation of generator frequency and voltage control response," *IEEE Transactions on Power Systems*, 2020.
- [85] J. Mohammadi, G. Hug, and S. Kar, "Agent-based distributed security constrained optimal power flow," *IEEE Transactions on Smart Grid*, vol. 9, no. 2, pp. 1118–1130, 2018.
- [86] W. Zhang, Y. Xu, Z. Dong, and K. P. Wong, "Robust security constrained-optimal power flow using multiple microgrids for corrective control of power systems under uncertainty," *IEEE Transactions on Industrial Informatics*, vol. 13, no. 4, pp. 1704–1713, 2017.
- [87] E. Karangelos and L. Wehenkel, "An iterative AC-SCOPF approach managing the contingency and corrective control failure uncertainties with a probabilistic guarantee," *IEEE Transactions on Power Systems*, vol. 34, no. 5, pp. 3780–3790, 2019.
- [88] A. Velloso and P. Van Hentenryck, "Combining deep learning and optimization for preventive security-constrained DC optimal power flow," *IEEE Transactions on Power Systems*, 2021.

- [89] Q. Wang, J. D. McCalley, T. Zheng, and E. Litvinov, "Solving corrective risk-based security-constrained optimal power flow with Lagrangian relaxation and Benders decomposition," *International Journal of Electrical Power & Energy Systems*, vol. 75, pp. 255–264, 2016.
- [90] O. Alsac and B. Stott, "Optimal load flow with steady-state security," *IEEE Transactions on Power Apparatus and Systems*, vol. 93, no. 3, pp. 745 – 751, 1974.
- [91] R. Madani, J. Lavaei, and R. Baldick, "Constraint screening for security analysis of power networks," *IEEE Transactions on Power Systems*, vol. 32, no. 3, pp. 1828–1838, 2017.